AN ABSTRACT OF THE DISSERTATION OF

Atipong Suriya for the degree of Doctor of Philosophy in Industrial Engineering presented on August 19, 2013.
Title: Modeling and Optimization of Radio Frequency Identification Networks for Inventory Management

Abstract approved:_____
J. David Porter

Stock loss and out-of-stocks are outcomes of poorly designed inventory management systems and can lead to significant revenue losses. Inventory management systems (IMS) based on radio frequency identification (RFID) have the potential to minimize these losses if they are properly designed and deployed. However, the placement of RFID readers to support IMS is often done on a trial and error basis which is time consuming and results in less than optimal coverage.

A methodology to model and optimize the design of RFID networks for IMS was developed in this research. The main objective of this methodology is to find the optimal *location* and *number* of RFID readers to ensure a desired level of coverage. Finding a solution that ensures the complete coverage of an entire facility (e.g., a warehouse) would allow an RFID network to support real-time inventory tracking and localization which can minimize shrinkage and prevent theft. Two model formulations that incorporate critical RFID network design parameters known to have an effect on the performance of RFID-based IMS were developed. When compared to prior work, the underlying assumptions that guided the construction of the model formulations make the modeling of the RFID-based IMS more realistic and applicable to warehouse environments. These

important assumptions included the use of elliptical antenna coverage, the consideration of the uplink communication channel (i.e., tag-to-reader), the utilization of appropriate propagation models for the downlink and for the uplink communication channels, and the consideration of obstacles. The heuristic optimization algorithms particle swam optimization (PSO) and genetic algorithm (GA) were applied to the model formulations to search for feasible solutions that ensured appropriate coverage for the warehouse facility, with less interference and within reasonable computation time.

The results show that the proposed methodology works very well with small rectangular facilities and small inverted-T facilities, but there are some limitations when applying it to large facilities.

Modeling and Optimization of Radio Frequency Identification Networks for Inventory Management

by

Atipong Suriya

A DISSERTATION

submitted to

Oregon State University

in partial fulfillment of
the requirements for the
degree of

Doctor of Philosophy

Presented August 19, 2013
Commencement June 2014

Doctor of Philosophy dissertation of Atipong Suriya presented on August 19, 2013.

APPROVED:

Major Professor, representing Industrial Engineering

Head of the School of Mechanical, Industrial and Manufacturing Engineering

---

Dean of the Graduate School

I understand that my dissertation will become part of the permanent collection of Oregon State University libraries. My signature below authorizes release of my dissertation to any reader upon request.

Atipong Suriya, Author

ACKNOWLEDGEMENTS

First and foremost, I would like to express my sincere appreciation to my advisor, Prof. J. David Porter, for his continuous support, nurturing, and guidance throughout my graduate studies. His personal and professional standards will have a lasting influence in my life. Without him, this dissertation would never have been possible. His kindness is greatly appreciated. I would like to express my gratitude to committee members, Prof. David Kim, Prof. John Sessions, Prof. Mario Magaña, and Prof. Roger Graham for their valuable suggestions and willingness to make time to support me in this effort.

The Royal Thai Government, who gave me this valuable opportunity to study abroad in a well-known university and to work with competent professors, is gratefully acknowledged for all their financial support. Special thanks to Mr. Wichai Pakayanont (P Wichai) for his great advice and administration of my fellowship.

I am thankful to the School of Mechanical, Industrial and Manufacturing Engineering for their additional financial support and for giving me the great opportunity and experience to work as a graduate teaching assistant and a graduate research assistant.

I would like to thank all the members of the Mobile Technology Solution Laboratory (MTSL) for their friendship and the good discussions about my research. Very special thanks to all my Thai friends at Oregon State University during these years for making my time in Corvallis enjoyable and memorable, and my friends in Thailand for keeping in touch throughout this long period.

I would like to thank all the good spirits and angels who take care of me and my family. I am indebted to Buddhism and Buddha. His teachings substantially helped me walk through the difficulties in my PhD training with the least suffering possible.

Most importantly, I would like to express my deepest gratitude to my dad Anon, my mom Paichit, my brother Sarunyoo, my sister Sasiwan, and my relatives, for their unconditional love, encouragement, and support through the good and difficult times of my PhD studies.

TABLE OF CONTENTS

Page

1. INTRODUCTION..... 1

1.1. Research Motivation..... 2

1.2. Research Objective..... 3

1.3. Research Contribution..... 4

2. BACKGROUND..... 7

2.1. Radio Frequency Identification..... 7

2.1.1. RFID System Configuration..... 7
2.1.2. Types of RFID Technology..... 8

2.2. Path Loss Propagation Models..... 17

2.2.1. Free Space Propagation Model..... 20
2.2.2. Two-Ray Propagation Model..... 21
2.2.3. Multipath Propagation Model..... 23
2.2.4. Radar Cross Section Propagation Model..... 25
2.2.5. Comparison of Propagation Models..... 26

2.3. Basics Antenna Concepts..... 28

2.3.1. Antenna Radiation Pattern..... 28
2.3.2. Antenna Gain..... 29
2.3.3. Antenna Effective Aperture and Aperture Efficiency..... 30
2.3.4. Antenna Polarization..... 31
2.3.5. Effective Isotropic Radiated Power and Equivalent Radiated Power.... 32

2.4. Optimization Techniques..... 33

2.4.1. Genetic Algorithm..... 33
2.4.2. Particle Swarm Optimization..... 36

3. LITERATURE REVIEW..... 39

3.1. Signal Coverage..... 39

3.2. Signal Propagation..... 43

TABLE OF CONTENTS (Continued)

Page

3.3. Interference..... 47

3.4. Optimization of an RFID System Design..... 50

3.4.1. Genetic Algorithm..... 51
3.4.2. Particle Swarm Optimization..... 52

3.5. Literature Review Summary..... 54

4. RESEARCH METHODOLOGY..... 56

4.1. EPCglobal® C1G2 Standard for RFID Network Planning..... 58

4.2. The Circular Antenna Coverage Model Formulation..... 61

4.2.1. CAC Model Formulation and Constraints..... 67
4.2.2. The Coverage Area of an Omnidirectional Antenna..... 71

4.3. Application of the CAC Model Formulation..... 73

4.3.1. Facility Dimensions and Forbidden Grids..... 74
4.3.2. Radius of the Antenna Coverage Area..... 74
4.3.3. Initial Number of RFID Readers..... 75
4.3.4. Downlink Communication Channel..... 76
4.3.5. Uplink Communication Channel..... 81
4.3.6. Assembling the Multi-Objective Function..... 84

4.4. The Elliptical Antenna Coverage Model Formulation..... 87

4.4.1. EAC Model Formulation and Constraints..... 90
4.4.2. The Coverage Area of a Directional Antenna..... 91

4.5. Application of the EAC Model Formulation..... 98

4.5.1. Major Axis (2a) and Minor Axis (2b) of the Antenna Coverage Area... 98
4.5.2. Initial Number of RFID Readers..... 98
4.5.3. Downlink Communication Channel..... 100
4.5.4. Uplink Communication Channel..... 102
4.5.5. Assembling the Multi-Objective Function..... 103

TABLE OF CONTENTS (Continued)

Page

4.6. Effect of Passive Interference on RFID Antenna Coverage..... 106

4.6.1. Modeling the Effect of Passive Interference on a Circular Antenna Coverage Area..... 106
4.6.2. Modeling the Effect of Passive Interference on an Elliptical Antenna Coverage Area..... 121

4.7. Heuristic Optimization Algorithms..... 140

4.7.1. Particle Swarm Optimization..... 140
4.7.2. Genetic Algorithm..... 148
4.7.3. Algorithm to Find the Optimum Number of RFID Readers..... 153

4.8. Experimental Design..... 157

4.8.1. Facility Shape..... 158
4.8.2. Facility Size..... 159
4.8.3. Grid Size..... 163
4.8.4. Power Levels..... 163
4.8.5. Model Formulation..... 164
4.8.6. Optimization Algorithm..... 164

4.9. Hardware and Software Specification..... 164

5. RESULTS AND DISCUSSION..... 165

5.1. Validation of Optimization Algorithms and CAC Model Formulation..... 167

5.1.1. Problem Description..... 167
5.1.2. Fitness Function Evaluation..... 170
5.1.3. Parameters of the GA and PSO algorithms..... 172
5.1.4. Covering the ITF using Ten RFID Readers..... 173
5.1.5. Covering the entire Indoor Test Facility..... 178

5.2. Effectiveness and Efficiency Evaluation of Optimization Algorithms..... 184

5.2.1. Results for the First Test Scenario..... 185
5.2.2. Results for the Second Test Scenario..... 188

5.3. Results from the Experimental Design with Six RFID Network Design Factors..... 191

TABLE OF CONTENTS (Continued)

Page

5.3.1. Model Adequacy Checking..... 191
5.3.2. Result of the Statistical Analyses based on Six RFID Network Design Factors..... 193

5.4. Results of the Statistical Analyses for Fixed Facility Shape and Fixed Facility Size..... 203

5.4.1. Results with a Small Rectangular Facility..... 203
5.4.2. Results with a Small Inverted-T Facility..... 208
5.4.3. Results with a Large Rectangular Facility..... 213
5.4.4. Results with a Large Inverted-T Facility..... 218

6. CONCLUSIONS AND OPPORTUNITIES FOR FUTURE WORK..... 223

6.1. Research Conclusions..... 225

6.2. Research Limitations..... 228

6.3. Opportunities for Future Work..... 230

Bibliography..... 231

Appendices..... 237

APPENDIX A: Detailed description of some parameters in the notation of the CAC model formulation..... 238
APPENDIX B: Order of experiments and results from the experimental design... 240
APPENDIX C: Calculation of radius (r), semi-major axis (a) and semi-minor axis (b)..... 247

LIST OF FIGURES

Figure — Page

2.1 Components of a typical RFID system..... 7

2.2 Passive RFID technology..... 9

2.3 Semi-passive RFID technology..... 10

2.4 Active RFID technology..... 11

2.5 RFID operating frequency band (Dobkin, 2007)..... 13

2.6 Summary of worldwide UHF RFID band allocations (Dobkin, 2007)..... 15

2.7 Path loss propagation model..... 19

2.8 Two-ray propagation model..... 22

2.9 The graphical representation of the radar system..... 25

2.10 E-plane and H-plane radiation patterns of a dipole antenna (Wikipedia, 2010) 29

2.11 The steps of a basic genetic algorithm (GA)..... 35

2.12 The steps of a basic particle swarm optimization (PSO) algorithm..... 38

3.1 Coverage patterns of omnidirectional and directional antennas..... 40

3.2 Three-dimensional representation of the radiation pattern of a dipole antenna (Dobkin, 2004)..... 41

3.3 E-plane and H-plane radiation patterns of a dipole antenna (Wikipedia, 2010).. 41

3.4 Two-dimensional elliptical representation of an RFID antenna's coverage area using the equation in Marrocco et al. (2009)..... 43

3.5 Reader-to-reader interference in UHF RFID systems..... 49

4.1 Main phases of the research methodology..... 56

4.2 Discretized facility to illustrate how to determine if an RFID tag is located within the coverage area on an omnidirectional antenna..... 73

4.3 Discretized rectangular facility..... 73

LIST OF FIGURES (Continued)

Figure — Page

4.4 Coverage of the rectangular facility using the concept of circle packing..... 75

4.5 Correction to the initial circle packing coverage to reduce interference..... 76

4.6 Pseudocode for computing the members in the set N_i and $D_i(max)$ 78

4.7 Pseudocode for computing the members in the set N_i and $U_i(max)$ 82

4.8 Important elements of the elliptical antenna coverage..... 89

4.9 Area of biggest square enclosed by a circle in CAC model formulation and area of biggest rectangle enclosed by an ellipse in EAC model formulation..... 91

4.10 The placement of RFID readers using the elliptical antenna coverage..... 95

4.11 Coverage of the rectangular facility using the concept of ellipse packing..... 99

4.12 Correction to the initial ellipse packing coverage to be eligible in the system.. 99

4.13 Regular grids and forbidden grids covered by the circular coverage area..... 107

4.14 Slope values of perimeter points and locations within the circular coverage area..... 109

4.15 Modified circular coverage area with 16 rays..... 118

4.16 Modified circular coverage area with 360 rays..... 119

4.17 Example of how to check if a grid under consideration (grid 4) is covered by the real coverage area..... 120

4.18 Important geometric features of an ellipse..... 121

4.19 Candidate grids and forbidden grids covered by the elliptical coverage area.... 123

4.20 Perimeter points of the elliptical coverage area with (a) $\alpha = 45^\circ$ and (b) $\alpha = 0^\circ$ 124

4.21 The coordinate on the perimeter (x_θ, y_θ) of the rotation elliptical coverage area..... 127

LIST OF FIGURES (Continued)

Figure Page

4.22 Modified elliptical coverage area..... 135

4.23 Modified elliptical coverage area with 16 rays from the center (*h*,*k*)..... 136

4.24 Modified elliptical coverage area with 360 rays..... 138

4.25 The format of a PSO particle representation..... 143

4.26 Discretized rectangular facility..... 146

4.27 Steps of the inertia-weighted PSO algorithm..... 147

4.28 The GA's crossover process..... 150

4.29 Steps of the GA algorithm..... 152

4.30 The original algorithm to find the optimum number of RFID readers..... 153

4.31 The algorithm to find the optimum number of RFID readers..... 156

4.32 Rectangular shape of facility and its layout (Tang et al., 1997)..... 160

4.33 Non-rectangular (Inverted-T) shape of facility and its layout (Ji et al., 2002).. 161

4.34 Small rectangular shape of facility and its layout..... 162

4.35 Small non-rectangular shape of facility and its layout..... 162

5.1 Structure of the results chapter..... 166

5.2 The indoor test facility (Chen et al., 2011)..... 168

5.3 Coverage of the ITF by Chen et al. (2011)..... 174

5.4 Coverage of the ITF by the PSO algorithm..... 174

5.5 Evolution of the fitness function during the search for PSO algorithm..... 175

5.6 Coverage of the ITF by the GA..... 176

5.7 Evolution of the fitness function during the search for GA..... 176

LIST OF FIGURES (Continued)

Figure Page

5.8 The optimum location and number of RFID readers to cover all tags in the ITF using PSO algorithm..... 179

5.9 Evolution of the fitness function during the search of PSO algorithm to cover the entire ITF..... 180

5.10 The optimum location and number of RFID readers to cover all RFID tags in the ITF using the GA..... 181

5.11 Evolution of the fitness function during the search of GA to cover entire ITF. 182

5.12 Normal probability plot of the residuals from the fitness..... 192

5.13 Residual plot of the fitness versus the treatment combinations..... 193

5.14 LSD interval plot of the RFID network design factor *facility shape*..... 196

5.15 LSD interval plot of the RFID network design factor *facility size*..... 196

5.16 LSD interval plot of the RFID network design factor *grid size*..... 197

5.17 LSD interval plot of the RFID network design factor *power levels*..... 197

5.18 LSD interval plot of the RFID network design factor *model formulation*..... 198

5.19 LSD interval plot of the RFID network design factor *optimization algorithm*.. 198

5.20 LSD interval plot of the RFID network design factor *grid size*..... 204

5.21 LSD interval plot of the RFID network design factor *power levels*..... 205

5.22 LSD interval plot of the RFID network design factor *model formulation*..... 205

5.23 The placement of RFID readers in a small rectangular facility using the best configuration of RFID network design factors..... 206

5.24 The placement of RFID readers in a small rectangular facility using the best configuration of RFID network design factors with entire coverage..... 207

5.25 The interaction plot of power levels and model formulation..... 209

LIST OF FIGURES (Continued)

Figure — Page

5.26 LSD interval plot of the RFID network design factor *grid size*..... 210

5.27 LSD interval plot of the RFID network design factor *power levels*..... 210

5.28 LSD interval plot of the RFID network design factor *optimization algorithm*.. 211

5.29 The placement of RFID readers in a small inverted-T using the best configuration of RFID network design factors with entire coverage..... 212

5.30 LSD interval plot of the RFID network design factor *optimization algorithm*.. 214

5.31 LSD interval plot of the RFID network design factor *power levels*..... 215

5.32 LSD interval plot of the RFID network design factor *model formulation*..... 215

5.33 The placement of RFID readers in a large rectangular facility using the best configuration of RFID network design factors..... 217

5.34 LSD interval plot of the RFID network design factor *optimization algorithm*.. 219

5.35 LSD interval plot of the RFID network design factor *grid size*..... 220

5.36 LSD interval plot of the RFID network design factor *power levels*..... 220

5.37 The placement of RFID readers in a large inverted-T facility using the best configuration of RFID network design factors..... 222

LIST OF TABLES

Table — Page

2.1 The comparison of RFID in different operating frequency band (Sanghera, 2007)..... 14

2.2 Path loss exponent *n* and standard deviation measured in different buildings (Huang & Boyle, 2008)..... 24

2.3 Advantages and disadvantages of different propagation models..... 26

2.4 Description of the parameters of the PSO formulation..... 37

3.1 Summary of the research studies conducted by (Guan et al., 2006), (Chen et al., 2011), and (Giampaolo et al., 2010)..... 55

4.1 RFID system parameters compliant with EPCglobal® C1G2 standard..... 59

4.2 Location of an FGj based on the relationship between its slope and the signs of the coordinates (x_j,y_j) of its center..... 110

4.3 Location of FGs for the example in Figure 4.14..... 111

4.4 Criteria for slope comparison of the ray with no slope or infinite slope..... 113

4.5 Criteria for slope comparison of the ray with positive or negative slope..... 114

4.6 Slope comparison between R_6 and the corner points of the FGs located in Q2.. 115

4.7 The number of walls crosses by each $R_i \ \forall \ i = 1,2,...,16$ 117

4.8 Parameters needed to calculate coordinates (x_i, y_i) of perimeter points P_i..... 125

4.9 Location of FGs for the example in Figure 4.19..... 129

4.10 Slope comparison between ray 6 and the corner points of the FGs located in Q1..... 131

4.11 Number of walls crosses by each of the 16 rays of elliptical coverage area..... 132

4.12 New coordinates $P_i^{'}(x_i^{'}, y_i^{'})$ of each ray, the relative incremental angle $\theta_{relative}$ and the relative length $d_{relative}$ 137

LIST OF TABLES (Continued)

Table	Page
4.13 Conditions identifying the fields required in a particular particle.....	144
4.14 Experimental controlled factors in the experimental design.....	157
5.1 Parameters of the GA and PSO algorithms.....	172
5.2 Summary of results from Chen et al. (2011), GA and PSO for partial ITF coverage with 10 RFID readers.....	177
5.3 Summary of results for the GA and PSO algorithms to cover entire ITF.....	183
5.4 Exhaustive enumeration results for the first test scenario.....	185
5.5 Effectiveness and efficiency of the PSO for the first test scenario.....	186
5.6 Effectiveness and efficiency of the GA for the first test scenario.....	187
5.7 Exhaustive enumeration results for the second test scenario.....	189
5.8 Effectiveness and efficiency of the PSO algorithm for the second test scenario.	190
5.9 Effectiveness and efficiency of the GA for the second test scenario.....	190
5.10 Multi-factor ANOVA results based on six RFID network design factors.....	194
5.11 Multi-factor ANOVA results for the small rectangular facility.....	203
5.12 Multi-factor ANOVA results for the small inverted-T facility.....	208
5.13 Multi-factor ANOVA results for the large rectangular facility.....	213
5.14 Multi-factor ANOVA results for the large inverted-T facility.....	218
6.1 The best configuration for a specific facility shape and facility size and its fitness.....	228

Modeling and Optimization of Radio Frequency Identification Networks for Inventory Management

1. INTRODUCTION

Radio frequency identification (RFID) is an Automatic Identification and Data Capture (AIDC) technology that has gained significant attention in recent years as a means of enhancing the traceability of items throughout the supply chain. Market trends indicate a rapid growth in the demand for RFID-based technologies, with an expected 18% compound annual growth rate for the three-year period 2011-2014, culminating in a projected $19.3 billion industry by the end of 2014 (RNCOS Industry Research Solutions, 2012).

RFID technology, when properly implemented, has several benefits over more conventional AIDC technology (i.e., bar codes), including tracking physical objects in real time and reductions in process times, labor, and the amount of paperwork needed in day-to-day operations. Applications of RFID technology are becoming more common in the supply chain (and particularly in warehouse facilities) to enable product tracking and to support inventory management systems (IMSs).

An RFID-based IMS can be designed to have localized coverage or to cover the entire warehouse facility. However, an RFID-based IMS with entire warehouse facility coverage will result in several advantages when compared to one with localized coverage including:

- **Real time inventory tracking, shrinkage and theft prevention.** With entire warehouse facility coverage, an organization can monitor and track inventory levels in real time. An RFID system with localized coverage cannot track

inventory levels in real time because it is unable to track inventory items when they are moving. Ernst & Young (2003) found that retailers lose $46 billion annually to inventory shrinkage including employee theft, shoplifting, administrative error and vendor fraud and the biggest problem is from employee thefts. An RFID-based IMS with entire warehouse facility coverage and continuous tracking has the potential to reduce shrinkage, theft and loss of inventory.

- **Localization.** An RFID-based IMS with entire warehouse facility coverage can provide the capability of inventory/item localization and/or positioning.
- **Travel time estimation and warehouse layout improvement.** With comprehensive tracking, location, and identification, the movement history of tagged items can be obtained. Also, the average travel time it takes employees to get to the desired items during picking and put away operations can be calculated. Item movement history may also be useful for adjusting a route to access items with shortest path and improving the efficiency of the warehouse facility layout.

1.1. Research Motivation

One of the most important decisions when designing RFID-based IMSs is where to locate the RFID readers within a warehouse facility to maximize performance. However, the placement of RFID readers in practice is often done on a trial-and-error basis, which is very time consuming and generally results in less-than-optimal coverage of the warehouse facility area. This directly affects the reliability of RFID-based IMSs in terms of reader-to-tag communication and tag read rate. RFID network installations based on trial and error also typically results in a more expensive system since more RFID readers are needed. RFID

readers used in IMS applications cost between $1,000 and $9,000 per unit depending on the features in the device; antennas can cost anywhere from $200 to $500 (RFID Journal LLC, 2012). Comparatively, wireless LAN access points cost between $30 and $200 (Amazon.com Inc., 2012).

Furthermore, models developed in prior research in the area of RFID network planning have been based on questionable assumptions. For example, some models have only assumed circular (i.e., omnidirectional) antenna coverage and have mainly employed free space propagation models while others have not taken into account the attenuation caused by obstacles located within a facility or considered the modeling of the uplink and downlink communication channels.

1.2. Research Objective

The main objective of this research was to develop an effective and automated approach for optimizing the placement of RFID readers in a facility. Optimally locating RFID readers within a facility is referred to as the RFID network planning (RNP) problem.

The methodology followed in this research to accomplish this objective involved the development of two model formulations that incorporated critical RFID network design parameters known to have an effect on the performance of RFID-based IMSs. The underlying assumptions made in constructing the model formulations were improved when compared to prior work to make the modeling of the RFID-based IMS more realistic and applicable to warehouse environments. These important assumptions included the use of elliptical antenna coverage, the consideration of the uplink communication channel (i.e., tag-to-reader), the utilization of appropriate propagation models for the downlink and for the uplink communication channels, and the consideration of obstacles.

The heuristic optimization algorithms particle swam optimization (PSO) and genetic algorithm (GA) were applied to the model formulations to search for feasible solutions to the RNP problem that ensured coverage for the entire warehouse facility, with less interference and within reasonable computation time.

Finally, a designed experiment was conducted to evaluate the effect that different RFID network design factors had on the effectiveness of the developed GA and PSO algorithms to find the optimal number and location of RFID readers in a facility.

1.3. Research Contribution

Several contributions have been made by this research. To achieve the goal of the design of RFID networks for inventory management, the *circular antenna coverage* (CAC) and *elliptical antenna coverage* (EAC) model formulations were developed based on the type of antenna used by the RFID reader in the system. Most of the prior work in the literature proposed models to solve the RFID network problem (RNP) assuming that the antenna of the RFID readers produced a circular coverage; very few developed models under the assumption of an elliptical antenna coverage area. In this research, a dipole antenna having a circular coverage area was assumed in the CAC model formulation. However, RFID readers that use directional antennas with an elliptical coverage area are more common in RFID networks. Therefore, the EAC model formulation was developed assuming the use of a patch antenna. The development of both the CAC and the EAC model formulations would help to get a better understanding of the effect of both types of antennas on the performance of an RFID network.

The consideration of the downlink communication and the uplink communication channels was also included in the CAC and EAC model formulations using the multipath

propagation model and the radar cross section propagation model, respectively. The consideration of the uplink communication channel was found in only one previous work from the literature. The more realistic assumption of an antenna with an elliptical coverage area as well as the use of two propagation models make the model formulations more practical and more accurate.

Finding solutions to the CAC and EAC model formulations is an NP-hard problem. Therefore, an automated tool was developed that implements two heuristic optimization algorithms based on GA and PSO to find good solutions to the CAC and EAC model formulations within a reasonable computation time. In the process of finding good solutions, the attenuation due to the effect of obstructions (i.e., passive interference) was taken into account. The shape and size of the *maximum antenna coverage area* without the effect of obstructions, i.e., perfect circle or ellipse, was changed to a *modified antenna coverage area* after the effect of obstructions was assessed by using a *ray-tracing* method. The consideration of obstructions made the GA and PSO algorithms more constrained when searching for good solutions. None of the prior research found in the literature considered the effect of obstructions in their RFID network design problem.

A full factorial experimental design was conducted to investigate the effect of the six RFID network design factors *facility shape, facility size, grid size, power levels, model formulation,* and *optimization algorithm* on the value of fitness (i.e., the response variable). The results of this experiment were analyzed using multi-factor ANOVA. Further experimentation was conducted to investigate the effect of the four RFID network design factors *grid size, power levels, model formulation,* and *optimization algorithm* on the value of fitness with scenarios where it was assumed that the size and shape of the facility (as well as the locations of obstructions) were known. Understanding the effect of the six RFID network

design factors in the first scenario would be beneficial when the designers would like to design an RFID network before a facility is built. If a facility is already available, the latter scenario could be applied to identify the effect of *grid size*, *power levels*, *model formulation*, and *optimization algorithm* on the value of fitness.

2. BACKGROUND

2.1. Radio Frequency Identification

The term Automatic Identification and Data Capture (AIDC) refers to a family of technologies that enable the automatic collection and storage of data in a computer system. Radio frequency identification (RFID) is one AIDC technology that has gained significant attention in recent years. RFID is one method of communicating data via electromagnetic waves in a radio frequency (RF) band between a transmitter and a receiver.

2.1.1. RFID System Configuration

A basic RFID system, such as the one depicted in Figure 2.1, includes four main components: a host computer system, a reader, an antenna, and a transponder (or tag).

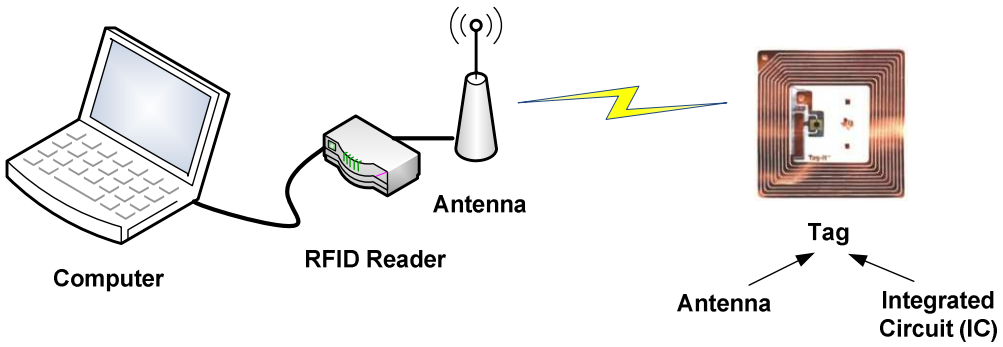

Figure 2.1 Components of a typical RFID system

The tag is electronically programmed with unique information. The host computer system issues specific commands to the reader that are transformed into electromagnetic (EM) signals that radiate from the RFID reader's antenna to the tag. After the tag receives the

EM signal, it sends its identification (ID) number back to the RFID reader using a backscattering method. The tag's ID number is ultimately forwarded to the host computer system for further processing or storage.

RFID technology, when properly implemented, has the potential of providing several benefits including reductions in process times, labor, and the amount of paperwork needed in day-to-day operations. This is because the RFID reader can automatically read tags within the coverage area of its antenna and multiple tags can be read at one time. RFID does not require line of sight (LOS) communication, which is necessary with more conventional AIDC technology (e.g., bar codes). RFID has the capability of tracking physical objects in real time and therefore is becoming a popular choice in several applications such as supply chain management (Angeles, 2005), retail (Jones et al., 2005b), inventory control (Chande et al., 2005), animal tracking and detection (Wismans, 1999), food traceability (Jones et al., 2005a), health care (Venkatesan & Grauer, 2004), access control (Almanza-Ojeda et al., 2006) and library services (Kern, 2004).

2.1.2. Types of RFID Technology

RFID technology can be categorized into several different types based upon tag power source, operating frequency, and coupling.

2.1.2.1. Tag Power Source

In RFID applications, the RFID reader is usually attached to a host computer and thus it has its own power supply. However, RFID tags can be categorized as *passive*, *semi-passive*, or *active* depending upon their power source.

2.1.2.1.1. Passive RFID Technology

In passive RFID technology, the tag does not have its own power source. Instead, the tag receives an electromagnetic signal from the RFID reader via the antenna and converts it to current that is supplied to its integrated circuit (IC). Finally, the IC utilizes the supplied energy for processing and then sends the signal and the ID number of the tag back to the reader. This process is illustrated in Figure 2.2.

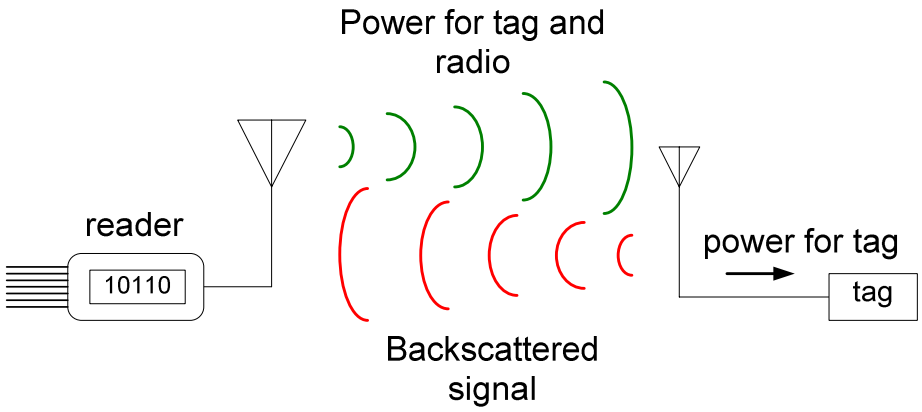

Figure 2.2 Passive RFID technology

A passive RFID tag has the following characteristics:

- **Operation.** The passive tag must be within the coverage area of the RFID reader since it utilizes the energy supplied by the reader to operate. Also, the passive tag cannot initiate communications with the RFID reader.
- **Size and range**. The passive tag is normally small and its operating range is shorter compared with semi-passive and active tags.
- **Lifespan**. The passive tag has a long lifespan because it uses the energy from the RFID reader to operate (i.e., it does not use batteries).

- **Memory**. The passive tag has a small memory capacity (i.e., 1-128 bits). However, modern passive tags sometimes have up to 64 kilobytes (KB) of memory.

Passive RFID tags can operate in the low frequency (LF), high frequency (HF), and ultra high frequency (UHF) frequency bands, as depicted in Figure 2.5. Compared to semi-active and active tags, passive tags are comparatively inexpensive. Therefore, they are very popular and have been used in several applications, particularly in the supply chain.

2.1.2.1.2. Semi-Passive RFID Technology

In semi-passive RFID technology, the tag has its own power supply in the form of a battery. The energy from the battery is used to supply power to the IC in the tag, but it still utilizes the power received from the RFID reader for processing and for sending its ID number back to the RFID reader. This process is illustrated in Figure 2.3.

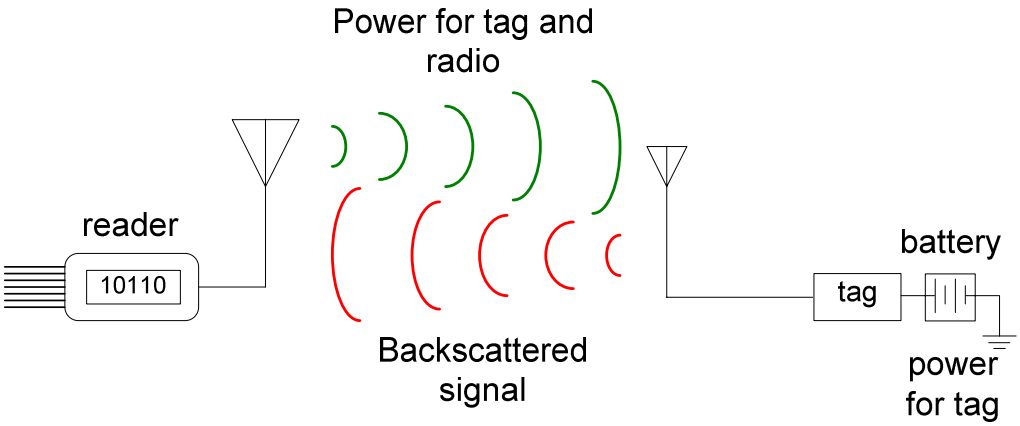

Figure 2.3 Semi-passive RFID technology

A semi-passive RFID tag has the following characteristics:

- **Operation.** The semi-passive tag uses the energy from the RFID reader to initiate the communication link, just like a passive tag
- **Size and range**. The semi-passive tag is typically larger in size and has a longer operating range when compared to the passive tag.
- **Lifespan**. The lifespan of the semi-passive tag is dependent upon the life of its battery.
- **Memory**. The semi-passive tag has a larger memory capacity when compared to a passive tag.

2.1.2.1.3. Active RFID Technology

Unlike the first two types of RFID tags, an active tag has its own power source and can initiate the communication link with the RFID reader, as depicted in Figure 2.4.

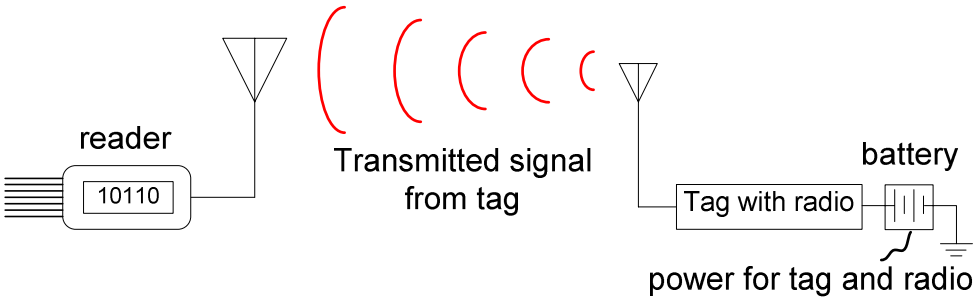

Figure 2.4 Active RFID technology

An active RFID tag has the following properties:

- **Operation.** The active tag can initiate the communication link with the RFID reader at any time. Therefore, it is very flexible and can be used in several applications.
- **Size and range.** The size of an active tag is large when compared to passive and semi-passive tags. Active tags can be read within several meters and up to one kilometer.
- **Lifespan.** The lifespan of an active tag is about ten years and depends on the type of battery it uses.
- **Memory.** The active tag has a large memory capacity of up to 8 megabytes (MB).

The biggest disadvantage of active RFID tags is that they are much more expensive than passive or semi-passive tags. Active RFID tags commonly operate in the UHF and microwave frequency bands and are attached to high cost items such as cars and shipping containers.

2.1.2.2. Types of RFID by Operating Frequency

Operating frequency refers to the carrier frequency the RFID reader and the RFID tag use to communicate with each other. Most RFID systems in the U.S. operate in the unlicensed industrial, scientific and medical (ISM) bands. RFID systems can be classified into four operating frequency bands, i.e., low frequency (LF), high frequency (HF), ultra high frequency (UHF), and microwave frequency. These RFID operating frequency bands are shown in Figure 2.5.

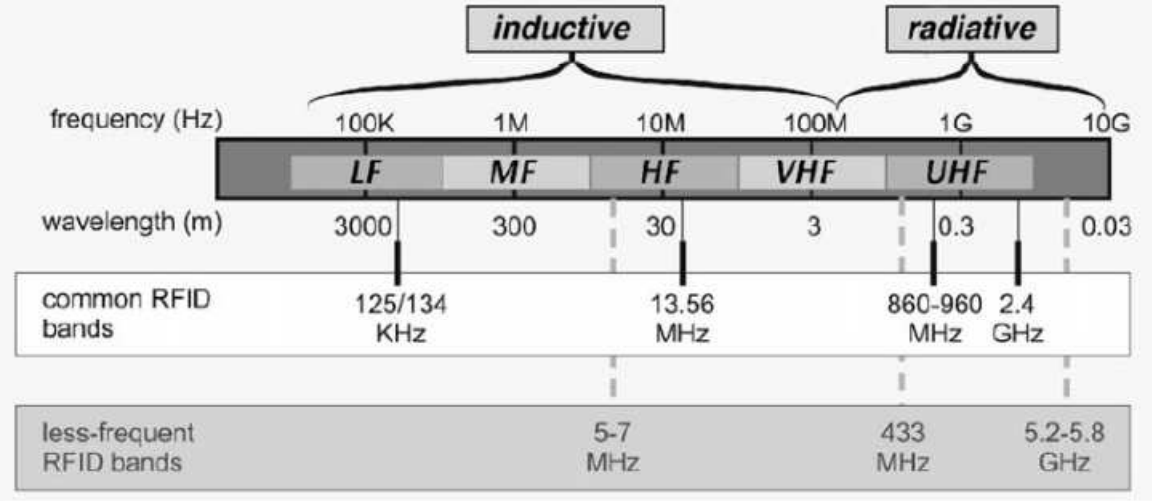

Figure 2.5 RFID operating frequency band (Dobkin, 2007)

Several parameters have to be considered when selecting the appropriate operating frequency for the RFID readers and tags for certain applications. These parameters include the expected maximum read distance (particularly for passive tags), reading speed, sensitivity to water and humidity, etc. Some of the common values for these parameters for the different operating frequency bands are shown in Table 2.1.

Table 2.1 The comparison of RFID in different operating frequency band (Sanghera, 2007)

	FREQUENCY BANDS			
Parameters	**LF** 125 kHz / 134 kHz	**HF** 13.56 MHz	**UHF** 433 MHz, 860-960 MHz	**Microwave** 2.45 GHz / 5.8 GHz
Maximum read distance for passive tag	< 50 cm	< 3 m	< 9 m	> 10 m
Reading speed	Slow	Medium	Fast	Very Fast
Sensitive to water and humidity	No	No	Yes	Yes. Very sensitive.
ISO Standard	ISO 11784/85 and ISO 14223	ISO 14443, ISO 18000, and ISO 15693	ISO 18000-6, and EPC Class 0/ Class 1/ Class 1 Gen 2	ISO 18000-4
Applications	Access control, Immobilizer, Gas, Laundry, Animal tracking and detection	Smart cards, Electronic ID, Ticketing, Library, Baggage handling at airports, Boarding pass, Postal, and Pharmacy	Logistic and supply chain, Inventory control, Trucks and trailer tracking	Road tolling, Container tracking

RFID systems must use different operating frequencies depending on the region of the world where they are located, as shown in Figure 2.6 (Dobkin, 2007).

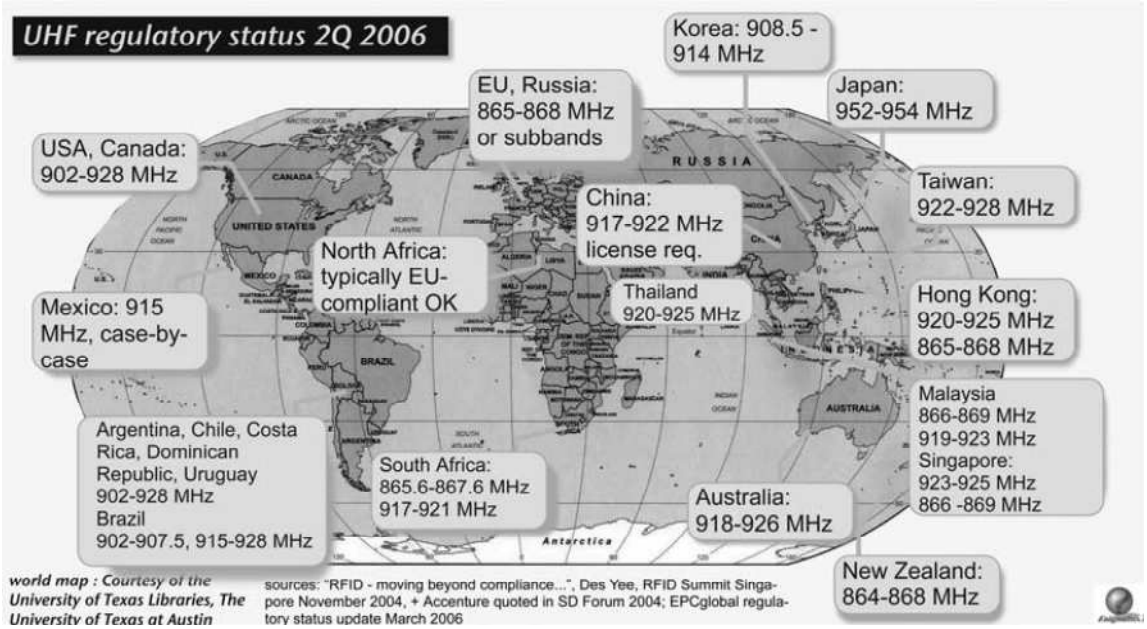

Figure 2.6 Summary of worldwide UHF RFID band allocations (Dobkin, 2007)

2.1.2.3. Types of RFID by Coupling

An RFID system bases its operation on an electromagnetic signal travelling through space at the speed of light (i.e., 3×10^8 meters/second). The relationship among wavelength (λ), operating frequency (f) and the speed of light (c) can be expressed using equation 2.1.

$$\lambda = \frac{c}{f} \tag{2.1}$$

Equation 2.1 shows that the wavelength of an electromagnetic signal is inversely proportional to the operating frequency. As a consequence, RFID systems can also be categorized by comparing the size of the wavelength of the electromagnetic signal relative to the size of the antenna. The regions referred to as *near-field* and *far-field* are considered to identify whether the RFID system operates in *inductive coupling* or *radiative coupling*,

respectively. An RFID system is said to operate in the *near-field* region if equation 2.2 is satisfied.

$$R < \frac{2D^2}{\lambda} \tag{2.2}$$

In equation 2.2, *R* is the distance between the antenna of the RFID reader and the antenna of the RFID tag and *D* represents the largest physical linear dimension of the antenna. If equation 2.2 is not satisfied, then the RFID system is said to operate in the *far-field* region.

2.1.2.3.1. Inductive Coupling

RFID systems in which the wavelength of the electromagnetic signal is much larger than the largest physical linear dimension of the antenna operate according to the principle of inductive coupling. Under inductive coupling, the majority of the available energy from the antenna of the RFID reader is contained within a region near the reader. Therefore, inductive coupling occurs in the near-field region. Inductive coupling is common in RFID systems that operate in the LF and HF bands (i.e., up to 30 MHz) because the value of λ tends to be much larger than *D*. Consequently, the ratio $\frac{2D^2}{\lambda}$ will be small. As a result, the maximum read distance of inductive coupling RFID systems is relatively short compared to those RFID systems that operate in the UHF or microwave frequency bands.

2.1.2.3.2. Radiative Coupling

Radiative (i.e., backscattered) coupling occurs in the far-field region. Radiative coupling RFID systems operate in the UHF and microwave frequency bands, i.e., at frequencies greater than 30 MHz. As a result, the wavelength of the electromagnetic signal is smaller than that used in inductive systems (Finkenzeller, 2003).

In radiative coupling RFID systems, designing the antenna with the largest physical linear dimension comparable to or greater than the wavelength of the electromagnetic signal allows the antenna to have much higher efficiency than that of inductive coupling RFID systems. This results in an increment of the power available for the tag. When the power increases, it can also increase the operating or maximum read distance between the reader and the tag. As a result, RFID systems operating in the UHF or microwave frequency bands are more flexible for applications requiring longer read distances, such as in supply chain management.

2.2 Path Loss Propagation Models

The selection of a path loss propagation model is one of the most important decisions when modeling an RF-based communications system. A path loss propagation model is formulated using the radio wave propagation path loss, which is defined as the difference between the transmitted power from the source antenna and the received power at the destination antenna. A propagation model is needed to accurately estimate the radio signal coverage or, in the case of an RFID system, the coverage area of the RFID reader.

An RFID system has two communication links, i.e., the communication link from the reader to the tag and the communication link from the tag to the reader. These

communication links are referred to as the *downlink* and *uplink* communication channels, respectively. The signals that use these channels are attenuated not only by the distance between the reader and tag, but also by the interference from adjacent readers and obstacles in the system.

Some of the most common path loss propagation models and their parameters are depicted in Figure 2.7. These models are grouped based on whether they are used to model the downlink or the uplink communication channel. The three main models used to model the downlink channel are *free space*, *two-ray* and *multipath* models. These same path loss propagation models can be used to model the uplink channel with the addition of the *radar cross section* (RCS) model, which can be used for more precise calculations. The following sections describe each type of path loss propagation model in more detail.

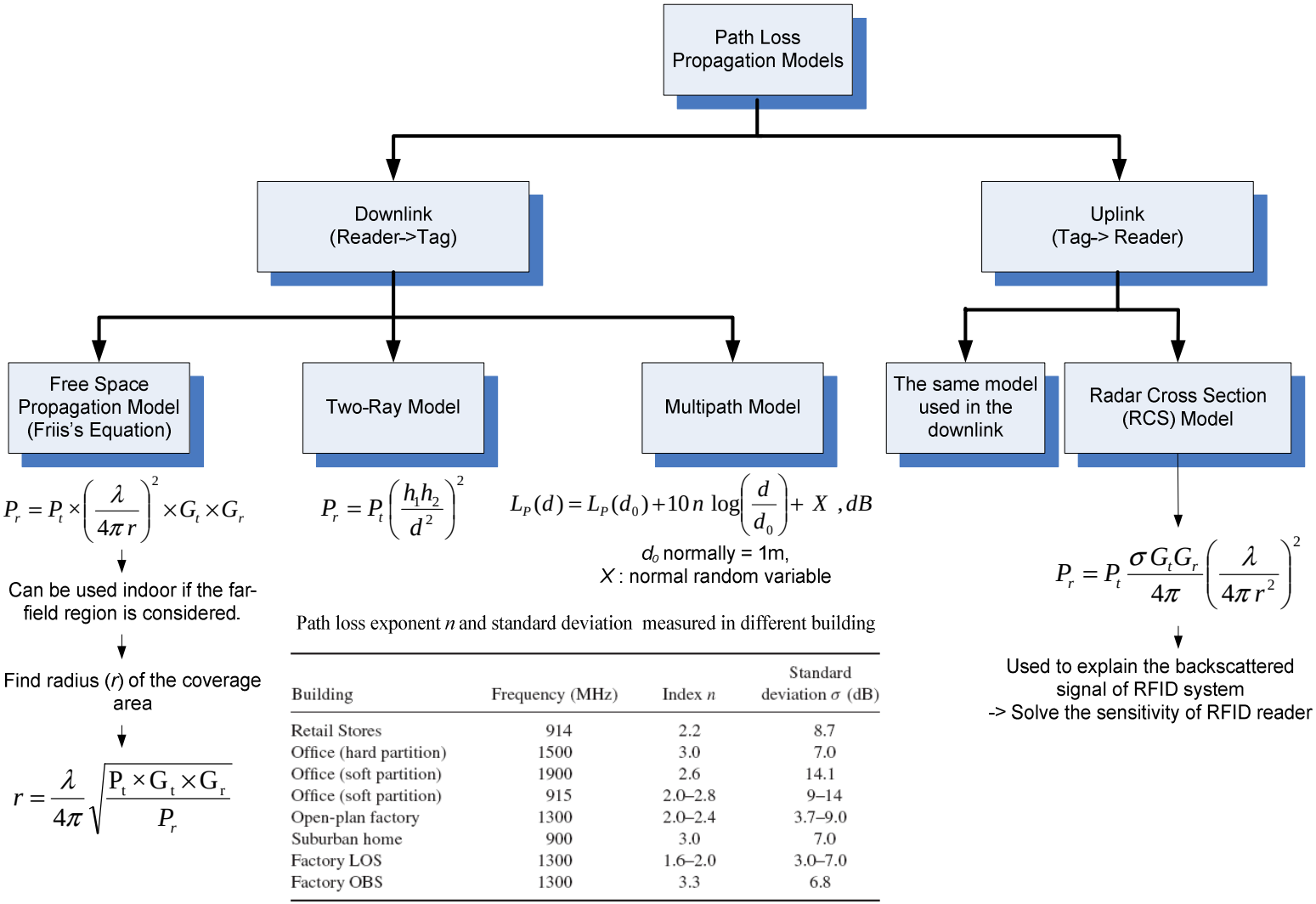

Path loss exponent n and standard deviation measured in different building

Building	Frequency (MHz)	Index n	Standard deviation σ (dB)
Retail Stores	914	2.2	8.7
Office (hard partition)	1500	3.0	7.0
Office (soft partition)	1900	2.6	14.1
Office (soft partition)	915	2.0–2.8	9–14
Open-plan factory	1300	2.0–2.4	3.7–9.0
Suburban home	900	3.0	7.0
Factory LOS	1300	1.6–2.0	3.0–7.0
Factory OBS	1300	3.3	6.8

Figure 2.7 Path loss propagation models

2.2.1. Free Space Propagation Model

The free space (FS) propagation model assumes direct LOS communication between the transmitting antenna and receiving antenna. The FS propagation model is suitable to model outdoor RF communications with no obstructions in the environment. However, Greene (2006) suggested that it can be used in an indoor environment in the far-field region. The equation for computing the received signal power at the receiving antenna is shown in equation 2.3. This equation is known as the *Friis transmission formula* or *Friis's equation*.

$$P_r = P_t \times \left(\frac{\lambda}{4\pi r} \right)^2 \times G_t \times G_r \tag{2.3}$$

In equation 2.3, P_r is the received power, P_t is the transmitted power, λ is the wavelength of the transmitted signal, *r* is the distance between the transmitting and receiving antennas, and G_t and G_r are the gains of the transmitting and receiving antennas, respectively.

After some mathematical manipulation, the Friis's equation can also be expressed in units of decibel (dB), as shown in equation 2.4.

$$[P_r]_{dB} = [P_t]_{\mathrm{dB}} + [G_t]_{dB} + [G_r]_{dB} - [path\ \ loss]_{dB} \tag{2.4 a}$$

$$[P_r]_{dB} = [P_t]_{\mathrm{dB}} + [G_t]_{dB} + [G_r]_{dB} - 20\log\left(\frac{4\pi r}{\lambda} \right) \tag{2.4 b}$$

$$[P_r]_{dB} = [P_t]_{\mathrm{dB}} + [G_t]_{dB} + [G_r]_{dB} - 20\log\left(\frac{4\pi f r}{c} \right) \tag{2.4 c}$$

$$[P_r]_{dB} = [P_t]_{\text{dB}} + [G_t]_{dB} + [G_r]_{dB} - 20\log f - 20\log r - 20\log\left(\frac{4\pi}{c}\right) \quad \text{(2.4 d)}$$

$$[P_r]_{dB} = [P_t]_{\text{dB}} + [G_t]_{dB} + [G_r]_{dB} - 20\log f - 20\log r + 147.6\,dB \quad \text{(2.4 e)}$$

The path loss term in equation 2.4a is due to the attenuation loss along the distance between transmitter and receiver and is represented by the term $\left(\frac{\lambda}{4\pi r}\right)^2$. Since the path loss is proportional to the square of the operating frequency and the distance, RFID systems that operate in higher frequency bands (i.e., UHF and microwave) tend to have a larger path loss than those that operate in the LF and HF frequency bands. The radius of the coverage area of an RFID system can be calculated from the Friis's equation using equation 2.5.

$$r = \frac{\lambda}{4\pi}\sqrt{\frac{\mathrm{P_t} \times \mathrm{G_t} \times \mathrm{G_r}}{P_r}} \quad \text{(2.5)}$$

2.2.2. Two-Ray Propagation Model

The two-ray propagation model assumes that there are two paths in the communication link between transmitter and receiver, i.e., a *direct path* and a *reflected path from the surface*. These paths are illustrated in Figure 2.8.

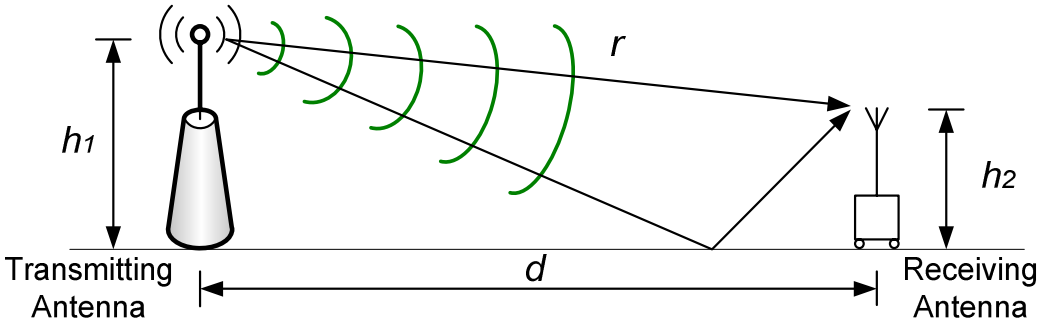

Figure 2.8 Two-ray propagation model

The two-ray propagation model can be applied to terrestrial communications such as radio broadcasting. It can also be used in an indoor environment as in the work conducted by Giampaolo et al. (2010). The received signal at the receiving antenna has components due to the direct path and the reflected path which may combine constructively or destructively depending on the reflection coefficient of the surface and the phase difference of these two rays.

Equation 2.6 shows the path difference (i.e., Δr) between the direct path and the reflected path based on the assumption that *d* is much larger than the summation of h_1 and h_2 (i.e., $d >> (h_1 + h_2)$), where h_1 and h_2 represent the height of the transmitting and receiving antennas, respectively. In the two-ray propagation model, the heights of both the transmitting and receiving antennas have to be known.

$$\Delta r = \sqrt{(h_1 + h_2)^2 + d^2} - \sqrt{(h_1 - h_2)^2 + d^2} \approx \frac{2h_1 h_2}{d} \tag{2.6}$$

The received signal power of the two-ray propagation model can be calculated using equation 2.7.

$$P_r = P_t \left(\frac{h_1 h_2}{d^2} \right)^2 \tag{2.7}$$

Equation 2.7 can also be expressed in units of dB, as shown in equation 2.8.

$$[P_r]_{dB} = [P_t]_{dB} - [40\log(d)]_{dB} + [20\log(h_1 h_2)]_{dB} \quad (2.8)$$

Equation 2.8 shows that for a constant transmit power and distance between the transmitted and receiving antenna, the higher the transmitting and receiving antennas are from the ground, the smaller the signal path loss is.

2.2.3. Multipath Propagation Model

The multipath propagation model assumes that the signals received at the receiving antenna come from more than two rays, i.e., the direct path and several reflected paths. This is because signals transmitted by the transmitting antenna may be reflected, diffracted, or scattered by the obstructions in the environment resulting in the multipath signal received at the receiving antenna. Since signals from different paths arrive at the receiving antenna in different time periods, their phase difference may combine constructively or destructively causing an effect known as *delay spread*.

Several empirical and statistical representations are available to estimate the radio propagation path loss for the multipath case. For outdoor environments, most of the path loss estimation tools are based on a formulation developed by Okumura and Hata (Circuit Design, Inc., 2009). For indoor environments, the path loss as a function of distance between transmitting antenna and receiving antenna in units of dB can be calculated using equation 2.9.

$$L_P(d) = L_P(d_0) + 10\,n\,\log\left(\frac{d}{d_0}\right) + X\ , dB \tag{2.9}$$

Where:

- d_0 is the reference distance (normally 1 meter),
- *n* is the path loss exponent term which depends on the operating frequency and the surrounding environment, and
- *X* is a normal random variable (in dB) referred to as the multipath fading term having a standard deviation of σ dB.

Different values for the index *n* and standard deviation σ are shown in Table 2.2. For the free space case, the typical value of *n* is 2. Therefore, the value of *n* for indoor environments for the multipath propagation model is normally greater than 2. The use of higher transmitting frequencies also results in larger value for the index *n*.

Table 2.2 Path loss exponent *n* and standard deviation measured in different buildings (Huang & Boyle, 2008)

Building	Frequency (MHz)	Index *n*	Standard Deviation σ (dB)
Retail stores	914	2.2	8.7
Office (hard partition)	1500	3.0	7.0
Office (soft partition)	1900	2.6	14.1
Office (soft partition)	915	2.0-2.8	9.0-14.0
Open-plan factory	1300	2.0-2.4	3.7-9.0
Suburban home	900	3.0	7.0
Factory LOS	1300	1.6-2.0	3.0-7.0
Factory OBS	1300	3.3	6.8

2.2.4. Radar Cross Section Propagation Model

In the radar cross section (RCS) propagation model, the radar equation can be used to estimate the power reflected or scattered from an object to a receiver. The radar equation can be derived in a similar manner as that of the Friis's equation. However, the receiving object is not an antenna but rather a target which will not have an associated gain term. Thus, it is necessary to introduce the new term *radar cross section* (RCS) to describe how the object receives, reflects or scatters power. The RCS of an object is defined as "the area intercepting that amount of power which, when scattered isotropically, produces at the receiver a power density which is equal to that scattered by the actual target" (Balanis, 2005). Figure 2.9 shows a graphical representation of the radar system where the radar equation can be used.

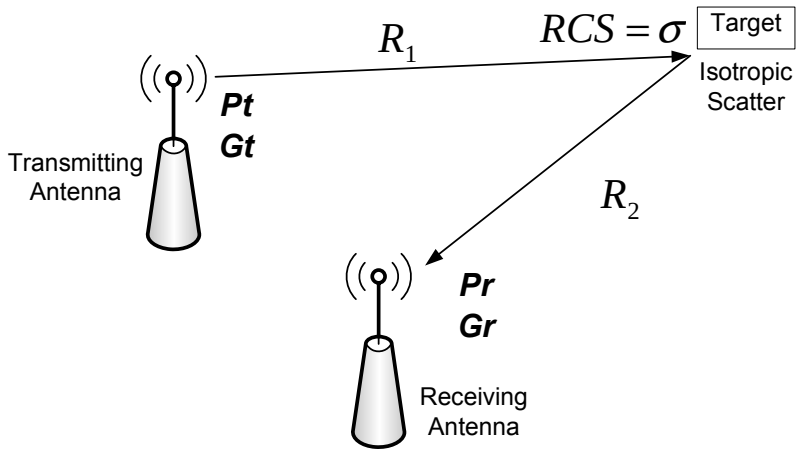

Figure 2.9 The graphical representation of the radar system

The received power at the receiving antenna can be calculated using equation 2.10.

$$P_r = P_t \frac{\sigma G_t G_r}{4\pi} \left(\frac{\lambda}{4\pi R_1 R_2} \right)^2 \tag{2.10}$$

In RFID systems, equation 2.10 can be simplified as shown in equation 2.11 because the transmitting and receiving antennas are co-located (i.e., $R_1 = R_2$).

$$P_r = P_t \frac{\sigma G_t G_r}{4\pi} \left(\frac{\lambda}{4\pi r^2} \right)^2 \tag{2.11}$$

2.2.5. Comparison of Propagation Models

Table 2.3 presents the advantages and disadvantages of each propagation model introduced in the prior sections.

Table 2.3 Advantages and disadvantages of different propagation models

Downlink communication		
Model	**Advantages**	**Disadvantages**
Free space	- Simple calculation - The radius of the coverage area of the RFID reader can be approximated using Friis's equation.	- Normally applied to outdoor environments and indoor environments (far-field region) with no obstacles. - The environment in this research is an indoor warehouse environment with obstacles; therefore, this propagation model does not meet the requirement.
Two-ray	- Simple calculation - Can be used in an indoor environment.	- Need to know the height of the transmitter (reader) and receiver (tag) antenna. - The antenna gain is not taken into consideration making the calculation less accurate.

Table 2.3 (continued) Advantages and disadvantages of different propagation models

Downlink communication (continued)		
Model	**Advantages**	**Disadvantages**
Multipath	- The most accurate model of the three propagation models for the downlink channel. - Appropriate for use in indoor environment with obstacles. - The index *n* can be selected to be suitable for the conditions of the environment. - Represents the real situation in which several paths of signal propagation will be received at the receiver (tag).	- The random variable *X* (referred to as the multipath fading term) makes the calculation of the received signal power at the receiving antenna (P_r) more complicated than with the free space and two-ray models.
Uplink communication		
Model	**Advantages**	**Disadvantages**
Radar Cross Section (RCS)	- The UHF RFID system uses the concept of backscattering. This model can represent and explain the backscattered signal from a tag to an RFID reader. - Can be used to calculate the sensitivity of the RFID reader to meet the designed specifications and requirements.	- Can only be used for indoor environments in the far-field region. However, UHF RFID systems normally operate in the far-field region.

2.3. Basics of Antenna Theory

This section introduces basic concepts and some important properties of antenna theory. Having a basic understanding of these concepts is important since both the RFID reader and the RFID tag require an antenna to operate.

2.3.1. Antenna Radiation Pattern

The radiation pattern of an antenna is defined as “a mathematical function or graphical representation of the radiation properties of the antenna as a function of space coordinates. In most cases, the radiation pattern is determined in the far-field region and is represented as a function of the directional coordinates” (Greene, 2006). In other words, the antenna radiation pattern shows how the antenna radiates power around its placement location. It is generally represented in polar coordinates and depicts the magnitude of the antenna gain as a function of angle varied from 0° to 360°.

The three-dimensional (3D) pattern of an antenna is an excellent representation of the radiated power distribution as a function of angle. However, in practice, it is very time-consuming and also difficult to measure the 3D pattern of an antenna. Therefore, the radiation pattern of the antenna is typically illustrated as a two-dimensional (2D) pattern of two main planes: the E-plane and the H-plane. The E-plane is the plane where the electric field (*E*) lies on, whereas the H-Plane is the plane where the magnetic field (*H*) lies on. Figure 2.10 gives an example of the 2D radiation pattern of a dipole antenna showing both the E-plane and the H-plane.

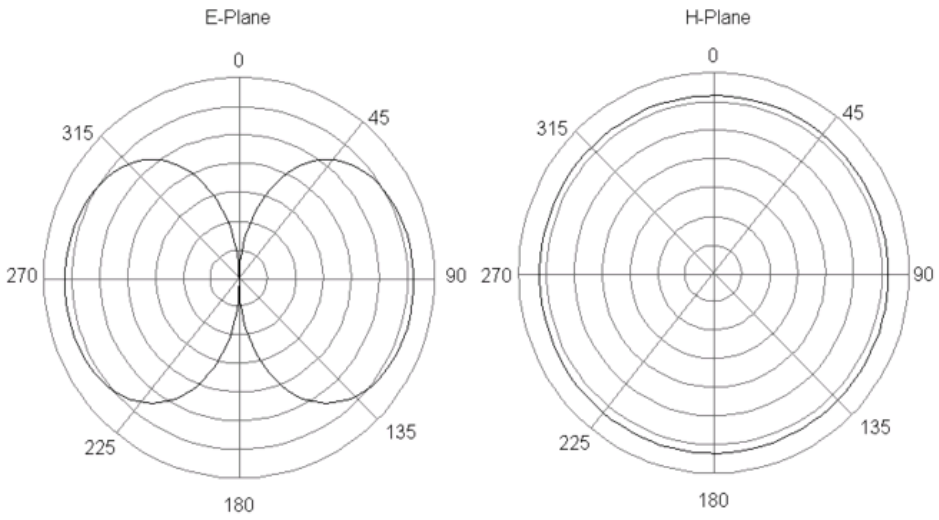

Figure 2.10 E-plane and H-plane radiation patterns of a dipole antenna (Wikipedia, 2010)

2.3.2. Antenna Gain

The gain of an antenna is defined as "the ratio of the radiation intensity in a given direction from the antenna to the total input power accepted by the antenna divided by 4π" (Huang & Boyle, 2008), and is expressed as in equation 2.12.

$$\text{Antenna Gain (G)} = \frac{U}{\left(\frac{P_{in}}{4\pi}\right)} = \frac{4\pi U}{P_{in}} \tag{2.12}$$

Where:

- U represents the radiation intensity in Watts/unit solid angle.
- P_{in} is the total input power accepted by the antenna in Watts.

It should be noted that the gain calculated with equation 2.12 has no units (i.e., it is dimensionless). Thus, the gain of an antenna is also measured using a reference antenna with

a known gain value. The reference antenna normally has to be placed at a fixed position and the test antenna is rotated within the E-plane and the H-plane. The received power at the reference antenna is used to calculate the gain of the test antenna at different angles. The entire gain pattern can be plotted from the calculated gain in various angles and represented as a radiation pattern in two major planes. Therefore, the antenna gain is a relative value which is dependent on the type of reference antenna. The units of *dB isotropic* (dBi) and *dB dipole* (dBd) are used to represent the antenna gain when the reference antenna is an isotropic antenna or a dipole antenna, respectively. Antenna gain is usually given as the maximum value in the preferred direction (e.g., 2.15 dBi for a dipole antenna). The relationship between the units of dBi and dBd is shown in equation 2.13.

$$\text{dBd} = \text{dBi} - 2.15 \tag{2.13}$$

2.3.3. Antenna Effective Aperture and Aperture Efficiency

The antenna effective aperture or effective area is defined as "the ability of the antenna to collect an incident radio wave and deliver it as an electrical current at the antenna's terminals" (Orfanidis, 2010). The effective aperture (A_e) is the ratio of power delivered to load and the power density per square meter of incoming radio wave as shown in equation 2.14.

$$A_e = \frac{P_R}{S} \tag{2.14}$$

Where:

- P_R is the power received at the load in Watts, and
- S is the incident power density in Watts per square meter.

The effective aperture (A_e) is normally less than the physical aperture (A_p). Therefore, the aperture efficiency is defined as the ratio of these two quantities, as shown in equation 2.15.

$$\eta_{ap} = \frac{A_e}{A_p} \tag{2.15}$$

The antenna effective aperture is also related to antenna gain. The formula for calculating effective area as a function of its power gain is shown in equation 2.16.

$$A_e = \frac{\lambda^2}{4\pi} G \tag{2.16}$$

2.3.4. Antenna Polarization

The polarization of an antenna in a given direction is defined as "the polarization of the wave transmitted (radiated) by the antenna. The polarization is the property of an electromagnetic wave describing the time-varying direction and relative magnitude of the electric-field vector" (Balanis, 2005). In other words, polarization describes the orientation of the E-field in a given direction. There are three main types of polarization: *linear*, *circular* and *elliptical*. The type of polarization an antenna uses depends on how the current moves in the antenna. For linear polarization, the current travels along one axis, while two orthogonal currents having the same magnitude (but 90° phase difference) are generated on an antenna with circular polarization. The elliptical polarization can be generated in a similar manner as that of circular polarization; however, the two orthogonal currents need to have different magnitudes.

In a communication link, antenna polarization has to be matched in order to transmit and receive maximum signal power. A linearly polarized antenna can be easily created; however, it is very sensitive to antenna orientation and can result in polarization loss. An antenna with circular polarization is less sensitive to orientation; however, the implementation of this type of antenna is more complicated. Some antennas have mixed polarization to deal with the problem of orientation.

2.3.5. Effective Isotropic Radiated Power and Equivalent Radiated Power

The effective isotropic radiated power (EIRP) is the amount of power that has to be radiated by an isotropic antenna to generate the peak power density in the preferred antenna direction which has the maximum gain. The path loss between the transmitting antenna and the receiving antenna can be obtained easily by calculating the ratio of the transmitted EIRP to the received EIRP. As shown in equation 2.17, EIRP is calculated by multiplying the transmitting power (P_t) by the antenna gain (G).

$$EIRP = P_t G \tag{2.17}$$

Another term related to EIRP that is widely used in industry is the effective radiated power (ERP). ERP is calculated using a half-wave dipole antenna instead of an isotropic antenna. The relationship between EIRP and ERP is shown in equation 2.18.

$$ERP\,(dBW) = EIRP\,(dBW) - 2.15\,dBi \tag{2.18}$$

2.4. Optimization Techniques

The exact solution of a linear optimization problem can be obtained using linear programming given an objective function and its constraints. There are several algorithms that can be applied to solve the formulated linear programming problem and one of the most well-known is the simplex method. However, if the problem to be solved is considered a combinatorial optimization problem, the computation time increases exponentially as the number of decision variables increases. In this case, a very long computation time will be required to obtain an exact solution. In addition, if the non-linear optimization problem is considered, the problem formulation and the method to find an exact solution are much more complicated.

Heuristic or meta-heuristic optimization techniques can be used to solve combinatorial optimization problems so that the optimum (or near optimum solution) can be obtained within a reasonable computation time. There are a large number of meta-heuristics that have been developed to solve combinatorial optimization problems. In this research, the focus will be on *genetic algorithm* and *particle swarm optimization*. Thus, both heuristic optimization techniques are explained in more detail in the following sections.

2.4.1. Genetic Algorithm

A generic algorithm (GA) is a meta-heuristic based on the evolutionary process of natural systems used to solve complex combinatorial problems (Holland, 1975). GAs belong to the class of probabilistic algorithms and combine elements of directed and stochastic search (Michalewicz, 1998). An evolution usually begins with a population of randomly generated individuals. The characteristics of a system under investigation are encoded in chromosomes.

Feasible solutions are modeled as individuals known as *genomes*. The term *genome* also refers to an arrangement of several chromosomes. Genetic operations such as crossover and mutation are performed to produce new individuals in subsequent generations. Crossover is the process of creating new offspring from the selected parents by exchanging their corresponding genes, while mutation refers to the process of creating a new offspring by exchanging gene positions within the same chromosome. The new population is then used in the next iteration of the algorithm. Usually, the best individual of each generation is transferred over to the next generation. As the search evolves, the population includes better solutions and the one with the best fitness value is selected upon attaining a predetermined termination criteria. Figure 2.11 depicts a flowchart of the process used to find the optimum solution with a GA.

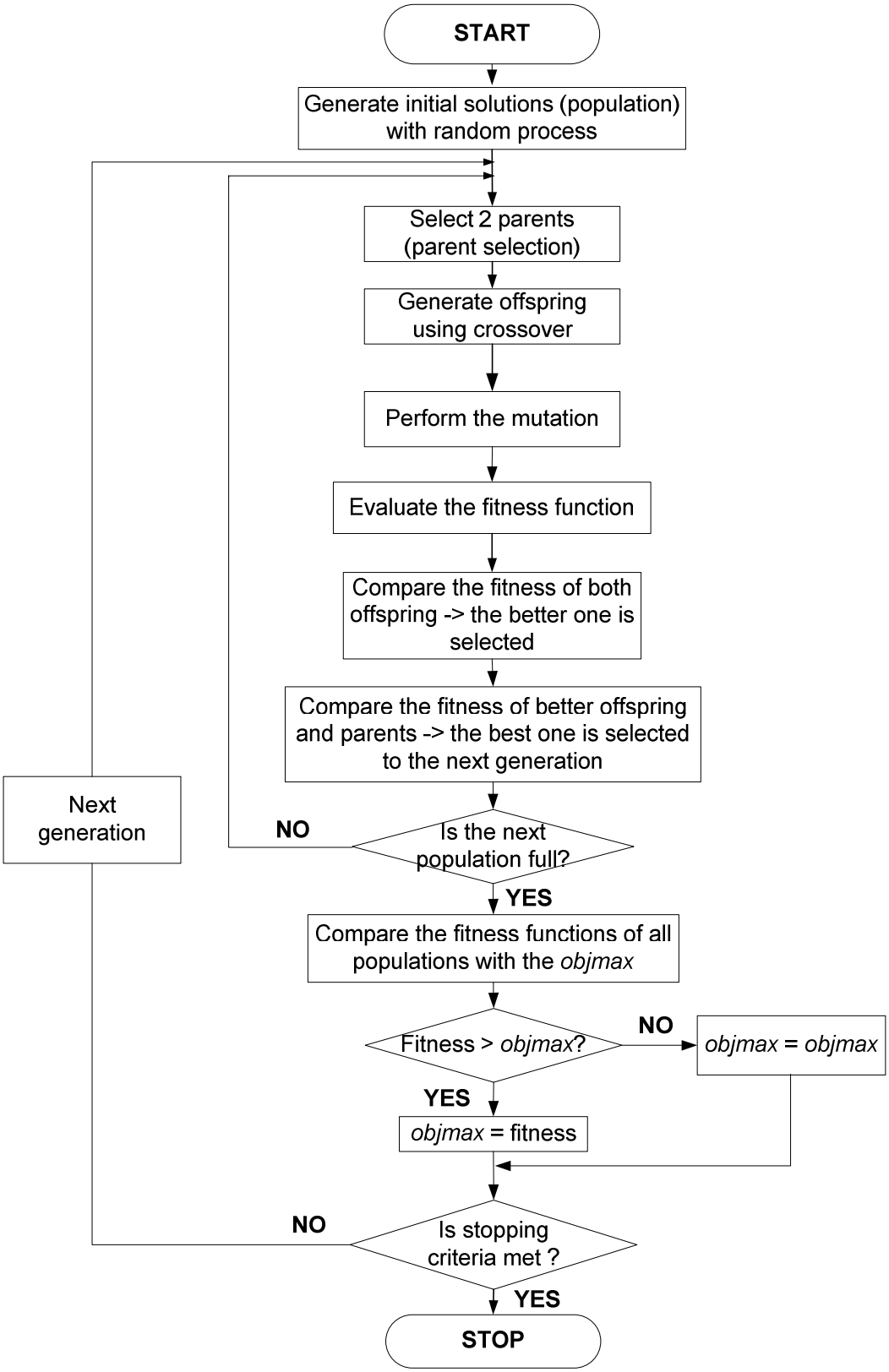

Figure 2.11 The steps of a basic genetic algorithm (GA)

2.4.2. Particle Swarm Optimization

Particle swarm optimization (PSO) was first introduced by Kennedy & Eberhart (1995) and was inspired by social behavior of bird flocking or fish schooling. PSO starts with a group of initial solutions called *particles,* each having an initial position and velocity. Then, the fitness of each particle is evaluated and compared against the best fitness it has achieved, called *personal best* (*pbest*). A comparison among the fitness of all particles is performed and the best one is called *global best* (*gbest*). After finding *pbest* and *gbest,* each particle updates its velocity and position by following the current optimum particles. The new velocity and position can be calculated using the mathematical formulation shown in equation 2.19. The parameters in equation 2.19 are described in Table 2.4.

$$v(i,j) = w \times v(i,j) + c_1 \times rand \times \left(pxbest(i,j) - x(i,j)\right) + c_2 \times rand \times \left(gxbest(j) - x(i,j)\right)$$

$$x(i,j) = x(i,j) + v(i,j) \tag{2.19}$$

Table 2.4 Description of the parameters of the PSO formulation

Parameter	Description
$x(i, j)$	Current particle (solution)
$v(i, j)$	Particle velocity
w	Inertia
c_1	Local cognitive component
c_2	Global social component
$gxbest\,(j)$	Global best position so far
$pxbest\,(i, j)$	Personal best position so far

The PSO algorithm does not have the evolution operators performed with GAs (i.e., crossover and mutation). The PSO algorithm will stop when the termination criterion is met. Several parameters in the algorithm have to be adjusted so that the best solution can be achieved, i.e., number of particles, inertia (w), local cognitive component (c_1), and global social component (c_2). Eberhart & Shi (2001) suggested how these parameters should be adjusted to make them appropriate for certain types of problems which lead the search to the best solution. Figure 2.12 depicts the flowchart of the algorithm used in PSO to find the optimum solution.

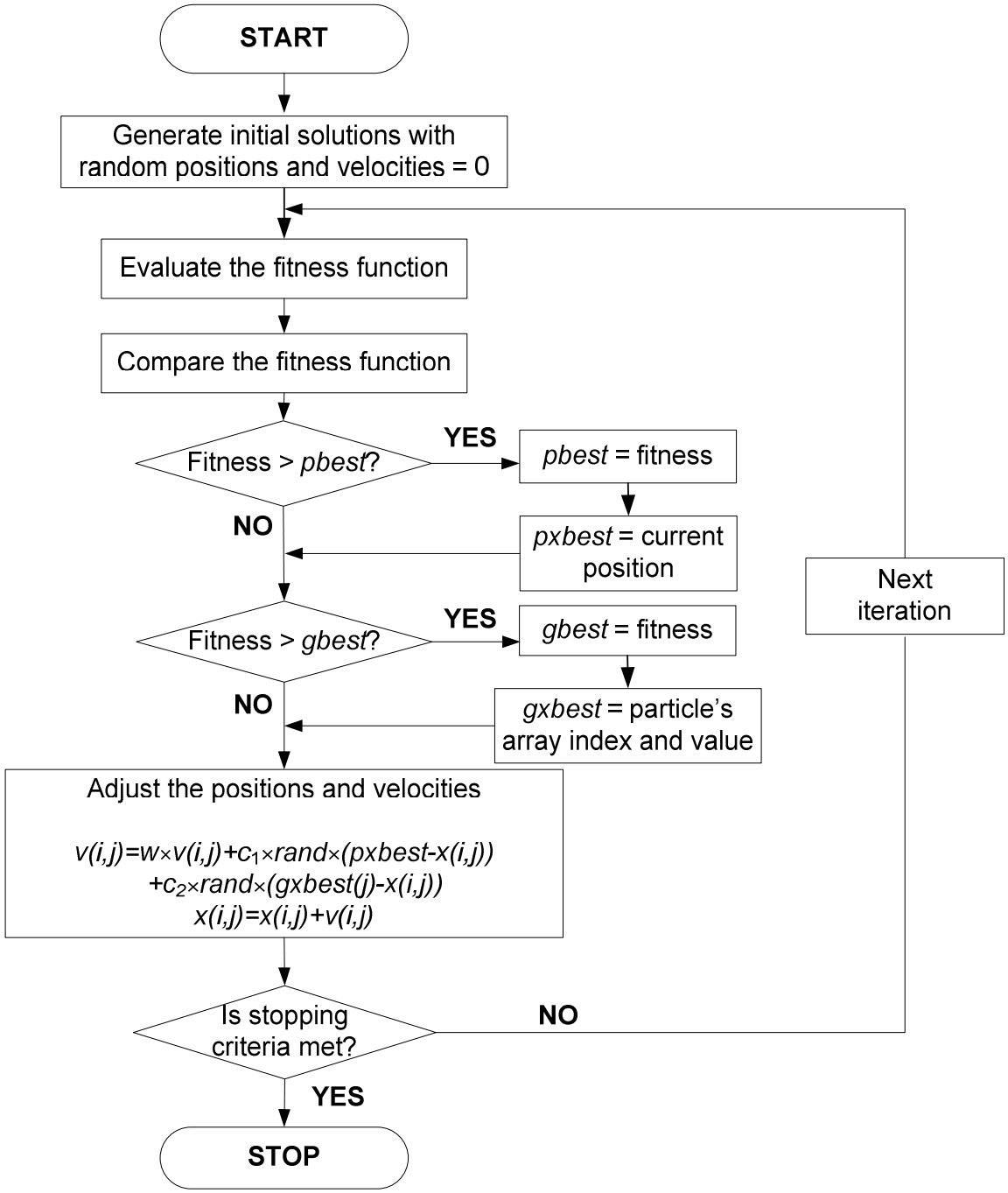

Figure 2.12 The steps of a basic particle swarm optimization (PSO) algorithm

3. LITERATURE REVIEW

One of the most important decisions when designing RFID-based inventory management systems (IMSs) is where to locate the RFID readers within a warehouse facility to maximize performance. Optimally locating RFID readers within a facility is referred to as the RFID network planning (RNP) problem. Providing an optimal solution to the RNP problem is a complex task that may be affected by several factors such as signal coverage, signal propagation, and interference (i.e., both passive and active).

Traditionally, the placement of RFID readers in RFID-based IMSs has been done on a trial-and-error basis, which is a time consuming process that generally results in less than optimal signal coverage. Thus, a methodology to optimize the placement and number of RFID readers required to cover a facility is needed. Critical steps in such a methodology are the development of a model formulation and the selection of an appropriate optimization technique to ensure that quality solutions are obtained within a reasonable computation time.

The following sections present a synthesis of relevant prior work that has been done to address some of the challenges in the area of RFID system optimization design. This material is followed by a literature review summary, where the gap in the state-of-the-art is identified and the expected contributions of the proposed work are outlined.

3.1. Signal Coverage

Most of the prior work in the area of computer-based models aimed at optimizing the placement of RFID readers has made the assumption that antenna coverage is omnidirectional (Anusha & Iyer, 2005; Guan et al. 2006; Gupta & Iyer, 2007; Reza & Geok, 2009).

It is a well known fact that the size and shape of the RFID reader's antenna coverage patterns affect the number of RFID readers required to cover a given warehouse facility. For example, Figure 3.1 depicts the difference between the 2-D patterns of an ideal isotropic antenna (i.e., omnidirectional) and a directional antenna.

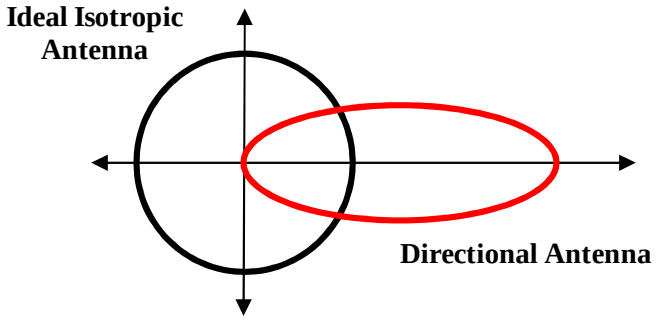

Figure 3.1 Coverage patterns of omnidirectional and directional antennas

The assumption of omnidirectional antenna coverage is quite reasonable for the design of wireless local area networks (WLAN), where large areas need to be covered (Adickes et al., 2002; Prommak et al., 2002). However, most types of antennas used by RFID systems in IMSs applications are directional in nature. Nevertheless, researchers have assumed ideal isotropic antennas (Anusha & Iyer, 2005; Gupta & Iyer, 2007) or dipole antennas (Guan et al., 2006; Reza & Geok, 2009) with circular coverage in their work mainly to simplify the modeling process.

An isotropic antenna is an ideal radiator whose radiation patterns in both the vertical (E-plane) and horizontal (H-plane) planes are circular. However, an isotropic antenna can only be used as a reference because it does not really exist (hence the term "ideal"). Therefore, a dipole antenna is typically used instead for modeling purposes in a 2-D space because its H-plane appears to provide good omnidirectional coverage. A dipole antenna's

3-D radiation pattern has a doughnut-like shape, as depicted in Figure 3.2. Its 2-D radiation patterns in the E-plane and H-plane are shown in Figure 3.3. As Figure 3.2 clearly shows, there are some uncovered areas above and below the doughnut-like 3-D radiation pattern.

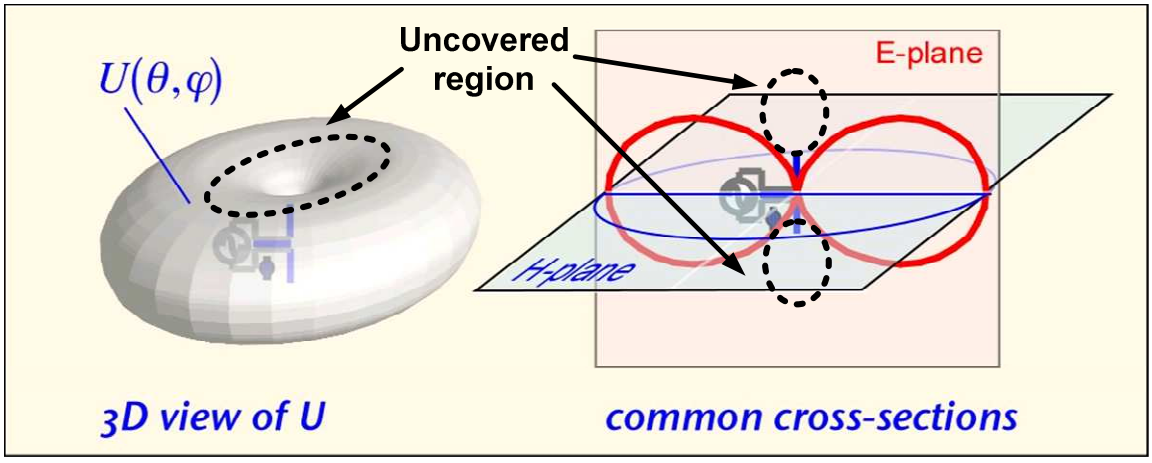

Figure 3.2 Three-dimensional representation of the radiation pattern of a dipole antenna (Dobkin, 2004)

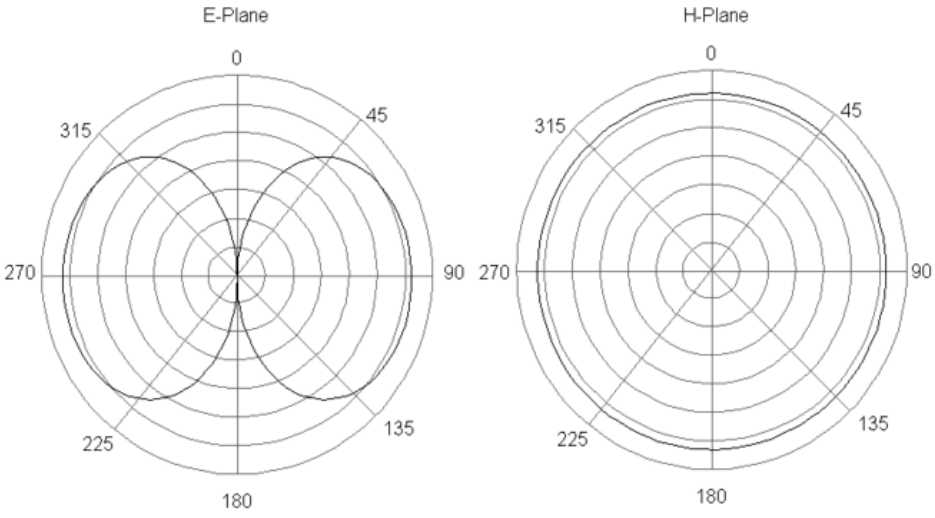

Figure 3.3 E-plane and H-plane radiation patterns of a dipole antenna (Wikipedia, 2010)

Most UHF RFID reader's antennas such as a patch or a microstrip antenna are directional, meaning that they have more gain in a preferred direction than the dipole antenna (Greene, 2006; Phongcharoenpanich, 2009; Chen et al., 2009; Huang & Chang, 2011). These antennas can also be fabricated with circular polarization to effectively communicate with tags presented to the antenna of the RFID reader in several different orientations. Therefore, the assumption of a circular shape to depict signal coverage when designing RFID-based IMSs is not appropriate and an elliptical-like shape should be used instead.

The research conducted by Marrocco et al, (2009) suggested that equation 3.1 can be used to approximate the 3-D coverage area of an UHF RFID reader's antenna with an ellipsoid. The antenna is placed at $x = 0$, $y = 0$ and $z = 0$ and it radiates signal toward $x > 0$.

$$\frac{(x-a_x)^2}{a_x^2} + \frac{y^2}{a_y^2} + \frac{z^2}{a_z^2} = 1 \tag{3.1}$$

The term $\frac{z^2}{a_z^2}$ in equation 3.1 can be eliminated if a 2-D representation of the ellipsoid is needed, resulting in equation 3.2. Figure 3.4 depicts the resulting 2-D ellipsoidal coverage pattern generated in MATLAB using equation 3.2 and the constant values $a_x = 5$ and $a_y = 3$.

$$\frac{(x-a_x)^2}{a_x^2} + \frac{y^2}{a_y^2} = 1 \tag{3.2}$$

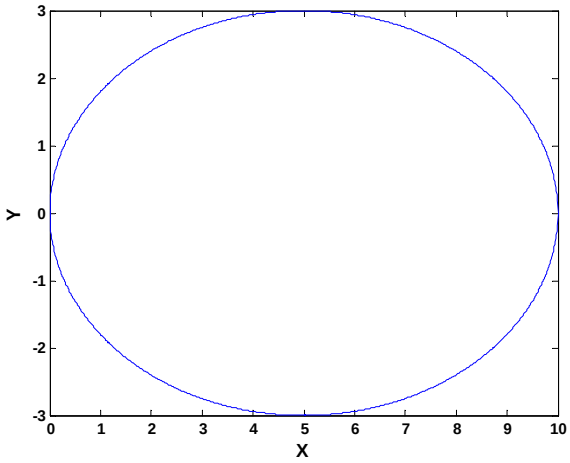

Figure 3.4 Two-dimensional elliptical representation of an RFID antenna's coverage area using the equation in Marrocco et al. (2009)

3.2. Signal Propagation

Careful consideration needs to be given to the selection of the signal propagation model when designing RFID-based IMSs. Unlike other wireless communication systems, the downlink signals (i.e., reader-to-tag) and uplink signals (i.e., tag-to-reader) in an RFID system are not equal. This implies that the coverage area of the RFID reader is much greater than that of the tag. Additionally, as signals propagate from adjacent readers in overlapped coverage areas, they may impede the accurate decoding of backscattered signals from tags causing serious deficiencies on the performance of the RFID system (Kim et al., 2009).

Anusha & Iyer (2005), Gupta & Iyer (2007) and Reza & Geok (2009) assumed free space propagation when calculating the RFID reader coverage area, represented as *r*, and therefore used the Friis's free propagation model shown in equation 3.3.

$$P_{r,tag} = P_t \times \left(\frac{\lambda}{4\pi r} \right)^2 \times G_{reader} \times G_{tag} \tag{3.3}$$

In equation 3.3, $P_{r,tag}$ is the minimum power required at the RFID tag's antenna to enable communication with the RFID reader; P_t is the transmitted power from the RFID reader's antenna; G_{reader} is the gain of the RFID reader's antenna; and G_{tag} is the gain of tag's antenna. After some algebraic manipulation, the RFID reader's coverage area, *r*, can be calculated using equation 3.4.

$$r = \frac{\lambda}{4\pi}\sqrt{\frac{P_t \times G_{reader} \times G_{tag}}{P_{r,tag}}} \tag{3.4}$$

The free space propagation model is appropriate for outdoor environments; however, inventory management activities are typically carried indoors (i.e., a warehouse facility). Since warehouse environments contain many different types of physical obstacles, a propagation model that considers multipath is more appropriate. For example, Marrocco et al. (2009) estimated the reading regions of an UHF RFID system in a real indoor environment. Several propagation models were utilized including the free space model, two-ray model, and ray-tracing model. The ray-tracing model provided superior performance compared to the other two models because signal strength is measured in all directions, i.e., the azimuth angles of the antenna are varied and a measurement of the signal path loss is performed at each angle so that the antenna coverage in all directions is obtained. However, the disadvantage of the ray-tracing model is that it is complicated and time consuming. The tradeoff between complexity, computation time and accuracy of estimations needs to be considered carefully. The mathematical formulas derived from each propagation model mentioned above can be used to estimate the 3D reading regions for the planning and optimization of RFID reader-tag networks.

For the downlink channel, the multipath propagation model is the most appropriate because it has several advantages over the free space and two-ray models (Rappaport, 2002; Nikitin & Rao, 2008) as discussed in Table 2.3. The basic formulas used with the multipath propagation model are shown in equation 3.5 and equation 3.6.

$$[P_{r,tag}]_{dBm} = [P_t]_{dBm} + [G_{reader}]_{dB} + [G_{tag}]_{dB} - [\textit{path loss from multipath } (L_P(d))]_{dB} \quad (3.5)$$

$$[L_P(d)]_{dB} = L_P(d_0) + 10n \log\left(\frac{d}{d_0}\right) + X \quad (3.6)$$

In equation 3.6, $L_P(d)$ represents the path loss from multipath as a function of distance (d); d_0 is normally 1 meter; and X is a log normally distributed random variable. This model represents the situation of a transmitted signal in an indoor environment with some obstructions following several paths from a reader to a tag. Also, the index n can be changed to be suitable to the conditions of the communications environment and includes a multipath fading term (i.e., the random variable X), which has to be modeled appropriately. With a careful design and model parameter selection, the multipath propagation model can be used to represent a real practical system and it can also result in the most accurate estimation of the downlink signal propagation for the RFID system.

Aside from a couple of exceptions, the majority of the prior work reviewed neglected the modeling of the uplink communication channel. Guan et al. (2006) developed a discrete model for the location of RFID transceivers. Equation 3.7 represents this model which considered the uplink communication and the received signal power at the RFID readers

backscattered from tags. The term Γ_{tag}^2 shown in equation 3.7 is the reflection efficiency of the tag.

$$P_{r,reader} = P_t\left(\frac{\lambda}{4\pi}\right)^2 G_{reader}G_{tag}\Gamma_{tag}^2\left(\frac{1}{2d}\right)^2 \tag{3.7}$$

When compared to the free space propagation model presented in equation 3.3, equation 3.7 includes the new factor $\frac{\Gamma_{tag}^2}{4}$. However, Guan et al. (2006) did not provide an explanation of how the equation was derived.

Greene (2006) conducted a study to find the area of operation for an RFID tag in the far-field region. This reserach considered both the downlink and uplink communication channels when modeling the RFID system. The radar cross section (RCS) model (shown in equation 3.8) was recommended to model the RFID uplink communication channel.

$$P_{r,reader} = P_t\frac{\sigma G_{trasmitter}G_{receiver}}{4\pi}\left(\frac{\lambda}{4\pi R_1 R_2}\right)^2 \tag{3.8}$$

In equation 3.8, σ is the radar cross section area, R_1 is the distance from the reader to the tag, and R_2 is the distance from the tag to the reader.

Since RFID readers are considered transceivers (i.e., they both transmit and receive RF signals), then R_1 and R_2 can be considered equal. Under this assumption, equation 3.8 can be reduced and expressed as shown in equation 3.9a.

$$P_{r,reader} = P_t \frac{\sigma G_{trasmitter} G_{receiver}}{4\pi} \left(\frac{\lambda}{4\pi r^2} \right)^2 \quad (3.9a)$$

Equation 3.9b shows the radar cross section propagation model with the consideration of path loss exponent (n) and loss from the multipath fading (X).

$$P_{r,reader} = \frac{P_t \times G_{trasmitter} \times G_{receiver} \times \sigma \times \lambda^2}{(4\pi)^3} \times \frac{1}{r^{2n}} \times \frac{1}{10^{\frac{X}{10}}} \quad (3.9b)$$

3.3. Interference

An important concern in designing and implementing RFID-based IMSs is signal interference. There are two main types of interference that RFID systems may be exposed to, i.e., interference from physical obstacles and interference from RFID readers and/or tags. The size and the material of the physical obstacles in the vicinity of the RFID readers may affect the propagation characteristics of the signal emitted by the RFID reader's antenna in different ways. Some materials tend to absorb the signal's energy (e.g., cardboard), thus increasing the signal loss/attenuation in the communication channel. Other materials may reflect, diffract, or scatter the signal resulting in multipath (i.e., multiple copies of the signal with varying delays being received by either the RFID reader or the tag). The interference from RFID readers and tags themselves includes multiple-tag-to-reader interference (tag collision), multiple-reader-to-tag interference (tag interference), and reader-to-reader interference (frequency interference) (Engels & Sarma, 2002).

Laboratory experiments have provided a useful means of investigating the performance of RFID technology in environments where different levels and types of signal

interference may be present. For example, Porter et al. (2006) developed a test protocol for the characterization of RFID systems in the presence of active signal interference, whereas Sydänheimo et al. (2006) developed a test bed to study the effect of size and shape of metallic objects on the performance of passive RFID technology. Both studies considered the maximum reliable read range and read rate as the performance metrics of interest. In the latter study, three different types of RFID tag antennas were tested, i.e., a printed inverted-F antenna, a microstrip patch antenna with regular ground plane and a patch antenna with photonic band gap (PBG) ground plane. It was found that the size and shape of metallic objects significantly affected the maximum reliable read range and read rate of the RFID system. The patch antenna with PBG ground plane worked well when the RFID tag was attached to metallic plates of different sizes. The results showed a slight increase in read range but the read rates deteriorated. It was also found that using an RFID tag with a patch antenna with regular ground plane resulted in the maximum read range when the tag was attached to the non-uniform surface of metallic cans. The patch antenna with PBG ground plane produced the best performance on uniform metallic surfaces (i.e., an air compressor).

Kim et al. (2008) studied the effect of interference in UHF RFID systems and found that reader-to-reader interference directly reduced the RFID reader's maximum read distance from 4.25 meters to 1.70 meters (i.e., worst case) in a dense reader environment. The term interrogation range-reduction ratio (IRRR) was introduced in this research to refer to the reduction in maximum read distance. IRRR is calculated as shown in equation 3.10.

$$IRRR = \left(\frac{R_{\max} - R_{actual}}{R_{\max}} \right) \times 100 \tag{3.10}$$

Reader-to-reader interference occurs when an adjacent reader transmits a signal that interferes with the communication between the "desired" reader and a tag located within its interrogation range (see Figure 3.5). The backscattered signal from the tag to the "desired" reader is attenuated by the signal from the *i*-th interfering reader, thus decreasing the "desired" RFID reader's interrogation range. As Figure 3.5 clearly shows, the interrogation range of the "desired" RFID reader is reduced from maximum interrogation range ($R_{\max}$) to actual interrogation range (R_{actual}).

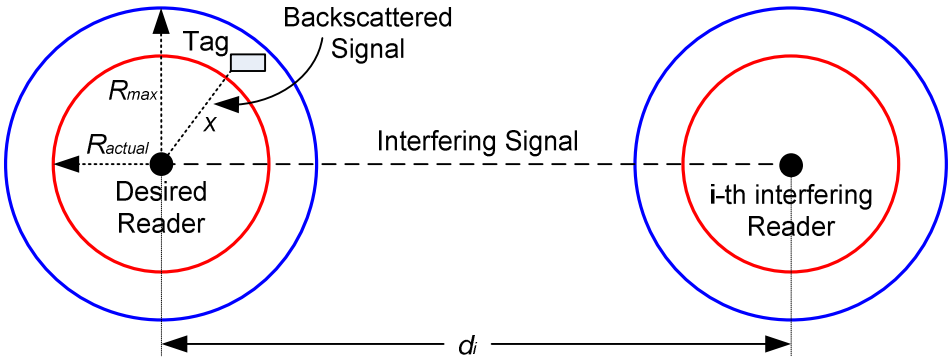

Figure 3.5 Reader-to-reader interference in UHF RFID systems

The IRRR can take values from 0% (i.e., no reader-to-reader interference) to 100%. In the extreme case where the IRRR is 100%, the RFID system cannot capture any tags in the system. Kim et al. (2008) showed that IRRR is inversely proportional to the distance between RFID readers. For example, IRRR is about 60% when the readers are one meter apart in a dense reader environment (i.e., more than 50 RFID readers). In other words, the RFID reader's interrogation range decreases from 4.25 meters to 1.70 meters, i.e., $\left(\frac{4.25-1.70}{4.25}\right)\times 100\% = 60\%$.

3.4. Optimization of an RFID System Design

RFID readers must be placed strategically within a facility to maximize the number of tags read. The read rate of an RFID system is usually defined as the ratio of successfully read RFID tags and the number of read attempts. RFID tags are attached to physical objects at unit level or pallet level for items stored in bulk.

Various techniques have been used to determine the optimal location of transceivers in wireless systems that use IEEE 802.11 technology (i.e., wireless local area networks) or RFID technology. Although IEEE 802.11 technology is different from RFID, the algorithms used to determine placement of transceivers within a facility can be also useful in determining the optimal location of RFID readers. A common goal of these procedures is to simultaneously maximize the signal coverage while minimizing the level of electromagnetic field interference. These techniques include simulated annealing (e.g., Anderson & McGeehan, 1994), genetic algorithms (e.g., Han et al., 2001; Adickes et al., 2002; Guan et al., 2006; Chang & Lin, 2007; Huang et al., 2009), and particle swarm optimization (e.g., Bhattacharya & Roy, 2010; Guan et al., 2006; Giampaolo et al., 2010).

No prior research was found that used simulated annealing to deal with the problem of the placement of RFID readers in an RFID-based IMS. On the other hand, genetic algorithms (GA) and particle swarm optimization (PSO) have been widely used to solve the reader location problem with multi-objective functions. There are several parameters in both algorithms that can be adjusted giving researchers an opportunity to investigate the resulting effects on the solutions.

The following sections describe prior work where GA and PSO have been used in the design of RFID-based IMS.

3.4.1. Genetic Algorithms

Konak et al. (2006) developed criteria for the selection of each component in multi-objective genetic algorithms (GAs), including fitness functions; diversity (which includes fitness assignment, fitness sharing, and niching); elitism; constraint handling; and parallel and hybrid multi-objective GA. Several examples are also provided of the application of multi-objective GAs in engineering system design and it was found that multi-objective GAs can deal very well with the problem of reliability optimization. Applying multi-objective GAs to the problem of the placement of RFID readers can help in finding solutions to optimize the performance of the system. In this case, two main objectives are pursued so that reliable communication between a reader and a tag can be achieved, i.e., good signal coverage of the entire facility and low levels of signal interference. Thus, multi-objective GAs is one of the most appropriate optimization techniques that can effectively solve the proposed problem in this research.

Adickes et al. (2002) developed a computerized layout simulation system that utilized heuristic optimization methods to solve the problem of locating IEEE 802.11 transceivers. They assumed omnidirectional transceivers with circular coverage, which enabled the use of the geometric circle covering technique, whose goal is to place *n* circles over a given area so as to completely cover the area with the minimum number of circles. A GA was used to find the best solution. Three objective functions were considered, i.e., the percentage of area covered, average regional capacity, and average signal strength across all points. These three objective functions could not be satisfied simultaneously, so a preferential Pareto ranking was used for fitness evaluation. Model effectiveness was assessed by comparing its solutions to those obtained by Tang et al. (1997) in identical facilities, and also via actual site surveys. It was found that the developed GA could achieve 100% coverage and lower path losses

when compared to the solutions obtained by Tang et al. (1997). The average signal strength measured using the transceiver placement recommended by the developed GA was higher when compared to the measurement that resulted when an experienced RF engineer manually placed the transceivers in the facility.

Guan et al. (2006) developed a discrete model for the location of RFID transceivers. The geographical working area was first discretized into a finite number of points on which radio signals were tested. A GA was developed to solve a multi-objective mathematical model to maximize coverage, minimize the number of RFID readers, and minimize the level of interference. The number of readers was the key performance indicator directly related to the deployment cost. Different propagation models were used for the downlink and uplink communication channels. However, a circular shape was assumed for the signal coverage of the RFID reader's antenna. The model's fitness function was evaluated using a weighted sum approach and the single solution obtained is dependent on the selection of the weights (which might be obtained based on the researchers' preferences). Another approach, such as Pareto optimality (Konak et al., 2006), could be used instead if the trade-offs among multiple solution is of interest.

3.4.2. Particle Swarm Optimization

Particle swarm optimization (PSO) is one of the most effective optimization techniques and it has been widely used to solve several kinds of problems including the RNP problem.

Bhattacharya & Roy (2010) proposed a PSO algorithm to find the minimal number of RFID readers with 100% coverage of tagged items in an RFID network. They considered coverage, number of readers required (cost), and interference as the objective functions. A weighted sum approach was used for fitness assignment and evaluation. The values used for

w, c_1, and c_2 were 0.01, 0.1 and 0.1, respectively. These values are very small compared to the values recommended by Eberhart & Shi (2001). This may explain why the resulting algorithm takes a large number of iterations (i.e., 10,000) to achieve an optimum solution.

Chen et al. (2011) developed a novel algorithm called PS^{2}O that extends the single population PSO to interacting multi-swarms. Basically, there are two values influencing the movement of particles in the standard PSO algorithm, i.e., global best (*gbest*) and personal best (*pbest*). In the PS^{2}O algorithm, a community best (*cbest*) value is added. The PS^{2}O was then used to solve a multi-objective mathematical model and the results were compared to those obtained with other well-known optimization techniques, including GAs, evolutionary strategies (ES) and PSO. Interestingly, the PS^{2}O algorithm showed superior results for all objective functions (i.e., coverage, interference, load balance, and economic efficiency). Two new objective functions, i.e., load balance and economic efficiency were introduced in this research (economic efficiency was used instead of deployment cost). The propagation model and the consideration of the uplink communication channel were not clearly described and the impact of obstacles was not reflected in the model.

Finally, Giampaolo et al. (2010) also used PSO as the optimization technique to find the optimum placement of RFID readers and derived the reading region using formulations estimated from Marrocco et al. (2009). Three different propagation models (i.e., free space, two-ray, and ray-tracing) were used to model the downlink channel. However, the modeling of the uplink communication channel was neglected. The multi-objective functions consisted of the coverage efficiency, overall overlapping, total power radiated by the RFID readers' network, and cost of the network. The authors used a weighted sum as the fitness for the multi-objective functions. Obstacles were not considered in the model and the methodology cannot guarantee the coverage of the entire facility area.

Interestingly, all three articles mentioned above applied a weighted sum approach for fitness evaluation. It is sometimes difficult to identify the appropriate pre-defined weighted value of each objective function. Thus, other approach for fitness assignment and evaluation can be used instead, such as Pareto optimality or solving the objectives in a hierarchical manner. Moreover, several parameters of the PSO, i.e., number of particles, *w*, c_1, and c_2, have to be adjusted appropriately. The value of *w* gives the algorithm the search ability while c_1 and c_2 indicates how much global best and local best influences movement, respectively.

3.5. Literature Review Summary

The research studies discussed in this chapter focused on different aspects of RFID technology that could impact the effectiveness of an RFID-based IMS, especially in a warehouse environment. In particular, this research will attempt to improve on the research done by Guan et al. (2006), Chen et al. (2011), and Giampaolo et al. (2010).

It is clear that there are still critical technical gaps and challenging issues to be addressed in the design of an RFID-based system to support inventory management. Table 3.1 summarizes these challenges and indicates how these issues will be addressed in the proposed research. A three color scheme is used in this table. The color green identifies the strong points of the research performed by Guan et al., 2006, Chen et al., 2011, and Giampaolo et al., 2010. The weaknesses are represented by the color red and are considered the technical gaps and challenging issues that this research will try to address. Finally, the color yellow identifies parameters that are reasonable, but the performance of the overall system may be improved if a different type of parameter or method were used instead.

Table 3.1 Summary of the research studies conducted by Guan et al., 2006, Chen et al., 2011, and Giampaolo et al., 2010

	Parameters	Guan et al. (2006)	Chen et al. (2011)	Giampaolo et al. (2010)	Proposed research
1	Signal Coverage	Circular	Circular	Ellipsoid	Circular and Elliptical
2	Propagation model				
	Downlink (Reader->Tag)	Multipath	Free-space (N/A)	Free-space, 2-ray, Ray-tracing	Multipath
	Uplink (Tag->Reader)	Reflection Coefficient	Not considered	Not considered	Radar Cross Section (RCS)
3	Obstacles	Not considered	Not considered	Not considered	Considered
4	Interference	Reader-to-Reader (Overlapped area)	Reader-to-Reader (Overlapped area)	Reader-to-Reader (Overlapped area)	Reader-to-Reader, Signal-to-Interference Ratio (SIR)
5	Multi-Objective Function	Cost	Coverage	Coverage	Coverage
		Interference	Interference	Overall Overlapping	Interference
		Coverage	Load Balance	Avg. EIRP	Cost
			Economic Efficiency	Cost	
6	Fitness	Weighted Sum	Weighted Sum	Weighted Sum	Weighted sum
7	Optimization Techniques	GA	Multi-PSO, GA, ES, PSO	PSO	GA, PSO
8	Cover entire facility	Not considered (Static tags)	Not considered (Static tags)	Not considered (Static tags)	Considered (Dynamic tags)
9	Randomly add tags first	Required	Required	Required	Not required
10	Shape of facility area	Rectangular	Rectangular	L-Shape	Rectangular and inverted-T shape

4. RESEARCH METHODOLOGY

The main phases of the methodology followed in this research are depicted in Figure 4.1. The first step involved a thorough review of the EPCglobal® class 1 generation 2 (C1G2) standard to identify the most critical parameters for RFID network planning for warehouse inventory management. These parameters were later used in the development of two model formulations and as input parameters when generating feasible solutions for the model formulations.

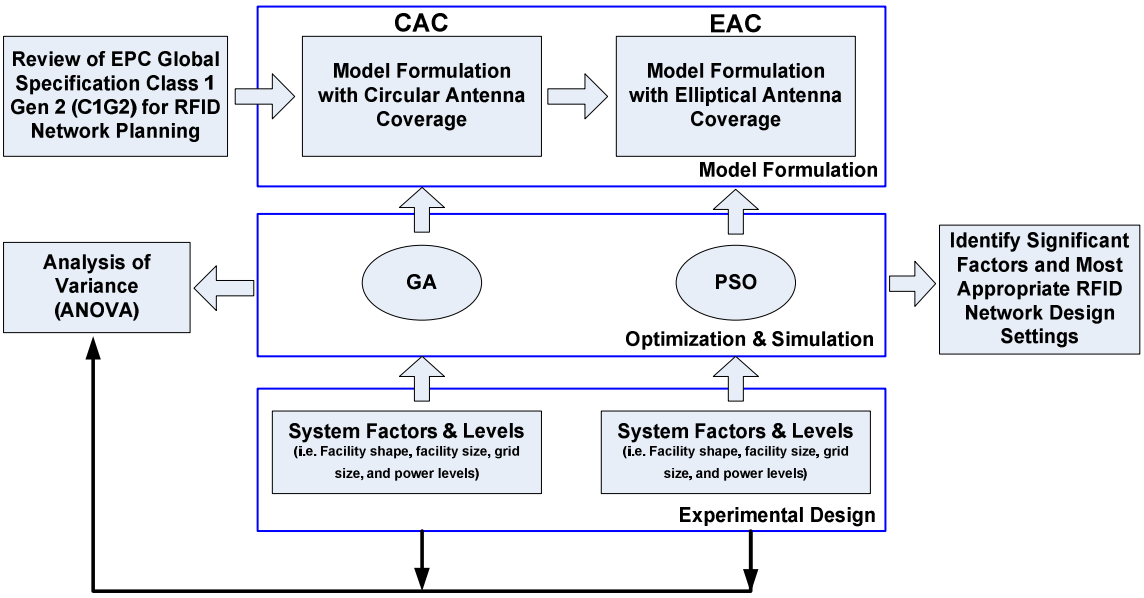

Figure 4.1 Main phases of the research methodology

Next, a model formulation was developed based on the assumption that the antenna attached to the RFID reader generated a circular coverage area. The assumption that the antenna produced a circular coverage area provided the opportunity to validate certain aspects of the model formulation before utilizing an elliptical antenna coverage area, which is

more realistic for RFID systems utilized in warehouse inventory management. More specifically, the development of the baseline optimization algorithm in MATLAB was easier under the assumption of a circular coverage area. Furthermore, since most of the prior literature related to the RIFD network planning problem assumed circular antenna coverage exclusively, several examples were available for validation. An model formulation with elliptical antenna coverage was subsequently developed which incorporated new antenna parameters such as the length of the major axis, the length of the minor axis, and the orientation angle. Both model formulations dealt with a multi-objective problem by combining three objectives, i.e., signal coverage, interference, and implementation cost, into a single objective.

The heuristic optimization techniques genetic algorithm (GA) and particle swarm optimization (PSO) were used to find good solutions for the model formulations. Several factors of the RFID network planning (RNP) problem as well as specific parameters of each heuristic optimization technique were adjusted to improve the quality of the solutions. A designed experiment was conducted followed by a multi-factor analysis of variance (ANOVA) to identify those factors that had the most significant effect on the quality of the solutions. Finally, the most appropriate RFID network design settings are determined. When the specific facility shape, facility size, and location of obstructions are known, the developed research methodology can be applied to optimize both the number and the placement of RFID readers in the system

The rest of this chapter is organized as follows. Section 4.1 describes the EPCglobal® C1G2 standard for RFID network planning. Section 4.2 describes the circular antenna coverage model formulation. An application example of the circular antenna coverage model formulation is presented in section 4.3. Section 4.4 describes the elliptical antenna coverage

model formulation, followed by an application example of this model formulation in section 4.5. Section 4.6 presents the effect of passive interference on RFID antenna coverage. Section 4.7 describes the details of the heuristic optimization algorithms used in this research, i.e., GA and PSO. Finally, section 4.8 presents the details of the experimental design.

4.1 EPCglobal® C1G2 Standard for RFID Network Planning

The Electronic Product Code (EPC) is designed as a universal identifier for a single physical object in an RFID system. The EPC is programmed and stored in the memory of an RFID tag. When the RFID tag is attached to the physical object, an RFID reader can uniquely identify this particular object.

EPCglobal® is the organization that developed the industry-wide EPC standard to be used by RFID systems. The EPCglobal® Class 1 Generation 2 standard (also known as *EPC C1G2*, *EPC Gen 2* or *Gen 2*) defines the physical and logical requirements for a passive-backscatter, interrogator-talks-first, RFID system operating in the frequency range of 860 MHz to 960 MHz (EPCglobal®, 2011).

The EPCglobal® C1G2 standard mainly focuses on the UHF air interface protocol of the RFID reader and the RFID tag. Several parameters were obtained from this standard and incorporated as input parameters into the model formulations developed in this research. These parameters included the RFID reader's operating frequency, the RFID reader's transmitting power, the RFID reader's effective isotropic radiated power (EIRP), the RFID reader's antenna gain, the RFID reader minimum power or sensitivity, the RFID tag's antenna gain and RFID tag's minimum operating power or sensitivity. The specific values of these parameters are shown in Table 4.1.

Table 4.1 RFID system parameters compliant with EPCglobal® C1G2 standard

Parameters	Values in C1G2 Standard
RFID Reader System Operating Frequency	UHF band: 902-928 MHz, Center Frequency: 915 MHz
RFID Reader EIRP	CAC†: 1 Watts EAC†: 4 Watts
RFID Reader Transmitting Power	1 Watt
RFID Reader Antenna Gain	CAC†: 0 dB (1 as a ratio) EAC†: 6 dB (4 as a ratio)
RFID Tag Antenna Gain	2.15 dB (1.64 as a ratio)
RFID Reader Minimum Power (RFID Reader Sensitivity)	0.316 nanowatts (-95 dBm)
RFID Tag Minimum Power (RFID Tag Sensitivity)	10 microwatts (-20 dBm)

† CAC: Circular Antenna Coverage, EAC: Elliptical Antenna Coverage

RFID readers and RFID tags compliant with the EPCglobal® CIG2 standard operate on two basic UHF frequency bands depending upon the region of the world where they are located. These frequency bands are 860 MHz - 868 MHz and 902 MHz - 928 MHz. RFID systems in North America operate in the UHF band of 902 - 928 MHz with a center frequency of 915 MHz.

The RFID reader's EIRP is computed by multiplying the RFID reader's transmitting power by its antenna gain. The RFID reader's EIRP is always established in accordance with local regulations. Therefore, RFID systems that operate in the U.S. must adhere to the 4-Watt limit for the EIRP set by the Federal Communication Commission (FCC). Thus, the RFID reader's transmitting power is equal to 1 watt and the RFID reader's antenna gain for the

circular antenna coverage (CAC) model formulation and the *elliptical antenna coverage* (EAC) model formulation are limited to 0 dB and 6 dB, respectively (see APPENDIX C).

The EPCglobal® C1G2 standard suggests that the RFID tag's antenna gain should be 2.15 dB (i.e., 1.64 as a ratio). Commercially available RFID readers and RFID tags (Impinj, Inc., 2013) compliant with the EPCglobal® C1G2 standard require a specific power for the chip or integrated circuit (IC) to operate properly known as *sensitivity* which are equal to 0.316 nanowatts (-95 dBm) and 10 microwatts (-20 dBm), respectively.

4.2. The Circular Antenna Coverage Model Formulation

In this section, the model formulation developed under the assumption that the antenna attached to the RFID reader generates a circular coverage area is described. This specific model formulation is referred to as the *circular antenna coverage* (CAC) model formulation. Several characteristics of the RFID system were incorporated into this model, including critical operational parameters specific to the RFID reader, the RFID tag, and the signal propagation model. Also, the characteristics of the test facility, such as shape and size, were considered.

The underlying assumptions made in the development of the CAC model formulation were:

1. The shape and size of the warehouse facility and the location of obstacles within the warehouse facility are known. The area of the warehouse facility is discretized into *grids* of equal height and width.
2. The term *RFID reader* refers to the combination of an RFID interrogator and a single antenna.
3. The RFID reader and the RFID tags are compliant with the EPCglobal® C1G2 standard.
4. Only one type of RFID reader and RFID tag were utilized, i.e., all RFID readers and RFID tags have the same operating frequency, maximum transmitting power, minimum receiving power, antenna type, and antenna gain. Mixed brands of RFID systems and/or multiple detection frequencies were not considered.
5. The polarization and impedance of the antennas match perfectly.
6. Dipole antennas are used for both the RFID reader and the RFID tag. These antennas produced a circular coverage area in a 2D representation.

7. The antenna for the RFID reader is placed at the center of a *grid* and in a manner that maximizes signal coverage (e.g., on the ceiling of the warehouse facility)
8. The radius of the signal coverage area produced by the antenna is known and can be calculated using a propagation model.
    a) The multipath propagation model is used for the downlink channel (i.e., reader-to-tag).
    b) The radar cross section (RCS) propagation model is used for the uplink channel (i.e., tag-to-reader).

The notation used to represent the parameters of the RFID system in the CAC model formulation is described below. A more detailed description of selected parameters in the notation is included in APPENDIX A.

Notation	Description	Units
n	Number of grids in the system, $n = C \times R$	# of grids
i	The index of a grid, $i = 1, 2, ..., n$	-
j	The index of a grid where an RFID reader is placed, $j = 1, 2, ..., n$	-
k	The index of a grid where an interfering RFID reader is located, $k \in IS_i$	-
N	Initial number of RFID readers (see APPENDIX A and equation 4.3)	# of RFID readers
r	Radius of the signal coverage area of the RFID reader's antenna (see APPENDIX C)	meters (m)

Notation	Description	Units
W	Width of the facility area	meters (m)
H	Height of the facility area	meters (m)
C	Total number of grid columns in the facility area; $C = \left\lceil \frac{W}{w_i} \right\rceil$	# of columns
R	Total number of grid rows in the facility area; $R = \left\lceil \frac{H}{h_i} \right\rceil$	# of rows
w_i	Width of grid i	meters (m)
h_i	Height of grid i	meters (m)
FG	Set of forbidden grids. It refers to the set of grids where RFID readers cannot be located due to physical obstructions or other restrictions. $FG = \{ i \mid i \text{ is the forbidden grid} \}$	set {}
t	Number of installed RFID readers	# of RFID readers
RS	Set of installed RFID readers $RS = \{ j \mid x_j = 1 \}$	set {}
FA	Feasible area	square meters (m^2)
TA	Total area	square meters (m^2)
$D_{i,j}$	Signal power levels received at grid i from the RFID reader located at grid j $D_{i,j} = P_t \times G_{reader} \times G_{tag} \times \left(\frac{\lambda}{4\pi} \right)^2 \times \frac{1}{d^n} \times \frac{1}{10^{\frac{X}{10}}} = C_1 \times \frac{1}{d_{ij}^{2.2}}$ Where $C_1 = P_t \times G_{reader} \times G_{tag} \times \left(\frac{\lambda}{4\pi} \right)^2 \times \frac{1}{10^{\frac{X}{10}}}$, $n = 2.2$	watts or dBm

Notation	Description	Units
$D_i(\max)$	Set of maximum signal power levels received at grid *i* from the RFID reader located at grid j, $j \in N_i$, $D_i(\max)=\{\max(D_{i,j})\}$	set {}
IS_i	Set of RFID readers that generate interference at grid *i*, $i=1,2,...,C\times R$	set {}
$ID_i(\max)$	Set of maximum signal power levels received at grid *i* from the RFID reader located at grid j, and interfered by the neighboring RFID reader(s) located at grid k, $k \in IS_i$, $ID_i(\max)=\{(D_i(\max))_k\}$	set {}
$U_{i,j}$	Signal power levels (backscattered) received at the RFID reader located at grid j from grid *i* $U_{i,j}=\frac{P_t\times G_{trasmitter}\times G_{receiver}\times\sigma\times\lambda^2}{(4\pi)^3}\times\frac{1}{r^{2n}}\times\frac{1}{10^{\frac{X}{10}}}=C_2\times\frac{1}{r^{4.4}}$ Where $C_2=\frac{P_t\times G_{trasmitter}\times G_{receiver}\times\sigma\times\lambda^2}{(4\pi)^3}\times\frac{1}{10^{\frac{X}{10}}}$, $n=2.2$	watts or dBm
$U_i(\max)$	Set of maximum signal power levels (backscattered) received at the RFID reader located at grid j from grid *i*, $U_i(\max)=\{\max(U_{i,j})\}$	set {}
$IU_i(\max)$	Set of maximum signal power levels (backscattered) received at the RFID reader located at grid j from grid *i* and interfered by neighboring RFID readers located at grid k, $IU_i(\max)=\{(U_i(\max))_k\}$	set {}
x_j	Binary decision variable to identify whether or not an RFID reader is located at grid *j*: $x_j=$ 1 *if an RFID reader is located at grid j*; 0 *otherwise*	binary (0,1)

Notation	Description	Units
y_i	Binary decision variable to identify whether or not grid i is covered by at least one RFID reader: $y_i = \tau D_i \cdot \tau U_i \cdot \beta_i$ Grid i is covered by the RFID reader located at grid j ($y_i = 1$) if and only if the following three requirements are satisfied: 1) The downlink communication from the RFID reader located at grid j to grid i is successfully established. 2) The uplink communication from grid i to the RFID reader located at grid j is successfully established. 3) Grid i is not a forbidden grid.	binary (0,1)
τD_i	Successful transmission from the RFID reader located at grid j to grid i $\tau D_i = \max\left(\frac{D_i(\max) - TD}{\lvert D_i(\max) - TD \rvert}, 0\right)$ TD is the specific downlink power threshold (29 microwatts or -15.4 dBm)	binary (0,1)
τU_i	Successful transmission from grid i to the RFID reader located at grid j, i.e., the backscattered signal from the RFID tag to the RFID reader $\tau U_i = \max\left(\frac{U_i(\max) - TU}{\lvert U_i(\max) - TU \rvert}, 0\right)$ TU is the specific uplink power threshold (0.316 nanowatts or -95 dBm)	binary (0,1)
β_i	Feasible coverage of grid i $\beta_i = 1$ *if* $i \notin FG$ 0 *otherwise*	binary (0,1)

Notation	Description	Units
N_i	The set of RFID readers ($j \in RS$) that can cover grid *i*, $N_i = \{ j \mid d_{ij} \leq r \cap i \notin FG \}$	set {}
DN_i	The set of signal power levels received at grid *i* from the RFID reader located at grid *j* for downlink channel $DN_i = \{ D_{i,j} \mid \forall j \in N_i \}$	set {}
UN_i	The set of signal power levels received at grid *i* from the RFID reader located at grid *j* for uplink channel $UN_i = \{ U_{i,j} \mid \forall j \in N_i \}$	set {}
d_{ij}	The Euclidean distance from the center of grid *j* to the center of grid *i* $d_{ij} = \sqrt{(\lvert i-j \rvert \bmod w)^2 + \left(\left\lfloor \frac{\lvert i-j \rvert}{w} \right\rfloor \right)^2}$ $\lvert i-j \rvert \bmod w$ is the remainder when $\lvert i-j \rvert$ is divided by w $\left\lfloor \frac{\lvert i-j \rvert}{w} \right\rfloor$ rounds down $\frac{\lvert i-j \rvert}{w}$ to the nearest integer	meters (m)
W_1	Weight assigned to the first objective, i.e., total coverage	-
W_2	Weight assigned to the second objective, i.e., total signal to interference ratio (SIR)	-
W_3	Weight assigned to the third objective, i.e., total cost	-
C_i	Cost of the RFID reader at grid *i*	US dollars (USD)

4.2.1. CAC Model Formulation and Constraints

The objective function and constraints of the CAC model formulation are as follows:

$$Maximize:\ Z \;=\; W_1 \cdot \frac{\sum_{i=1}^{n} y_i}{\sum_{i=1}^{n} \beta_i} \qquad \textit{(Coverage)} \qquad (4.1a)$$

$$+\ W_2 \cdot \frac{\sum_{i=1}^{n} \sum_{j \in N_i} \left(\max\left(D_{i,j}\right)\right)}{\sum_{i=1}^{n} \sum_{j \in N_i} \left(\max\left(D_{i,j}\right)\right) + \sum_{i=1}^{n} \sum_{j \in N_i} \sum_{k \in IS_i} \left(\left(\max\left(D_{i,j}\right)\right)_k\right)} \qquad \textit{(Downlink SIR)} \qquad (4.1b)$$

$$+\ W_2 \cdot \frac{\sum_{i=1}^{n} \sum_{j \in N_i} \left(\max\left(U_{i,j}\right)\right)}{\sum_{i=1}^{n} \sum_{j \in N_i} \left(\max\left(U_{i,j}\right)\right) + \sum_{i=1}^{n} \sum_{j \in N_i} \sum_{k \in IS_i} \left(\left(\max\left(U_{i,j}\right)\right)_k\right)} \qquad \textit{(Uplink SIR)} \qquad (4.1c)$$

$$+\ W_3 \cdot \frac{Budget - (C_i \times t)}{Budget} \qquad \textit{(Cost)} \qquad (4.1d)$$

Subject to:

$$y_i \;\le\; \sum_{j \in N_i} x_j \;\le\; y_i \times t \quad ;\ \forall i \qquad where \qquad N_i = \left\{ j \;\middle|\; d_{ij} \;\le r \cap i \notin FG \right\} \qquad (4.2)$$

$$\left\lceil \frac{TA}{\pi r^2} \right\rceil \le t \;\le\; N \qquad where \qquad N \approx \left\lceil \frac{TA}{2r^2} \right\rceil \qquad (4.3)$$

$$\sum_{j=1}^{n} x_j = t \qquad (4.4)$$

$$C_i \times t \le Budget \qquad (4.5)$$

$$\sum_{i=1}^{3} W_i \;=\; 1 \qquad (4.6)$$

$$0 \le D_i(\max) \le y_i \times 4\,watts \quad \forall i \;\; ; \;\; D_i(\max) = \left\{ \max\left(D_{i,j}\right) \right\} \tag{4.7}$$

$$0 \le ID_i(\max) \le y_i \times \left(\sum_{j \in N_i} DN_i - D_i(\max) \right) \quad \forall i \;\; ; \;\; ID_i(\max) = \left\{ \left(D_i(\max)\right)_k \right\} \tag{4.8}$$

$$0 \le U_i(\max) \le y_i \times 4\,watts \quad \forall i \;\; ; \;\; U_i(\max) = \left\{ \max\left(U_{i,j}\right) \right\} \tag{4.9}$$

$$0 \le IU_i(\max) \le y_i \times \left(\sum_{j \in N_i} UN_i - U_i(\max) \right) \quad \forall i \;\; ; \;\; IU_i(\max) = \left\{ \left(U_i(\max)\right)_k \right\} \tag{4.10}$$

$$x_j \in (0,1) \quad ; \quad j = \{1, 2, ..., n\}$$

$$y_i \in (0,1) \quad ; \quad i = \{1, 2, ..., n\}$$

As equation 4.1 shows, the CAC model formulation is a maximization problem that consists of three objective functions combined using a weighted sum or linear combination with specific weight values. All objectives are normalized; therefore, their values range from zero to one.

Equation 4.1a represents the first objective which is to maximize the area of the facility covered by the installed RFID reader network. The binary decision variable y_i is calculated as the product of three terms, i.e., $y_i = \tau D_i \cdot \tau U_i \cdot \beta_i$. The term τD_i indicates whether or not the downlink signal transmission from RFID reader *j* to grid *i* is successful. If the maximum signal power level received at grid *i* is greater than or equal to the downlink power threshold (i.e., 29 microwatts or -15.4 dBm), the communication link is established successfully and the value of τD_i is set to one. Otherwise, it is equal to zero. The term τU_i indicates whether or not the uplink signal transmission from grid *i* to an RFID reader located at grid *j* is successful. If the maximum signal power level received at a desired RFID reader

located at grid j is greater than or equal to the uplink power threshold (e.g., 0.316 nanowatts or -95 dBm), the communication link is established successfully and the value of τU_i is set to one. Otherwise, it is equal to zero. Finally, the term β_i indicates whether or not the RFID reader can be placed at grid *i*. If grid *i* is not a forbidden grid, the value of β_i is equal to one; otherwise, it is set to zero. Therefore, a particular grid *i* is considered as *covered* by an RFID reader if and only if the decision variables $\tau D_i, \tau U_i$, and β_i are all equal to one.

The second objective, represented by equation 4.1b and equation 4.1c, is to minimize the reader-to-reader interference. Since the term signal-to-interference ratio (SIR) is used as the measure of interference, minimizing interference means maximizing SIR. Equation 4.1b reflects the SIR in the downlink channel, whereas equation 4.1c quantifies the SIR in the uplink channel. The total SIR is then calculated as the summation of the downlink SIR and the uplink SIR.

The third objective is to minimize the implementation cost of an RFID network for inventory management. However, the overall objective function (or fitness function) seeks a maximization objective. To transform the objective of implementation cost into a maximization objective, the ratio of the budget minus the cost of the installed RFID readers divided by the budget can be used to calculate the cost of implementation, as shown in equation 4.1d.

Constraint (4.2) ensures that if $\sum_{j \in N_i} x_j \geq 1$, at least one RFID reader in the set N_i covers grid i $(y_i = 1)$. On the other hand, if $N_i = \phi$ (i.e., $\sum_{j \in N_i} x_j = 0$), grid i will not be covered $(y_i = 0)$. In addition, the number of RFID readers that cover grid *i* must not be greater than the number of installed RFID readers in the system (i.e., $\sum_{j \in N_i} x_j \leq y_i \times t$).

The lower bound and the upper bound for the total number of RFID readers installed can be calculated using constraint (4.3). This constraint allows the optimization algorithms to search for the optimum number of RFID readers required in the system that would result in the best value of fitness. Originally, constraint (4.3) used the feasible area *(FA)* of the facility as the numerator, i.e., $\left\lceil \frac{FA}{\pi r^2} \right\rceil \leq t \leq N$, where $N \approx \left\lceil \frac{FA}{2r^2} \right\rceil$. However, constraint (4.3) was only satisfied if the effect of obstructions in the facility was not considered. Once the effect of obstructions is considered, the coverage area of the RFID readers decreases due to the effect of factors such as attenuation loss and passive interference. As a result, more RFID readers are required. Thus, constraint (4.3) had to be relaxed by replacing *FA* with the total area of the facility (*TA)*. With this modification, the GA and PSO optimization algorithms can find feasible solutions to the RNP. Constraint (4.4) implies that the number of grids where an RFID reader is installed must be equal to the total number of RFID readers installed.

Constraint (4.5) specifies that the implementation cost of the RFID reader network must be less than or equal to the available budget. Constraint (4.6) specifies that the linear combination of weights must not exceed one.

Constraint (4.7) ensures that if grid *i* is covered (i.e., $y_i = 1$), the maximum signal power levels received at grid *i* from the RFID reader located at grid *j* must not be greater than the 4-watt EIRP limitation set by the Federal Communication Commission (FCC).

In constraint (4.8), the set $DN_i \; \forall \; j \in N_i$ consists of the signal power levels received at a particular grid *i* from the RFID readers located at the grid(s) $j \in N_i$ for the downlink communications channel. Only one signal power element in this set is considered as the maximum signal power level (i.e., $D_i(\max)$), whereas the other signal power elements

(if any) are considered as *interference*. Therefore, the maximum value of signal interference power affecting a particular grid *i* can be calculated by summing all elements in the set DN_i and then subtracting the maximum signal power level $D_i(\max)$. Thus, constraint (4.8) specifies that if grid *i* is covered (i.e., $y_i = 1$), the level of interference affecting this grid can vary between zero and $\sum_{j \in N_i} DN_i - D_i(\max)$.

Constraints (4.9) and (4.10) implement similar concepts as that of constraints (4.7) and (4.8) but applied to the uplink communications channel. In this case, the maximum signal power level and the signal power levels received at a particular grid *i* from the RFID readers located at the grid(s) $j \in N_i$ are represented as $U_i(\max)$ and UN_i, respectively.

4.2.2. The Coverage Area of an Omnidirectional Antenna

One of the most important geometric features of a circle is its radius. A circle does not have a rotation angle because the distance from its center to any point on its circumference is the same. Thus, the equation of a circle with a constant radius (*r*) and center coordinates (*h*, *k*) is as shown in equation 4.11.

$$(x-h)^2 + (y-k)^2 = r^2 \tag{4.11}$$

If the coordinates (*h*, *k*) of the location of the RFID reader and the radius (*r*) are known, it is straightforward to represent the coverage area generated by an RFID reader with an omnidirectional antenna. Furthermore, if the coordinates (*x*, *y*) of the location of the RFID tag are known, the method for identifying whether or not the tag is located within the circular

coverage area of the RFID reader is to substitute the coordinates (*h, k*) of the location of the RFID reader and the coordinates (*x, y*) of the location of the RFID tag in equation 4.11. If the tag is within the circular coverage area of the RFID reader, the summation of the terms on the left hand side of equation 4.11 should be less than or equal to the square of the radius, r^2, as shown in equation 4.12.

$$(x-h)^2+(y-k)^2 \leq r^2 \tag{4.12}$$

Figure 4.2 depicts a facility where the location of an RFID reader and the locations of two RFID tags are known. These known locations will be used to demonstrate the concept of determining whether or not an RFID tag is located within the circular coverage area of the RFID reader. The antenna of the RFID reader is located at coordinates (0.5, 0.5) and its coverage area has a radius of 1.5 meters. Two RFID tags are located at coordinates (0.5, 1.5) and (2.5, 1.5). The result obtained from equation 4.8 after replacing the known values of *(h, k), (x, y)* and *r*, for the RFID tag located at (0.5, 1.5) is $(0.5-0.5)^2+(1.5-0.5)^2 \leq 1.5^2$ $\because\ 1 < 2.25$. Thus, the RFID tag located at coordinates (0.5, 1.5) is within the circular coverage area of the RFID reader. On the other hand, the RFID tag located at coordinates (2.5, 1.5) does not satisfy equation 4.12 since $5 > 2.25$, indicating that this RFID tag is not located within the circular coverage area of the RFID reader.

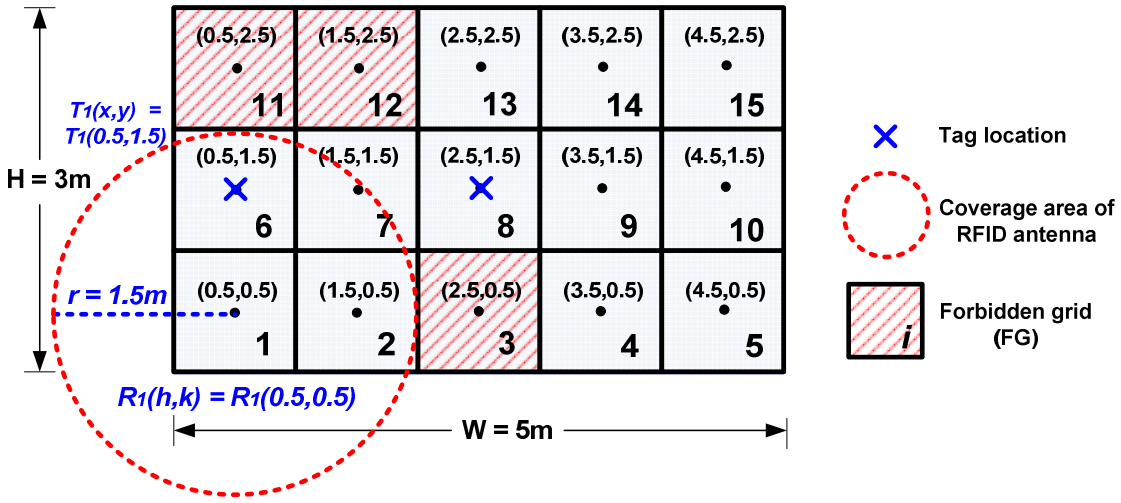

Figure 4.2 Discretized facility to illustrate how to determine if an RFID tag is located within the coverage area on an omnidirectional antenna

4.3. Application of the CAC Model Formulation

In this section, an example is presented to demonstrate the application of the CAC model formulation. A rectangular facility, depicted in Figure 4.3, has already been discretized into grids to illustrate the decomposition of the RNP problem.

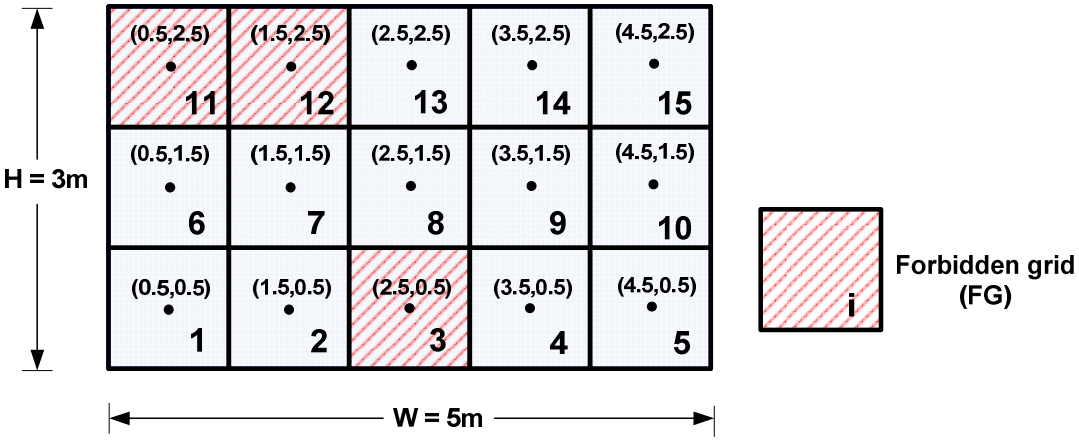

Figure 4.3 Discretized rectangular facility

4.3.1. Facility Dimensions and Forbidden Grids

The width (W) and height (H) of the rectangular facility are 5 meters and 3 meters, respectively. The width (w_i) and height (h_i) of each grid *i* in the rectangular facility are 1 meter and 1 meter, respectively. Therefore, the total number of columns (C) is five computed as $C = \left\lceil \frac{W}{w_i} \right\rceil = \left\lceil \frac{5}{1} \right\rceil = 5$. The total number of rows is calculated in a similar manner using the formula $R = \left\lceil \frac{H}{h_i} \right\rceil = 3$. The total number of grids in the facility is the product of C and R, i.e., $C \times R = 5 \times 3 = 15$.

Figure 4.3 shows that there are three forbidden grids in the rectangular facility. The values for index *i* for these grids are 3, 11, and 12. Therefore, the set of forbidden grids (FG) in this example is $FG = \{3, 11, 12\}$. RFID readers cannot be placed in these forbidden grids and the antennas of the installed RFID readers do not have to cover these areas either. Moreover, the feasible area (FA) can be computed using the equation $FA = (W \times H) - size\,of\ set\ FG \times (w_i \times h_i)$. As a result, the parameter FA is equal to 12 square meters.

4.3.2. Radius of the Antenna Coverage Area

The radius *(r)* of the circular coverage area of the antenna of the RFID reader is calculated by taking into account the gain and directionality of the antenna in the horizontal plane (H-Plane) and a propagation model. APPENDIX C includes a detailed example of how *r* is calculated. For the purposes of this example, the radius of the circular coverage area of the antenna of the RFID reader is assumed to be 1.5 meters.

4.3.3. Initial Number of RFID Readers

The initial number of RFID readers (N) needed to cover the example rectangular facility is calculated using the circle packing (CP) algorithm. The CP algorithm consists of packing the biggest square enclosed by a circle in the rectangular-shaped facility (Heppes & Melissen, 1996; Hougardy, 2011). Figure 4.4 shows that for the example rectangular facility, the CP algorithm determines that the initial number of RFID readers is four. However, using four RFID readers will result in significant antenna coverage overlap and, as a consequence, interference. Thus, only three RFID readers should be used to reduce the interference in the system, as shown in Figure 4.5. The placement of the RFID readers shown in Figure 4.5 was obtained by manually placing RFID readers at eligible locations, i.e., the center of qualified grids, and one RFID reader was manually removed from Figure 4.4 in order to avoid interference. The RFID reader coverage scenario depicted in Figure 4.5 will be used to further demonstrate the problem and validate the CAC model formulation.

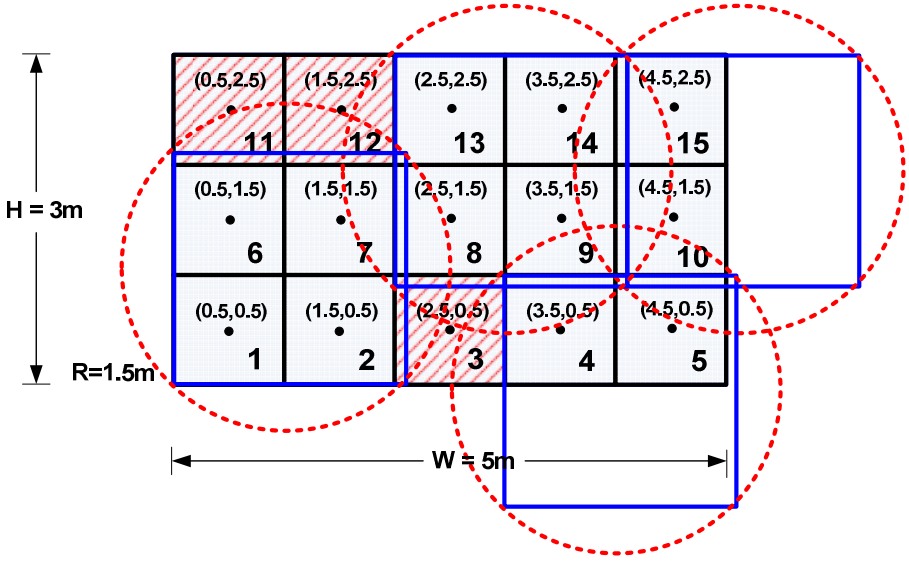

Figure 4.4 Coverage of the rectangular facility using the concept of circle packing

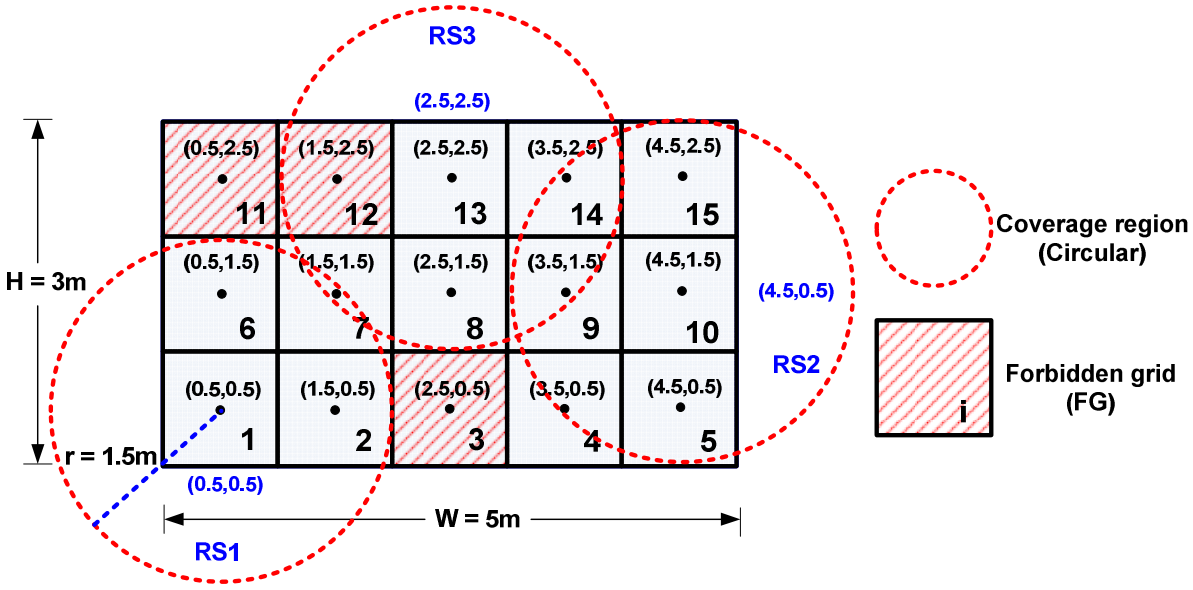

Figure 4.5 Correction to the initial circle packing coverage to reduce interference

Figure 4.5 shows RFID readers located at the center of grids 1, 10 and 13. Therefore, the set of installed RFID readers is $RS = \{1, 10, 13\}$ and the number of installed RFID readers t = 3. The coordinates of the center of grids 1, 10 and 13 are (0.5, 0.5), (4.5, 0.5), and (2.5, 2.5), respectively.

4.3.4. Downlink Communication Channel

The signal transmission power of the downlink communication channel, i.e., reader-to-tag, is determined next. The set of RFID readers that can cover grid i (i.e., N_i) is determined first using equation 4.13.

$$N_i = \left\{ j \,\middle|\, d_{ij} \le r \cap i \notin FG \right\} \tag{4.13}$$

Equation 4.13 implies that for an RFID reader (located at grid *j*) to cover grid *i*, the following two conditions must be met:

1) The Euclidean distance (d_{ij}) calculated from the center of grid *j* to the center of grid *i* must be less than or equal to the radius (*r*) of the circular coverage area of the RFID reader located at grid *j*, and
2) The grid *i* is not a forbidden grid.

For the rectangular facility depicted in Figure 4.5, the sets $N_i \ \forall i$ are computed using the pseudocode shown in Figure 4.6.

Algorithm: Determine the members of the set N_i and $D_i(\max)$

for i = 1 → n **do**
  if $i \in FG$ **then**
    $N_i = \phi$
  else
    $N_i = \phi$
    for $j \in RS$ **do**
      Calculate Euclidean distance d_{ij}
      if $d_{ij} \le r$ **then** *(Grid i can be covered by the RFID reader located at grid j)*
        Add $j \in RS$ to N_i
      end if
    end for
  end if
  if $N_i = \phi$ **then** *(No RFID reader can cover grid i)*
    $D_i(\max) = \phi$
  else if $|N_i| = 1$ **then** *(Exactly one RFID reader can cover grid i)*
    $D_i(\max) = D_{i,j}$
  else *(more than one RFID reader can cover grid i)*
    for $j \in N_i$ **do**
      Calculate and add $D_{i,j}$ to D
    end for
    Find $D_i(\max) = \{\max(D)\}$
    if $|D_i(\max)| \ge 2$ **then**
      Select the $D_{i,j}$ with the lowest j index
    end if
  end if
end for

Figure 4.6 Pseudocode for computing the members in the set N_i and $D_i(max)$

The resulting sets $N_i \ \forall i$ are:

$$N_1 = \{1\}, \quad N_2 = \{1\}, \quad N_3 = \phi, \quad N_4 = \{10\}, \quad N_5 = \{10\},$$

$$N_6 = \{1\}, \quad N_7 = \{1,13\}, \quad N_8 = \{13\}, \quad N_9 = \{10,13\}, \quad N_{10} = \{10\},$$

$$N_{11} = \phi, \quad N_{12} = \phi, \quad N_{13} = \{13\}, \quad N_{14} = \{10,13\}, \quad N_{15} = \{10\}$$

Next, the set of maximum signal power levels received at grid *i* from the RFID reader located at grid *j* is determined using the equation $D_i(\max)=\{\max(D_{i,j})\}$. Figure 4.5 clearly shows that a single grid may receive signals from several RFID readers. The members of the set $D_i(\max)$ are determined from N_i using the pseudocode shown in Figure 4.6.

For the rectangular facility depicted in Figure 4.5, the members of the set $D_i(\max)$ are computed as follows:

$$D_1(\max)=\{\max(D_{1,1})\}=\{D_{1,1}\}$$

$$D_2(\max)=\{\max(D_{2,1})\}=\{D_{2,1}\}$$

$$D_3(\max)=\phi \quad \because \ Grid\ 3 \in FG$$

$$\cdots$$

$$D_7(\max)=\{\max(D_{7,1}, D_{7,13})\}=\{D_{7,1}\}$$

$$\cdots$$

$$D_{14}(\max)=\{\max(D_{14,10}, D_{14,13})\}=\{D_{14,13}\}$$

$$D_{15}(\max)=\{\max(D_{15,10})\}=\{D_{15,10}\}$$

The level of interference in the downlink communication channel also needs to be quantified. This parameter is substituted in the second term of the denominator of equation 4.1b so that the downlink SIR can be obtained. To do so, the set of interfering readers for each grid *i* (i.e., IS_i) must be calculated.

The set IS_i contains the number of interfering readers that correspond to each grid *i.* An RFID reader is labeled as an *interfering reader* if and only if the coverage area of its

antenna covers the center of grid *i* but it is not the strongest signal received (i.e., it is not the $D_i(\max)$). The set of IS_i can be calculated using the information in the sets N_i and $D_i(\max)$. Reader-to-reader interference can only occur in the sets $N_i\ \forall i$ that contain more than one member. For the rectangular facility depicted in Figure 4.5, sets N_7, N_9 and N_{14} meet this criterion, so reader-to-reader interference can only occur in grids 7, 9, and 14. The interfering RFID reader for grid 7 is that located at grid 13, since the strongest signal (i.e., $D_i(\max)$) received at grid 7 is from the RFID reader located at grid 1. The interfering readers for grid 9 and grid 14 are identified in the same manner.

For the rectangular facility depicted in Figure 4.5, the complete sets $IS_i\ \forall i$ are as follows:

$$IS_1=\phi, \quad IS_2=\phi, \quad IS_3=\phi, \quad IS_4=\phi, \quad IS_5=\phi,$$
$$IS_6=\phi, \quad IS_7=\{13\}, \quad IS_8=\phi, \quad IS_9=\{13\}, \quad IS_{10}=\phi,$$
$$IS_{11}=\phi, \quad IS_{12}=\phi, \quad IS_{13}=\phi, \quad IS_{14}=\{10\}, \quad IS_{15}=\phi,$$

After the members of the sets N_i, $D_i(\max)$ and IS_i are known, the set of received signal power levels at grid *i* from the preferred RFID reader located at grid *j*, and interfered by the neighboring RFID readers located at grid *k* are computed using the equation $ID_i(\max)=\{(D_i(\max))_k\}$. It should be noted that if the size of $IS_i = 0$, then $\{(D_i(\max))_k\}=\phi\ \forall i;\ j\in N_i$; and $k\in IS_i$. For the rectangular facility depicted in Figure 4.5, the members of the sets $ID_i(\max)\forall i$ that are not empty, i.e., $ID_7(\max)$, $ID_9(\max)$, and $ID_{14}(\max)$, are determined as follows:

$$ID_7(\max) = \{(D_7(\max))_{13}\} = \{(D_{7,1})_{13}\}$$

$$ID_9(\max) = \{(D_9(\max))_{13}\} = \{(D_{9,10})_{13}\}$$

$$ID_{14}(\max) = \{(D_{14}(\max))_{10}\} = \{(D_{14,13})_{10}\}$$

4.3.5. Uplink Communication Channel

The signal transmission power, interference and SIR of the uplink communication channel are computed in the same manner to that of the downlink communication channel. The set of maximum signal power levels (backscattered) received at the RFID reader located at grid *j* from grid *i* $(U_i(max))$ is computed using the pseudocode shown in Figure 4.7.

$$U_i(\max) = \{\max(U_{i,j})\}\ ; \quad where\ D_i(\max) = \{\max(D_{i,j})\}$$

Algorithm: Determine the members of the set N_i and $U_i(\max)$

for i = 1 → n **do**
  if $i \in FG$ **then**
    $N_i = \phi$
  else
    $N_i = \phi$
    for $j \in RS$ **do**
      Calculate Euclidean distance d_{ij}
      if $d_{ij} \le r$ **then** *(Grid i can be covered by the RFID reader located at grid j)*
        Add $j \in RS$ to N_i
      end if
    end for
  end if
  if $N_i = \phi$ **then** *(No RFID reader can cover grid i)*
    $U_i(\max) = \phi$
  else if $|N_i| = 1$ **then** *(Exactly one RFID reader can cover grid i)*
    $U_i(\max) = U_{i,j}$
  else *(more than one RFID reader can cover grid i)*
    for $j \in N_i$ **do**
      Calculate and add $U_{i,j}$ to U
    end for
    Find $U_i(\max) = \{\max(U)\}$
    if $|U_i(\max)| \ge 2$ **then**
      Select the $U_{i,j}$ with the lowest j index
    end if
  end if
end for

Figure 4.7 Pseudocode for computing the members in the set N_i and U_i *(max)*

For the rectangular facility depicted in Figure 4.5, the members of the sets $U_i(\max)\ \forall i$ are as follows:

$$U_1(\max) = \{\max(U_{1,1})\} = \{U_{1,1}\}$$

$$U_2(\max) = \{\max(U_{2,1})\} = \{U_{2,1}\}$$

$$U_3(\max)=\phi \quad \because \quad Grid\ 3 \in FG$$

$$\cdots$$

$$U_7(\max)=\{\max(U_{7,1}, U_{7,13})\}=\{U_{7,1}\}$$

$$\cdots$$

$$U_{14}(\max)=\{\max(U_{14,10}, U_{14,13})\}=\{U_{14,13}\}$$

$$U_{15}(\max)=\{\max(U_{15,10})\}=\{U_{15,10}\}$$

The set of signal power levels (backscattered) received at the RFID reader located at grid *j* from grid *i* and interfered by neighboring RFID readers located at grid *k* $(IU_i(max))$ can be calculated using the equation $IU_i(\max)=\{(U_i(\max))_k\}$. It should be noted that if the size of IS_i = 0, then $\{(U_i(\max))_k\}=\phi \ \ \forall i\,;\, j \in N_i$; and $k \in IS_i$.

For the rectangular facility depicted in Figure 4.5, the members of the sets $IU_i(max) \forall i$ that are not empty, i.e., $IU_7(\max)$, $IU_9(\max)$ and $IU_{14}(\max)$ are as follows:

$$IU_7(\max)=\{(U_7(\max))_{13}\}=\{(U_{7,1})_{13}\}$$

$$IU_9(\max)=\{(U_9(\max))_{13}\}=\{(U_{9,10})_{13}\}$$

$$IU_{14}(\max)=\{(U_{14}(\max))_{10}\}=\{(U_{14,13})_{10}\}$$

4.3.6. Assembling the Multi-Objective Function

Once all the necessary parameters are known, they are input into equation 4.1 to compute the objective function for the rectangular facility scenario. Since each objective has a different importance, their weights are different. Coverage is the most important objective; thus, its weight (W_1) is set to 0.6. Interference (W_2) and cost (W_3) have the same importance, so both have a weight of 0.2. In addition, the cost of an RFID reader located at grid *i* and the available budget are assumed to be \$1,000 and \$10,000, respectively. The objective function of the CAC model formulation for the rectangular facility depicted in Figure 4.4 is derived as follows:

$$Maximize:\ Z = 0.6 \cdot \frac{\sum_{i=1}^{15} y_i}{\sum_{i=1}^{15} \beta_i}$$

$$+\ 0.2 \cdot \frac{\sum_{i=1}^{15} \sum_{j=N_i} \left(\max\left(D_{i,j}\right)\right)}{\sum_{i=1}^{15} \sum_{j=N_i} \left(\max\left(D_{i,j}\right)\right) + \sum_{i=1}^{15} \sum_{j=N_i} \sum_{k=IS_i} \left(\left(\max\left(D_{i,j}\right)\right)_k\right)}$$

$$+\ 0.2 \cdot \frac{\sum_{i=1}^{15} \sum_{j=N_i} \left(\max\left(U_{i,j}\right)\right)}{\sum_{i=1}^{15} \sum_{j=N_i} \left(\max\left(U_{i,j}\right)\right) + \sum_{i=1}^{15} \sum_{j=N_i} \sum_{k=IS_i} \left(\left(\max\left(U_{i,j}\right)\right)_k\right)}$$

$$+\ 0.2 \cdot \frac{10{,}000 - (1{,}000 \times t)}{10{,}000}$$

$$Maximize: Z = 0.6 \cdot \frac{\left[(\pi D_1 \cdot \pi U_1 \cdot \beta_1) + (\pi D_2 \cdot \pi U_2 \cdot \beta_2) + \ldots + (\pi D_{14} \cdot \pi U_{14} \cdot \beta_{14}) + (\pi D_{15} \cdot \pi U_{15} \cdot \beta_{15})\right]}{12}$$

$$+ \ 0.2 \cdot \frac{\left[\sum_{j=\{1\}} \max\left(D_{1,j}\right) + \sum_{j=\{1\}} \max\left(D_{2,j}\right) + \ldots + \sum_{j=\{10,13\}} \max\left(D_{14,j}\right) + \sum_{j=\{10\}} \max\left(D_{15,j}\right)\right]}{\left[\sum_{j=\{1\}} \max\left(D_{1,j}\right) + \sum_{j=\{1\}} \max\left(D_{2,j}\right) + \ldots + \sum_{j=\{10,13\}} \max\left(D_{14,j}\right) + \sum_{j=\{10\}} \max\left(D_{15,j}\right)\right] + \left[\begin{array}{c} \sum_{j=\{1\}} \left(\left(\max\left(D_{1,j}\right)\right)_0\right) + \sum_{j=\{1\}} \left(\left(\max\left(D_{2,j}\right)\right)_0\right) + \sum_{j=\phi} \left(\left(\max\left(D_{3,j}\right)\right)_0\right) + \ldots + \\ \sum_{j=\{10,13\}} \left(\left(\max\left(D_{14,j}\right)\right)_{10}\right) + \sum_{j=\{10\}} \left(\left(\max\left(D_{15,j}\right)\right)_0\right) \end{array}\right]}$$

$$+ \ 0.2 \cdot \frac{\left[\sum_{j=\{1\}} \max\left(U_{1,j}\right) + \sum_{j=\{1\}} \max\left(U_{2,j}\right) + \ldots + \sum_{j=\{10,13\}} \max\left(U_{14,j}\right) + \sum_{j=\{10\}} \max\left(U_{15,j}\right)\right]}{\left[\sum_{j=\{1\}} \max\left(U_{1,j}\right) + \sum_{j=\{1\}} \max\left(U_{2,j}\right) + \ldots + \sum_{j=\{10,13\}} \max\left(U_{14,j}\right) + \sum_{j=\{10\}} \max\left(U_{15,j}\right)\right] + \left[\begin{array}{c} \sum_{j=\{1\}} \left(\left(\max\left(U_{1,j}\right)\right)_0\right) + \sum_{j=\{1\}} \left(\left(\max\left(U_{2,j}\right)\right)_0\right) + \sum_{j=\phi} \left(\left(\max\left(U_{3,j}\right)\right)_0\right) + \ldots + \\ \sum_{j=\{10,13\}} \left(\left(\max\left(U_{14,j}\right)\right)_{10}\right) + \sum_{j=\{10\}} \left(\left(\max\left(U_{15,j}\right)\right)_0\right) \end{array}\right]}$$

$$+ \ 0.2 \cdot \frac{10{,}000 - (1{,}000 \times 3)}{10{,}000}$$

$$Maximize: Z = 0.6 \cdot \frac{\left[\begin{array}{c} (1 \cdot 1 \cdot 1) + (1 \cdot 1 \cdot 1) + (0 \cdot 0 \cdot 0) + (1 \cdot 1 \cdot 1) + (1 \cdot 1 \cdot 1) + \\ (1 \cdot 1 \cdot 1) + (1 \cdot 1 \cdot 1) + (1 \cdot 1 \cdot 1) + (1 \cdot 1 \cdot 1) + (1 \cdot 1 \cdot 1) + \\ (0 \cdot 0 \cdot 0) + (1 \cdot 1 \cdot 0) + (1 \cdot 1 \cdot 1) + (1 \cdot 1 \cdot 1) + (1 \cdot 1 \cdot 1) \end{array}\right]}{12}$$

$$+ 0.2 \cdot \frac{\left[D_{1,1} + D_{2,1} + 0 + \ldots + D_{14,13} + D_{15,10}\right]}{\left[D_{1,1} + D_{2,1} + 0 + \ldots + D_{14,13} + D_{15,10}\right] + \left[\left(D_{7,1}\right)_{13} + \left(D_{9,10}\right)_{13} + \left(D_{14,13}\right)_{10}\right]}$$

$$+ 0.2 \cdot \frac{\left[U_{1,1} + U_{2,1} + 0 + \ldots + U_{14,13} + U_{15,10}\right]}{\left[U_{1,1} + U_{2,1} + 0 + \ldots + U_{14,13} + U_{15,10}\right] + \left[\left(U_{7,1}\right)_{13} + \left(U_{9,10}\right)_{13} + \left(U_{14,13}\right)_{10}\right]}$$

$$+ \ 0.2 \cdot 0.7$$

$$Maximize: Z = 0.74$$

$$+ 0.2 \cdot \left[\begin{array}{c} \dfrac{\left[D_{1,1} + D_{2,1} + 0 + \ldots + D_{14,13} + D_{15,10}\right]}{\left[D_{1,1} + D_{2,1} + 0 + \ldots + D_{14,13} + D_{15,10}\right] + \left[\left(D_{7,1}\right)_{13} + \left(D_{9,10}\right)_{13} + \left(D_{14,13}\right)_{10}\right]} \\ + \dfrac{\left[U_{1,1} + U_{2,1} + 0 + \ldots + U_{14,13} + U_{15,10}\right]}{\left[U_{1,1} + U_{2,1} + 0 + \ldots + U_{14,13} + U_{15,10}\right] + \left[\left(U_{7,1}\right)_{13} + \left(U_{9,10}\right)_{13} + \left(U_{14,13}\right)_{10}\right]} \end{array} \right]$$

4.4. The Elliptical Antenna Coverage Model Formulation

In this section, the model formulation developed under the assumption that the antenna attached to the RFID reader generates an elliptical coverage area is described. This model is referred to as the *elliptical antenna coverage* (EAC) model formulation. It is important to note that the CAC model formulation described in section 4.2 is the foundation of the EAC model formulation. However, different assumptions are made and additional parameters and model constraints have been added.

In the CAC model formulation, it was assumed that both the RFID reader and the RFID tag used a dipole antenna, which results in a circular (i.e., omnidirectional) coverage area. However, most RFID readers used in warehouse inventory management applications use a directional antenna which produces an elliptical coverage area (Greene, 2006; Chen et al., 2009; Phongcharoenpanich, 2009; Huang & Chang, 2011).

The underlying assumptions made in the development of the EAC model formulation were:

- The assumptions 1 – 5 stated in section 4.2 used in the development of the CAC model formulation still hold true in the development of the EAC model formulation.
- Assumptions 6 and 7 were modified as follows:

    6. A directional patch antenna is used for the RFID reader. This antenna radiates a 2D elliptical coverage area. The antenna for the RFID reader is placed at the center of a *grid* and in a manner that maximizes signal coverage (e.g., on the ceiling of the warehouse facility). A dipole antenna is still used for the RFID tag because it is the most common type of antenna currently in use. Since a

dipole antenna is less sensitive to changes in orientation, it provides a great advantage to the RFID tag.

7. The lengths of major axis (*2a*) and minor axis (*2b*) of the antenna's coverage area are known and can be calculated using a propagation model.
   a) The multipath propagation model is used for the downlink channel (i.e., reader-to-tag).
   b) The radar cross section (RCS) propagation model is used for the uplink channel (i.e., tag-to-reader).

The additional parameters added to the notation of the EAC model formulation are shown below.

Notation	Description	Units
a	Half of the major axis of an elliptical antenna coverage	meters (m)
b	Half of the minor axis of an elliptical antenna coverage (see APPENDIX C for the detailed calculation of *a* and *b*)	meters (m)
AR	Set of rotation angles relative to the x-axis of the installed RFID readers (e.g., if three (3) RFID readers are installed, i.e., $RS = \{1,10,13\}$) $AR = \{\theta_1, \theta_{10}, \theta_{13}\} = \{45^\circ, 225^\circ, 0^\circ\}$, One of eight (8) rotations angles (in degrees) are allowed, i.e., $(0^\circ, 45^\circ, 90^\circ, 135^\circ, 180^\circ, 225^\circ, 270^\circ, 315^\circ)$	set {}
$f1_j$	Coordinate (x,y) of the first focal point of the elliptical antenna coverage area of the RFID reader located at grid *j*	(x,y)
$f2_j$	Coordinate (x,y) of the second focal point of the elliptical antenna coverage area of the RFID reader located at grid *j*	(x,y)

A few parameters in the notation of the CAC model formulation were changed to make them applicable to the EAC model formulation, as follows:

Notation	Description	Units
N_i	The set of RFID readers ($j \in RS$) that can cover the center of grid *i* $N_i = \{ j \mid d1_{ij} + d2_{ij} \le 2a \cap i \notin FG \}$	set {}
$d1_{ij}$	The Euclidean distance from the first focal point of the antenna coverage area of the RFID reader located at grid *j* to the center of grid *i*	meters (m)
$d2_{ij}$	The Euclidean distance from the second focal point of the antenna coverage area of the RFID reader located at grid *j* to the center of grid *i*	meters (m)

Figure 4.8 depicts the location of axes *a* and *b*, the rotation angle θ_i, and important elements of the elliptical antenna coverage.

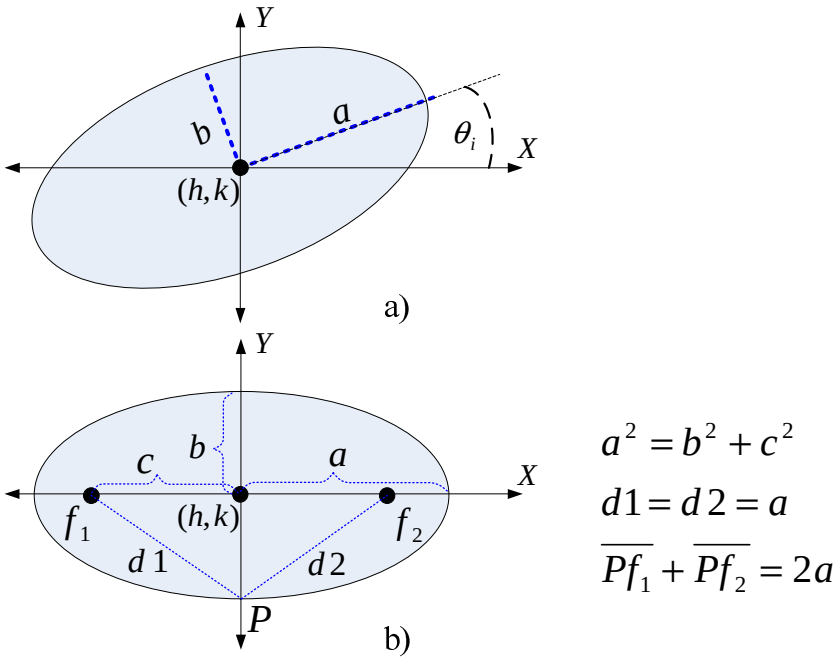

Figure 4.8 Important elements of the elliptical antenna coverage

4.4.1. EAC Model Formulation and Constraints

Constraints (4.4) through (4.10) defined for the CAC model formulation can be applied in their current form in the EAC model formulation. However, constraints (4.2) and (4.3) were modified in the EAC model formulation given the assumption of elliptical antenna coverage. In the CAC model formulation, constraint (4.2) was added to ensure that if $\sum_{j \in N_i} x_j \geq 1$, at least one RFID reader in the set N_i covers grid i $(y_i = 1)$. On the other hand, if $N_i = \phi$ (i.e., $\sum_{j \in N_i} x_j = 0$), grid i will not be covered $(y_i = 0)$. Additionally, the number of RFID readers that cover grid i must not be greater than the number of installed RFID readers in the system (i.e., $\sum_{j \in N_i} x_j \leq y_i \times t$). A similar constraint is needed in the EAC model formulation but, in this case, the condition to identify whether or not the particular RFID reader located at grid j covers the center of grid i has to be changed from $N_i = \{ j \mid d_{ij} \leq r \cap i \notin FG \}$ to $N_i = \{ j \mid d1_{ij} + d2_{ij} \leq 2a \cap i \notin FG \}$. Therefore, constraint (4.2) was re-written in the EAC model formulation as shown in equation 4.14.

$$y_i \leq \sum_{j \in N_i} x_j \leq y_i \times t \;\; ; \;\; \forall i \quad where \quad N_i = \{ j \mid d1_{ij} + d2_{ij} \leq 2a \cap i \notin FG \} \tag{4.14}$$

Moreover, the lower and upper bounds for the total number of RFID readers installed in constraint (4.3) were changed. The lower bound for the number of installed RFID readers in the EAC model formulation is derived from the total area (*TA*) in the facility divided by the RFID reader's elliptical coverage area (πab). The initial number of required RFID readers (i.e., the upper bound for the total number of installed RFID readers) is computed

from the total area (*TA*) in the facility divided by the area of the biggest rectangle enclosed by an ellipse, as shown in Figure 4.9.

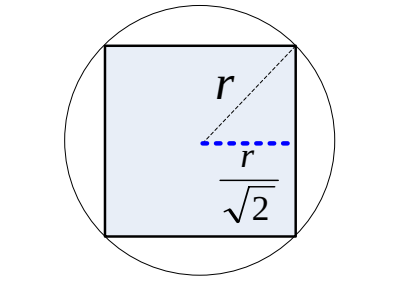

Area of a biggest square enclosed by a circle $= \left(2 \cdot \frac{r}{\sqrt{2}}\right)^2 = 2 \cdot r^2$

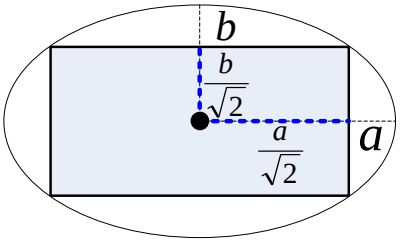

Area of a biggest rectangle enclosed by an ellipse $= 4 \cdot \frac{a}{\sqrt{2}} \cdot \frac{b}{\sqrt{2}} = 2 \cdot a \cdot b$

Figure 4.9 Area of biggest square enclosed by a circle in the CAC model formulation and area of biggest rectangle enclosed by an ellipse in the EAC model formulation

Therefore, the final form of constraint (4.3) for the EAC model formulation is as shown in equation 4.15.

$$\left\lceil \frac{TA}{\pi ab} \right\rceil \leq t \leq N, \ \ where\ N \approx \left\lceil \frac{TA}{2ab} \right\rceil \tag{4.15}$$

4.4.2. The Coverage Area of a Directional Antenna

A concept similar to that described in section 4.2.2 can be applied when an RFID reader with an elliptical coverage area is utilized. An ellipse has two important geometric features, i.e., the length of its major axis (*2a*) and the length of its minor axis (*2b*), as previously shown in

Figure 4.8. As opposed to a circle, the distance from the center of an ellipse to any point on its boundary is not constant. Because of this, the equation of an ellipse changes as the rotation angle is changed, thus making the calculation of the equation of a coverage area with an elliptical shape more challenging than that of a coverage area with circular shape.

Once the equation of a coverage area with an elliptical shape that considers the changes in rotation angle has been obtained, it can be used to determine whether or not an RFID tag is located within the elliptical coverage area of an RFID reader. There are several steps needed to accomplish this, as follows:

1. The standard form of the equation of the ellipse can be used to approximate the elliptical antenna coverage area in the H-Plane of the directional patch antenna, as shown by equation 4.16.

$$\frac{(x-h)^2}{a^2}+\frac{(y-k)^2}{b^2}=1 \tag{4.16}$$

2. However, equation 4.16 changes as the rotation angle changes. Thus, the standard form of the equation of the ellipse has to be re-written to account for this, as shown in equation 4.17. Equation 4.17 considers the concept of the rotation of axes found in Hughes & Chraibi (2011) and reduces to equation 4.16 if the rotation angle is zero.

$$\frac{\left[\cos(\theta_i)\cdot(x-h)+\sin(\theta_i)\cdot(y-k)\right]^2}{a^2}+\frac{\left[-\sin(\theta_i)\cdot(x-h)+\cos(\theta_i)\cdot(y-k)\right]^2}{b^2}=1 \tag{4.17}$$

Equation 4.13 can be expressed in an implicit form as shown in equation 4.18.

$$Ax^2+Bxy+Cy^2+Dx+Ey+F=0 \tag{4.18}$$

Where:

$$A = \frac{[\cos(\theta_i)]^2}{a^2} + \frac{[\sin(\theta_i)]^2}{b^2} \tag{4.18a}$$

$$B = 2\frac{\cos(\theta_i)\sin(\theta_i)}{a^2} - 2\frac{\cos(\theta_i)\sin(\theta_i)}{b^2} \tag{4.18b}$$

$$C = \frac{[\sin(\theta_i)]^2}{a^2} + \frac{[\cos(\theta_i)]^2}{b^2} \tag{4.18c}$$

$$D = 2\frac{(-\cos(\theta_i)\cdot h - \sin(\theta_i)\cdot k).\cos(\theta_i)}{a^2} - 2\frac{(\sin(\theta_i)\cdot h - \cos(\theta_i)\cdot k).\sin(\theta_i)}{b^2} \tag{4.18d}$$

$$E = 2\frac{(-\cos(\theta_i)\cdot h - \sin(\theta_i)\cdot k).\sin(\theta_i)}{a^2} + 2\frac{(\sin(\theta_i)\cdot h - \cos(\theta_i)\cdot k).\cos(\theta_i)}{b^2} \tag{4.18e}$$

$$F = \frac{(-\cos(\theta_i)\cdot h - \sin(\theta_i)\cdot k)^2}{a^2} + \frac{(\sin(\theta_i)\cdot h - \cos(\theta_i)\cdot k)^2}{b^2} - 1 \tag{4.18f}$$

3. The semi-major axis (*a*), the semi-minor axis (*b*), and the location coordinates of the center of ellipse (*h*, *k*) have to be determined and input into equation 4.17 or 4.18 to verify whether or not an RFID tag is located within the elliptical coverage area of the RFID reader. The semi-major axis (*a)* and the semi-minor (*b)* axis are approximated using equation 4.19 and equation 4.20, respectively (Marrocco et al., 2009).

$$a = \frac{\lambda}{8\pi}\sqrt{\chi\frac{EIRP}{P_R}} \tag{4.19}$$

$$b = a\sqrt{\tan\frac{HPBW}{2} \times \frac{\sin\frac{HPBW}{2}}{\sqrt{2} - \cos\frac{HPBW}{2}}} \tag{4.20}$$

Where:

$EIRP = P_t G_t =$ Transmitted Power × Gain

χ : Polarization coefficient

P_R : Received threshold power

$HPBW$: Half power beam width of the RFID reader antenna.

In the EAC model formulation, the patch antenna of the RFID reader is assumed to have either circular or elliptical polarization, whereas the dipole antenna of the RFID tag is assumed to have linear polarization. This polarization mismatch is the reason why a polarization loss value (i.e., χ) of 0.5 is applied in the calculation of the semi-major axis (Marrocco et al., 2009). The polarization coefficient χ would have a value of one if both antennas had the same polarization type.

The HPBW is sometimes referred to as the *-3 dB beam width* because it is calculated from the position in the radiation patterns of the E-plane and the H-plane where the gain of an antenna is reduced by 3 dB from the maximum gain in the preferred direction.

4. Since the placement coordinates, *a*, *b*, and θ_i of the RFID reader are known, the center of the ellipse (*h, k*) can be calculated using trigonometry. As an example, consider Figure 4.10 that shows an RFID reader located at coordinates (*i, j*) = (0.5, 0.5). The rotation angle of the elliptical coverage area produced by this RFID reader is 45 degrees and *a* is assumed to be 1.5 meters.

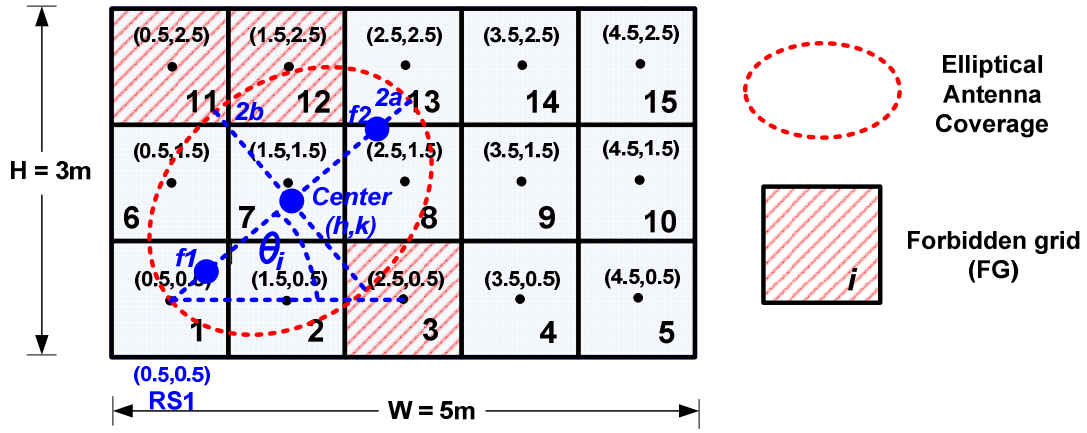

Figure 4.10 The placement of RFID readers using the elliptical antenna coverage

Considering the values of the parameters depicted in Figure 4.10, the coordinates of the center of the ellipse (*h*, *k*) are derived using equation 4.21 and result in the values (1.56, 1.56).

$$(h,k) = \left(i + a \cdot \cos(\theta_i),\ j + a \cdot \sin(\theta_i)\right) = \left(0.5 + 1.5 \cdot \cos(45^\circ),\ 0.5 + 1.5 \cdot \sin(45^\circ)\right) \quad (4.21)$$

5. After the center of the ellipse (*h*, *k*) is derived and a, b, *and* θ_i are also known, the elliptical coverage area of a directional patch antenna at any rotation angle can be calculated and expressed in the format shown in equation 4.18. The coefficients of this equation can be computed using equations 4.18a to 4.18f.
6. To identify whether or not each grid *i* and RFID tags located at coordinates (*x*, *y*) in the system are covered by the elliptical antenna coverage area, equation 4.22 has to be satisfied.

$$Ax^2 + Bxy + Cy^2 + Dx + Ey + F \leq 0 \quad (4.22)$$

The elliptical shape of the coverage area of a directional antenna can also be derived from the focal points, i.e., *f1* and *f2* (see Figure 4.10) and the Euclidean distance from each focal point to the center of grid *i*. The values of *a, b,* θ_i and the center of ellipse *(h, k)* are derived using the same procedure described in step 3 and step 4 above. The calculation of the coordinates of the focal points; the calculation of the Euclidean distance from each focal point to the center of a particular grid *i*; and the justification of whether or not grid *i* is covered by the RFID reader is accomplished via the following steps:

1. In order to find the (*x, y*) coordinates of the focal points of the elliptical antenna coverage area, the distance from the center of the elliptical coverage area to the focal points has to be computed first. This distance (referred to as *c*) is calculated using the values *a* and *b*, as shown in equation 4.23.

$$c = \sqrt{a^2 - b^2} \tag{4.23}$$

2. The (*x, y*) coordinates of the first focal point (*f1*) and the second focal point (*f2*) are then calculated using equations 4.24 and 4.25, respectively. The (*x, y*) coordinates of the first focal point (*f1*) are calculated as follows:

$$x_1 = h - c\cos\theta_i \tag{4.24a}$$

$$y_1 = k - c\sin\theta_i \tag{4.24b}$$

The (x, y) coordinates of the second focal point (*f2*) are calculated as follows:

$$x_2 = h + c\cos\theta_i \tag{4.25a}$$

$$y_2 = k + c\sin\theta_i \tag{4.25b}$$

3. For the elliptical antenna coverage, two Euclidean distances need to be calculated:

   (1) $d1_{ij}$ = distance from the first focal point $f_1(x_1, y_1)$ to the center of grid $i(x, y)$.

   (2) $d2_{ij}$ = distance from the second focal point $f_2(x_2, y_2)$ to the center of grid $i(x, y)$.

   These Euclidean distances are calculated using equations 4.26 and 4.27, respectively.

$$d1_{ij} = \sqrt{(x - x_1)^2 + (y - y_1)^2} \tag{4.26}$$

$$d2_{ij} = \sqrt{(x - x_2)^2 + (y - y_2)^2} \tag{4.27}$$

4. To identify whether or not each grid i and RFID tags located at coordinates (x, y) in the system are covered by the elliptically-shaped coverage area, equation 4.28 has to be satisfied.

$$d1_{ij} + d2_{ij} \leq 2a \tag{4.28}$$

4.5. Application of the EAC Model Formulation

The facility depicted in Figure 4.3 is also used to demonstrate the application of the EAC model formulation. Therefore, the facility dimensions, forbidden grids and feasible area are the same as those mentioned in section 4.3.1.

4.5.1. Major Axis (2a) and Minor Axis (2b) of the Antenna Coverage Area

The semi-major axis *(a)* and the semi-minor axis *(b)* of the elliptical coverage area of the RFID reader's antenna are calculated using equation 4.19 and equation 4.20. For the purposes of this example, the major axis and minor axis of the elliptical coverage area of the RFID reader's antenna are assumed to be approximately 3.60 and 2.50 meters, respectively. If the values a = 1.8 meters and b = 1.25 meters are then used to calculate the area of an ellipse with the formula $Area = \pi \cdot a \cdot b$, the resulting coverage area is the same as that assumed in the CAC model formulation using a radius of 1.50 meters and the formula $Area = \pi \cdot r^2$.

4.5.2. Initial Number of RFID Readers

As before, an initial number of RFID readers (N) is calculated first. In the EAC model formulation, the ellipse packing (EP) algorithm is used to calculate *N*. The objective of this algorithm is to pack the biggest rectangle enclosed by an ellipse in the rectangular-shaped facility (Efrat et al., 2004). For the rectangular facility used in this example, Figure 4.11 shows that the EP algorithm determines that the initial number of RFID readers is three. However, placing three RFID readers as shown in Figure 4.11 will not be allowed because all three RFID readers cannot be located at a forbidden grid or outside of the facility. Thus, the location of the three RFID readers is modified as shown in Figure 4.12 so that their

placements are valid. The RFID reader coverage scenario depicted in Figure 4.12 will be used to further demonstrate the problem and to validate the EAC model formulation.

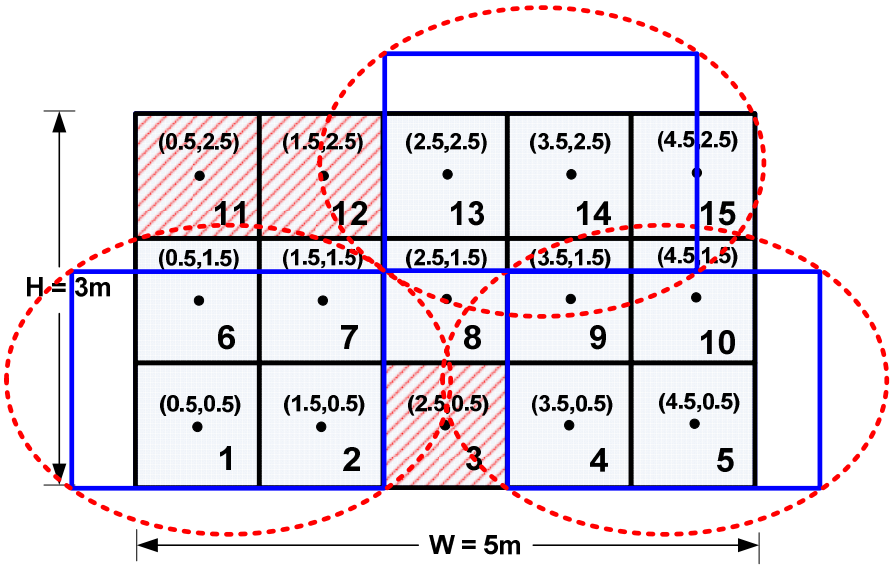

Figure 4.11 Coverage of the rectangular facility using the concept of ellipse packing

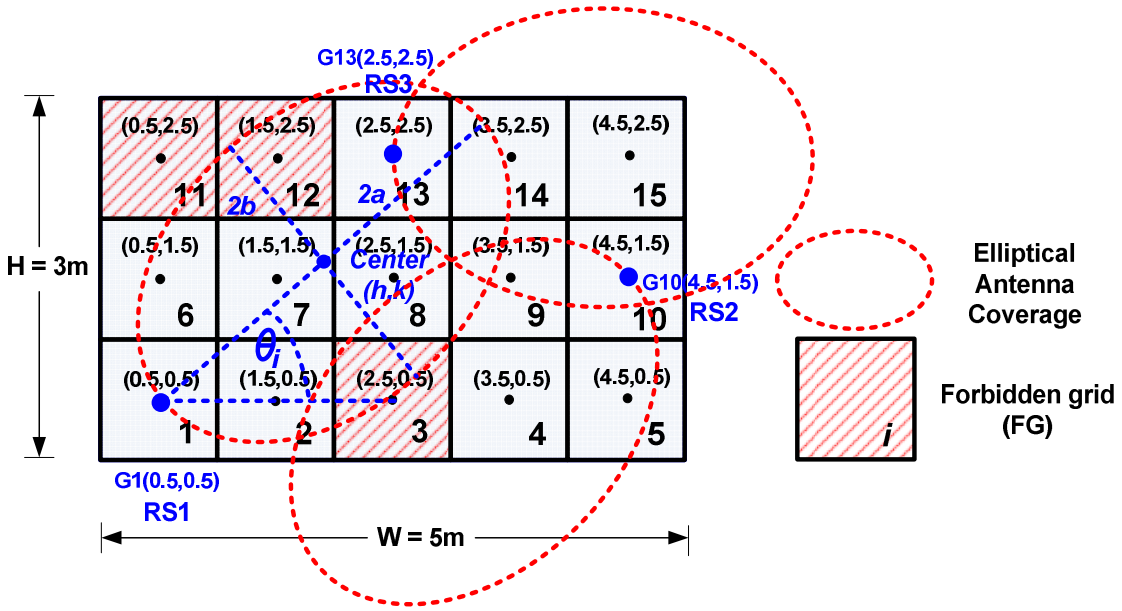

Figure 4.12 Correction to the initial ellipse packing coverage to be eligible in the system

Figure 4.12 shows RFID readers located at the center of grids 1, 10 and 13. Therefore, the set of installed RFID readers is $RS = \{1,10,13\}$ and the number of RFID readers installed t = 3. The coordinates of the grids 1, 10 and 13 are (0.5, 0.5), (4.5, 0.5), and (2.5, 2.5), respectively.

4.5.3. Downlink Communication Channel

The signal transmission power of the downlink communication channel in the EAC model formulation can be obtained by applying the same concept used in the CAC model formulation.

Two Euclidean distances (i.e., $d1_{ij}$ and $d2_{ij}$) need to be calculated before the set of RFID readers that can cover the center of grid *i* (i.e., N_i) can be identified. Therefore, the calculation of the set N_i in the EAC model formulation is different from that of the CAC model formulation. The set N_i is calculated using equation 4.29.

$$N_i = \left\{ j \,\middle|\, d1_{ij} + d2_{ij} \le 2a \cap i \notin FG \right\} \tag{4.29}$$

Equation 4.29 implies that for an RFID reader (located at grid *j*) to cover grid *i*, the following two conditions must be met:

1) The summation of the Euclidean distances $d1_{ij}$ and $d2_{ij}$ must be less than or equal to the length of the major axis (*2a*) of the elliptical coverage area of the RFID reader located at grid *j*, and
2) The grid *i* is not a forbidden grid.

For the rectangular facility depicted in Figure 4.12, the sets $N_i \ \forall i$ are as follows:

$$N_1 = \{1\}, \quad N_2 = \{1\}, \quad N_3 = \phi, \quad N_4 = \{10\}, \quad N_5 = \{10\},$$
$$N_6 = \{1\}, \quad N_7 = \{1\}, \quad N_8 = \{1\}, \quad N_9 = \{10,13\}, \quad N_{10} = \{10,13\},$$
$$N_{11} = \phi, \quad N_{12} = \phi, \quad N_{13} = \{1,13\}, \quad N_{14} = \{13\}, \quad N_{15} = \{13\}$$

Next, the set of maximum signal power levels received at grid *i* from the RFID reader located at grid *j* is determined using the equation $D_i(\max) = \{\max(D_{i,j})\}$. This can be computed using a similar procedure to that used in the CAC model formulation (see Figure 4.6). However, the process for calculating the Euclidean distance needs to be changed as previously mentioned at the beginning of this section. Thirteen out of fifteen sets of $D_i(\max)$ are the same as in section 4.3.4. However, sets $D_8(\max)$ and $D_{15}(\max)$ are different. In the case of the EAC model formulation, the maximum signal power levels received at grid 8 and 15 are from the RFID readers located at grids 1 and 13, respectively. This results in the sets $D_8(\max)$ and $D_{15}(\max)$ being:

$$D_8(\max) = \{\max(D_{8,1}, D_{8,10}, D_{8,13})\} = \{D_{8,1}\}$$
$$D_{15}(\max) = \{\max(D_{15,1}, D_{15,10}, D_{15,13})\} = \{D_{15,13}\}$$

In order to quantify the SIR in the downlink communication channel in the EAC model formulation, the sets of IS_i and $ID_i(\max)$ have to be obtained. The same definition of an *interfering reader* used in the CAC model formulation applies for the EAC model

formulation, i.e., an RFID reader is labeled as an *interfering reader* if and only if the coverage area of its antenna covers the center of grid *i* but it is not the strongest signal received (i.e., it is not the $D_i(\max)$). For the example depicted in Figure 4.12, interference can occur only in grids 9, 10, and 13. Additionally, the sets IS_i and $ID_i(\max)$ are defined as follows:

$$IS_1 = \phi, \quad IS_2 = \phi, \quad IS_3 = \phi, \quad IS_4 = \phi, \quad IS_5 = \phi,$$
$$IS_6 = \phi, \quad IS_7 = \phi, \quad IS_8 = \phi, \quad IS_9 = \{13\}, \quad IS_{10} = \{13\},$$
$$IS_{11} = \phi, \quad IS_{12} = \phi, \quad IS_{13} = \{1\}, \quad IS_{14} = \phi, \quad IS_{15} = \phi,$$

$$ID_9(\max) = \{(D_9(\max))_{13}\} = \{(D_{9,10})_{13}\}$$
$$ID_{10}(\max) = \{(D_{10}(\max))_{13}\} = \{(D_{10,10})_{13}\}$$
$$ID_{13}(\max) = \{(D_{13}(\max))_1\} = \{(D_{13,13})_1\}$$

4.5.4. Uplink Communication Channel

The signal transmission power, interference and SIR of the uplink communication channel are computed in a same manner to that of the downlink communication channel. The results for the EAC model formulation are very similar to those presented for the CAC model formulation, with some exceptions:

$$U_8(\max) = \{\max(U_{8,1}, U_{8,10}, U_{8,13})\} = \{U_{8,1}\}$$
$$U_{15}(\max) = \{\max(U_{15,1}, U_{15,10}, U_{15,13})\} = \{U_{15,13}\}$$

$$IU_9(\max) = \{(U_9(\max))_{13}\} = \{(U_{9,10})_{13}\}$$

$$IU_{10}(\max) = \{(U_{10}(\max))_{13}\} = \{(U_{10,10})_{13}\}$$

$$IU_{13}(\max) = \{(U_{13}(\max))_{1}\} = \{(U_{13,13})_{1}\}$$

4.5.5. Assembling the Multi-Objective Function

After all necessary parameters are known, they are substituted into equation 4.1 in order to compute the objective function for the rectangular facility scenario. The objective function of the EAC model formulation for the rectangular facility depicted in Figure 4.12 is derived as follows:

$$\begin{aligned} Maximize:\ Z \;=\;& 0.6 \cdot \frac{\sum_{i=1}^{15} y_i}{\sum_{i=1}^{15} \beta_i} \\ &+\ 0.2 \cdot \frac{\sum_{i=1}^{15} \sum_{j=N_i} \left(\max\left(D_{i,j}\right)\right)}{\sum_{i=1}^{15} \sum_{j=N_i} \left(\max\left(D_{i,j}\right)\right) + \sum_{i=1}^{15} \sum_{j=N_i} \sum_{k=IS_i} \left(\left(\max\left(D_{i,j}\right)\right)_k\right)} \\ &+\ 0.2 \cdot \frac{\sum_{i=1}^{15} \sum_{j=N_i} \left(\max\left(U_{i,j}\right)\right)}{\sum_{i=1}^{15} \sum_{j=N_i} \left(\max\left(U_{i,j}\right)\right) + \sum_{i=1}^{15} \sum_{j=N_i} \sum_{k=IS_i} \left(\left(\max\left(U_{i,j}\right)\right)_k\right)} \\ &+\ 0.2 \cdot \frac{10{,}000 \;-\; (1{,}000 \times t)}{10{,}000} \end{aligned}$$

$$Maximize: Z = 0.6 \cdot \frac{\left[(\pi D_1 \cdot \pi U_1 \cdot \beta_1) + (\pi D_2 \cdot \pi U_2 \cdot \beta_2) + \ldots + (\pi D_{14} \cdot \pi U_{14} \cdot \beta_{14}) + (\pi D_{15} \cdot \pi U_{15} \cdot \beta_{15})\right]}{12}$$

$$+ \ 0.2 \cdot \frac{\left[\sum_{j=\{1\}} \max\left(D_{1,j}\right) + \sum_{j=\{1\}} \max\left(D_{2,j}\right) + \sum_{j=\phi} \max\left(D_{3,j}\right) + \ldots + \sum_{j=\{13\}} \max\left(D_{14,j}\right) + \sum_{j=\{13\}} \max\left(D_{15,j}\right)\right]}{\left[\sum_{j=\{1\}} \max\left(D_{1,j}\right) + \sum_{j=\{1\}} \max\left(D_{2,j}\right) + \sum_{j=\phi} \max\left(D_{3,j}\right) + \ldots + \sum_{j=\{13\}} \max\left(D_{14,j}\right) + \sum_{j=\{13\}} \max\left(D_{15,j}\right)\right] + \left[\begin{array}{c} \sum_{j=\{1\}} \left(\left(\max\left(D_{1,j}\right)\right)_0\right) + \sum_{j=\{1\}} \left(\left(\max\left(D_{2,j}\right)\right)_0\right) + \sum_{j=\phi} \left(\left(\max\left(D_{3,j}\right)\right)_0\right) + \ldots + \\ \sum_{j=\{1,13\}} \left(\left(\max\left(D_{13,j}\right)\right)_1\right) + \sum_{j=\{13\}} \left(\left(\max\left(D_{14,j}\right)\right)_0\right) + \sum_{j=\{13\}} \left(\left(\max\left(D_{1,j}\right)\right)_0\right) \end{array}\right]}$$

$$+ \ 0.2 \cdot \frac{\left[\sum_{j=\{1\}} \max\left(U_{1,j}\right) + \sum_{j=\{1\}} \max\left(U_{2,j}\right) + \sum_{j=\phi} \max\left(U_{3,j}\right) + \ldots + \sum_{j=\{13\}} \max\left(U_{14,j}\right) + \sum_{j=\{13\}} \max\left(U_{15,j}\right)\right]}{\left[\sum_{j=\{1\}} \max\left(U_{1,j}\right) + \sum_{j=\{1\}} \max\left(U_{2,j}\right) + \sum_{j=\phi} \max\left(U_{3,j}\right) + \ldots + \sum_{j=\{13\}} \max\left(U_{14,j}\right) + \sum_{j=\{13\}} \max\left(U_{15,j}\right)\right] + \left[\begin{array}{c} \sum_{j=\{1\}} \left(\left(\max\left(U_{1,j}\right)\right)_0\right) + \sum_{j=\{1\}} \left(\left(\max\left(U_{2,j}\right)\right)_0\right) + \sum_{j=\phi} \left(\left(\max\left(U_{3,j}\right)\right)_0\right) + \ldots + \\ \sum_{j=\{1,13\}} \left(\left(\max\left(U_{13,j}\right)\right)_1\right) + \sum_{j=\{13\}} \left(\left(\max\left(U_{14,j}\right)\right)_0\right) + \sum_{j=\{13\}} \left(\left(\max\left(U_{1,j}\right)\right)_0\right) \end{array}\right]}$$

$$+ \ 0.2 \cdot \frac{10{,}000 - (1{,}000 \times 3)}{10{,}000}$$

$$Maximize: Z = 0.6 \cdot \frac{\left[\begin{array}{c} (1 \cdot 1 \cdot 1) + (1 \cdot 1 \cdot 1) + (1 \cdot 1 \cdot 0) + (1 \cdot 1 \cdot 1) + (1 \cdot 1 \cdot 1) + \\ (1 \cdot 1 \cdot 1) + (1 \cdot 1 \cdot 1) + (1 \cdot 1 \cdot 1) + (1 \cdot 1 \cdot 1) + (1 \cdot 1 \cdot 1) + \\ (0 \cdot 0 \cdot 0) + (1 \cdot 1 \cdot 0) + (1 \cdot 1 \cdot 1) + (1 \cdot 1 \cdot 1) + (1 \cdot 1 \cdot 1) \end{array}\right]}{12}$$

$$+ 0.2 \cdot \frac{\left[D_{1,1} + D_{2,1} + 0 + \ldots + D_{14,13} + D_{15,13}\right]}{\left[D_{1,1} + D_{2,1} + 0 + \ldots + D_{14,13} + D_{15,13}\right] + \left[\left(D_{9,10}\right)_{13} + \left(D_{10,10}\right)_{13} + \left(D_{13,13}\right)_1\right]}$$

$$+ 0.2 \cdot \frac{\left[U_{1,1} + U_{2,1} + 0 + \ldots + U_{14,13} + U_{15,13}\right]}{\left[U_{1,1} + U_{2,1} + 0 + \ldots + U_{14,13} + U_{15,13}\right] + \left[\left(U_{9,10}\right)_{13} + \left(U_{10,10}\right)_{13} + \left(U_{13,13}\right)_1\right]}$$

$$+ \ 0.2 \cdot 0.7$$

$$Maximize: Z = 0.74 + 0.2 \cdot \left[\begin{array}{c} \dfrac{\left[D_{1,1} + D_{2,1} + 0 + \ldots + D_{14,13} + D_{15,13}\right]}{\left[D_{1,1} + D_{2,1} + 0 + \ldots + D_{14,13} + D_{15,13}\right] + \left[\left(D_{9,10}\right)_{13} + \left(D_{10,10}\right)_{13} + \left(D_{13,13}\right)_{1}\right]} \\ + \dfrac{\left[U_{1,1} + U_{2,1} + 0 + \ldots + U_{14,13} + U_{15,13}\right]}{\left[U_{1,1} + U_{2,1} + 0 + \ldots + U_{14,13} + U_{15,13}\right] + \left[\left(U_{9,10}\right)_{13} + \left(U_{10,10}\right)_{13} + \left(U_{13,13}\right)_{1}\right]} \end{array} \right]$$

4.6. Effect of Passive Interference on RFID Antenna Coverage

Warehouse facilities contain multiple sources of passive interference such as walls and material handling equipment. Therefore, the strength of an RF signal in these environments is affected not only by attenuation due to the distance from the source but also by attenuation as the RF signal travels through obstructions. The resulting effect of these combined factors is an antenna coverage area that is not a perfect circle and a perfect ellipse, as it is initially assumed by the CAC and EAC model formulations, respectively.

Therefore, the effect of passive interference on the shape of the RFID antenna coverage was considered and modeled prior to finding feasible solutions to the RNP for both the CAC and EAC model formulations. The following sections describe the approaches used to accomplish this.

4.6.1. Modeling the Effect of Passive Interference on a Circular Antenna Coverage Area

The modified shape of the coverage area of an RFID omnidirectional antenna due to the effect of passive interference was derived using its idealized circular coverage area as a basis and then applying a *ray tracing* technique. In ray tracing, RF signals emitted from the transmitter (i.e., RFID reader) are treated as rays, which are traced geometrically as they interact with the surrounding objects before finally arriving at the receiver (i.e., RFID tag) (Imai, 2007). The main objective in ray tracing is to obtain the path length of each ray after the propagation losses due to passive interference are considered, thus enabling the generation of the modified shape of the antenna coverage area. The steps needed to accomplish this were as follows:

1. Determine the candidate grids and forbidden grids (FGs) covered by the circular coverage area of the omnidirectional antenna. Figure 4.13 shows an example where the omnidirectional antenna of an RFID reader is located at the center of candidate grid 7 with coordinates (h, k) = (1.5, 1.5). The circular coverage area of the omnidirectional antenna covers candidate grids 1, 2, 4, 6, 7, 8, 13, 14, and 18 and the FGs 3, 9, 11, 12, 16, and 17.

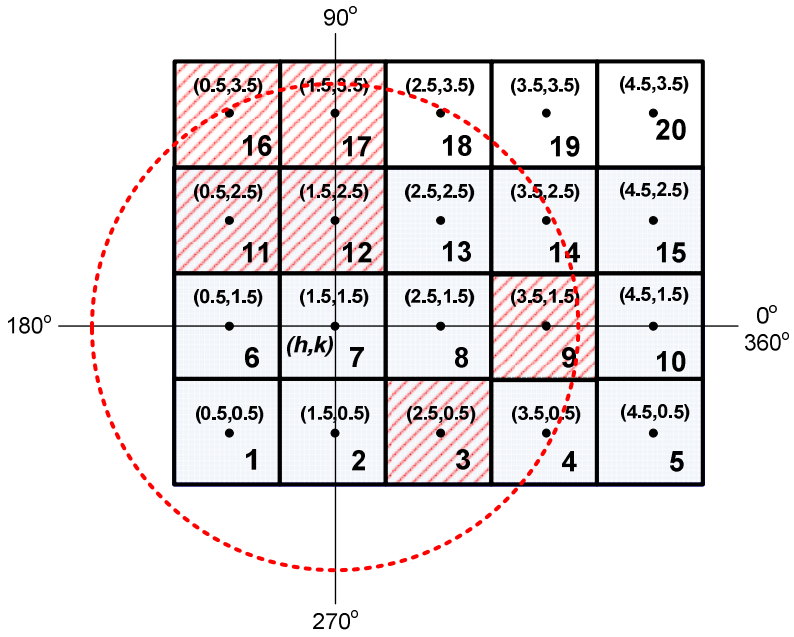

Figure 4.13 Regular grids and forbidden grids covered by the circular coverage area

2. Starting at zero degrees and using increments of 22.5 degrees, define 16 points $P_i \; \forall \, i = 1,2,...,16$ on the perimeter of the circular coverage area and determine their coordinates $(x_i, y_i) \forall \, i = 1,2,...,16$ using equations 4.30a and 4.30b, where the variable r represents the *radius* of the circular coverage area.

$$x_i = h + r\cos\theta \tag{4.30a}$$

$$y_i = k + r\sin\theta \tag{4.30b}$$

It is important to note that the degree increment in this step is adjustable. However, preliminary experiments showed that increments of 22.5 degrees allow the optimization algorithms (i.e., GA and PSO) to obtain good results within a reasonable computation time.

3. Each of the 16 perimeter points P_i identified in step 2 represents the end point of a ray $R_i \; \forall \, i = 1,2,...,16$. Using equation 4.31, calculate the slope $S_i \; \forall \, i = 1,2,...,16$ of each ray $R_i \; \forall \, i = 1,2,...,16$ originating from the center (*h*,*k*) of the circular coverage area and ending on a perimeter point $P_i \; \forall \, i = 1,2,...,16$ with coordinates (x_i,y_i).

$$Slope_i \, (S_i) = tan \, \theta = \frac{k - y_i}{h - x_i} \; ; \;\; i = 1,2,3,...,16 \tag{4.31}$$

As an example, Figure 4.14 shows rays R_1, R_2, …, R_6, their perimeter points P_1, P_2, …, P_6 and a table with their corresponding slope values S_1, S_2, …, S_6. The top part of Figure 4.14 illustrates how the value of the slope S_i of a ray R_i can be used to identify its location within the circular coverage area, as follows:

- A ray R_i whose slope S_i is *positive* is located in either quadrant 1 (Q1) or quadrant 3 (Q3).
- A ray R_i whose slope S_i is *negative* is located in either quadrant 2 (Q2) or quadrant 4 (Q4).
- A ray R_i whose slope S_i is *zero* lies on the X-axis.
- A ray R_i whose slope S_i is *infinity* (i.e., $+\infty$ or $-\infty$) lies on the Y-axis.

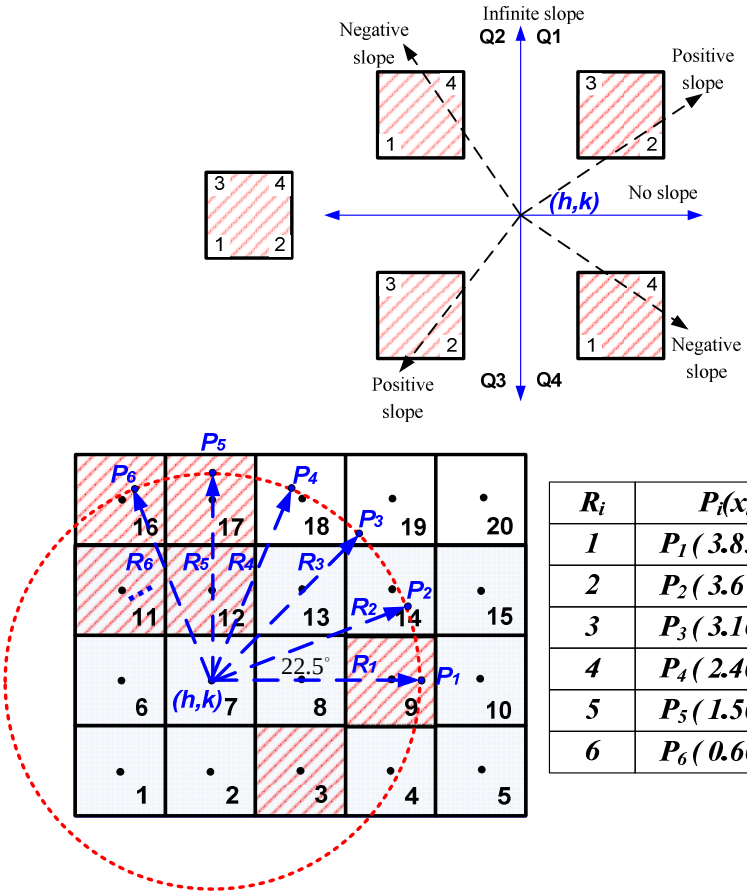

R_i	$P_i(x_i, y_i)$	$Slope_i$ (S_i)
1	P_1 (3.85, 1.50)	0.000
2	P_2 (3.67, 2.40)	0.414
3	P_3 (3.16, 3.16)	1.000
4	P_4 (2.40, 3.67)	2.414
5	P_5 (1.50, 3.85)	$+\infty$
6	P_6 (0.60, 3.67)	-2.414

Figure 4.14 Slope values of perimeter points and locations within the circular coverage area

4. Compute the number of obstructions (i.e., walls) that each ray $R_i \; \forall \, i = 1,2,...,16$ crosses. This is done in several steps:

   a) Calculate the slopes $S_j \; \forall \, j$ of the lines originating from the center (*h*, *k*) of the circular coverage area and ending at the center (x_j, y_j) of each FG_j covered by the circular coverage area. The slopes $S_j \; \forall \, j$ can be either *positive*, *negative*, *zero*, or *infinity*. From Figure 4.14, the center (*h*, *k*) of the circular coverage area is located at (1.5, 1.5), whereas the coordinates (x_j, y_j) of FG_3 and FG_{12} are (2.5, 0.5) and (1.5, 2.5), respectively. Using equation 4.31, the

slopes of the lines from (h, k) to the centers (x_j, y_j) of FG_3 and FG_{12} are -1 and $+\infty$, respectively.

b) To determine the quadrant(s) and/or axis in which each FG_j covered by the circular coverage area is located, the slopes $S_j \ \forall \ j$ calculated in the previous step are used in conjunction with the signs of the coordinates (x_j,y_j) of the center of the FG_j. The signs of the coordinates (x_j, y_j) are set relative to the quadrants formed by the center (h, k) of the circular coverage area, as shown in Table 4.2.

Table 4.2 Location of an FGj based on the relationship between its slope and the signs of the coordinates (x_j, y_j) of its center

		SLOPE			
		(1)	***(2)***	***(3)***	***(4)***
		+	-	0	$\pm\infty$
(x,y) Center of FG	*x +*	*Q1*	*Q4*	*X-Axis, Q1, Q4*	-
	x −	*Q3*	*Q2*	*X-Axis, Q2, Q3*	-
	y +	*Q1*	*Q2*	-	*Y-Axis, Q1, Q2*
	y −	*Q3*	*Q4*	-	*Y-Axis, Q3, Q4*

For example, the value of the slope for FG_3 is -1 and the signs of its coordinates (x_j, y_j) are ($+x$, $-y$). Thus, from Table 4.2, FG_3 is located in Q4. On the other hand, the slope of FG_{12} is $+\infty$ and the signs of its coordinates (x_j, y_j) are (0, $+y$). From Table 4.2, this indicates that FG_{12} lies on the Y-axis of the circular coverage area and it is also located in both Q1 and Q2. As the latter example illustrates, a FG_j can be located in one quadrant or in more

than one quadrant and an axis (i.e., X or Y). Table 4.3 shows the location(s) of all FG_j in Figure 4.14.

Table 4.3 Location of FGs for the example in Figure 4.14

	(1)	(2)	(3)	(4)	(5)	(6)
FG_j	**Q1**	**Q2**	**Q3**	**Q4**	**X-Axis**	**Y-Axis**
3				✓		
9	✓			✓	✓	
11		✓				
12	✓	✓				✓
16		✓				
17	✓	✓				✓

c) Once the location of all $FG_j \; \forall \; j$ is known, compare the slope $S_i \; \forall \; i = 1,2,...,16$ of each ray $R_i \; \forall \; i = 1,2,...,16$ to the cases shown in Table 4.4 and Table 4.5. The $FG_j \; \forall \; j$ considered in the comparison to the slope S_i of each ray R_i are only those that are located in the same quadrant or that lie on the same axis as the ray R_i. For instance, only FG_9 is considered for R_1 because both the FG and the ray lie on the X-axis of the circular coverage area (see Figure 4.14 and column 5 in Table 4.3). On the other hand, since R_6 is located in Q2, then FG_{11}, FG_{12}, FG_{16}, and FG_{17} are considered in the slope comparison because they are also located in Q2 (see Figure 4.14 and column 2 in Table 4.3). If the ray R_i has no slope (i.e., slope is *zero*) or an infinite

slope, the criteria in Table 4.4 must be used. If the ray R_i has either a positive or a negative slope, the criteria in Table 4.5 must be used. In the latter case, the slope S_i of the ray R_i is compared to the slopes of two lines originating from the center (*h*, *k*) of the circular coverage area and ending at two specific corners of the $FG_j \ \forall \ j$ covered by the circular coverage area.

Consider R_1 in Figure 4.14 which lies on the X-axis of the circular coverage area and has a slope of zero (see equation 4.31). Column 5 of Table 4.3 shows that only FG_9 lies on the X-axis and, therefore, Case 1 in Table 4.4 is applied. The sign of the x_j coordinate of the center of FG_9 is checked to determine where the FG_9 is located. In general, if the sign of the x_j coordinate of the center of a particular FG_j is *positive*, that FG_j lies on the X-axis at 0°, i.e., it follows the same direction as R_1. If the sign of the x_j coordinate of the center of a particular FG_j is *negative*, then that FG_j lies on the X-axis at 180^o, i.e., it follows the same direction as R_9. The number of walls used to modify the path length of a ray that is located at 0^o (e.g., ray 1) is the number of FGs that lay on the X-axis and that have a *positive* x_j coordinate. The number of walls of a ray that is located at 180^o (e.g., R_9) is the number of FGs that lie on the X-axis and that have a *negative* x_j coordinate. In this example, the sign of the x_j coordinate of the center of FG_9 is *positive*; therefore, FG_9 is located at 0^o and R_1 passes through one wall.

Table 4.4 Criteria for slope comparison of the ray with no slope or infinite slope

	FG on X-Axis	**FG on Y-Axis**
Case 1: No slope. ***The ray lies along the X-axis of the circular coverage area (i.e., slope is zero).***	No slope comparison with slopes of two corners of FGs. Check the sign of the coordinate x_j of the center of the $FG_j \ \forall \ j$ having a slope of zero corresponding to angle 0° or angle 180° and determine (i.e., count) how many FGs the ray crosses.	-
Case 2: Infinite slope. ***The ray lies along the Y-axis of the circular coverage area.***	-	No slope comparison with slopes of two corners of FGs. Check the sign of the coordinate y_j of the center of the $FG_j \ \forall \ j$ having a slope of infinity corresponding to angle 90° or angle 270° and determine (i.e., count) how many FGs the ray crosses.

Table 4.5 Criteria for slope comparison of the ray with positive or negative slope

	Quadrant 1 (Q1)		**Quadrant 2 (Q2)**		**Quadrant 3 (Q3)**		**Quadrant 4 (Q4)**	
	FG not on Y-Axis	**FG on Y-Axis**	**FG not on Y-Axis**	**FG on Y-Axis**	**FG not on Y-Axis**	**FG on Y-Axis**	**FG not on Y axis**	**FG on Y-Axis**
Case 1: Positive slope. The ray points to Q1 or Q3.	Slope of corner 2 and 3	Slope of corner 2 and $+\infty$	-	-	Slope of corner 2 and 3	Slope of corner 3 and $-\infty$	-	-
Case 2: Negative slope. The ray points to Q2 or Q4.	-	-	Slope of corner 1 and 4	Slope of corner 1 and $-\infty$	-	-	Slope of corner 1 and 4	Slope of corner 4 and $+\infty$

In Figure 4.14, R_6 is used as an example of a ray that does not lie on an axis. R_6 points to Q2 at 112.5° and the value of S_6 is -2.414. Four FG_j are located in Q2, i.e., FG_{11}, FG_{12}, FG_{16} and FG_{17}, as shown in Table 4.3. Therefore, Case 2 in Table 4.5 is applied. Two categories of FGs located in Q2 are considered, i.e., *FGs not on Y-axis* (FG_{11} and FG_{16}) and *FGs on Y-axis* (FG_{12} and FG_{17}). For FGs that do not lie on the Y-axis, the slope of the ray must be compared to the slopes of two lines originating from the center *(h, k)* of the circular antenna coverage area and ending at the coordinates (x_m, y_m) of corner 1 and corner 4 of the FGs. For FGs that lie on the Y-axis, the slope of the ray must be compared to the slope of a line drawn from the center *(h, k)* of the circular antenna coverage area to the coordinate (x_m, y_m) of corner 1 of the FG and the slope of -∞. Table 4.5 shows the slope comparison between R_6 and the corner points for the FGs located in Q2.

Table 4.6 Slope comparison between R_6 and the corner points of the FGs located in Q2

FG_j	FG Location	S_6	FGS_1	FGS_4	$-\infty$	Crossed by R_6 ?
11	not on Y-axis	-2.41421	-0.3333	-3.0000	-	Yes
12	on Y-axis	-2.41421	-1.0000	-	$-\infty$	Yes
16	not on Y-axis	-2.41421	-1.0000	-5.0000	-	Yes
17	on Y-axis	-2.41421	-3.0000	-	$-\infty$	No

Table 4.6 shows that S_6 (i.e., -2.41421) is compared to the slope of corner 1 (FGS_1) and the slope of corner 4 (FGS_4) of FG_{11} and FG_{16},

because these FG*j* are not located on the Y-axis. Since FG_{12} and FG_{17} lie on the Y-axis, the slope of R_6 is compared to the slope of corner 1 (FGS_1) and $-\infty$. The number of walls used to modify the path length of a ray depends on how many times the slope of a ray lies "between" the slopes of the appropriate corner points or meets the criteria provided in Table 4.5. In this case, R_6 meets the criteria of the slope comparison three times; therefore, R_6 crosses three walls.

Each wall is assumed to produce an attenuation of 1 dB. Therefore, the actual length in meters of the ray (L_{R_i}) for each $R_i \; \forall \, i = 1,2,...,16$ is obtained after applying the attenuation produced by the obstructions in the propagation model. For the multipath propagation model, the actual length of the ray L_{R_i} for each $R_i \; \forall \, i = 1,2,...,16$ can be calculated using equation 4.32:

$$L_{R_i} = \frac{\lambda}{4\pi} \sqrt{\frac{P_t \times G_{reader} \times G_{tag}}{P_{r,tag} \times 10^{\frac{Multipath\,Loss(dB)}{10}} \times 10^{\frac{WCR_i}{10}}}} \text{ (meters)} \qquad (4.32)$$

Where:

WCR_i = Number of walls crossed by ray R_i

Since a larger number of walls results in a larger value of the denominator in equation 4.28, the actual length of the ray L_{R_i} decreases as the number of walls crossed by the ray $R_i \; \forall \, i = 1,2,...,16$ increases.

Table 4.7 shows the number of walls crossed by each $R_i \ \forall i = 1,2,...,16$, as well as the resulting value for L_{R_i}. The value of L_{R_i} is used to calculate the new coordinates $(x_i^{'}, y_i^{'})$ of the end point of each ray $R_i \ \forall i = 1,2,...,16$ using equations 4.30a and 4.30b. Figure 4.15 depicts the final lengths of all the rays $R_i \ \forall i = 1,2,...,16$. The numbers shown at the end of each ray indicate the number of walls it crosses. ***The shape now formed by the 16 rays is considered the basis for the modified shape of the coverage area***.

Table 4.7 The number of walls crosses by each $R_i \ \forall i = 1,2,...,16$

R_i	WCR_i	L_{R_i} **(m)**	R_i	WCR_i	L_{R_i} **(m)**
1	1	2.09	9	0	2.35
2	0	2.35	10	0	2.35
3	0	2.35	11	0	2.35
4	1	2.09	12	0	2.35
5	2	1.87	13	0	2.35
6	3	1.66	14	1	2.09
7	1	2.09	15	1	2.09
8	1	2.09	16	1	2.09

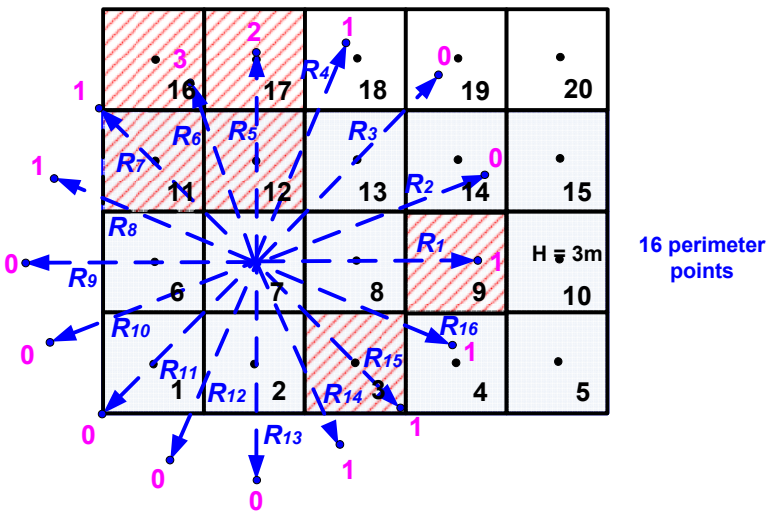

Figure 4.15 Modified circular coverage area with 16 rays

5. Perform a linear interpolation based on the path length of the original 16 perimeter points $P_i \; \forall \, i = 1,2,...,16$ defined in step 4 to estimate the path length of 360 points around the perimeter of the modified coverage area in increments of one degree.

   In this research, this process is completed using the MATLAB instant function for one-dimensional data interpolation known as *interp1*. The function *interp1* calculates the path length from the center (*h*, *k*) of the circular coverage area to each point on the perimeter of the modified coverage area in increments of one degree starting at zero degrees. The coordinates $(x_i^{'}, y_i^{'})$ of the new 360 perimeter points are then defined using equations 4.30a and 4.30b. Approximately 22 to 23 new perimeter points are defined in between pairs of the original 16 perimeter points. This translates into a smoother shape for the modified antenna coverage area after considering the effect of obstructions (i.e., passive interference), as depicted in Figure 4.16.

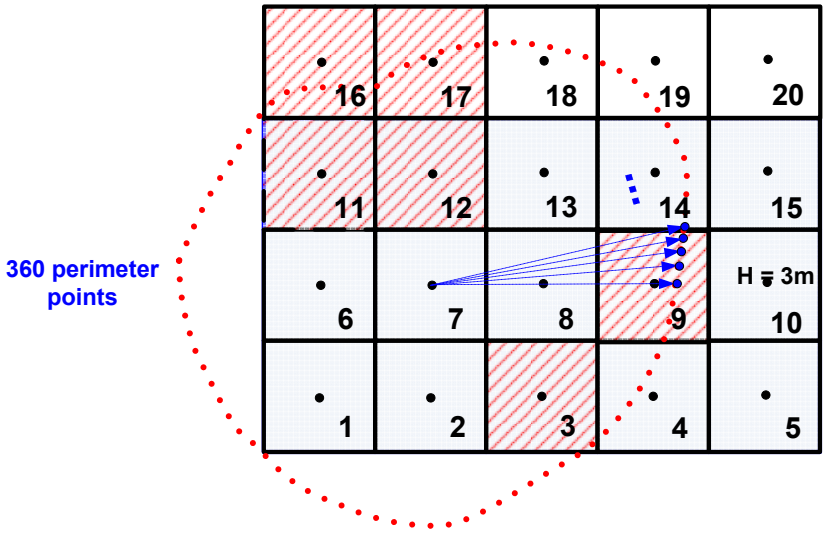

Figure 4.16 Modified circular coverage area with 360 rays

6. Find the number of candidate grids covered by the modified antenna coverage area. The procedure is as follows:
   a) Using equation 4.31, calculate the slope from the center (*h*, *k*) of the modified coverage area to each of the 360 perimeter points.
   b) Using equation 4.31, find the slope from the center (*h*, *k*) of the modified coverage area to the center of each candidate grid originally covered by the circular coverage area. In Figure 4.13, the candidate grids 1, 2, 4, 6, 7, 8, 13, 14, and 18 were covered by the circular antenna coverage area (see step 1).
   c) Identify the slopes values S_n and S_m of the modified coverage area in between which the value of the slope of each candidate grid falls (see Figure 4.17). Identify the perimeter points P_n and P_m that correspond to the slope values S_n and S_m, respectively.

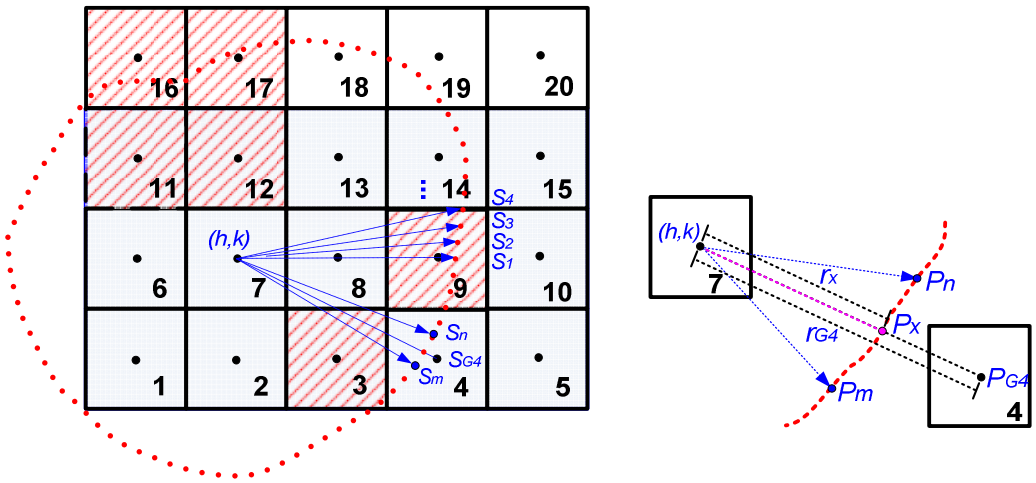

Figure 4.17 Example of how to check if a grid under consideration (grid 4) is covered by the real coverage area

d) Using equations 4.33a and 4.33b, calculate the coordinates of the mid-point P_x (see Figure 4.17) located on the perimeter of the modified coverage area in between the perimeter points P_m and P_n.

$$x = \frac{x_{Pm} + x_{Pn}}{2} \tag{4.33a}$$

$$y = \frac{y_{Pm} + y_{Pn}}{2} \tag{4.33b}$$

e) Calculate the distance r_x from the center (h, k) of the modified antenna coverage area to the mid-point P_x and the distance r_{G4} from the center (h, k) of the modified antenna coverage area to the center of grid 4.

f) Compare the lengths of r_x and r_{G4}. If $r_{G4} \leq r_x$, then grid 4 is still covered by the modified antenna coverage area. Otherwise, it is not covered. From Figure 4.17, grids 1, 2, 6, 7, 8, 13, 14 and 18 are still covered by the modified antenna coverage area. However, grid 4 is not covered anymore.

4.6.2. Modeling the Effect of Passive Interference on an Elliptical Antenna Coverage Area

A similar procedure to the one described in section 4.6.1 was used to model the effect of passive interference on the elliptical antenna coverage area of a directional antenna. A few important considerations have to be recognized when using an ellipse to represent the coverage area of the antenna attached to an RFID reader. These considerations are:

a) An ellipse has several important geometric features, including the length of its major axis (2a), the length of its minor axis (2b), and a rotation angle α.

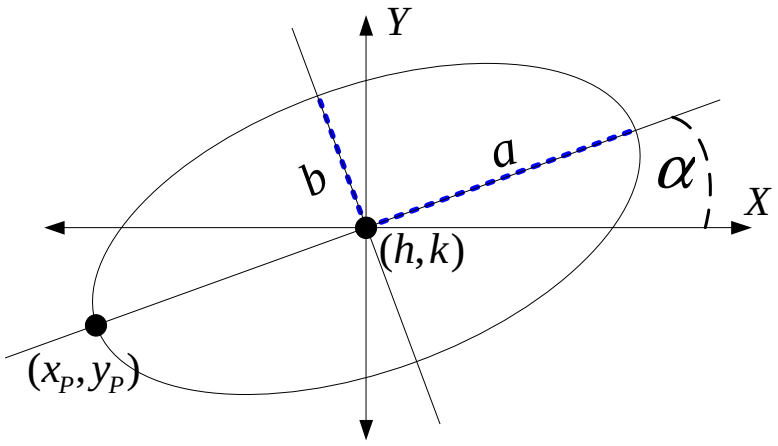

Figure 4.18 Important geometric features of an ellipse

b) The RFID reader is located at one of the points where the major axis and the perimeter of the ellipse intersect, as depicted in Figure 4.18. This intersecting point is identified with coordinates (x_p, y_p). Thus, the slope S_i of each ray R_i in the elliptical coverage area is the slope of the line originating from the RFID

reader placement location with coordinates (x_p, y_p) and ending at the point P_i where the ray intersects with the perimeter of the ellipse.

c) Because an ellipse has a rotation angle α, the length of the radius at each incremental angle from the center of the ellipse to a perimeter point P_i is not constant and depends on the rotation angle α.

The steps needed to model the effect of passive interference on an elliptical antenna coverage area were as follows:

1) Use equation 4.34a and equation 4.34b to find the coordinates of the center (*h*, *k*) of the elliptical coverage area at a different rotation angle α for an RFID reader located at coordinates (x_p, y_p).

$$h = x_p + a \cdot cos(\alpha) \tag{4.34a}$$

$$k = y_p + a \cdot sin(\alpha) \tag{4.34b}$$

2) Determine the candidate grids and forbidden grids (FGs) covered by the elliptical coverage area. Figure 4.19 depicts an example of a discretized facility area to illustrate this step. The RFID reader is located at grid 1. The coordinates of the center of grid 1 are (0.5, 0.5) and the values of *a* and *b* are 2.50 meters and 2.20 meters, respectively. The elliptical coverage area covers candidate grids 1, 2, 6, 7, 8, 13, 14, 18, and 19 and FGs 3, 9, 11, 12, and 17.

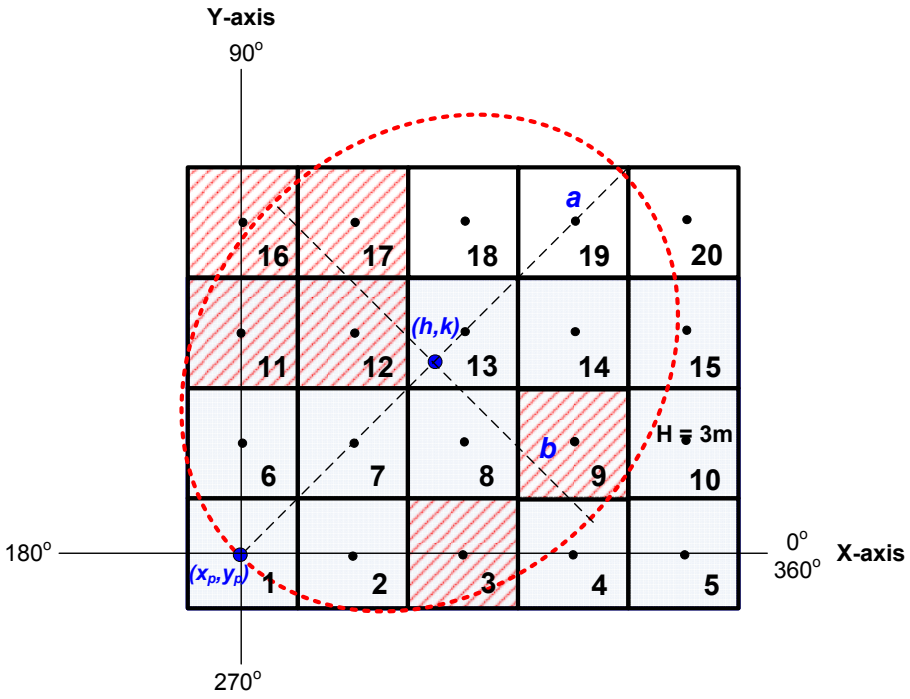

Figure 4.19 Candidate grids and forbidden grids covered by the elliptical coverage area

3) From the center (*h*, *k*) of the elliptical coverage area, draw a line parallel to the X-axis of grid 1 to the perimeter of the elliptical coverage area (see Figure 4.20a). Starting from this line (i.e., zero degrees), define 16 points $P_i \; \forall \, i = 1,2,...,16$ on the perimeter of the elliptical coverage area using increments of 22.5 degrees. The point with coordinates (x_p, y_p) is one of the perimeter points. Figure 4.20a shows six perimeter points on the elliptical coverage area with a rotation angle $\alpha = 45^\circ$. An elliptical coverage area with a rotation angle $\alpha \neq 0^\circ$ will be referred to as a *rotating* elliptical coverage area for the remainder of this section. Figure 4.20b shows all 16 perimeter points $P_i \; \forall \, i = 1,2,...,16$ on an elliptical coverage area with a rotation angle $\alpha = 0^\circ$. An elliptical coverage area with a rotation

angle $\alpha = 0^\circ$ will be referred to as the *reference* elliptical coverage area for the remainder of this section.

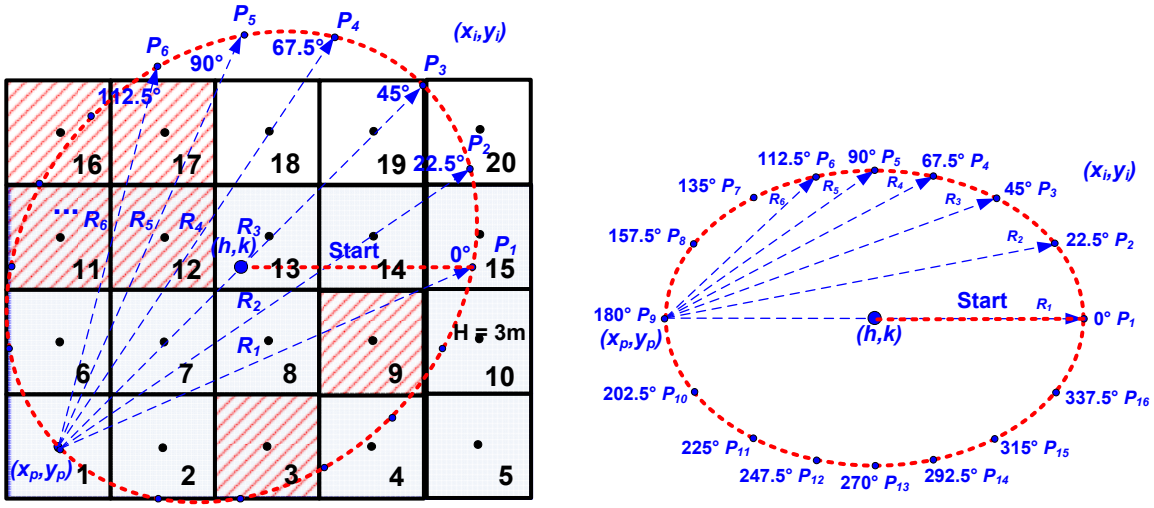

(a) rotation angle (α) = 45° **(b) rotation angle (α) = 0°**

Figure 4.20 Perimeter points of the elliptical coverage area with (a) $\alpha = 45^\circ$ and (b) $\alpha = 0^\circ$

In a circular coverage area, the radius (r) has constant length because a circle does not have a rotation angle. However, the length of the radius (r) in an ellipse changes depending on the value of the angle θ and also the value of the rotation angle α. Therefore, several parameters are required to determine the coordinates $(x_i, y_i) \forall i = 1,2,...,16$ for each of the perimeter points $P_i \forall i = 1,2,...,16$. These parameters are shown in Table 4.8.

Table 4.8 Parameters needed to calculate coordinates (x_i, y_i) of perimeter points P_i

Parameter	Description
θ	Angle on the perimeter of the elliptical coverage area relative to its center (*h*, *k*) $\theta = \{0^\circ, 1^\circ, 2^\circ, ..., 360^\circ\}$
α	Rotation angle of the elliptical coverage area relative to the X-axis (see Figure 4.20b). Eight rotation angles were considered in this research. $\alpha = \{0^\circ, 45^\circ, 90^\circ, 135^\circ, 180^\circ, 225^\circ, 270^\circ, 315^\circ\}$
r_θ	Radius (in meters) at angle θ on the *reference elliptical coverage area* (i.e., $\alpha = 0^\circ$).
d_θ	Radius (in meters) at angle θ on a *rotating* elliptical coverage area (i.e., $\alpha \neq 0^\circ$).

The length of the radius r_θ (in meters) on a *reference* elliptical coverage area (i.e., $\alpha = 0^\circ$) for angle θ is calculated with equation 4.35a. Then, the coordinates (x_i, y_i) of perimeter point $P_i(\theta, \alpha = 0^\circ)$ are calculated with equations 4.35b and 4.35c.

$$r_\theta = \frac{ab}{\sqrt{a^2 \sin^2(\theta) + b^2 \cos^2(\theta)}} \tag{4.35a}$$

$$x_\theta = h + r_\theta \cdot \cos(\theta) \tag{4.35b}$$

$$y_\theta = k + r_\theta \cdot \sin(\theta) \tag{4.35c}$$

The length of the radius $d_\theta = r_{(\theta-\alpha)}$ (in meters) of a *rotating* elliptical coverage area for angle θ and for a rotation angle $\alpha \neq 0°$ is calculated with equation 4.36a. Then, the coordinates (x_i, y_i) of perimeter point $P_i(\theta, \alpha \neq 0^\circ)$ are calculated with equations 4.36b and 4.36c.

$$d_\theta = r_{(\theta-\alpha)} = \frac{ab}{\sqrt{a^2 \sin^2(\theta-\alpha) + b^2 \cos^2(\theta-\alpha)}} \tag{4.36a}$$

$$x_\theta = h + d_\theta \cdot \cos(\theta) \tag{4.36b}$$

$$y_\theta = k + d_\theta \cdot \sin(\theta) \tag{4.36c}$$

Figure 4.21 depicts an example of the resulting values of r_θ and d_θ for different values of θ and for rotation angles of $\alpha = 0^\circ$ and $\alpha = 45^\circ$. The semi-major axis *(a)* has a value of 2.50 meters and the semi-minor axis *(b)* has a value of 2.20 meters.

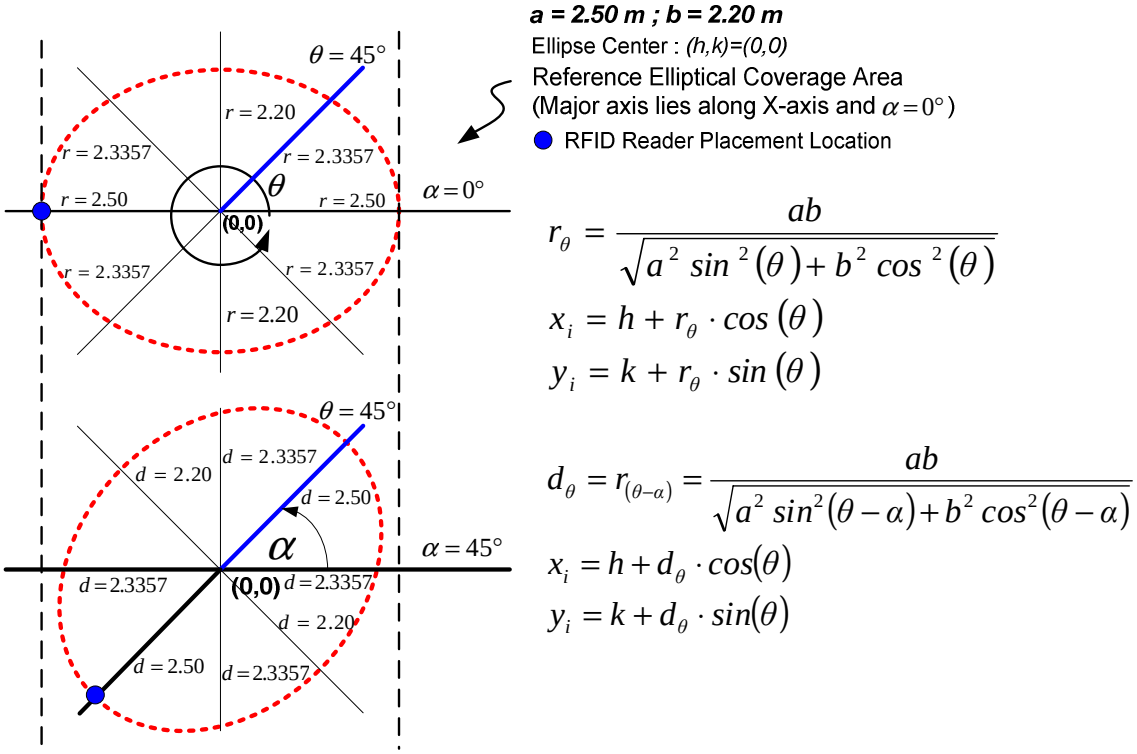

Figure 4.21 The coordinate on the perimeter (x_θ, y_θ) of the rotation elliptical coverage area

4) Each of the 16 perimeter points $P_i \; \forall \, i = 1,2,...,16$ identified in step 3 represents the end point of a ray. Use equation 4.37 to calculate the slope $S_i \; \forall \, i = 1,2,...,16$ of each ray originating from the RFID reader placement location (x_p, y_p) and ending on a perimeter point $P_i(x_i, y_i)$ (see Figure 4.20).

$$Slope_i \; (S_i) = \frac{y_P - y_i}{x_P - x_i} \; ; \; i = 1,2,3,...,16 \qquad (4.37)$$

The slope S_i of a ray R_i defines its location within the elliptical coverage area:

- A ray R_i whose slope S_i is *positive* is located in either quadrant 1 (Q1) or quadrant 3 (Q3).
- A ray R_i whose slope S_i is *negative* is located in either quadrant 2 (Q2) or quadrant 4 (Q4).
- A ray R_i whose slope S_i is *zero* lies on an X-axis.
- A ray R_i whose slope S_i is *infinity* (i.e., $+\infty$ or $-\infty$) lies on a Y-axis.

5) Compute the number of obstructions (i.e., walls) that each ray $R_i \; \forall \, i = 1,2,...,16$ crosses by following the same steps as those used with the circular coverage area. However, the slope calculation to determine the quadrant or axis in which each $FG_j \; \forall \; j$ covered by the elliptical coverage area is located is slightly different. More specifically, the slope S_j of the FG_j is computed for the line starting at the RFID placement location with coordinates (x_p, y_p) and ending at the center (x_j, y_j) of the FG_j covered by the elliptical coverage area.

To determine the quadrant(s) and/or axis in which each $FG_j \; \forall \; j$ covered by the elliptical coverage area is located, the slope values $S_j \; \forall \; j$ calculated are used in conjunction with the signs of the coordinates (x_j, y_j) of the center of the FG_j. The signs of the coordinates (x_j, y_j) are set relative to the quadrants formed by the center (*h*,*k*) of the elliptical coverage area, as shown in Table 4.9. As Table 4.9 shows, a FG_j can be located in one quadrant or in more than one quadrant and an axis (i.e., X or Y).

Table 4.9 Location of FGs for the example in Figure 4.19

	(1)	(2)	(3)	(4)	(5)	(6)
FG_j	Q1	Q2	Q3	Q4	X-Axis	Y-Axis
3	✓			✓	✓	
9	✓					
11	✓	✓				✓
12	✓					
17	✓					

In Figure 4.20a, R_6 is used as an example. The perimeter point P_6 and the slope S_6 of the line originating from the RFID placement location (x_P, y_P) and ending at P_6 can be computed by following steps 1 - 4. Equation 4.34a and 4.34b are used to compute the center of the elliptical coverage area, whereas the coordinates (x_6, y_6) of P_6 are calculated using equations 4.36a to 4.36c. The values $(x_p, y_p) = (0.5, 0.5)$, a = 2.50 meters, b = 2.20 meters, $\alpha = 45^\circ$, and $\theta = 112.5^\circ$ are entered into equations 4.34a, 4.34b, 4.36a, 4.36b and 4.36c as shown below:

$$h = 0.5 + 2.5 \cdot cos(\,45^\circ\,) = 2.268\ meters$$

$$k = 0.5 + 2.5 \cdot sin(\,45^\circ\,) = 2.268\ meters$$

$$d_{112.5^\circ} = r_{(112.5^\circ - 45^\circ)} = r_{67.5^\circ} = \frac{2.5 \times 2.2}{\sqrt{2.5^2 \cdot sin^2\left(67.5^\circ\right) + 2.2^2 \cdot cos^2\left(67.5^\circ\right)}} = 2.237\ meters$$

$$x_6 = 2.268 + 2.237 \cdot \cos(112.5^\circ) = 1.412$$

$$y_6 = 2.268 + 2.237 \cdot \sin(112.5^\circ) = 4.335$$

Once the coordinates (x_6, y_6) of P_6 are known, S_6 can be calculated using equation 4.37:

$$Slope_6\ (S_6) = \frac{0.5 - 4.335}{0.5 - 1.412} = 4.205$$

The result shows that S_6 is positive and it points to Q1. In fact, all FGs covered by the elliptical coverage area are located in Q1 (see column 1 in Table 4.9); therefore, all FGs have to be considered in the slope comparison and case 1 in Table 4.5 is applied (i.e., positive slope).

Two categories of FGs located in Q1 are considered, i.e., FGs that do not lie on the Y-axis (FG_3, FG_9, FG_{12}, and FG_{17}) and FGs that are located on the Y-axis (FG_{11}). For FGs that do not lie on the Y-axis, S_6 is compared to the slopes of two lines drawn from the placement location (x_P, y_P) to the coordinates (x_j,y_j) of corner 2 and corner 3 of FGs in the elliptical coverage area. For FGs located on the Y-axis, S_6 must be compared to the slope of a line originating from the placement location (x_P, y_P) and ending at the coordinate (x_j,y_j) of corner 2 and the slope of $+\infty$. Table 4.10 summarizes the slope comparison for R_6 and the corner points of FGs located in Q1. The last column in Table 4.10 shows that S_6 lies between the slopes of the

appropriate corner points or meets the criteria provided in Table 4.5 three times. Therefore, R_6 crosses three walls.

Table 4.10 Slope comparison between ray 6 and the corner points of the FGs located in Q1

FG_j	*FG Location*	S_6	FGS_2	FGS_3	$+\infty$	*Crossed by* R_6 *?*
3	not on Y-axis	4.205	-0.20	0.333	-	No
9	not on Y-axis	4.205	0.143	0.60	-	No
11	on Y-axis	4.205	3.0	-	$+\infty$	Yes
12	not on Y-axis	4.205	1.0	5.0	-	Yes
17	not on Y-axis	4.205	1.667	7.0	-	Yes

Column 3 in Table 4.11 shows the number of walls (*WCRi)* crossed by each of the 16 rays $R_i \; \forall \, i = 1,2,...,16$ for every 22.5 degree increment of the *relative* incremental angle $\theta^1_{relative}$ with respect to the center (*h*,*k*) of the elliptical coverage area. Column 4 in Table 4.11 shows the values for the actual incremental angle θ_{actual} relative to the placement location (x_p, y_p). The angle θ_{actual} was used to obtain (1) the maximum Euclidean distance $d_{\max}$ measured from the placement location (x_p, y_p) to the perimeter point $P_i(x_i, y_i)$, and (2) the actual length of the ray d_{actual} on the perimeter of the modified elliptical coverage area relative to its placement location (x_p, y_p).

Table 4.11 Number of walls crosses by each of the 16 rays of elliptical coverage area

(1)	(2)	(3)	(4)	(5)	(6)
R_i	**Relative incremental angle $\theta^1_{relative}$ with respect to the center (h,k) (degrees)**	WCR_i	**Actual incremental angle θ_{actual} relative to the placement location (x_p,y_p) (degrees)**	d_{max} **(m)**	d_{actual} **(m)**
1	0	1	23.31	4.47	3.98
2	22.5	0	33.87	4.85	4.85
3	45	0	45.00	5.00	5.00
4	67.5	1	56.13	4.85	4.33
5	90	2	66.69	4.47	3.55
6	112.5	3	76.63	3.94	2.79
7	135	1	86.35	3.33	2.97
8	157.5	1	96.51	2.64	2.35
9	180	1	107.81	1.86	1.65
10	202.5	0	120.74	0.97	0.97
11	225	0	*Placement location*	0.00	0.00
12	247.5	0	329.26	0.97	0.97
13	270	1	342.19	1.86	1.65
14	292.5	1	353.49	2.64	2.35
15	315	1	3.65	3.33	2.97
16	337.5	2	13.37	3.94	3.13

In Figure 4.20a, R_6 is used to demonstrate the procedure to calculate the actual length of the ray d_{actual} at the actual incremental angle θ_{actual} on the perimeter of the modified elliptical coverage area relative to its placement location (x_p, y_p).

The coordinates (x_6, y_6) of the perimeter point P_6 were calculated earlier as $(1.412, 4.335)$. The actual incremental angle θ_{actual} of R_6 relative to the placement location coordinates $(x_p, y_p) = (0.5, 0.5)$ is computed using equation 4.38.

$$\theta_{actual} = \arctan\left(\frac{y_i - y_p}{x_i - x_p}\right) \tag{4.38}$$

$$\theta_{actual} = \arctan\left(\frac{4.335 - 0.5}{1.412 - 0.5}\right) = 76.63^{\circ}$$

The actual length d_{actual} of R_6 is then calculated by multiplying the attenuation factor produced by the obstructions crossed by R_6, i.e., $\frac{1}{\sqrt{10^{\frac{WCR_i}{10}}}}$, by the maximum Euclidean distance $d_{\max}$ of R_6, as shown in equation 4.39.

$$d_{actual} = d_{max} \times \frac{1}{\sqrt{10^{\frac{WCR_i}{10}}}} \text{ (meters)} \tag{4.39}$$

First, the Euclidian distance $d_{\max}$ for R_6 is equal to $d_{\max} = \sqrt{(4.335 - 0.5)^2 + (1.412 - 0.5)^2} = 3.942$ meters. Then, $d_{\max}$ is multiplied by the attenuation factor to obtain d_{actual} for R_6, as follows:

$$d_{actual} = 3.942 \times \frac{1}{\sqrt{10^{\frac{3}{10}}}} = 2.791 \text{ meters}$$

The value of d_{actual} is used to calculate the new coordinates $(x_i^{'}, y_i^{'})$ for the end point of each ray using equations 4.40a and 4.40b.

$$x_i^{'} = x_p + d_{actual} \cdot \cos(\theta_{actual}) \tag{4.40a}$$

$$y_i^{'} = y_p + d_{actual} \cdot \sin(\theta_{actual}) \tag{4.40b}$$

For R_6, the new coordinate $P_6^{'}(x_6^{'}, y_6^{'})$ on the perimeter of the modified elliptical coverage area is calculated as follows:

$$x_6^{'} = 0.5 + 2.791 \cdot \cos(76.63^{\circ}) = 1.1454$$

$$y_6^{'} = 0.5 + 2.791 \cdot \sin(76.63^{\circ}) = 3.2154$$

Figure 4.22a shows detailed information for $\theta_{relative}^{1}$, θ_{actual}, $d_{\max}$, d_{actual}, $P_6(x_6, y_6)$ and $P_6^{'}(x_6^{'}, y_6^{'})$ regarding the calculation illustrated above for R_6. The final lengths of all 16 rays are depicted in Figure 4.22b. The numbers shown at the end of each ray indicate the number of walls it crossed. ***The shape now formed by the 16 rays is considered the basis for the modified shape of the coverage area***.

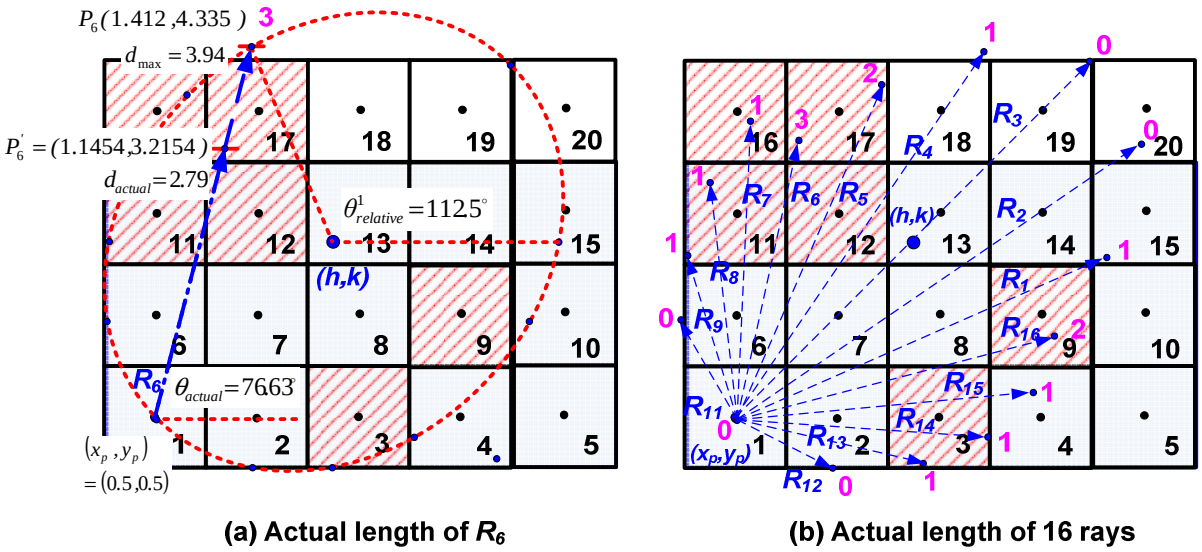

Figure 4.22 Modified elliptical coverage area

6) Calculate the modified length of each ray $R_i' \; \forall i = 1,2,...,16$ as a result of crossing obstructions. The end points of the modified rays $R_i' \; \forall i = 1,2,...,16$ are now the perimeter points $P_i'(x_i', y_i') \; \forall i = 1,2,...,16$ (see Figure 4.23). Also, calculate the value of the *relative* incremental angle $\theta^2_{relative}$ with respect to the center (*h*,*k*) of the elliptical coverage area for each ray $R_i' \; \forall i = 1,2,...,16$ using equation 4.41.

$$\theta^2_{relative} = arctan\left(\frac{y_i' - k}{x_i' - h}\right) \tag{4.41}$$

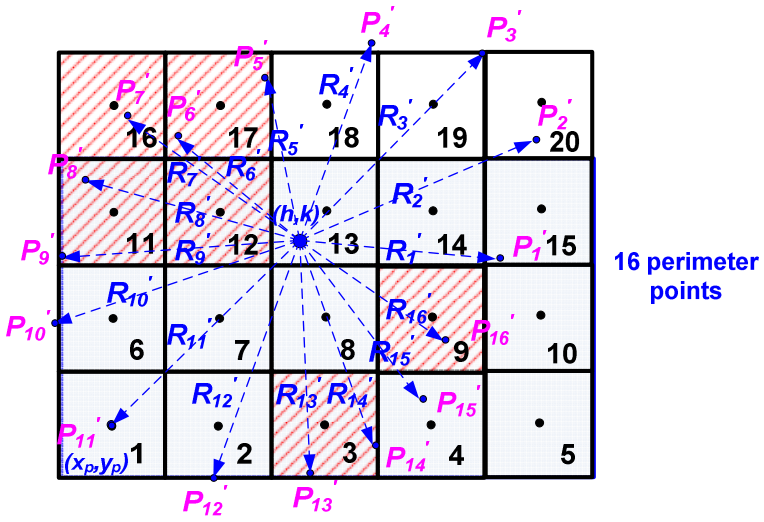

Figure 4.23 Modified elliptical coverage area with 16 rays from the center (*h*,*k*)

Table 4.12 shows the new coordinates $P_i^{'}(x_i^{'}, y_i^{'})$ for each $R_i^{'} \; \forall \, i = 1,2,...,16$, the *relative* incremental angle $\theta_{relative}^{1}$, and the *relative* incremental angle $\theta_{relative}^{2}$ that results after applying the attenuation due to obstructions. The relative length $d_{relative}$ measured from the center (*h*, *k*) to each of the 16 perimeter points $P_i^{'}(x_i^{'}, y_i^{'})$ of the modified elliptical coverage is calculated using the formula for the Euclidean distance (see column 5 of Table 4.12).

Table 4.12 New coordinates $P_i^{'}(x_i^{'}, y_i^{'})$ of each ray, the relative incremental angle $\theta_{relative}$ and the relative length $d_{relative}$

(1)	*(2)*	*(3)*	*(4)*	*(5)*
$R_i^{'}$	$P_i^{'}(x_i^{'}, y_i^{'})$	$\theta_{relative}^{1}$ (degrees)	$\theta_{relative}^{2}$ (degrees)	$d_{relative}$ (meters)
1	(4.16,2.08)	0	-5.81	1.90
2	(4.53,3.20)	22.5	22.50	2.45
3	(4.04,4.04)	45	45.00	2.50
4	(2.91,4.09)	67.5	70.58	1.93
5	(1.90,3.76)	90	103.70	1.54
6	(1.15,3.21)	112.5	139.84	1.47
7	(0.69,3.46)	135	142.89	1.98
8	(0.23,2.84)	157.5	164.33	2.11
9	(-0.01,2.08)	180	184.83	2.28
10	(0.01,1.33)	202.5	202.50	2.45
11	(0.5,0.5)	225	225.00	2.50
12	(1.33,0.01)	247.5	247.50	2.45
13	(2.08,-0.01)	270	265.17	2.28
14	(2.84,0.23)	292.5	285.67	2.11
15	(3.46,0.69)	315	307.11	1.98
16	(3.55,1.22)	337.5	320.77	1.65

7) Perform a linear interpolation based on the path length of the original 16 perimeter points defined in step 6 to estimate the path length of 360 points around the perimeter of the modified elliptical coverage area in increments of one degree starting from the first value of the new *relative* incremental angle ($\theta^2_{relative}$) in column 4 of Table 4.12. In this example, $\theta^2_{realtive} = -5.81^\circ$ is used as a starting point. As with the circular coverage area, the MATLAB instant function for one-dimensional data interpolation known as *interp1* was used in this step. The coordinates $(x_i^{'}, y_i^{'})$ of the new 360 perimeter points are then defined using equations 4.42a and 4.42b. This results into a smoother shape for the modified antenna coverage area, as depicted in Figure 4.24.

$$x_i^{'} = h + d_{relative} \cdot cos\left(\theta^2_{relative}\right) \tag{4.42a}$$

$$y_i^{'} = k + d_{relative} \cdot sin\left(\theta^2_{relative}\right) \tag{4.42b}$$

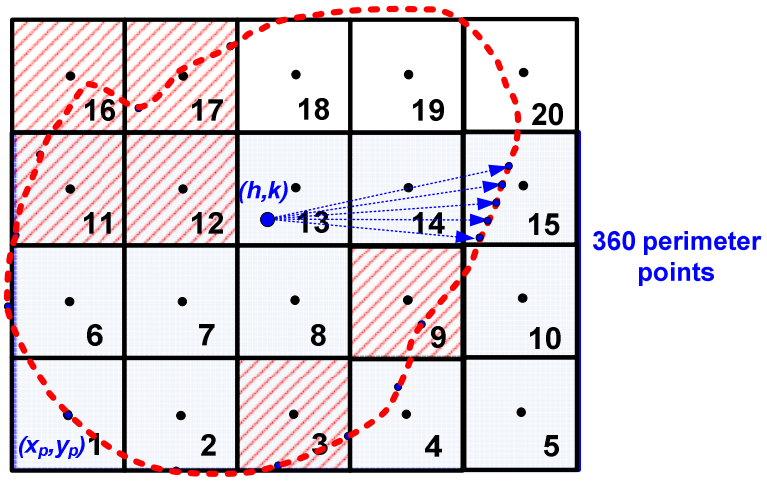

Figure 4.24 Modified elliptical coverage area with 360 rays

8) Find the number of candidate grids covered by the modified elliptical coverage area. A similar concept to that used in the modified coverage area for the omnidirectional coverage area can be applied. From Figure 4.24, it can be seen that candidate grids 1, 2, 6, 7, 8, 13, 14, 18, and 19 are still covered by the modified elliptical coverage area.

4.7. Heuristic Optimization Algorithms

Two heuristic optimization techniques were applied to find good solutions to the RFID network planning (RNP) problem in this research: Genetic Algorithm (GA) and Particle Swarm Optimization (PSO). Both GA and PSO have been applied previously to the RNP problem and have produced good solutions within reasonable computation time.

4.7.1. Particle Swarm Optimization

This section provides a detailed description of the PSO algorithm used to find good solutions for the CAC and the EAC model formulations. The PSO algorithm was developed as an inertia-weighted PSO algorithm. Three major parameters must be set appropriately in inertia-weighted PSO:

- Inertia (w),
- The local cognitive component (c_1), and
- The global social component (c_2).

The formulas for updating the velocity of the inertia-weighted PSO are shown in equations 4.43a and 4.43b.

$$v_{i,j} = w \cdot v_{i,j} + c_1 \cdot rand \cdot \left(local\ \ best_{i,j} - x_{i,j}\right) + c_2 \cdot rand \cdot \left(global\ best_j - x_{i,j}\right) \quad (4.43a)$$

$$x_{i,j} = x_{i,j} + v_{i,j} \quad (4.43b)$$

The inertia (w) parameter in the inertia-weighted PSO controls the velocity explosion. The original PSO does not have an inertia (w) parameter; therefore, a method for

limiting the maximum velocity in the range $[-v_{max}, v_{max}]$ is applied to control the velocity explosion. However, limiting the velocity explosion does not necessarily prevent particles from leaving the search space or guarantee convergence.

If the values of w, c_1, and c_2 are set correctly, the particles in the inertia-weighted PSO can converge without the use of v_{max}. Clerc & Kennedy (2002) introduced the constriction coefficient (χ) to prevent velocity explosion, ensure convergence, and eliminate the use of v_{max}. The equation for updating velocity for the inertia-weighted PSO after applying the constriction coefficient is shown in equations 4.44a and 4.44b.

$$v_{i,j} = \chi \cdot \left(v_{i,j} + \varphi_1 \cdot rand \cdot \left(local\ best_{i,j} - x_{i,j}\right) + \varphi_2 \cdot rand \cdot \left(global\ best_j - x_{i,j}\right)\right) \quad (4.44a)$$

$$\chi = \frac{2}{\left|2 - \varphi - \sqrt{\varphi^2 - 4\varphi}\right|} \quad (4.44b)$$

Where:

$$\varphi = \varphi_1 + \varphi_2\ ,\ \varphi > 4 \quad ; \quad w = \chi \quad ; \quad c_1 = \chi \cdot \varphi_1 \quad ; \quad c_2 = \chi \cdot \varphi_2$$

Clerc & Kennedy (2002) suggested that the values of w, c_1 and c_2 should be 0.7298, 1.49618 and 1.49618, respectively. However, the parameter values in an inertia-weighted PSO tend to be problem-specific and may need to be adjusted for better performance of the system.

Once the appropriate values of w, c_1 and c_2 are defined, the inertia-weighted PSO is then applied to the developed CAC model formulation (see section 4.2) and EAC model formulation (see section 4.4) to find good solutions for the RNP. The steps needed to apply

the inertia-weighted PSO with constriction coefficient to both the CAC and the EAC model formulations are as follows:

Step 1: Set input parameters so that they comply with the EPCglobal® Standard C1G2, i.e., RFID reader's transmitted power (P_t), RFID reader's antenna gain (G_{reader}), RFID reader's operating frequency (f), tag's antenna gain (G_{tag}), and tag's received power threshold ($P_{r,tag}$), as well as the important parameters for multipath propagation model and radar cross section propagation model, i.e., path loss exponent (n), loss from multipath fading (X), and radar cross section area (σ). Calculate the radius (*r*) of the RFID reader's coverage area for the CAC model formulation and calculate the semi-major axis (*a*) and semi-minor axis (*b*) of the RFID reader's coverage area for EAC model formulation.

Step 2: Set the level for the experimental factors facility shape, facility size, grid size, power levels, and type of model formulation. Each of these experimental factors is discussed in more detail in section 4.8.

Step 3: Initialize all parameters needed in the inertia-weighted PSO, which include the number of particles, the length of each particle, the total number of iterations (or the termination criteria), the initial values for the global best (*gbest*) and the local best (*pbest*), and the initial number of RFID readers.

In general, the values of *gbest* and *pbest* are equal to zero if a maximization objective is sought. Conversely, *gbest* and *pbest* should be large (e.g., 10^6) if a minimization objective is considered. In this research, a maximization problem is considered. Thus, the initial values of *gbest* and *pbest* are

both zero.

The initial number of RFID readers must meet the constraint in equation 4.3 for the CAC model formulation, and the constraint in equation 4.15 for the EAC model formulation. Both constraints provide the values of a lower bound and an upper bound for the number of RFID readers required in the system. The binary search algorithm described in section 4.7.3 is used to find the most appropriate number of RFID readers.

The three main field categories encoded into a particle include *site location*, *rotation angle* and *power levels*, as shown in Figure 4.25. Each of these field categories requires *n* variables, where *n* represents the number of RFID readers. The site location field is required regardless of the type of model formulation, whereas the rotation angle field is only required in the EAC formulation. Table 4.13 summarizes the conditions which identify the fields required in a specific type of particle and the number of variables required in a particle.

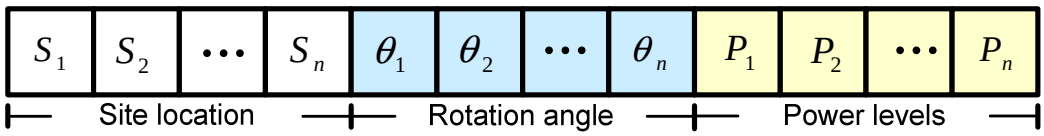

$S_n \in$ *all candidate grids*

$\theta_n \in \{1,2,...,8\} = \{0^\circ, 45^\circ, 90^\circ, 135^\circ, 180^\circ, 225^\circ, 270^\circ, 315^\circ\}$

$P_n \in \{1,2,...,8\} = \{9,12,15,18,21,24,27,30\ dBm\}$

n = *number of RFID readers*

Figure 4.25 The format of a PSO particle representation

Table 4.13 Conditions identifying the fields required in a particular particle

Condition		Required Fields	Number of Variables in a Particle
Optimization Formulation	**Power Levels**		
CAC	1	Site location	*n*
	8	Site location; power levels	*2n*
EAC	1	Site location; rotation angle	*2n*
	8	Site location; rotation angle; power levels	*3n*

For example, if the CAC optimization is applied with eight power levels and five RFID readers, then each particle requires only the fields *site location* and *power levels* for a total of 10 variables (i.e., *2n = 2*5 = 10*). The field *rotation angle* is not needed because a circular coverage area does not have one.

Step 4: Generate an initial solution with random values for positions and all velocities set to zero. At first, the algorithm randomly selects one grid out of all candidate grids in the facility for each bit of the site location field (see Figure 4.25). If a solution is being sought for the EAC model formulation, one out of eight rotation angles is randomly assigned to each bit of the rotation angle field. The same process is applied for the power levels field.

Step 5: For each particle, determine the modified antenna coverage area (see section 4.6)

and evaluate the value of fitness based on the values of the variables that represent the site location, rotation angle, and power levels.

Step 6: Compare the value of the fitness with the particle's local or personal best (*pbest*). If the current value of the fitness is greater than *pbest*, reset the value of *pbest* to be equal to the current value of the fitness. Then, update the *pbest* location (*pxbest*) to be equal to the current position of all variables in each particle.

Step 7: Compare the value of the fitness with the particle's global best (*gbest*). If the current value of the fitness is greater than *gbest*, reset the value of *gbest* to be equal to the current value of the fitness. Then, update the *gbest* location (*gxbest*) to be equal to the current particle's array index and value.

Step 8: Adjust the velocity and position of each particle using equations 4.43a and 4.43b. The RNP studied in this research is a discrete problem; therefore, the value of $x_{i,j}$ in equation 4.43b is rounded up to the nearest integer.

Step 9: Check the adjusted value $x_{i,j}$ in each of the field categories (i.e., site location, rotation angle, and power levels). If the adjusted value $x_{i,j}$ in a particular field category is less than one, then set it to one. Conversely, if the adjusted value of $x_{i,j}$ is greater than the largest value (*LV*) in the field category, set it equal to *LV*. Making these adjustments to the adjusted value $x_{i,j}$ will ensure that it stays in the feasible region.

- Consider the facility depicted in Figure 4.26 as an example for the site location field. This facility is $5m \times 3m$ in size and the forbidden grids are located at grid FG_3, FG_{11}, FG_{12}. Therefore, the RFID readers can be placed at the center of any of the candidate grids located at coordinates (0.5,0.5), (1.5,0.5),

(3.5,0.5), ..., (2.5,1.5), (3.5,.5), ..., (3.5,2.5), (4.5,2.5). There are 12 possible locations starting from site location 1 to site location 12, 12 being the largest possible value for *LV*.

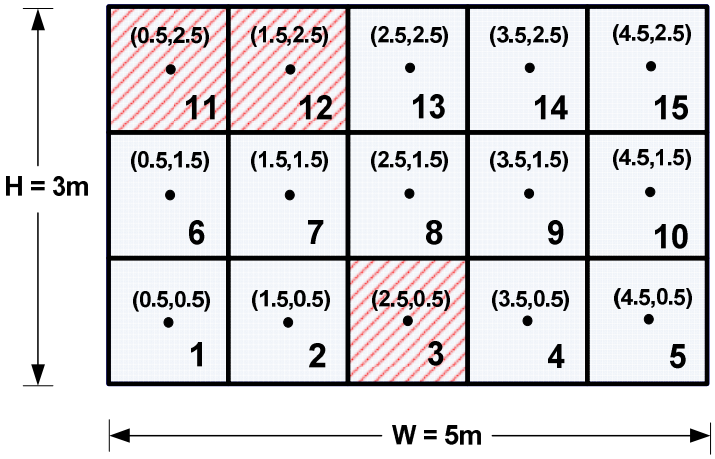

Figure 4.26 Discretized rectangular facility

Step 10: Loop back to step (5) until the termination criterion (i.e., 1,000 iterations) is met.

Step 11: Show results and plot the graph.

The steps needed to apply the inertia-weighted PSO to both the CAC and the EAC model formulations are summarized in the flowchart depicted in Figure 4.27.

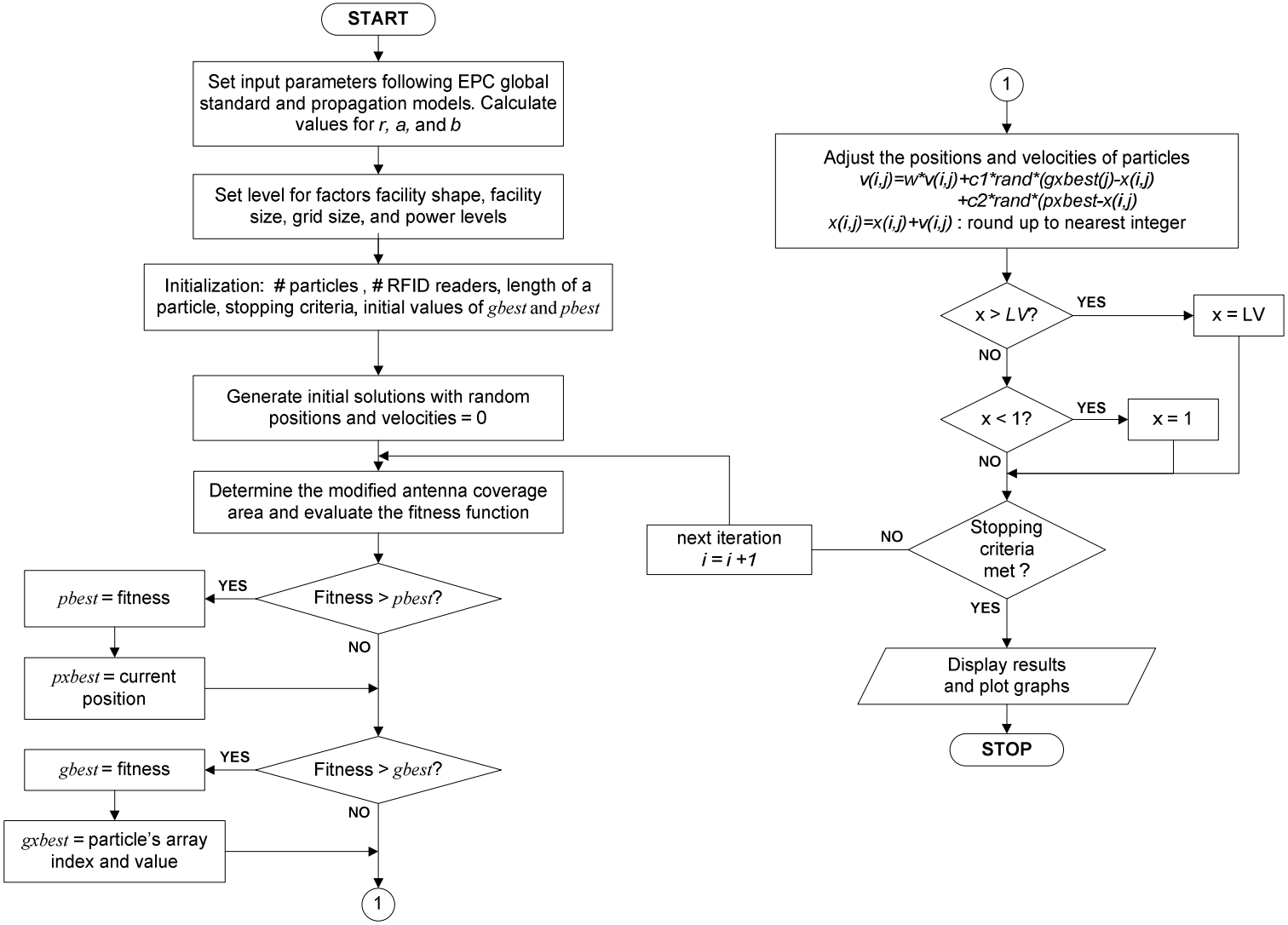

Figure 4.27 Steps of the inertia-weighted PSO algorithm

4.7.2. Genetic Algorithm

This section provides a detailed description of the GA that was applied to the CAC and the EAC model formulations to find good solutions to the RNP problem. The steps needed to apply the GA with both the CAC and the EAC model formulations are as follows:

Step 1: Set input parameters so that they comply with the EPCglobal® Standard C1G2, i.e., RFID reader's transmitted power (P_t), RFID reader's antenna gain (G_{reader}), operating frequency (f), tag's antenna gain (G_{reader}), and tag's received power threshold ($P_{r,tag}$), as well as the important parameters for multipath propagation model and radar cross section propagation model, i.e., path loss exponent (n), loss from multipath fading (X), and radar cross section area (σ). Calculate the radius (*r*) of the RFID reader's coverage area for the CAC model formulation and calculate the semi-major axis (*a*) and semi-minor axis (*b*) of the RFID reader's coverage area for EAC model formulation.

Step 2: Set the level for the experimental factors facility shape, facility size, grid size, power levels, and the type of model formulation. Each of these experimental factors is discussed in more detail in section 4.8.

Step 3: Initialize all parameters needed in the GA including the population size (*pop*); the initial number of variables or length of the chromosomes (*nVar*); the mutation rate (*m_rate*) which should be a small number between 0.01 and 0.05; the stopping criterion or the total number of generations (*nGen*); the maximum objective function (*objmax*); and the initial number of RFID readers required in

the system (*nReader*).

The format of the chromosome representation follows the same format as the particle of PSO. The three main field categories encoded into a chromosome include *site location*, *rotation angle* and *power levels*. Each of these field categories requires *n* genes, where *n* represents the number of RFID readers.

Step 4: Randomly generate initial chromosomes (i.e., solutions). The total number of chromosomes represents the initial population size of the GA. The algorithm randomly selects one grid out of all candidate grids for each gene of the site location field (see Figure 4.25). If a solution is being sought for the EAC model formulation, one out of eight rotation angles is randomly assigned to each bit of the rotation angle field. The same process is applied for the power levels field.

Step 5: Select two parent chromosomes from the population using a *roulette wheel selection* process (Goldberg & Deb, 1991). If the same chromosome is randomly selected in this process, a new selection takes place until two different parent chromosomes are identified.

Step 6: Generate two offspring chromosome by performing a crossover operation on the parent chromosomes. The details of the crossover operation are as follows:

- Randomly select a break location in the parent chromosomes, as shown in Figure 4.28.
- The first child chromosome includes all the genes up to the break location of the first parent chromosome plus all the genes of the second parent chromosome from the break location until the end of the chromosome, as shown in Figure 4.28. The second child uses the same crossover process, but with a reverse gene structure.

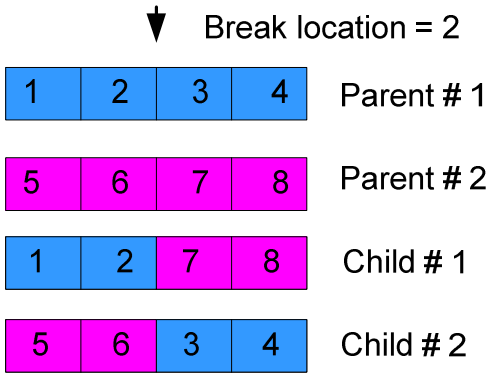

Figure 4.28 The GA's crossover process

Step 7: Perform the mutation operation as follows:

- Generate a random number between zero and one.
- If the random number is less than the mutation rate, then randomly select a gene position in the chromosome for mutation.
- Finally, randomly change the value of the gene in the chromosome. If the mutated gene is located in the site location field, the value of the random number is in the range between one and *LV* in the set of candidate grids; if the gene is located in the rotation angle field or power levels field, the value of the random number is in the range between one and eight.

Step 8: For each chromosome of the offspring, determine the modified antenna coverage area (see section 4.6) and evaluate the value of fitness of the offspring after the crossover and mutation operations. Select the better offspring to the next step.

Step 9: Compare the value of fitness of the better offspring with the value of fitness of the parents. The chromosome (i.e., solution) with the best value of fitness will be selected to the next generation.

Step 10: Loop back to step 5 until the required number of chromosomes in the population

of the next generation (i.e., *pop*) is reached.

Step 11: Evaluate the value of fitness for each chromosome in the population.

Step 12: Compare the value of the fitness with the value of the maximum objective (*objmax*). If the current value of the fitness is greater than *objmax*, reset the value of *objmax* to be equal to the current value of fitness.

Step 13: Loop to step 5 until the termination criterion (i.e., number of generations) is met.

Step 14: Show results and plot the graph.

The steps needed to apply the GA to both the CAC and the EAC model formulations are summarized in the flowchart depicted in Figure 4.29.

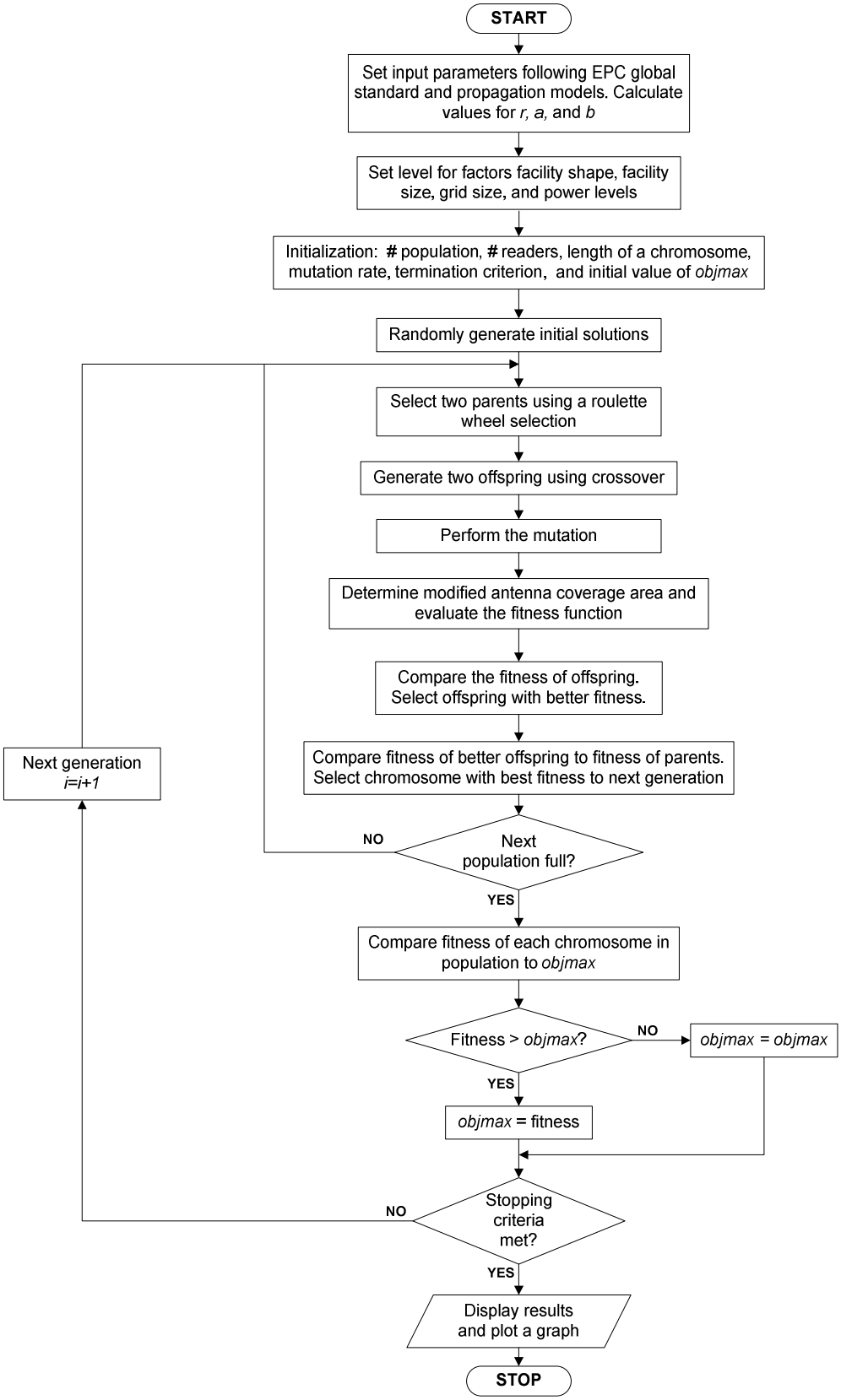

Figure 4.29 Steps of the GA algorithm

4.7.3. Algorithm to Find the Optimum Number of RFID Readers

An additional algorithm was designed to work with the GA and PSO algorithms to automatically find the optimum number of RIFD readers needed in the system. The required number of RFID readers was entered as an input parameter into the GA and PSO algorithms. Considering the fact that the optimum number of RFID readers needs to be less than the initial number of RFID readers (*N*) obtained from the concept of square or hexagonal packing, the original algorithm kept changing the number of RFID readers from *N* to one. At each number of RFID readers, the algorithm computed the best value of fitness and collected it in an array. After all of the best values of fitness from each number of RFID readers were collected, the algorithm compared all elements in the array and found the maximum value of fitness. The optimum number of RFID readers required in the system was set as the number of RFID readers that resulted in the maximum value of fitness. Figure 4.30 shows the pseudocode of the original algorithm.

Original Algorithm*: Find the optimum number of RFID readers required*

---

for *number_reader* = *intial_number_reader* to 1 **do**

    Enter *number_reader* as the input parameter of PSO or GA
    Find the best value of fitness using PSO or GA
    Collect all best values of fitness of each number of RFID readers in the array

end for

Find the maximum value of fitness in the array
Optimum number of RFID readers: Number of RFID readers giving a maximum value of fitness

---

Figure 4.30 The original algorithm to find the optimum number of RFID readers

The algorithm described in Figure 4.30 was able to compute the optimum number of RFID readers very well for small facility areas. A small facility requires a small initial number of RFID readers to cover the entire facility using the concept of square or hexagonal packing, e.g., 10 readers. Obtaining the optimum number of RFID readers required in the system by changing the value of the number of RFID readers from 10 to one did not take a very long time. On the other hand, a large facility also requires a large initial number of RFID readers, e.g., 100 RFID readers. Under this scenario, changing the value of the number of RFID readers from 100 to one required a significantly long period of time. Therefore, a more efficient algorithm was needed to find the optimum number of RFID readers in a reasonable period of time for any facility size.

The *Binary Search Algorithm (BSA)* was utilized to search for the optimum number of RFID readers that result in the maximum value of fitness. In the BSA, the number of RFID readers are sorted in an array starting from the lower bound to the upper bound of the number of installed RFID readers, i.e., the initial number of RFID readers required (N). Equations 4.3 and 4.15 were used to calculate the lower bound and upper bound of the number of installed RFID readers required for the CAC and the EAC model formulations, respectively. In order for the BSA to work properly, the values of fitness in the sorted array have to follow the shape of a *convex downward curve* where the maximum value of fitness lies between the fitness of the lower bound and the upper bound of the number of RFID readers required in the system. The BSA can significantly reduce the complexity of searching for the optimum number of RFID readers required in the system. In general, the complexity of the algorithm shown in Figure 4.30 is proportional to the length of the array. For example, if the initial number of RFID readers (N) is 33, then the array length is 33 and the original algorithm has to vary the value of the number of RFID readers 33 times (i.e., 33 to 1) to obtain the optimum number of RFID readers required.

However, the complexity of the search algorithm can be reduced by a factor equal to $\log_2(x)$, where *x* represent the length of the array (Knuth, 1998). Thus, if the length of the array is 12, i.e., lower bound of 21 RFID readers and upper bound of 33 RFID readers calculated from the constraint in equation 4.3, the proposed algorithm will take only four steps to find the optimum number of RFID readers. The pseudocode of the proposed algorithm to find the optimum number of RFID readers is shown in Figure 4.31.

Algorithm: ***Find the optimum number of RFID readers required***

Define the lower and upper bound of the number of RFID readers in the array. These bounds are obtained from equation 4.3 for the CAC model formulation and equation 4.15 for the EAC model formulation (e.g., [21 33]).

Define the array for collecting the values of the fitness during the search: $fitness\_array$

Find the midpoint between the lower and upper bound using $midpoint = \left\lfloor \frac{lower + upper}{2} \right\rfloor$

Insert the midpoint in the array (e.g., [21 27 33]).

for i =1 to $log_2(Upper\ Bound - Lower\ Bound) - 1$ **do**

Find midpoint between array value #1 and array value #2, and between array value #2 and array value #3

Insert two new midpoints in the array (e.g., [21 24 27 30 33])

Find the value of fitness for all the elements in the array (e.g., $[f_{21} \quad f_{24} \quad f_{27} \quad f_{30} \quad f_{33}]$)

Collect all value of fitness by appending them to the array:

$$fitness\_array = [fitness\_array \quad [f_{21} \quad f_{24} \quad f_{27} \quad f_{30} \quad f_{33}]]$$

Compare array value #2 and array value #4 in the array

if array value #2 > array value #4
Select only the first three array values (e.g., [21 24 27])
else
Select only the last three array values (e.g., [27 30 33])
end if

end for

Find the maximum value of fitness in the array, $fitness\_array$

Optimum number of RFID readers $\Rightarrow$ *Number of RFID readers giving the maximum value of fitness*

Figure 4.31 The algorithm to find the optimum number of RFID readers

4.8. Experimental Design

A 2^k full factorial experimental design was employed to evaluate the effect that different factors have on the effectiveness of the developed GA and PSO algorithms to find the optimal number and location of RFID readers in a facility. The effectiveness of the GA and PSO algorithms was measured by means of a value of fitness (i.e., the experimental response). Factorial experimental designs are widely used in experiments involving several factors when it is necessary to study the joint effect of the factors on a response (Montgomery, 2008).

Six experimental factors (i.e., $k = 6$) were investigated in this experiment. Each factor was tested at two levels (i.e., high and low). The experimental factors and their levels are summarized in Table 4.14. The next sections include a detailed description of each experimental factor.

Table 4.14 Experimental controlled factors in the experimental design

Factors	**Level of the Factor**	
	High (+)	**Low (-)**
A. Facility Shape	Non-rectangular shape Inverted-T (Ji's facility)	Rectangular shape (Tang's facility)
B. Facility Size	Large	Small
C. Grid Size	1 meter	0.25 meter
D. Power Levels	RFID readers have different power levels	RFID readers have the same power levels
E. Model formulation	EAC	CAC
F. Optimization Algorithm	PSO	GA

A total of 64 treatment combinations were created using the different levels of the experimental factors. Three replications were performed for each treatment combination. Therefore, a total of 192 experiments were conducted. All 192 replications were fully randomized before conducting the experiments, as shown in APPENDIX B.

4.8.1. Facility Shape

Two facility shapes were used in the experiment (i.e., rectangular or non-rectangular). The rectangular facility shape was found in the research conducted by Tang et al. (1997), whereas the non-rectangular facility shape (or inverted-T shape facility) was found in the research conducted by Ji et al. (2002). Both facility layouts had been used as test beds for research that involved the determination of optimal locations for wireless base stations for indoor environments. The main reasons these two facilities were selected were:

1. They are real facilities. Facility used in Tang et al. (1997) is the second floor of Whittemore Hall at Virginia Polytechnic Institute and State University and Facility used in Ji et al. (2002) is located on the third floor of Link Hall at Syracuse University in New York.
2. The authors provided very detailed information about the location of obstructions (i.e., walls) within the facilities which proved very useful in the modeling of passive interference.

Figure 4.32 depicts the rectangular facility shape, whereas Figure 4.33 depicts the non-rectangular facility shape.

4.8.2. Facility Size

A large and a small facility were considered in the experiment. The original size of the facility obtained from Tang et al. (1997) is 75 meters by 30 meters, whereas the facility obtained from Ji et al. (2002) measures 80 meters by 60 meters. These facility sizes were used as the high level for this factor.

The small facility size was obtained by scaling down the original facility size while maintaining the facility shape. The size of the small facilities is approximately one-ninth of that of the large facilities. The small facilities are depicted in Figure 4.34 and Figure 4.35, respectively.

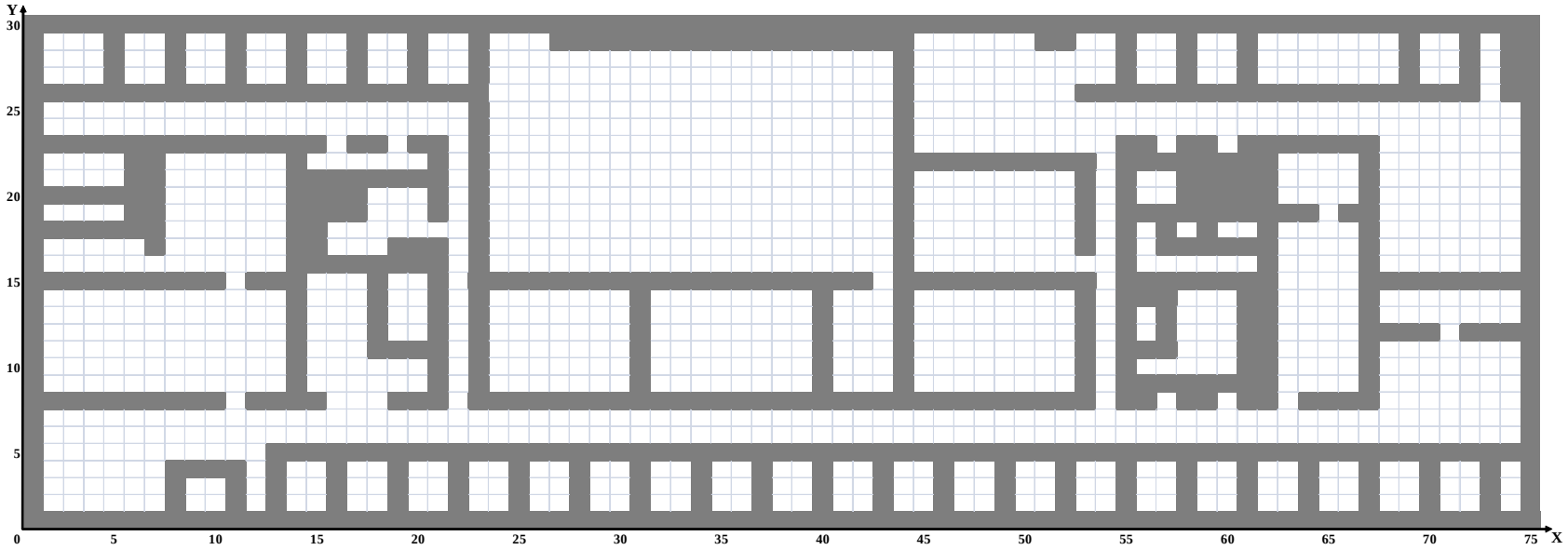

Figure 4.32 Rectangular shape of facility and its layout (Tang et al., 1997)

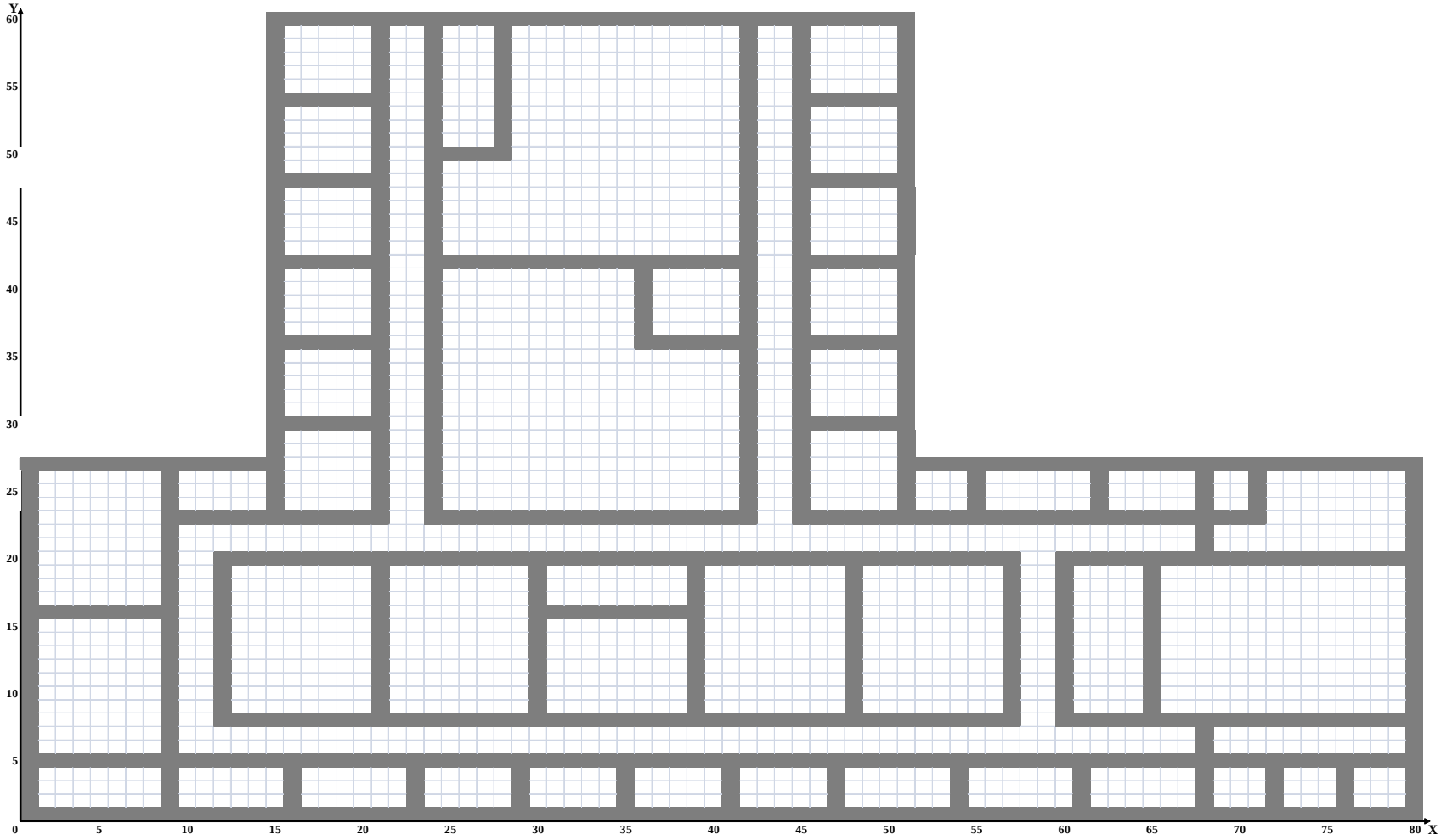

Figure 4.33 Non-rectangular (Inverted-T) shape of facility and its layout (Ji et al., 2002)

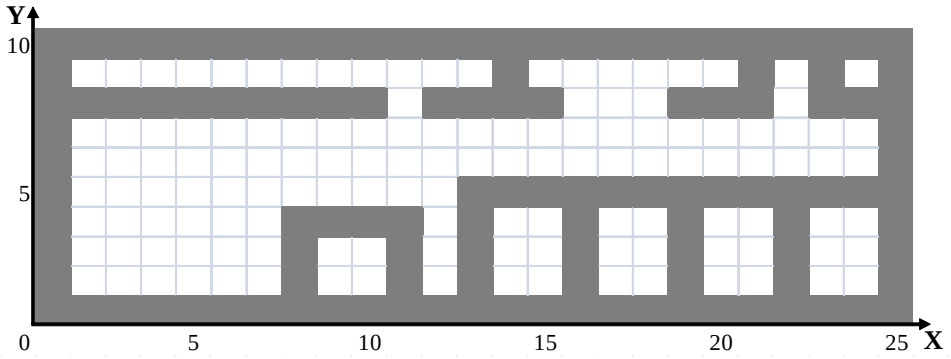

Figure 4.34 Small rectangular shape of facility and its layout

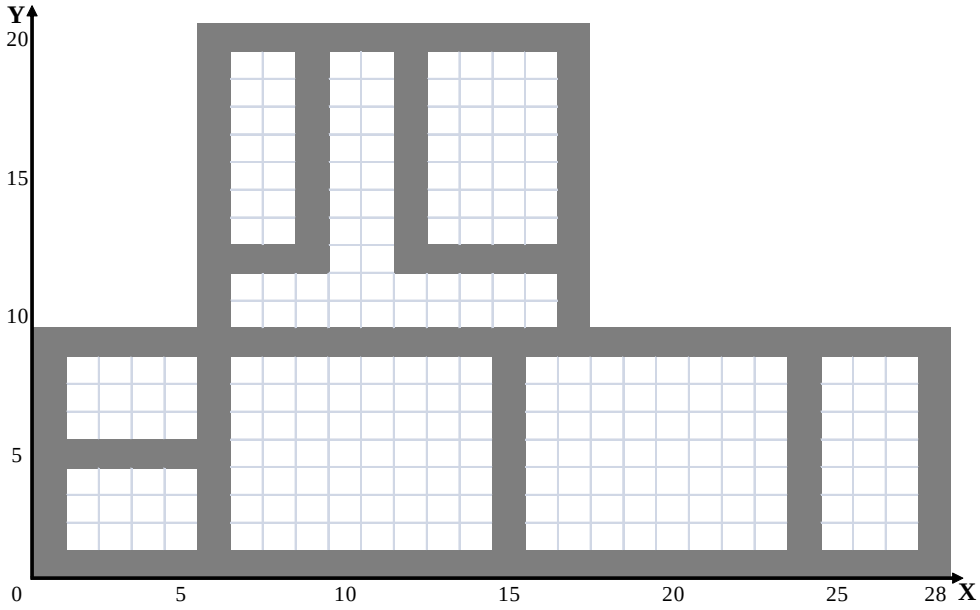

Figure 4.35 Small non-rectangular shape of facility and its layout

4.8.3. Grid Size

The objective of the GA and PSO algorithms is to place RFID readers at the center (*h*, *k*) of a particular grid in a facility. Decreasing the grid size may give these algorithms an opportunity to obtain a better solution by allowing them to place RFID readers at locations that otherwise would not be available. However, it might also increase the complexity of the problem because a larger number of site locations have to be considered as the grid size is reduced. The grids sizes considered in the experiment were one meter and 0.25 meter.

4.8.4. Power Levels

Commercially available RFID readers have power levels in the range of 10-30 dBm (Bolic et al., 2010). An RFID reader capable of adjusting its power levels (and thus its antenna coverage area) can overcome reader-to-reader interference more easily. This feature may translate into a larger or small number of RFID readers required to ensure a desired coverage level.

The high level for this factor is represented by all the RFID readers using the same power level (i.e., 30 dBm). In the low level, eight power levels are possible and the specific power level used by an RFID reader is selected randomly by the GA and PSO algorithms. The eight possible power levels are 30, 27, 24, 21, 18, 15, 12, and 9 dBm

4.8.5. Model Formulation

Each of the two model formulations developed in this research (i.e., CAC and EAC) represents a level for this factor. The EAC model formulation is the high level, whereas the CAC model formulation is the low level.

4.8.6. Optimization Algorithm

Each of the two optimization algorithms developed in this research (i.e., GA and PSO) represents a level for this factor. The POS optimization algorithm is the high level, whereas the GA optimization algorithm is the low level.

4.9. Hardware and Software Specification

The specifications of the computer used to conduct the experimental runs were as follows:

- Dell XPS 8500 personal computer.
- Intel® Processor Core™ i7-3770, 3.40 GHz.
- 16 GBytes RAM.
- Microsoft Windows 8 Professional Operating System.

The GA and PSO algorithms were implemented using MATLAB version 7.0.1

5. RESULTS AND DISCUSSION

This chapter presents and discusses the results obtained in this research. First, the GA and PSO algorithms developed in this research are validated by comparing the results obtained using the CAC model formulation against those obtained by Chen et al. (2011).

The effectiveness and the efficiency of the GA and PSO algorithms are evaluated next under two different scenarios: (1) in a small facility with 50 RFID tags placed at random locations, and (2) in a small facility with RFID tags located at the center of candidate grids. A different number of RFID readers is used in both scenarios (i.e., three and four, respectively) to show how fast the computation time needed to find the optimal solutions increases with the addition of only one RFID reader.

The results from conducting a full factorial experiment with the six RFID network design factors *facility shape*, *facility size*, *grid size*, *power levels*, *model formulation*, and *optimization algorithm* are then presented. The objective of this experiment was to better understand the effect that all these factors have on the quality of a solution as measured by the value of fitness.

Finally, the results from experiments conducted with the four RFID network design factors *grid size*, *power levels*, *model formulation*, and *optimization algorithm* assuming a specific facility shape and facility size are presented. The purpose of these experiments is to show the practical application of the modeling and optimization of the RFID network in a facility when the facility shape, facility size, and the locations of obstructions are known.

For clarity, the structure of this chapter is illustrated in Figure 5.1.

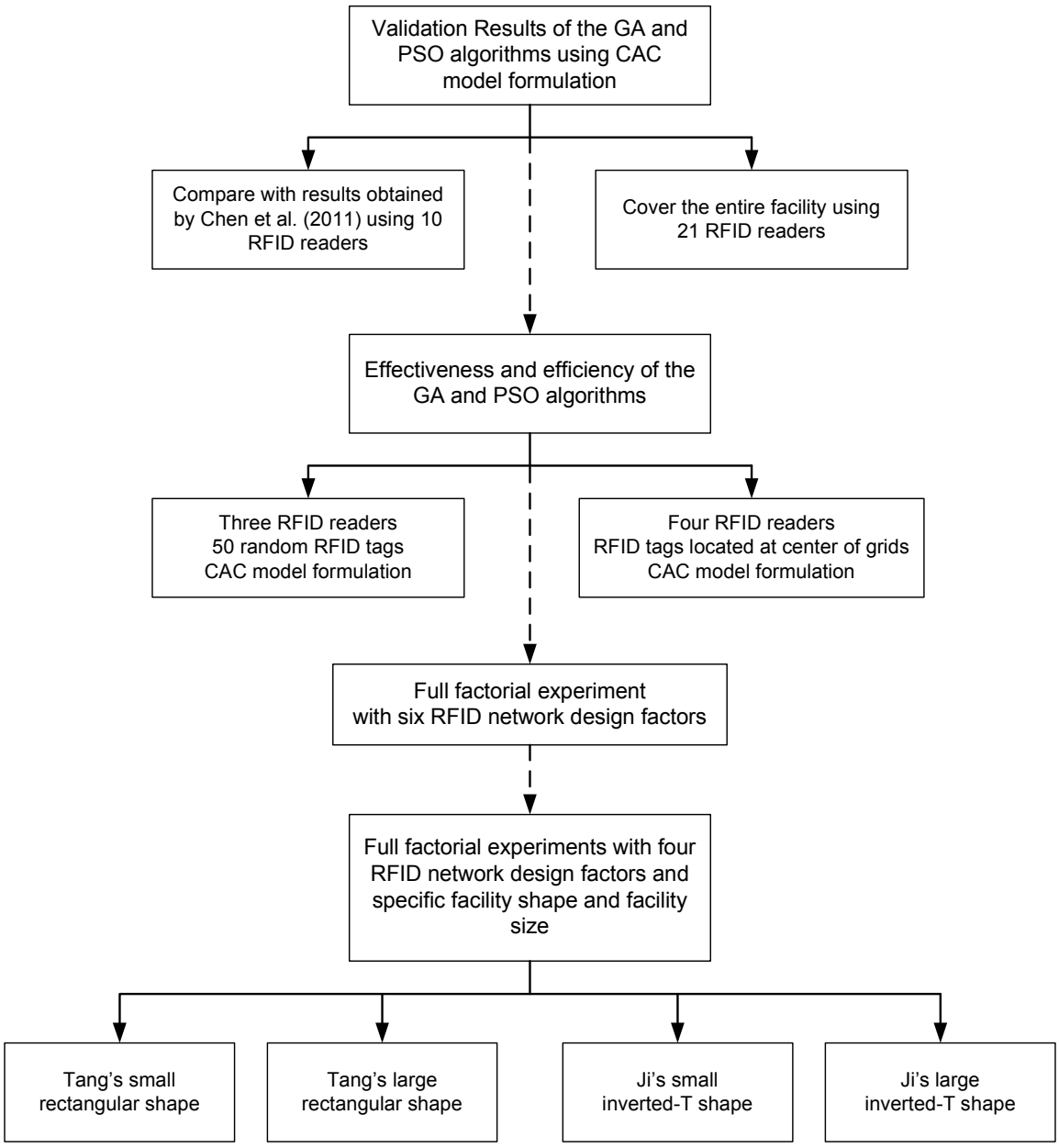

Figure 5.1 Structure of the Results Chapter

5.1. Validation of Optimization Algorithms and CAC Model Formulation

In this section, the results of validating the GA and PSO algorithms developed in this research are presented. The validation process involved applying both the GA and PSO algorithms to the CAC model formulation and comparing the results obtained to those reported by Chen et al. (2011). The research results reported by Chen et al. (2011) were used as the basis for validation because they provided the best level of detail regarding the specifics of the problem and the steps followed in their methodology.

5.1.1 Problem Description

The main objective in producing a solution to the RFID network planning (RNP) problem is to determine the *number* and *location* of the RFID readers in a facility to maximize a specific objective (or set of objectives). To this end, an indoor test facility (ITF) with a height of 30 meters and a width of 30 meters was utilized. The ITF, depicted in Figure 5.2, constitutes a free space environment with no obstructions. A total of 99 RFID tags (represented by the "x" marks in Figure 5.2) are placed randomly within the boundaries of the ITF. The solid black circles located in the ITF represent potential locations for the RFID readers (i.e., centers of candidate grids) and correspond to the coordinate points (0.5,0.5) to (29.5, 29.5). Thus, there is a total of 900 individual coordinate points that represent potential locations for the RFID readers.

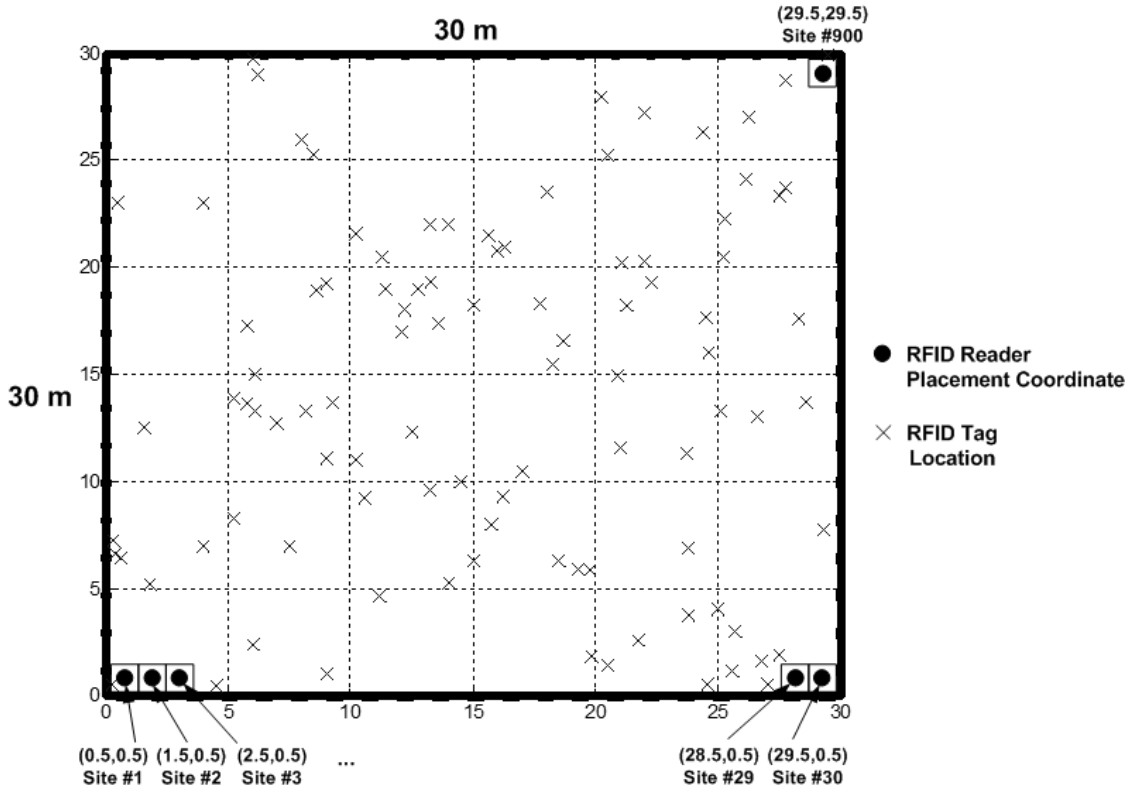

Figure 5.2 The indoor test facility (Chen et al., 2011)

Omnidirectional antennas with a circular coverage area were used to generate an initial set of RFID readers to cover the entire ITF. The radius (in meters) of the omnidirectional antenna's circular coverage can be calculated using the simple free space propagation formula shown in equation 5.1a and 5.1b.

$$P_{Rx} = P_{Tx}\frac{A_e}{4\pi r^2} \Rightarrow r = \sqrt{\frac{P_{Tx}}{P_{Rx}} \cdot \frac{A_e}{4\pi}} \tag{5.1a}$$

$$A_e = \frac{\lambda^2}{4\pi} \cdot G \tag{5.1b}$$

Where:

P_{Rx} = Power received by the RFID tag

P_{Tx} = Power transmitted by the RFID reader

A_e = Effective area of the antenna

λ = Wavelength of the signal

G= Gain of the antenna (assumed to be 1)

r = Radius of the antenna's coverage area

Assuming a transmission frequency of 915 MHz, a transmitted power of 2 W, and a received threshold power of 0.1 mW, the radius (r) of the coverage area for each omnidirectional antenna is calculated to be 3.69 meters. This value of r translates into an initial number of RFID readers required in the system in the range of 21 to 33 using the constraint in equation 4.3 of the CAC model formulation.

Finding an optimal number of RFID readers and their location to cover the ITF based on the initial number of RFID readers obtained from equation 4.3 is an NP-hard problem. Therefore, heuristic optimization procedures based on GA and PSO were utilized. The GA and PSO algorithms described in sections 4.7.1 and 4.7.2, respectively, were implemented as a software tool to solve the RNP problem in a reasonable computation time.

5.1.2 Fitness Function Evaluation

The objective functions of the CAC model formulation (shown in equation 4.1a to equation 4.1d) were used for the fitness function evaluation. Several competing system requirements were considered when optimizing the number and placement of RFID readers in the ITF. These system requirements were the following:

- Maximize RFID reader antenna coverage within the ITF.
- Minimize the interference in the downlink communication channel, i.e., the communication from an RFID reader to an RFID tag. This objective also maximizes the signal-to-interference ratio of the downlink communication channel (*Downlink SIR*).
- Minimize the interference in the uplink communication channel, i.e., the backscattered signal from an RFID tag to an RFID reader, thus also maximizing the signal-to-interference ratio of the uplink communication channel (*Uplink SIR*).
- Minimize the number of RFID readers required in the system. This objective also minimizes the implementation cost.

Since all the system requirements have to be satisfied simultaneously, this problem can be formulated as a multi-objective function model. All objectives have a value that can range between 0 and 1. They are combined into a fitness assignment using a weighted sum or linear combination, as shown in equation 5.2., where the sum of the weights assigned to the different objectives adds up to one.

No prior evidence was found that suggested a specific method to assign weights to the different objectives. In most cases, the suggestion was that this decision is the

responsibility of the modeler and relies heavily on prior experience with and knowledge of the system being modeled. In this research, the coverage objective was considered the most important objective and therefore was assigned a larger weight. After assigning a weight to the coverage objective, the remaining two objectives were assigned weights with equal values to respect the constraint that the summation of the weights must be equal to one.

The results showed that the GA algorithm obtained better fitness than the PSO algorithm in most cases. Therefore, the GA algorithm was used in the process of finding the most appropriate value for the weights for each objective in the fitness function. To find the most appropriate setting for the weight value of the coverage objective, its value was varied starting at 1.0 and then lowered in decrements of 0.1 until the GA algorithm could no longer cover all 99 RFID tags in the ITF. By using this approach, the GA algorithm could still ensure the entire coverage of the ITF, while also improving (i.e., reducing) interference and cost. Using this procedure, it was found that 0.6 was the lowest weight value of the coverage objective that allow the GA algorithm to still cover 99 RFID tags in the ITF. Thus, the interference and cost objectives were assigned equal values of 0.2, as shown in equation 5.2.

$$Fitness = 0.6 \times coverage + 0.2 \times (downlink\ SIR + uplink\ SIR) + 0.2 \times cost \quad (5.2)$$

5.1.3 Parameters of the GA and PSO Algorithms

Table 5.1 shows the parameters of the GA and PSO algorithms used to find good solutions to the RNP problem with the CAC model formulation. The parameters shown on the left side of Table 5.1 were common to both heuristics optimization algorithms. The right side of Table 5.1 shows the specific parameter values used with the GA or the PSO algorithms. It is important to note that the values for w, c_1 and c_2 of the PSO algorithm were set using the constricted coefficient procedure suggested by Clerc and Kennedy (2002).

Table 5.1 Parameters of the GA and PSO algorithms

Parameters	Values	Parameters	Values
Facility dimension	30m × 30m	**PSO parameters**	
Number of RFID tags	99	Number of particles	50
RFID tag distribution	Uniform	Stopping criteria	1000 iterations
Number of RFID readers	10† or 21	Inertia (w)	0.7298
Propagation model	Free space	Cognitive component (c_1) & social Component (c_2)	1.4962
Propagation equation	$P_{RX} = P_{TX} \frac{A_e}{4\pi r^2}$	**GA parameters**	
RFID tag power threshold (P_{RX})	-10 dBm (0.1 mW)	Number of populations	50
Transmitted power (P_{TX})	2 W	Mutation rate	0.05
Operating frequency	915 MHz	Stopping criteria	1000 generations
Effective aperture of antenna (A_e)	86cm^2 @ 915 MHz	Parent selection	Proportional to fitness
Signal coverage	Circular	Crossover	One-point crossover
Radius of signal coverage	3.69 m	Next generation selection	Strong child or parents

† **Number of RFID readers used to compare to results from Chen et al. (2011)**

5.1.4 Covering the ITF using Ten RFID Readers

Satisfying coverage is typically the most important objective in the RNP problem. Good algorithms should result in the coverage of as many RFID tags in the system as possible or coverage of the entire facility in the best case. Therefore, a simulation was conducted to assess the effectiveness of the PSO algorithm by comparing it to the results obtained in Chen et al. (2011). The modeling parameters shown in Table 5.1 were used in this simulation. It is also important to note that the number of RFID readers used was ten (the same as Chen's). The following sections present the validation results obtained from this experimentation.

5.1.4.1 Validation Results for the PSO Algorithm

Figure 5.3 shows that only 72 tags can be covered with ten RFID readers using the algorithm proposed by Chen et al. (2011). Figure 5.4 shows that the PSO algorithm developed in this research was able to cover 75 RFID tags and this solution was obtained in 269.56 seconds (no computation time was provided in Chen et al. (2011). This represents an improvement of 4.167% in terms of RFID tag coverage.

The optimum value of fitness was 0.7939 and was obtained after the PSO algorithm completed 520 iterations. The values obtained for the objectives *coverage*, *SIR* (the summation of *downlink SIR* and *uplink SIR*), and *cost* were 0.7576, 1.0, and 0.6970, respectively. The PSO algorithm stopped after the stopping criteria of 1,000 iterations was met. The evolution of the fitness function during the search is depicted in Figure 5.5.

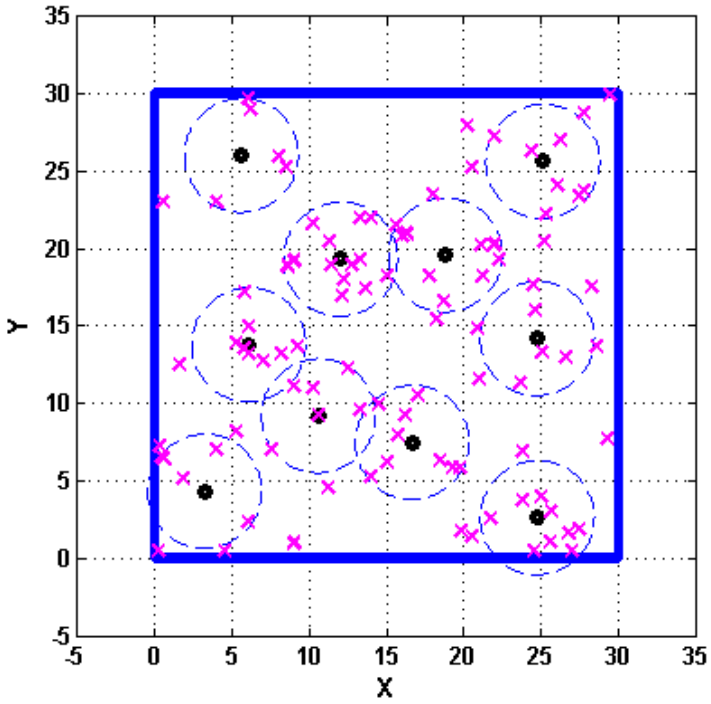

Figure 5.3 Coverage of the ITF by Chen et al. (2011)

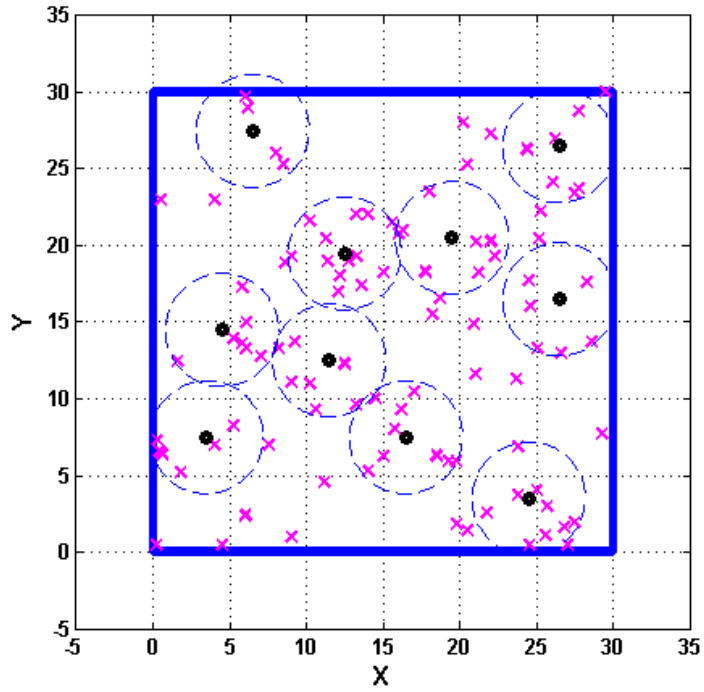

Figure 5.4 Coverage of the ITF by the PSO algorithm

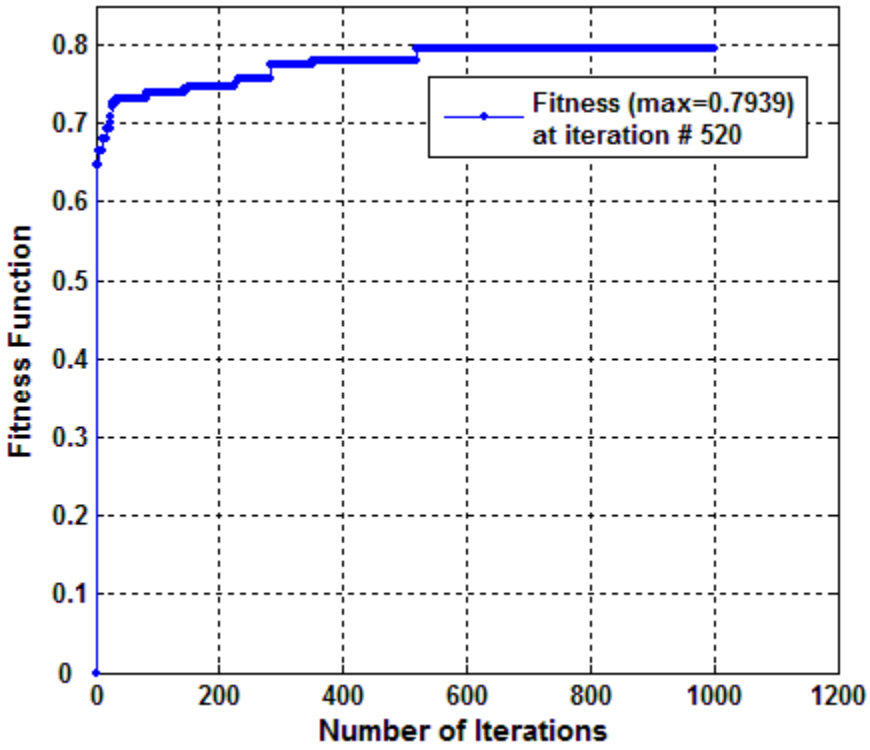

Figure 5.5 Evolution of the fitness function during the search for the PSO algorithm

5.1.4.2 Validation Results for the GA

Figure 5.6 shows that 76 tags were covered with the GA developed in this research, compared to only 33 tags covered with the procedure utilized by Chen et al. (2011). The result obtained with the GA represents and improvement of 5.556% and the solution was obtained in 539.15 seconds. Figure 5.7 shows the evolution of the fitness function during the search. The optimum value of fitness was 0.8000 and was reached after the algorithm ran approximately 392 generations. The objective of coverage, SIR, and cost were 0.7677, 1.0, and 0.6970, respectively.

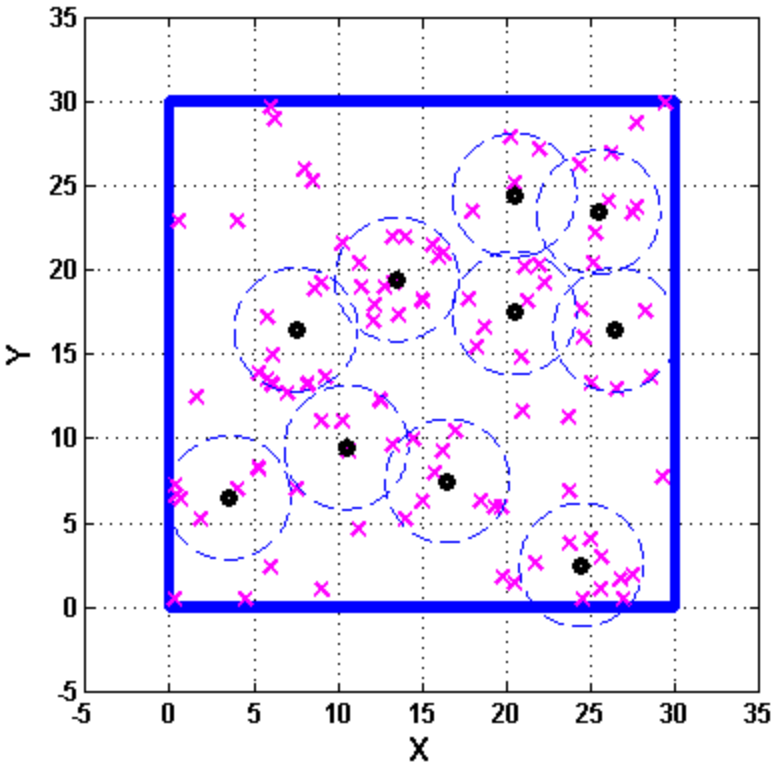

Figure 5.6 Coverage of the ITF by the GA

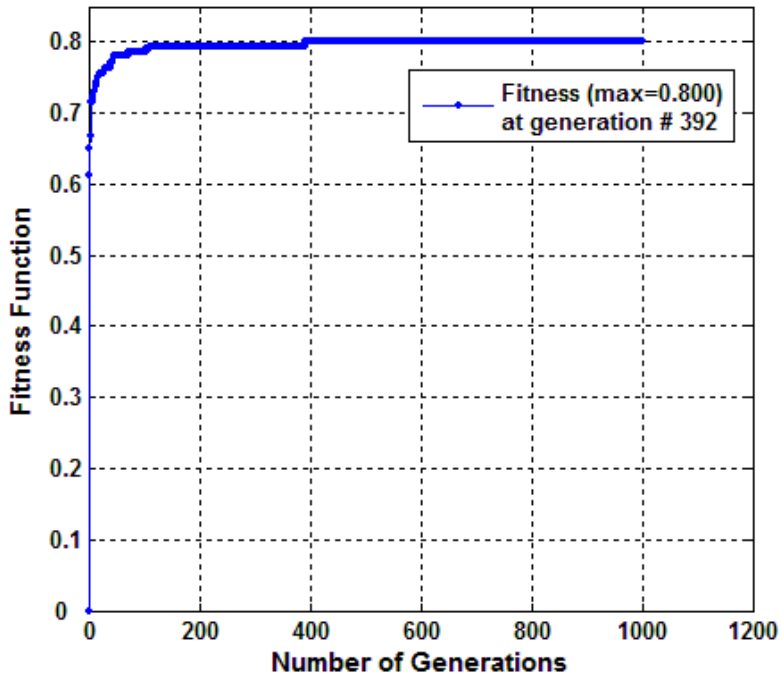

Figure 5.7 Evolution of the fitness function during the search for the GA

5.1.4.3 Summary of Validation Results

The results of validating both the GA and PSO algorithms with the CAC model formulation against the results obtained by Chen et al. (2011) are summarized in Table 5.2. Overall, the results show that the GA and the PSO algorithms have the ability to search and find good solutions to the RNP problem. When using ten RFID readers, the GA performed better than the PSO algorithm in terms of the number of RFID tags covered and the overall value of fitness. However, the GA required a longer computation time to reach this result than the PSO algorithm. The PSO algorithm had a better computation time per iteration (i.e., 0.26956 seconds per iteration) compared to about 0.53915 seconds per generation for the GA.

Table 5.2 Summary of results from Chen et al. (2011), GA and PSO for partial ITF coverage with 10 RFID readers

	Chen at al. (2011)	**PSO**	**GA**
Number of RFID readers used	10	10	10
Number of RFID tags covered	33	75	**76**
Value of fitness	N/A	0.7939	**0.8000**
Computation time (seconds)	N/A	**269.56**	539.15
Iterations	N/A	**1,000**	1,000
Computation time / iteration (seconds)	N/A	**0.26956**	0.53915

5.1.5 Covering the entire Indoor Test Facility

As mentioned in section 5.1.1, a total of 33 RFID readers would be required to cover the entire ITF. The coverage provided by this number of RFID readers would be very inefficient because:

- Large amounts of RF energy would be lost.
- Large amounts of overlapped coverage would be obtained, which would result in a high level of interference.
- It would not be cost-effective.

Logically, the number of required RFID readers should be in the range between 21 to 33 RFID readers. Therefore, the optimum location and the optimum number of RFID readers needed to cover all 99 RFID tags in the system were further investigated by applying the GA and PSO algorithms to the CAC model formulation. The following sections present the results obtained from this experimentation.

5.1.5.1 Results for the PSO Algorithm

The number of RFID readers started with a lower bound of 21 RFID readers and an upper bound of 33 RFID readers. The binary search algorithm (BSA) described in section 4.7 was then applied to evaluate and compare the value of fitness of each number of RFID readers. It was determined that 21 RFID readers was the optimum number to cover most RFID tags in the ITF.

The graphical results of this evaluation are depicted in Figure 5.8, where the coverage area of each RFID reader is represented by a dotted line. The blue solid line represents the boundary of the ITF and the "x" marks represent RFID tags that were randomly added onto

the ITF. Finally, the black circles in the center of the coverage areas indicate the optimum locations for the RFID readers, as determined by the PSO algorithm.

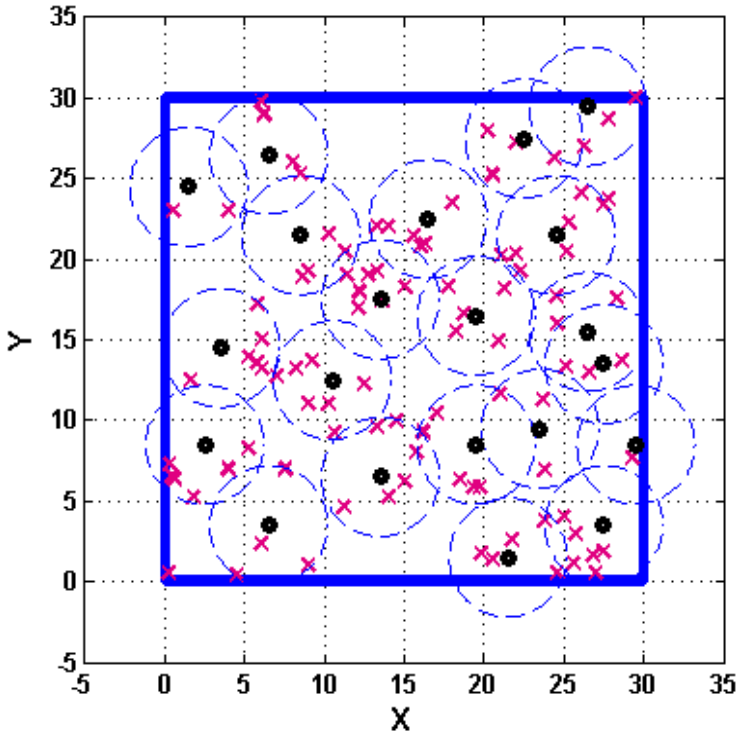

Figure 5.8 The optimum location and number of RFID readers to cover all tags in the ITF using the PSO algorithm

In terms of the fitness function, the value for coverage was 0.9798 meaning that 97 RFID tags are covered by at least one RFID reader in the system. The PSO algorithm could not achieve a complete coverage of all the RFID tags in the ITF after 1,000 iterations using 21 RFID readers. The value of SIR, i.e., the summation of downlink SIR and uplink SIR, was 0.8339. The value for cost, as calculated with equation 4.1d, was 0.3636. As a result, the value of fitness obtained with equation 5.2 was 0.8274. The PSO algorithm was terminated after 1,000 iterations with a total computation time of 2,193.57 seconds. The evolution of the fitness function during the search is depicted in Figure 5.9.

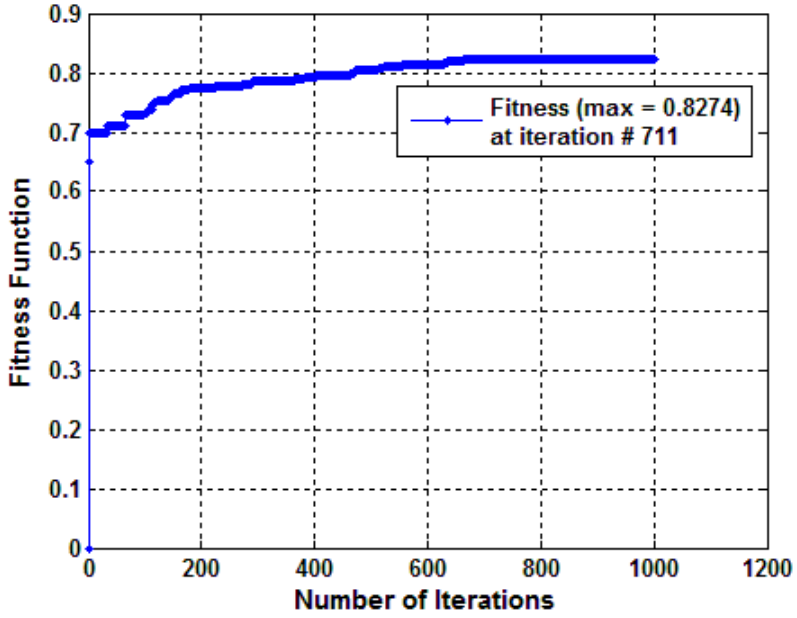

Figure 5.9 Evolution of the fitness function during the search of the PSO algorithm to cover the entire ITF

5.1.5.2 Results for the GA

The solution produced by the GA achieved complete coverage of all 99 tags in the ITF using 21 RFID readers, as depicted in Figure 5.10. However, more RFID tags were located in the overlapping areas of two or more RFID readers when compared to the results produced by the PSO algorithm. Therefore, the results produced by the GA may translate into more interference in both the downlink and uplink communication channels.

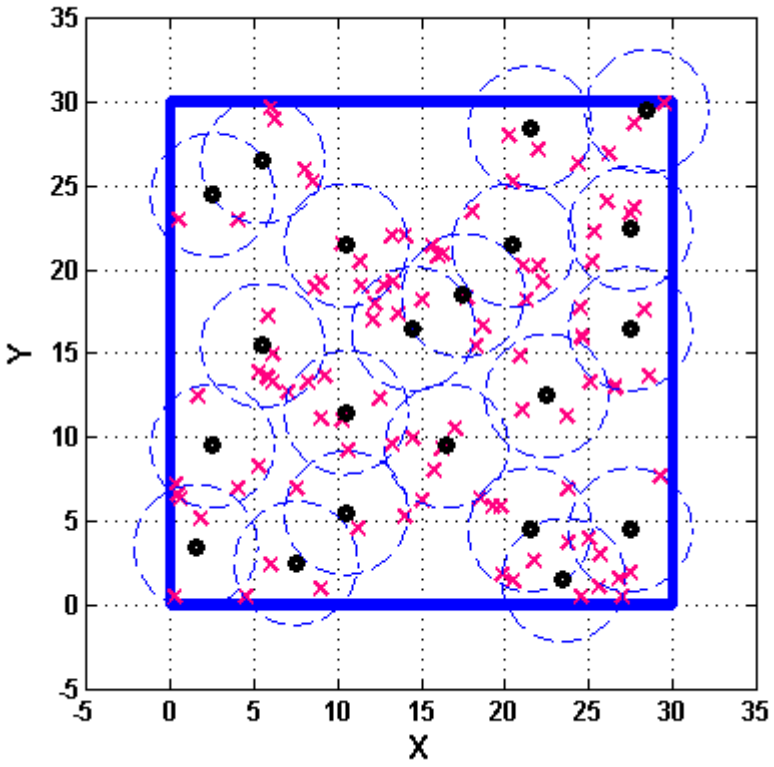

Figure 5.10 The optimum location and number of RFID readers to cover all RFID tags in the ITF using the GA

Additionally, the GA obtained a better value of fitness (i.e., 0.8325) than that of the PSO. The values of coverage, SIR, and cost were 1.0, 0.799, and 0.3636, respectively. The GA also achieved the maximum value of fitness faster than the PSO algorithm (i.e., at generation 546). The GA was terminated after 1,000 generations with a computation time of 4,587.38 seconds. The evolution of the fitness function during the search is depicted in Figure 5.11.

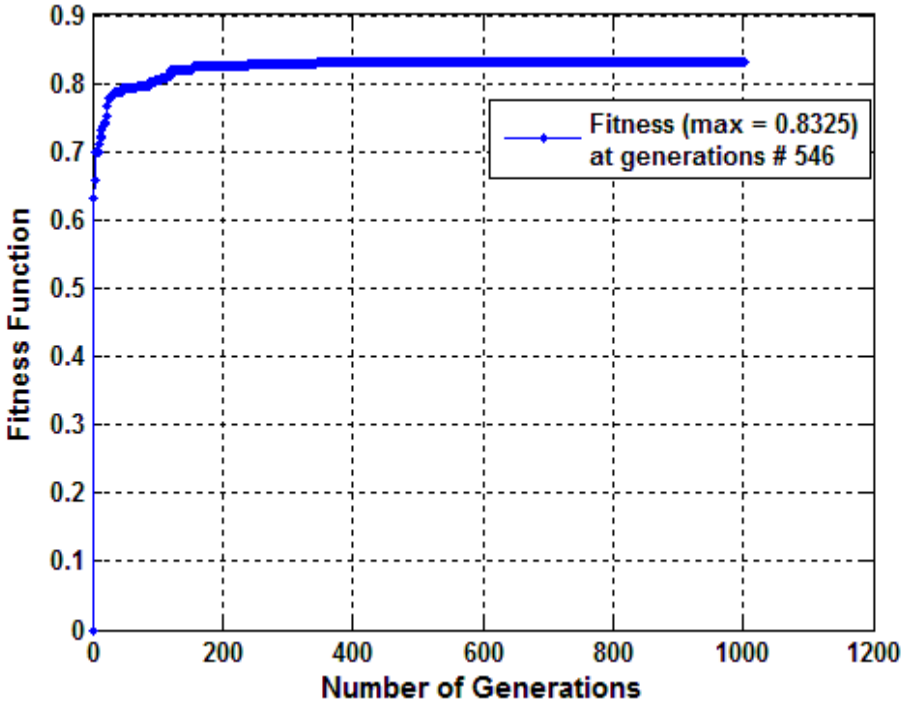

Figure 5.11 Evolution of the fitness function during the search of GA to cover entire ITF

5.1.5.3 Summary of Results

The results of covering the entire ITF using the CAC model formulation and the GA and PSO algorithms are summarized in Table 5.3. The cells highlighted in gray represent the categories in which one of the optimization algorithms outperformed the other.

The results in Table 5.3 show that both the GA and PSO algorithms have the ability to search and find good solutions to the RNP problem. When attempting to cover the entire ITF, the GA had a better performance when compared to the PSO algorithm in term of the value of fitness (i.e., 0.8325 versus 0.8274). The GA can also cover a larger number of RFID tags in the system (i.e., 99 versus 97). However, a larger number of RFID tags were located in the overlapping areas of two or more RFID readers which decreases the value of the SIR.

The GA needed a longer computation time, but it converged to the maximum value of fitness faster (i.e., lesser number of iterations) than the PSO algorithm.

Table 5.3 Summary of results for the GA and PSO algorithms to cover entire ITF.

	PSO	**GA**
Number of RFID readers used	21	21
Number of RFID tags covered	97	**99**
Value of fitness	0.8274	**0.8325**
Iterations	1,000	1,000
Computation time (seconds)	**2,193.57**	4,587.38
Computation time / iteration (seconds)	**2.194**	4.587

5.2. Effectiveness and Efficiency Evaluation of Optimization Algorithms

In this section, the results of assessing the *effectiveness* and *efficiency* of the GA and PSO algorithms are presented. First, the CAC model formulation was applied to a small facility (10 meters by 10 meters) using three or four RFD readers. The GA and PSO algorithms were then used to generate solutions to the resulting CAC model formulation. The reference utilized to assess the effectiveness and efficiency of the GA and PSO algorithms was an exact solution obtained through exhaustive enumeration for the same small facility.

The GA and PSO algorithms were ran five times each to obtain a solution to the CAC model formulation when applied to the small facility. A value for e*ffectiveness* (as a percentage) was obtained by evaluating how many times out of five each algorithm matched the exact solution obtained through exhaustive enumeration. *Efficiency* was assessed using equation 5.3:

$$Efficiency_{GA \text{ or } PSO} = \frac{T_{Exhaustive} - \overline{T}}{T_{Exhaustive}} \times 100\% \tag{5.3}$$

Where:

$T_{Exhaustive}$ = Computation time (in seconds) needed to obtain the exact solution via exhaustive enumeration.

$\overline{T}$ = Average computation time (in seconds) over five runs obtained via either the GA or PSO algorithms

Two different test scenarios were simulated. The first test scenario involved three RFID readers and 50 RFID tags placed randomly within a small facility. In the second test

scenario, four RFID readers were used and the RFID tags were located at the center of each candidate grid in a small facility.

5.2.1. Results for the First Test Scenario

Table 5.4 summarizes the results obtained through exhaustive enumeration for the first scenario, which involved three RFID readers with a coverage radius of 3.69 meters and 50 RFID tags placed randomly within a small facility. Table 5.4 shows that a total of 161,700 possible RFID reader placement combinations exist. Three optimal solutions were obtained with a value of fitness of 0.8260. The values for coverage, SIR, and cost were 0.96, 1.0, and 0.25, respectively. The computation time was 132.723 seconds.

Table 5.4 Exhaustive enumeration results for the first test scenario

Total Solutions	161,700
Total Optimum Solutions	3
Value of fitness	0.8260
Coverage	0.96
SIR	1.0
Cost	0.25
Computation Time (seconds)	132.723

Table 5.5 summarizes the effectiveness and efficiency results for the PSO algorithm. The effectiveness of the PSO was 80% since it achieved the optimal solution in four out of five replications. Its fastest computation time to reach the optimal solution was 0.744 seconds (23 iterations). The efficiency of the PSO algorithm was 88.34%, which means that the PSO

algorithm reduced the computation time by 88.34% compared to that of the exhaustive enumeration. However, it is clear that the computation time and number of iterations needed to obtain the optimum solution were inconsistent.

Table 5.5 Effectiveness and efficiency of the PSO for the first test scenario

Run #	Fitness Value	Optimal Solution?	Computation Time (seconds)	Number of Iterations to Achieve Optimal Solution
1	0.8260	Yes	1.853	84
2	0.8260	Yes	3.712	204
3	0.8033	No	69.818	5,000
4	0.8260	Yes	0.744	23
5	0.8260	Yes	1.22	43

Table 5.6 summarizes the effectiveness and efficiency results for the GA. The GA performed better than the PSO algorithm since it achieved the optimal solution in all five replications for an effectiveness of 100%. The efficiency of the GA was 98.85%, which means that the GA reduced the computation time by 98.85% compared to that of the exhaustive enumeration. Moreover, the computation time and the number of replications needed to achieve the optimal solution were more consistent with the GA. More specifically, the computation time was between one to two seconds and the number of generations were about 20.

Table 5.6 Effectiveness and efficiency of the GA for the first test scenario

Run #	Fitness Value	Optimal Solution?	Computation Time (seconds)	Number of Generations to Achieve Optimal Solution
1	0.8260	Yes	1.574	21
2	0.8260	Yes	1.15	14
3	0.8260	Yes	1.616	22
4	0.8260	Yes	1.595	21
5	0.8260	Yes	1.711	23

5.2.2. Results for the Second Test Scenario

The CAC model formulation was developed under the assumption that RFID tags are located at the center of all candidate grids in the facility. Therefore, the results presented in this section are more representative than those obtained in the scenario described in section 5.2.1.

Table 5.7 summarizes the results obtained through exhaustive enumeration for the second test scenario, which involved four RFID readers with a coverage radius of 3.69 meters and 100 RFID tags located at the center of each candidate grid in a small facility. Also, it is important to note that four RFID readers is not the optimum number to obtain the optimal value of fitness in this scenario. However, this number of RFID readers was used to investigate the effect of adding one more RFID reader on the computation time.

Table 5.7 shows that a total of 3,921,225 possible RFID reader placement combinations exist. Only one optimal solution was obtained with a value of fitness of 0.7760. The values for coverage, SIR, and cost were 0.96, 1.0, and 0, respectively. The computation time was 30,266.693 seconds or 8.4074 hours.

Table 5.7 shows that by just adding one more RFID reader, the computation time increased from a few minutes (when using three RFID readers) to more than eight hours. This reinforces the need for the GA and PSO algorithms when facing problems that involve large facilities and/or large numbers of RFID readers.

Table 5.7 Exhaustive enumeration results for the second test scenario

Total Solutions	3,921,225
Total Optimum Solutions	1
Value of Fitness	0.7760
Coverage	0.96
SIR	1.0
Cost	0
Computation Time (seconds)	30,266.693

Table 5.8 summarizes the effectiveness and efficiency results for the PSO algorithm. The PSO achieved the optimal solution in three out of five replications for an effectiveness of 60%. Its fastest computation time to reach the optimal solution was 10.439 seconds (230 iterations). The efficiency of the PSO algorithm was 99.29%.

Table 5.9 summarizes the effectiveness and efficiency results for the GA. The GA achieved the optimal solution in four out of five replications for an effectiveness of 80%. Its fastest computation time to reach the optimal solution was 6.102 second (41 generations). The efficiency of GA was 99.40%.

Table 5.8 Effectiveness and efficiency of the PSO algorithm for the second test scenario

Run #	Fitness Value	Optimal Solution?	Computation Time (seconds)	Number of Iterations to Achieve Optimal Solution
1	0.7639	No	503.26	5,000
2	0.7760	Yes	15.957	336
3	0.7582	No	482.56	5,000
4	0.7760	Yes	10.439	230
5	0.7760	Yes	63.828	1,255

Table 5.9 Effectiveness and efficiency of the GA for the second test scenario

Run #	Fitness Value	Optimal Solution?	Computation Time (seconds)	Number of Generations to Achieve Optimal Solution
1	0.7760	Yes	6.102	41
2	0.7638	No	750.58	5,000
3	0.7760	Yes	20.13	125
4	0.7760	Yes	80.19	523
5	0.7760	Yes	41.57	257

The increase in the complexity of the problem made both the GA and PSO algorithms more inconsistent when searching for the optimal solution and this was reflected by the variation in computation time and the number of iterations/generations needed to achieve the optimal solution. However, optimal solutions (or near optimal solutions) were obtained within comparatively short computation time when compared to the computation time needed with exhaustive enumeration (i.e., the longest computation time of 750.58 seconds for the GA versus 30,266.693 seconds for the exhaustive enumeration).

5.3. Results from the Experimental Design with Six RFID Network Design Factors

This section presents the statistical analyses of the results obtained from the experimental design. The effects of six RFID network design factors (see Table 4.14) on the value of fitness were identified by performing a multi-factor analysis of variance (ANOVA).

In the experiments, the value of the radius (r) of the circular antenna coverage used in the CAC model formulation was 5.19 meters. The values of the semi-major axis (a) and the semi-minor axis (b) of the elliptical antenna coverage used in the EAC model formulation were 5.84 meters and 4.63 meters, respectively. The detailed description and values of all parameters used to calculate the r, a, and b can be found in APPENDIX C.

The results are presented in two sections. In section 5.3.1, the results of validating the ANOVA assumptions are presented (i.e., model adequacy checking). Section 5.3.2 presents the detailed statistical analyses based mainly on multi-factor ANOVA and Fisher's least significant difference (LSD) plots.

5.3.1. Model Adequacy Checking

To be able to apply the ANOVA to evaluate the effect of the six RFID network design factors on the value of fitness, the ANOVA assumptions had to be validated first. These assumptions are as follows (Montgomery, 2008):

- Normality of the residuals (error term).
- Independence of observations within and between samples.
- Equal variance.

Figure 5.12 depicts the normal probability plot of the residuals created to validate the normality assumption of the values obtained for the fitness function. The plot shows that the distribution of the residuals complies quite well with the normality assumption.

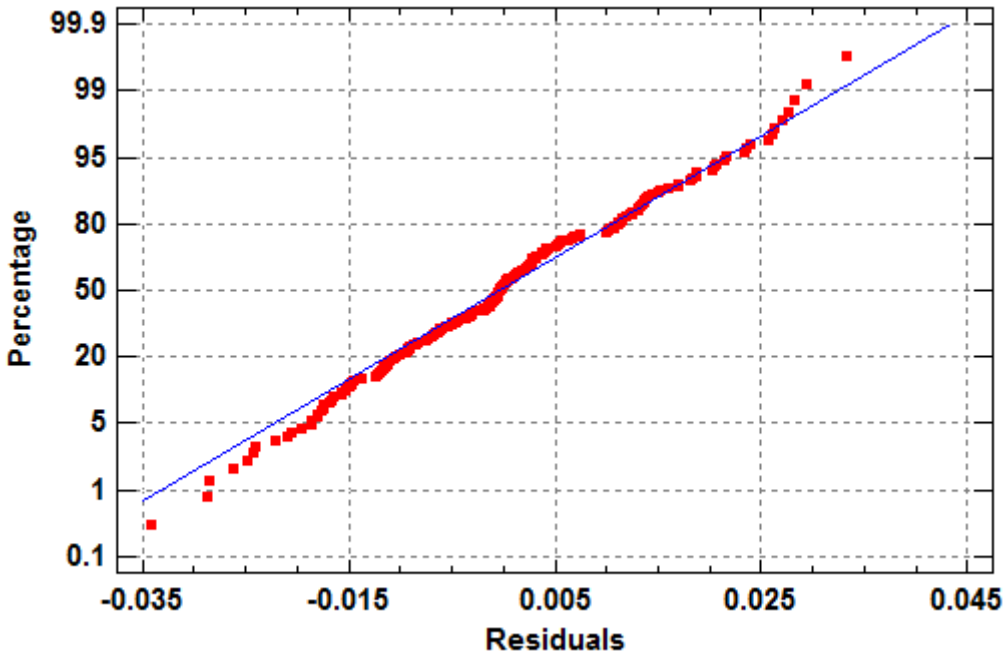

Figure 5.12 Normal probability plot of the residuals from the fitness

The assumption of the independence of observations within and between samples and the assumption of equal variance can be verified by a plot of residuals versus the variables of interest, i.e., the treatment combinations. Figure 5.13 shows that the residual plot is structureless. It can be concluded that there is no reason to suspect any violation of the independence or constant variance assumption.

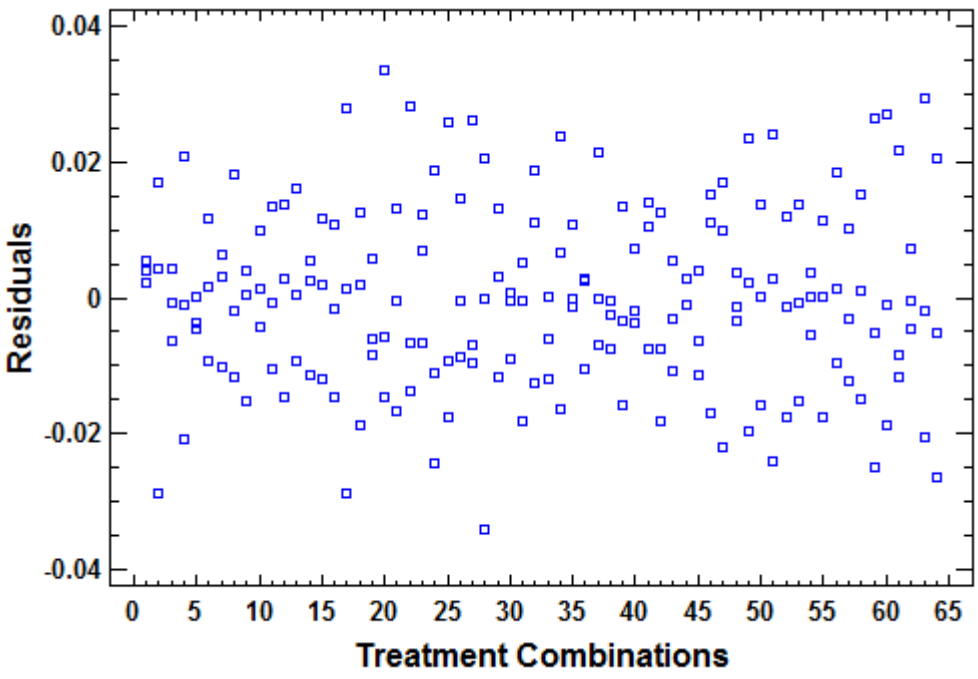

Figure 5.13 Residual plot of the fitness versus the treatment combinations

5.3.2. Result of the Statistical Analyses based on Six RFID Network Design Factors

This section presents the detailed statistical analyses of the effect of the six RFID network design factors on the performance of the system (i.e., the value of fitness). A multi-factor ANOVA was used to determine which main factors (i.e., the six RFID network design factors) and interactions had an effect on the quality of the fitness. The main factors and interactions were considered to be statistically significant if their p-value was less than 0.05. The multi-factor ANOVA table for the value of fitness based on six RFID network design factors is depicted in Table 5.10.

Table 5.10 Multi-factor ANOVA results based on six RFID network design factors

Source	*Sum of Squares*	*Df*	*Mean Square*	*F-Ratio*	*P-Value*
MAIN EFFECTS					
A: Facility shape	0.00325711	1	0.00325711	17.83	**0.0000**
B: Facility size	0.265206	1	0.265206	1451.74	**0.0000**
C: Grid Size	0.000181352	1	0.000181352	0.99	0.3209
D: Power levels	0.00839788	1	0.00839788	45.97	**0.0000**
E: Model formulation	0.00286907	1	0.00286907	15.71	**0.0001**
F: Optimization algorithm	0.0127368	1	0.0127368	69.72	**0.0000**
INTERACTIONS					
AC	0.00124542	1	0.00124542	6.82	**0.0100**
BC	0.00152325	1	0.00152325	8.34	**0.0045**
BD	0.0037843	1	0.0037843	20.72	**0.0000**
BF	0.00989576	1	0.00989576	54.17	**0.0000**
CD	0.000753667	1	0.000753667	4.13	**0.0442**
DF	0.001323	1	0.001323	7.24	**0.0080**
EF	0.000774413	1	0.000774413	4.24	**0.0414**
AEF	0.0010286	1	0.0010286	5.63	**0.0191**
BCD	0.00115346	1	0.00115346	6.31	**0.0132**
BDF	0.00148185	1	0.00148185	8.11	**0.0051**
ABDE	0.00103881	1	0.00103881	5.69	**0.0185**
ACDF	0.00101476	1	0.00101476	5.55	**0.0199**
BCEF	0.000999187	1	0.000999187	5.47	**0.0208**
RESIDUAL	0.024662	135	0.000182682		
TOTAL (CORRECTED)	0.349781	191			

Table 5.10 shows the main factors and the interactions that have a statistically significant effect on the value of fitness. The p-value of the RFID network design factors *facility shape*, *facility size*, *power levels*, *model formulation*, and *optimization algorithm* are less than 0.05 indicating that they all have a statistically significant effect on the value of fitness. The only RFID network design factor that does not have a statistically significant effect on the value of fitness is *grid size*.

The interaction effects in Table 5.10 that show a statistically significant effect are as follows:

- **Two-factor interactions**. Facility shape with grid size (AC); facility size with grid size (BC); facility size with power levels (BD); facility size with optimization algorithm (BF); grid size with power levels (CD); power levels with optimization algorithm (DF); and model formulation with optimization algorithm (EF).
- **Three-factor interactions**. Facility shape and model formulation with optimization algorithm (AEF); facility size and grid size with power levels (BCD); and facility size and power levels with optimization algorithm (BDF).
- **Four-factor interactions**. Facility shape, facility size, power levels, and model formulation (ABDE); facility shape, grid size, power levels, and optimization algorithm (ACDF); and the interaction of facility size, grid size, model formulation, and optimization algorithm (BCEF).

Fisher's least significant difference (LSD) interval plots of all RFID network design factors were produced at a 95% confidence level to illustrate how they influence the performance of the system in terms of the value of fitness. The LSD interval plots for *facility*

shape, *facility size*, *grid size*, *power levels*, *model formulation*, and *optimization algorithm* are depicted in Figure 5.14, Figure 5.15, Figure 5.16, Figure 5.17, Figure 5.18 and Figure 5.19, respectively.

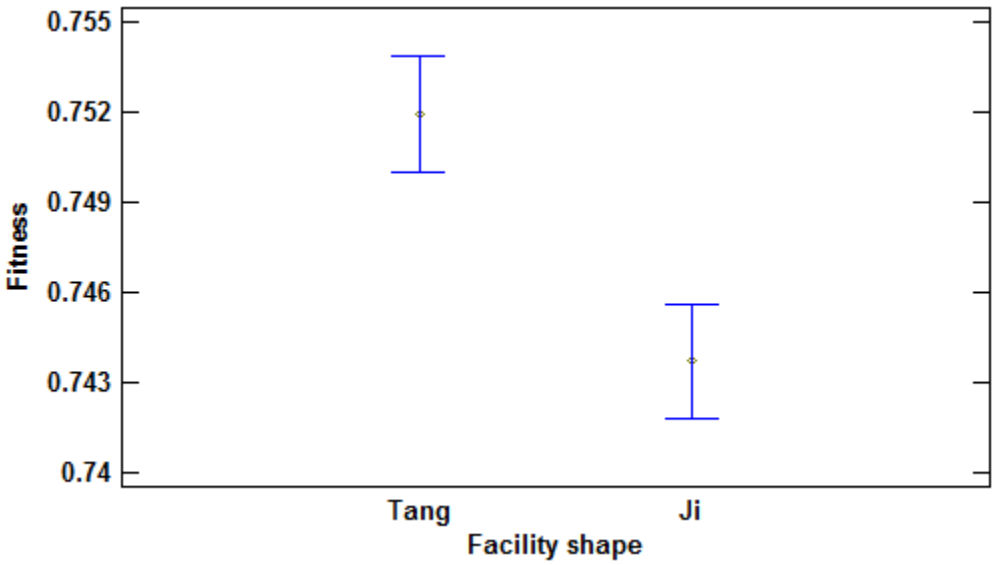

Figure 5.14 LSD interval plot of the RFID network design factor *facility shape*

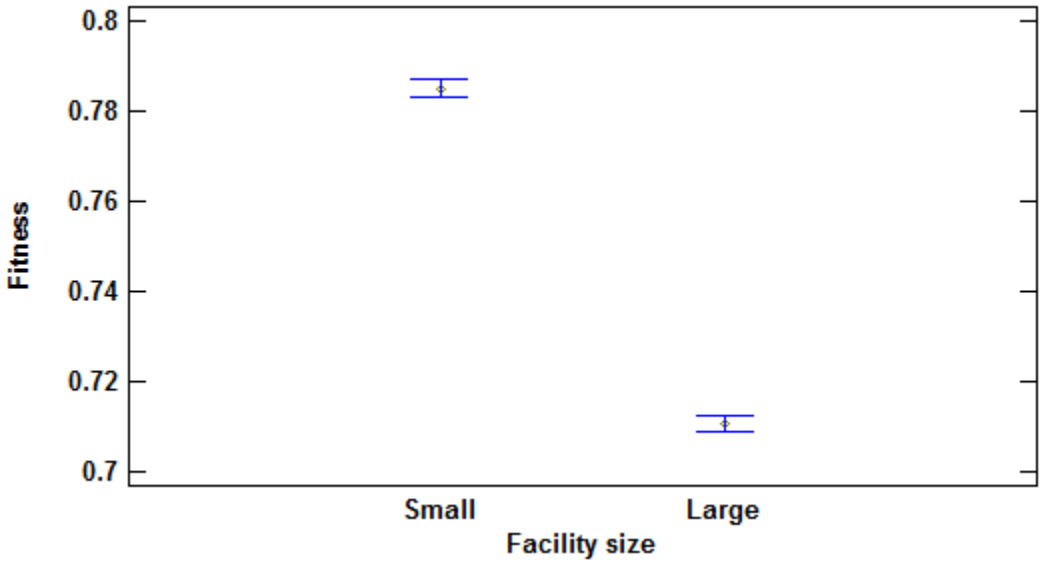

Figure 5.15 LSD interval plot of the RFID network design factor *facility size*

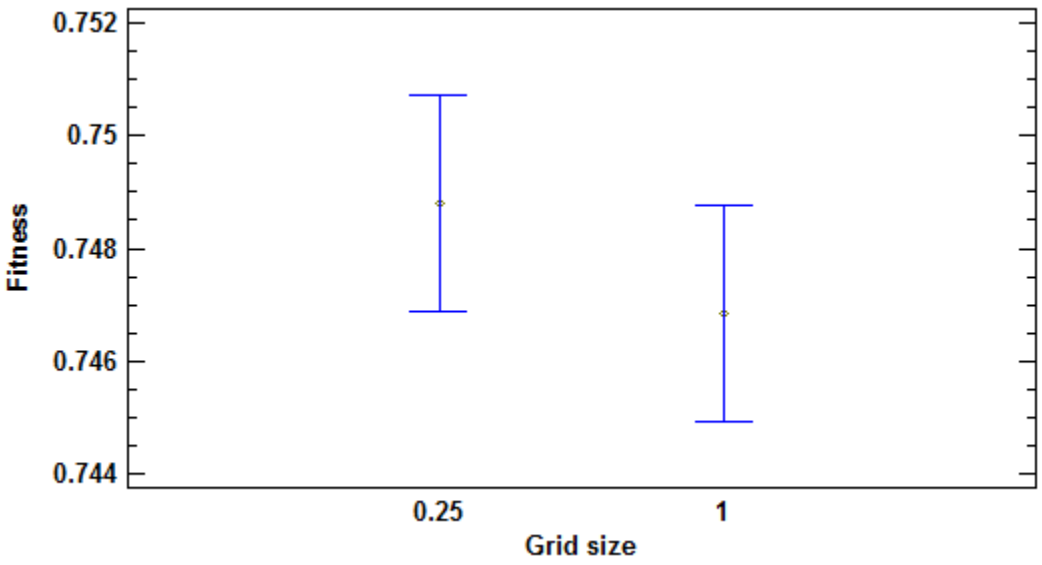

Figure 5.16 LSD interval plot of the RFID network design factor *grid size*

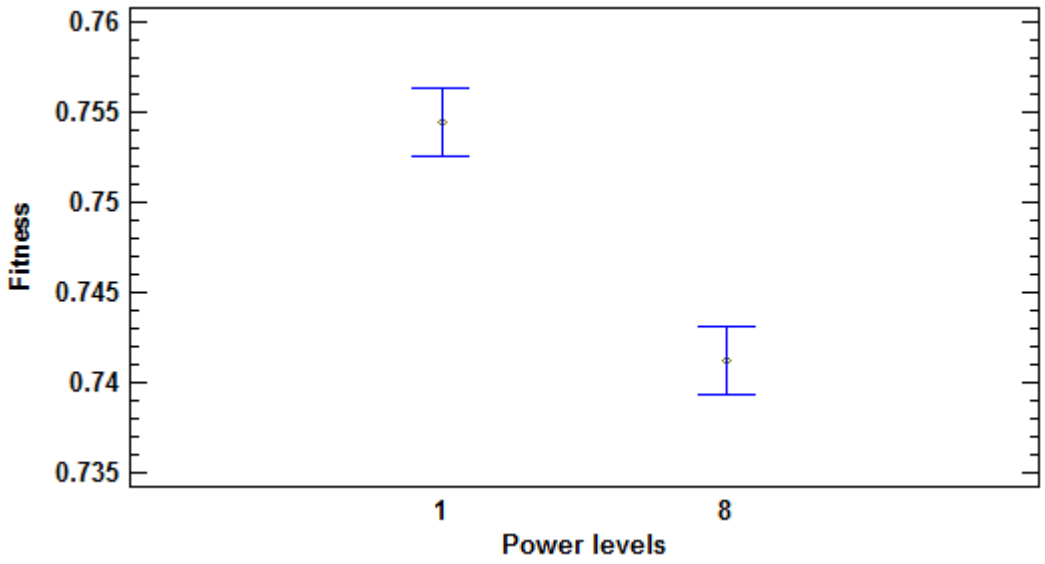

Figure 5.17 LSD interval plot of the RFID network design factor *power levels*

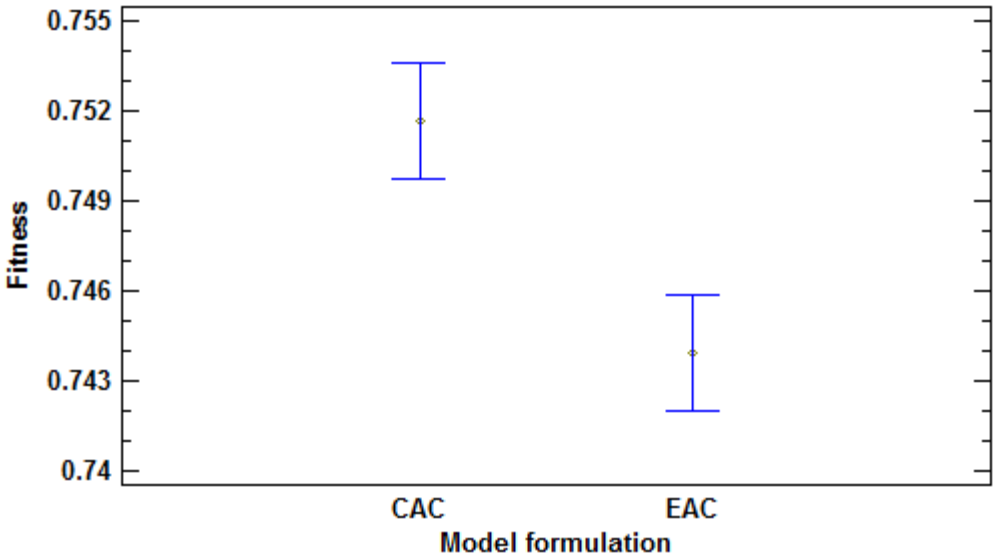

Figure 5.18 LSD interval plot of the RFID network design factor *model formulation*

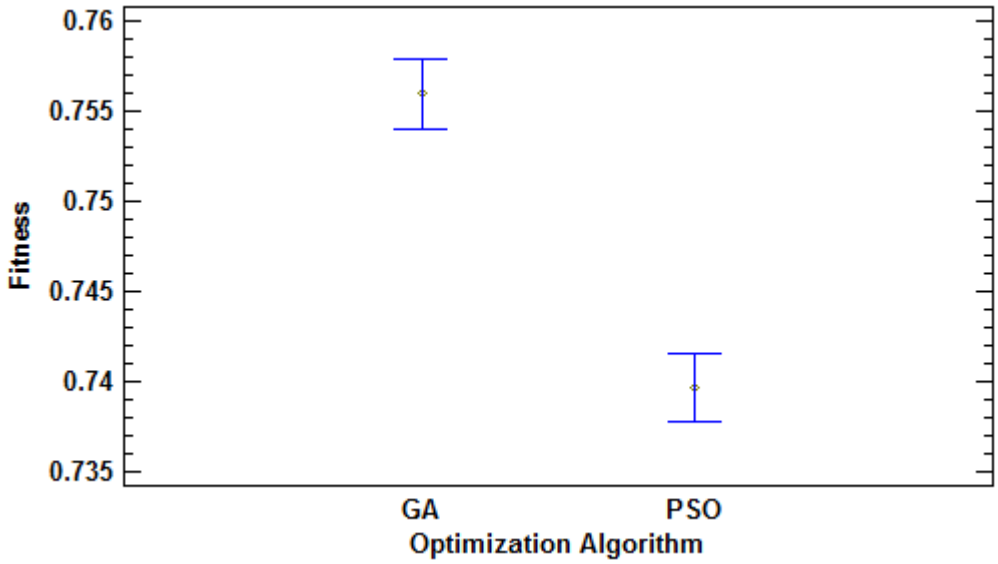

Figure 5.19 LSD interval plot of the RFID network design factor *optimization algorithm*

As shown by the results of the multi-factor ANOVA in Table 5.10 and the Fisher's LSD interval plots, five RFID network design factors have a statistically significant effect on the value of fitness. Furthermore, several two, three and four interaction effects also proved to

be statistically significant. The effect of each RFID network design factors on the value of fitness are discussed next.

5.3.2.1. Effect of Facility Shape

The results of the multi-factor ANOVA in Table 5.10 and the Fisher's LSD interval plot of the *facility shape* shown in Figure 5.14 indicate that the GA and PSO algorithms were able to search and find better fitness values when a rectangular facility (i.e., Tang's facility) was used than when a non-rectangular facility shape (i.e., Ji's inverted-T shape) was used. It was also observed that the best values of fitness were obtained when a *small* rectangular facility was used.

5.3.2.2. Effect of Facility Size

The Fisher's LSD interval plot depicted in Figure 5.15 show that there is a noticeable difference in the average value of fitness obtained from the experiments when the GA and PSO algorithms were applied to a small facility as opposed to a large facility (i.e., 0.7850 versus 0.7017). This difference can be attributed to the fact that a small facility presented a less complex search space. For example, a maximum of five to eight RFID readers were required to ensure entire coverage in a small facility compared to anywhere from 42 or 62 RFID readers that were required to ensure complete coverage of the large rectangular and inverted-T facilities.

5.3.2.3. Effects of the Grid Size

The results of the multi-factor ANOVA shown in Table 5.10 did not identify the RFID network design factor *grid size* as a statistically significant factor. However, the Fisher's LSD interval plot depicted in Figure 5.16 shows that the mean value of fitness for treatment combinations that use grid size of 0.25 meter was slightly higher than those that used the grid size of one meter, especially with a small facility. More specifically, the GA and PSO algorithms performed better when the small facility size and the smaller grid size were considered. However, when the large facility size was used, the grid size did not matter.

It was expected that decreasing the grid size may allow the GA and PSO algorithms more flexibility when searching for better fitness levels. However, the complexity of the system increased as grid size decreased and this rate of change in complexity was more than the solution improvement. Therefore, the GA and PSO algorithms could not perform any better.

5.3.2.4. Effects of the Power Levels

The multi-factor ANOVA results shown in Table 5.10 and the Fisher's LSD interval plot of the *power levels* shown in Figure 5.17 indicate that the GA and PSO algorithms found a better value of fitness when a single power level was used when conducting the experiments, especially in a large facility size.

It was expected that providing an increased number of available power levels would give the RFID readers more flexibility to adjust their power levels so that they could avoid the reader-to-reader interference that occurs in the overlapped coverage areas of two or more RFID readers. When the interference decreases, the value of fitness can be improved.

However, the complexity of the system when a large facility size is used increased rapidly when multiple power levels were also used (i.e., eight power levels). As a result, the use of multiple power levels had a negative effect on the value of fitness. In other words, the value of fitness decreased as the power levels increased. However, the power levels did not matter when a small facility size was considered.

5.3.2.5. Effects of the Model Formulation

The multi-factor ANOVA results shown in Table 5.10 and the Fisher's LSD interval plot of the *model formulation* shown in Figure 5.18 indicate that the GA and PSO algorithms found a better value of fitness when the CAC model formulation was used when conducting the experiments. This can be explained in part by the fact that the CAC model formulation is less complex than the EAC model formulation because a rotation angle is not considered when a circular antenna coverage is assumed.

When the GA and PSO algorithms were applied to solve the RFID network planning problem with the CAC or the EAC model formulation, the rotation angle also added complexity to both algorithms. The length of the chromosome for the GA and the length of the particle for the PSO algorithm were increased when the model formulation changed from the CAC to the EAC (see Table 4.13). A particle or a chromosome with a longer length resulted in more a complicated problem. As a result, higher values of fitness were obtained when the CAC model formulation was used compared to those obtained with the EAC model formulation.

5.3.2.6. Effects of the Optimization Algorithm

The multi-factor ANOVA results shown in Table 5.10 and the Fisher's LSD interval plot of the *optimization algorithm* shown in Figure 5.19 indicate that the GA found better values of fitness than the PSO algorithm, especially with the large facility size. When the small facility size was used, the optimization algorithm did not matter.

Moreover, the RFID network planning problem in this research is a discrete problem. From the literature, a GA can work very well with a discrete problem. However, the original PSO algorithm was developed to solve continuous problems. Therefore, some parameters of the PSO algorithm developed in this research had to be adjusted to effectively deal with a discrete problem and, in particular, when updating the position (x) by rounding it to the nearest integer. This approach is simple and, as it was proved by results reported in section 5.1 and section 5.2, it can be applied to solve a small facility size problem very well.

5.4. Results of the Statistical Analyses for Fixed Facility Shape and Fixed Facility Size

The analyses presented in this section were performed to gain a better understanding of the effect of a subset of the RFID network design factors if the facility shape, facility size, and location of obstructions are known. More specifically, the RFID network design factors *facility shape* and *facility size* were fixed when conducting these analyses. As a result, only the RFID network design factors *grid size, power levels, model formulations* and *optimization algorithms* were entered as the input for the multi-factor ANOVA and the Fisher's LSD interval plots.

5.4.1. Results with a Small Rectangular Facility

The multi-factor ANOVA results based on four RFID network design factors for a small rectangular facility (i.e., Tang's facility) are shown in Table 5.11.

Table 5.11 Multi-factor ANOVA results for the small rectangular facility

Source	*Sum of Squares*	*Df*	*Mean Square*	*F-Ratio*	*P-Value*
MAIN EFFECTS					
A: Grid size	0.00144102	1	0.00144102	37.53	**0.0000**
B: Power levels	0.000223603	1	0.000223603	5.82	**0.0205**
C: Model formulation	0.00182533	1	0.00182533	47.54	**0.0000**
INTERACTIONS					
AB	0.00011163	1	0.00011163	2.91	0.0959
AC	0.0000100833	1	0.0000100833	0.26	0.6112
BC	1.875E-7	1	1.875E-7	0.00	0.9446
ABC	0.0000156408	1	0.0000156408	0.41	0.5270
RESIDUAL	0.00153592	40	0.000038398		
TOTAL (CORRECTED)	0.00516342	47			

Table 5.11 shows that the RFID network design factors *grid size*, *power levels*, and *model formulation* have a statistically significant effect on the value of fitness. The only RFID network design factor that does not have a statistically significant effect on the value of fitness is *optimization algorithm*. There are no significant interaction effects when a small rectangular facility is used.

Both the GA and PSO algorithms performed very well in a small rectangular facility and their performances were comparable. The result from the Fisher's LSD interval plots for *grid size*, *power levels*, and *model formulation* depicted in Figure 5.20, Figure 5.21, and Figure 5.22, respectively, indicate that the GA and PSO algorithms found a better value of fitness when a grid size of 0.25 meter, a single power level, and the CAC model formulation were used when conducting the experiments.

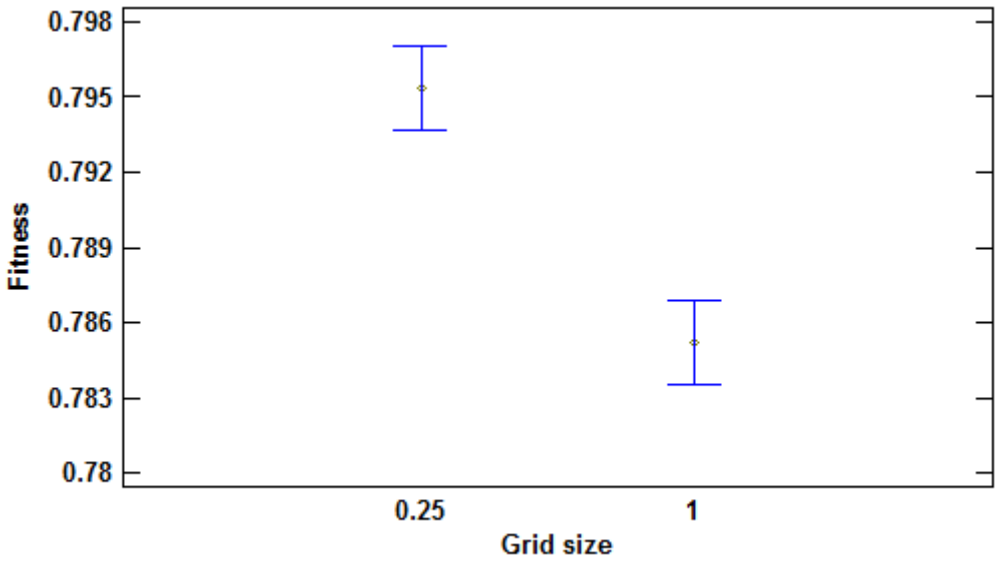

Figure 5.20 LSD interval plot of the RFID network design factor *grid size*

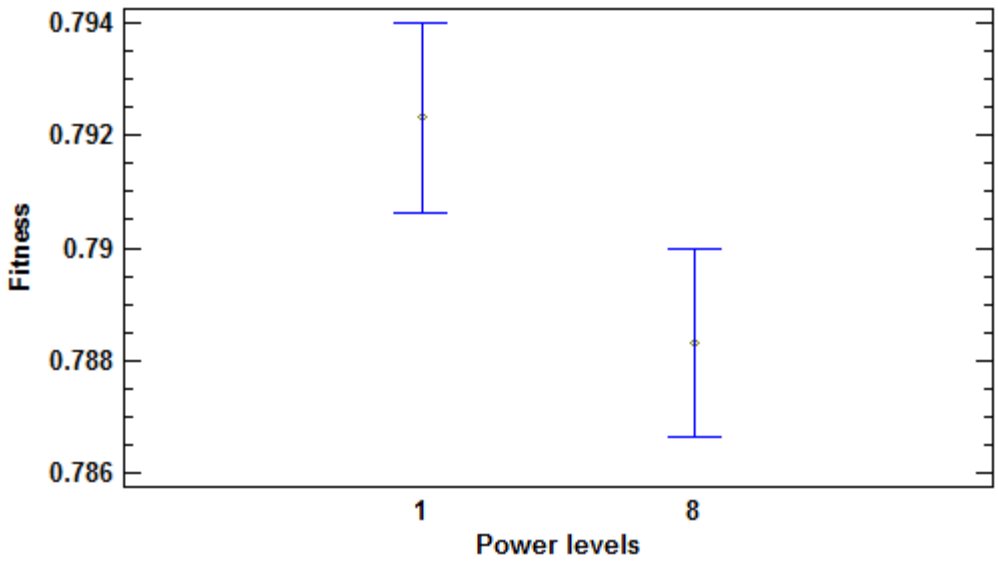

Figure 5.21 LSD interval plot of the RFID network design factor *power levels*

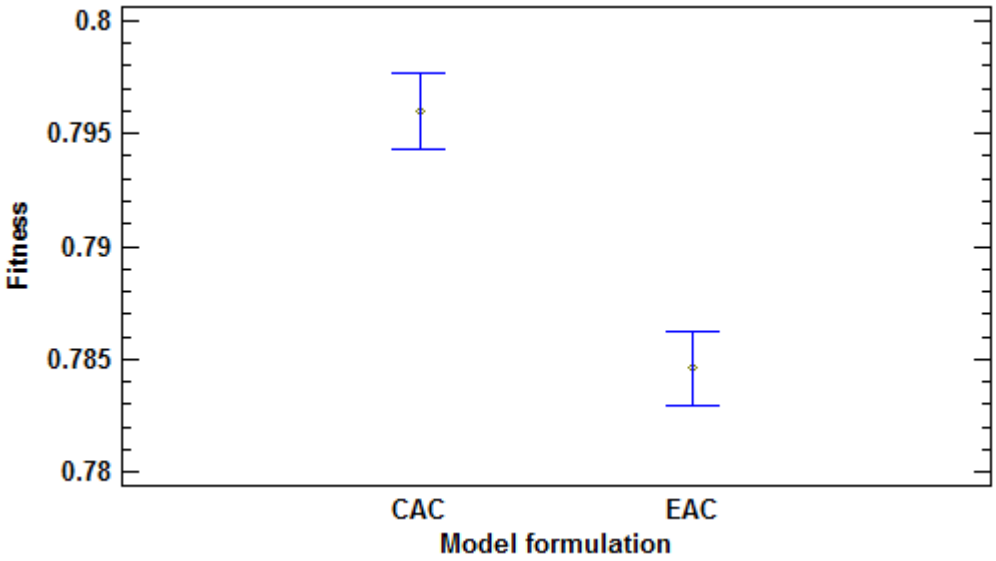

Figure 5.22 LSD interval plot of the RFID network design factor *model formulation*

Figure 5.23 depicts the graphical results of the placement of RFID readers in a small rectangular facility using the best configuration of RFID network design factors. The maximum coverage area of each RFID reader is represented by a dash-dotted line. The black

solid line represents the modified coverage area after obstructions are taken into account. The black dots represent RFID tags that were assumed to be placed at the center of all candidate grids. Shaded areas represent the locations of obstructions in the facility. Finally, the larger black dots at the center of the coverage areas indicate the optimum locations for the RFID readers, as determined by GA and PSO algorithms.

The GA and PSO algorithms can find the best value of fitness of 0.8052. In this case, 116 out of 131 RFID tags were covered which resulted in a value for the coverage objective of 0.8855. The objective of signal-to-interference ratio (SIR), i.e., the summation of downlink SIR and uplink SIR, and the objective of cost were 0.9695 and 0.40, respectively.

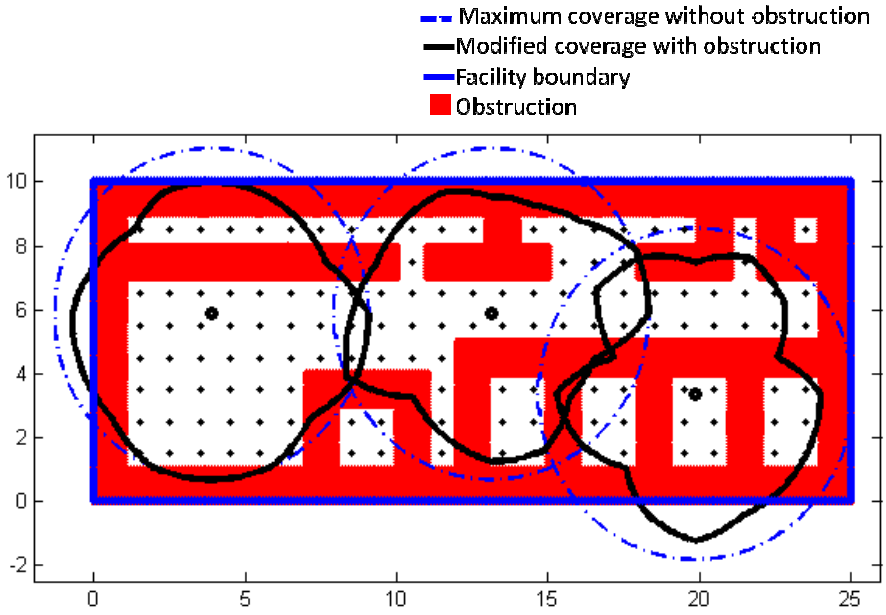

Figure 5.23 The placement of RFID readers in a small rectangular facility using the best configuration of RFID network design factors

As shown in Figure 5.23, three RFID readers cannot ensure the entire coverage of the facility. Therefore, the optimum location and optimum number of RFID readers needed to cover the entire facility, i.e., coverage of the center of all candidate grids in the system, were further investigated. The number of required RFID readers should be in the range between

three to five RFID readers, which is derived from the constraint of the CAC model formulation in equation 4.3. The improvement in the coverage can increase the value of fitness. However, the cost objective decreases as the number of RFID readers increase and the interference tends to increase as well with more RFID readers because of a denser environment. Therefore, the configuration with complete coverage did not guarantee the highest value of fitness.

Figure 5.24 depicts an alternative placement of RFID readers in the small rectangular facility. It was determined that five RFID readers was the optimum number to ensure entire coverage, which resulted in a value of fitness of 0.7740. The value for coverage was one; 0.8702 for signal-to-interference; and zero for cost. The cost was zero because the five RFID readers are the maximum number of RFID readers allowed which was derived from equation 4.3.

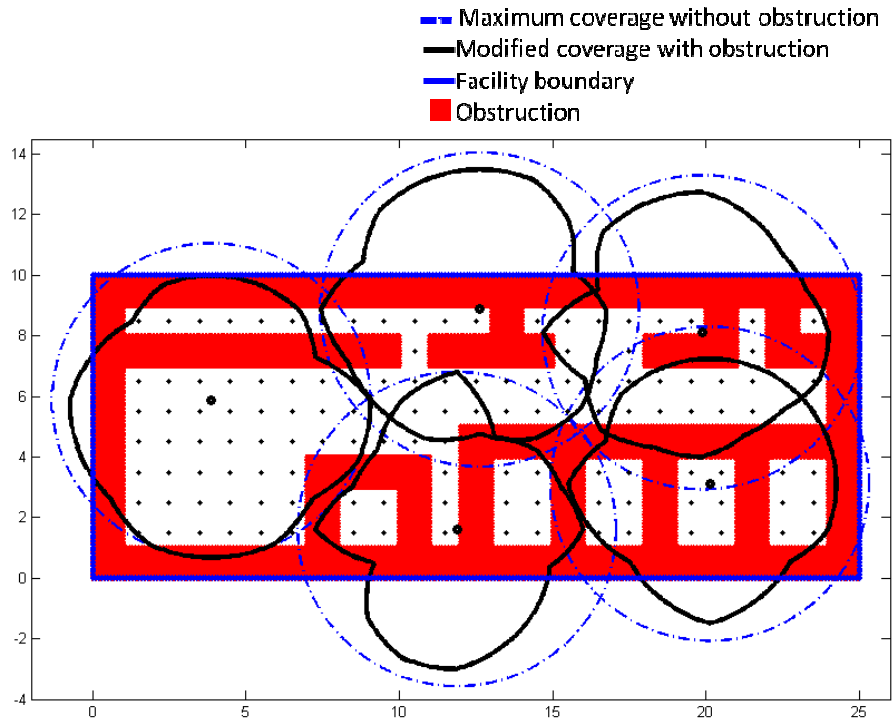

Figure 5.24 The placement of RFID readers in a small rectangular facility using the best configuration of RFID network design factors with entire coverage

5.4.2. Results with a Small Inverted-T Facility

The results of the multi-factor ANOVA for four RFID network design factors for a small inverted-T facility (i.e., Ji's facility) are shown in Table 5.12.

Table 5.12 Multi-factor ANOVA results for the small inverted-T facility

Source	*Sum of Squares*	*Df*	*Mean Square*	*F-Ratio*	*P-Value*
MAIN EFFECTS					
A: Grid size	0.000347979	1	0.000347979	6.37	**0.0168**
B: Power levels	0.000301201	1	0.000301201	5.51	**0.0252**
C: Model formulation	3.60533E-7	1	3.60533E-7	0.01	0.9358
D: Optimization algorithm	0.000109808	1	0.000109808	2.01	0.1659
INTERACTIONS					
AB	0.0000126075	1	0.0000126075	0.23	0.6342
AC	0.00000255763	1	0.00000255763	0.05	0.8301
AD	0.0000645888	1	0.0000645888	1.18	0.2850
BC	0.000443111	1	0.000443111	8.11	**0.0076**
BD	0.00000278403	1	0.00000278403	0.05	0.8228
CD	0.0000293907	1	0.0000293907	0.54	0.4686
ABC	0.0000199176	1	0.0000199176	0.36	0.5502
ABD	0.0000451632	1	0.0000451632	0.83	0.3700
ACD	0.000555424	1	0.000555424	10.17	**0.0032**
BCD	0.000374754	1	0.000374754	6.86	**0.0134**
ABCD	0.0000221952	1	0.0000221952	0.41	0.5284
RESIDUAL	0.00174824	32	0.0000546324		
TOTAL (CORRECTED)	0.00408008	47			

Table 5.12 shows that the RFID network design factors *grid size* and *power levels* have a statistically significant effect on the value of fitness. The RFID network design factors that do not have a statistically significant effect on the value of fitness are *model formulation* and *optimization algorithm*. However, *model formulation* and *optimization algorithm* have a statistically significant effect as part of interactions (i.e., two-factor interaction of power levels and model formulation; three-factor interaction of grid size, model formulation, and optimization algorithm; and three-factor interaction of power levels, model formulation, and optimization algorithm).

From the two-factor interaction of *power levels* and *model formulation* depicted in Figure 5.25, it can be seen that the GA and PSO algorithms performed better in experiments where a single power level for the RFID reader and the CAC model formulation were used. Figure 5.25 also shows that when the EAC model formulation was used, the RFID network design factor *power level* did not matter.

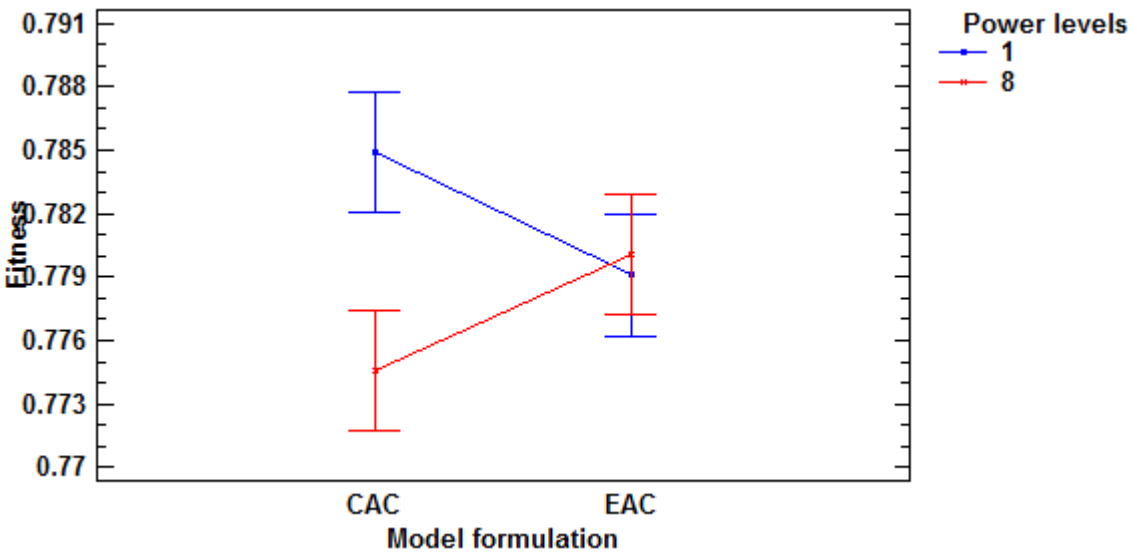

Figure 5.25 The interaction plot of *power levels* and *model formulation*

When a small inverted-T facility was used, both GA and PSO algorithms found better fitness values when the experiments were conducted using a grid size of 0.25 meters and a single power level. This is illustrated by the Fisher's LSD interval plots depicted in Figure 5.26 and Figure 5.27, respectively.

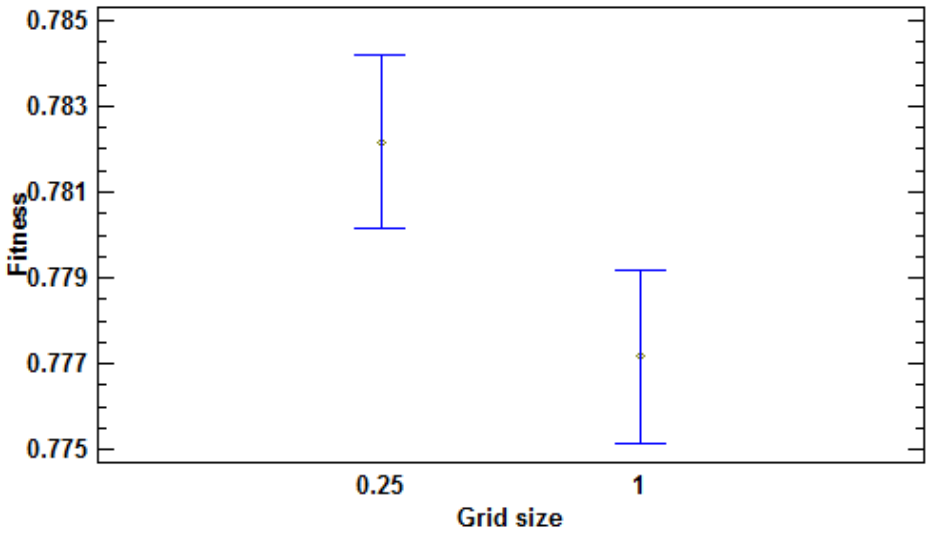

Figure 5.26 LSD interval plot of the RFID network design factor *grid size*

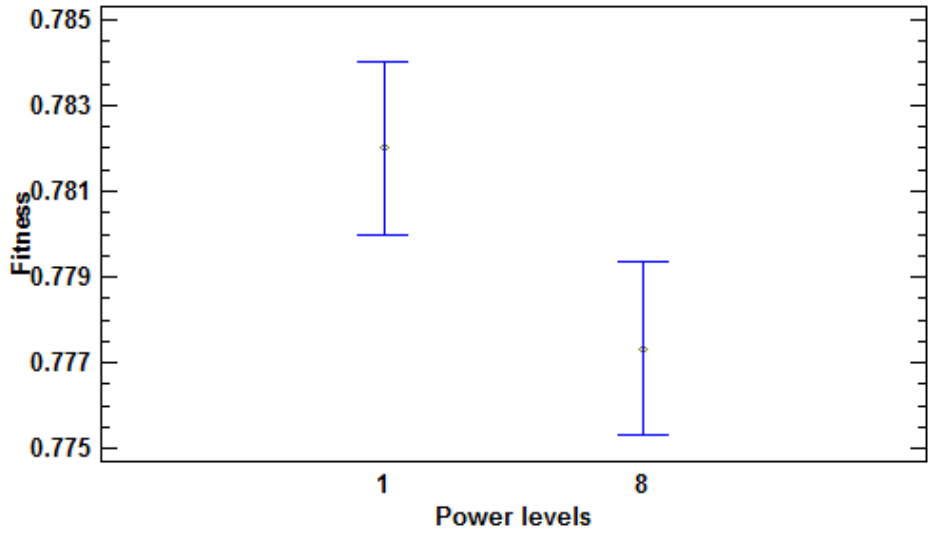

Figure 5.27 LSD interval plot of the RFID network design factor *power levels*

The results from the multi-factor ANOVA indicate that the RFID network design factor *optimization algorithm* did not have a significant effect on the value of fitness. However, the Fisher's LSD interval plot for the RFID network design factor *optimization algorithm* depicted in Figure 5.28 shows that the GA performed slightly better than the PSO algorithm in terms of the average fitness value obtained.

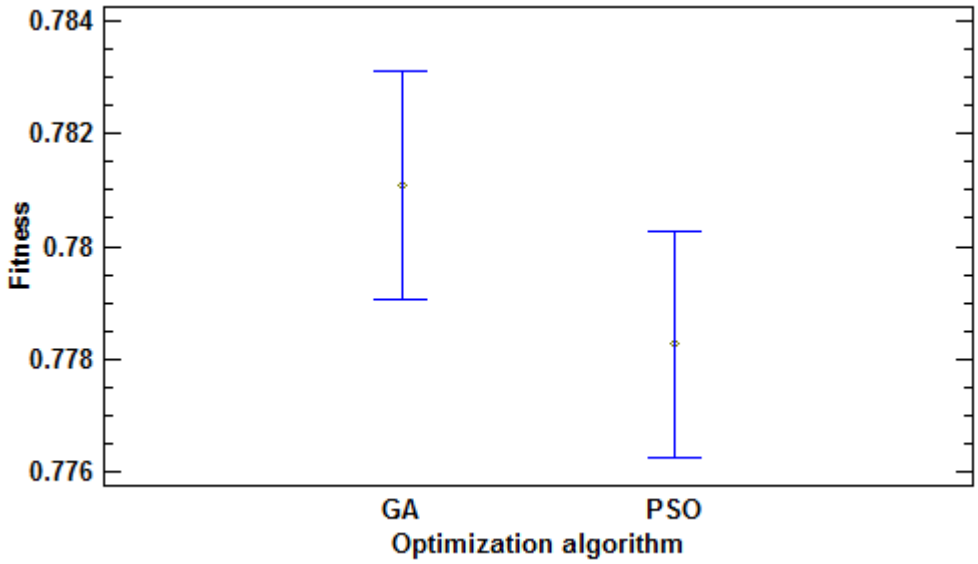

Figure 5.28 LSD interval plot of the RFID network design factor *optimization algorithm*

The configuration that resulted in the highest value of fitness for a small inverted-T facility included a grid size of 0.25 meter and a single power levels using the GA with either CAC or EAC optimization.

In the case of a small inverted-T facility, it is very interesting that the placement of RFID readers using the best configuration of RFID network design factors sometimes resulted in the entire coverage with the highest value of fitness. It was determined that seven RFID readers was the optimum number to cover the entire facility, as depicted in Figure 5.29.

In terms of the fitness function, the coverage reached the maximum value of one. This means that all centers of candidate grids are covered by at least one RFID reader in the system. The value of signal-to-interference ratio (SIR) was 0.8766. The cost objective was 0.125. As a result, the value of fitness obtained was 0.8003.

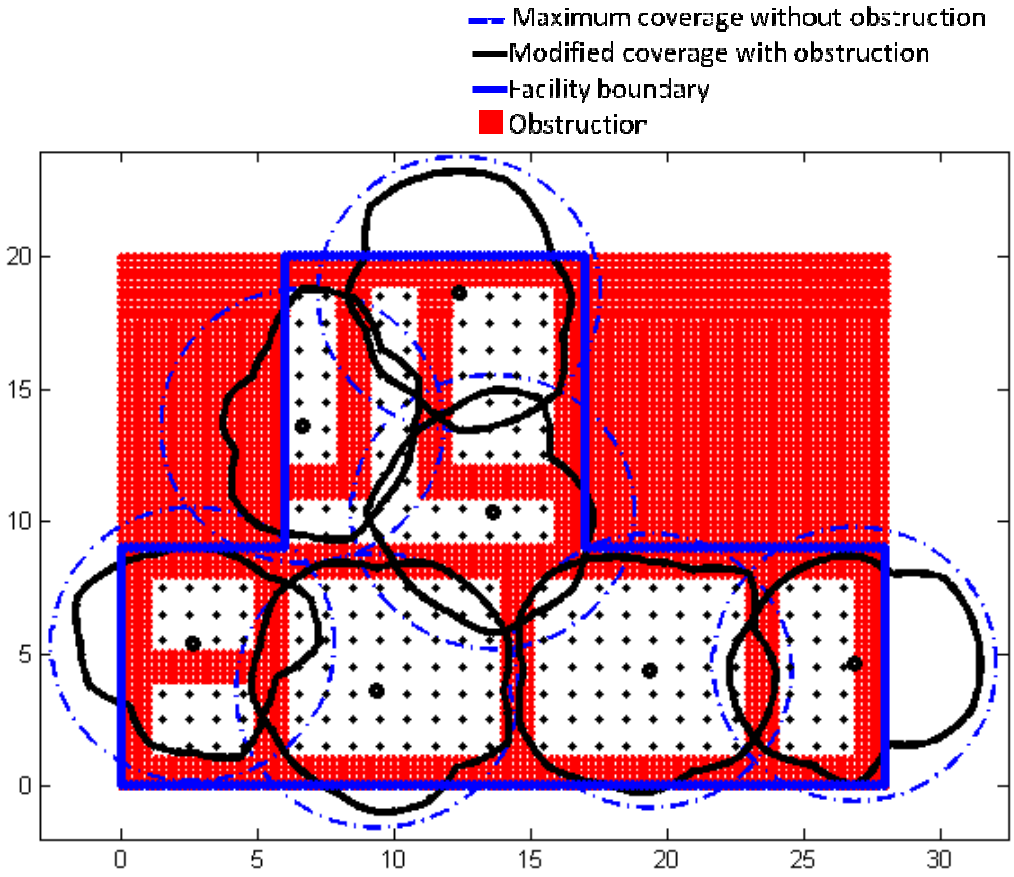

Figure 5.29 The placement of RFID readers in a small inverted-T using the best configuration of RFID network design factors with entire coverage

5.4.3. Results with a Large Rectangular Facility

The multi-factor ANOVA results for four RFID network design factors for a large rectangular facility (i.e., Tang's facility) are shown in Table 5.13.

Table 5.13 Multi-factor ANOVA results for the large rectangular facility

Source	*Sum of Squares*	*Df*	*Mean Square*	*F-Ratio*	*P-Value*
MAIN EFFECTS					
A: Grid size	0.00018526	1	0.00018526	0.59	0.4483
B: Power levels	0.00640101	1	0.00640101	20.37	**0.0001**
C: Model formulation	0.001201	1	0.001201	3.82	0.0594
D: Optimization algorithm	0.0128806	1	0.0128806	40.98	**0.0000**
INTERACTIONS					
AB	0.000171385	1	0.000171385	0.55	0.4656
AC	0.00000368521	1	0.00000368521	0.01	0.9144
AD	0.000713792	1	0.000713792	2.27	0.1416
BC	0.00086106	1	0.00086106	2.74	0.1077
BD	0.00171961	1	0.00171961	5.47	**0.0257**
CD	0.0023506	1	0.0023506	7.48	**0.0101**
ABC	0.0000910252	1	0.0000910252	0.29	0.5942
ABD	0.00158355	1	0.00158355	5.04	**0.0318**
ACD	0.0000926852	1	0.0000926852	0.29	0.5909
BCD	0.000233642	1	0.000233642	0.74	0.3950
ABCD	0.0000318502	1	0.0000318502	0.10	0.7523
RESIDUAL	0.0100575	32	0.000314298		
TOTAL (CORRECTED)	0.0385783	47			

Table 5.13 shows that the RFID network design factors *power levels* and *optimization algorithm* have a statistically significant effect on the value of fitness. The RFID network design factors that do not have a statistically significant effect on the value of fitness are *grid size* and *model formulation*. However, both *grid size* and *model formulation* have a statistically significant effect as part of interactions (i.e., two-factor interaction of model formulation and optimization algorithm; three-factor interaction of grid size, power levels, and optimization algorithm).

The Fisher's LSD interval plot depicted in Figure 5.30 shows that, in a large rectangular facility, the GA algorithm resulted in larger value of fitness than those obtained with the PSO algorithm. The Fisher's LSD interval plot depicted in Figure 5.31 shows that better values of fitness were also obtained when a single power level was used.

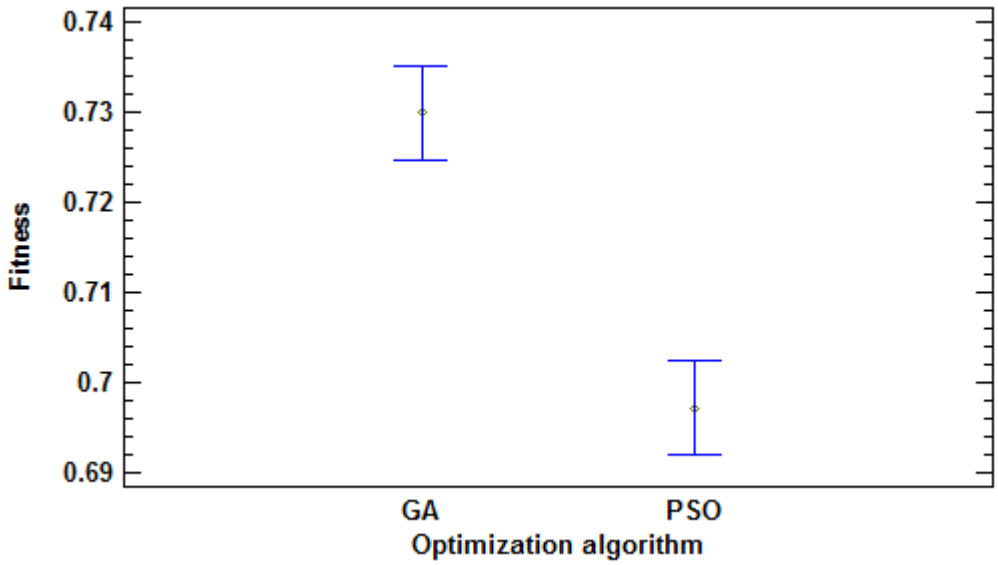

Figure 5.30 LSD interval plot of the RFID network design factor *optimization algorithm*

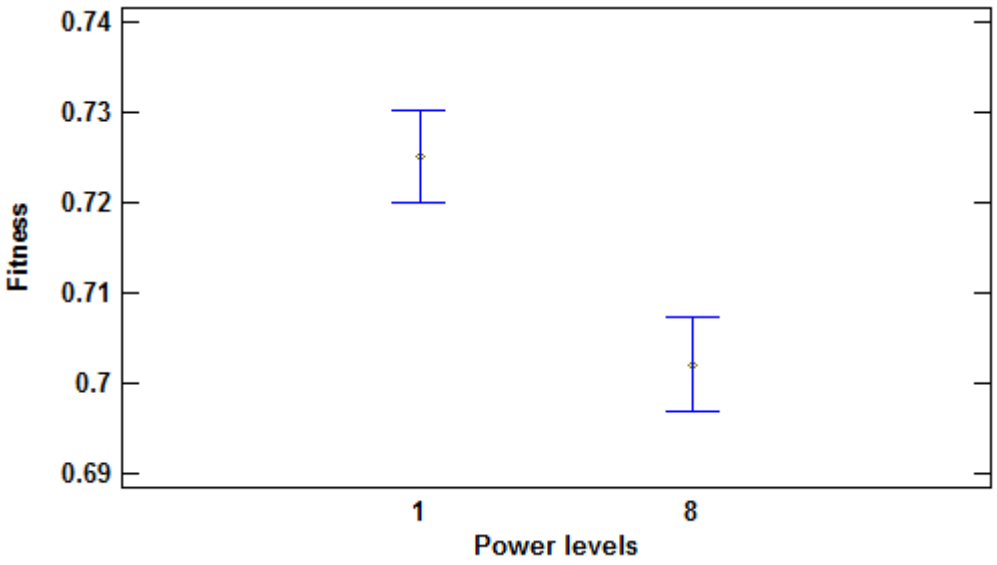

Figure 5.31 LSD interval plot of the RFID network design factor *power levels*

The results from the multi-factor ANOVA show that the type of model formulation did not have a statistically significant effect on the value of fitness. When the Fisher's LSD interval plot was investigated in more detail, it was found that on average the CAC model formulation performed slightly better than the EAC model formulation, as depicted in Figure 5.32.

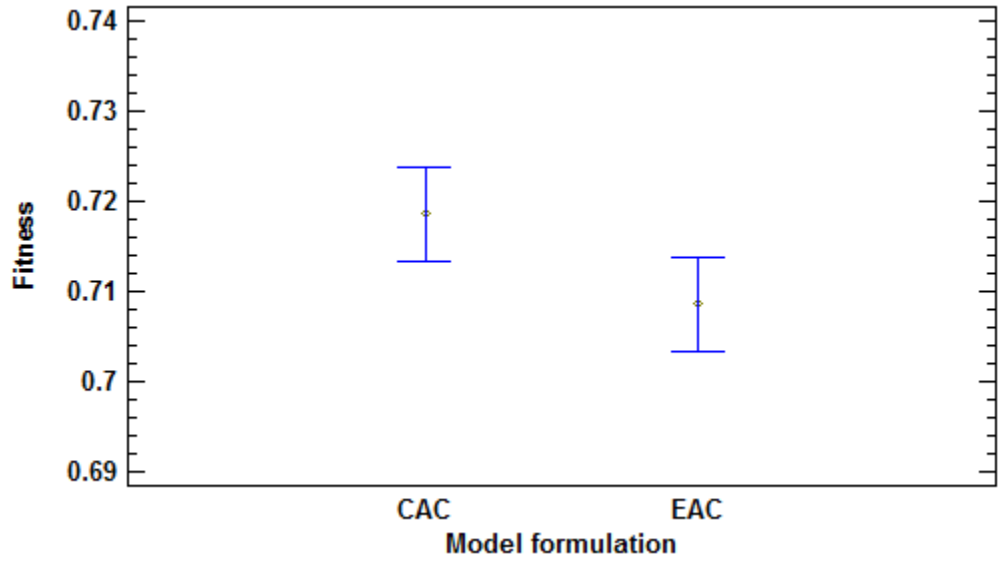

Figure 5.32 LSD interval plot of the RFID network design factor *model formulation*

The configuration that resulted in the highest value of fitness for a large rectangular facility included the use of a single power levels using the CAC model formulation and the GA algorithm. In terms of grid size, a grid size of one meter is preferable because it takes a shorter computation time.

The graphical results depicted in Figure 5.33 show the placement of RFID readers in a large rectangular facility using the best configuration of RFID network design factors. The GA algorithm can find the best value of fitness of 0.7674. In this case, 1,205 out of 1,432 RFID tags were covered resulting in a value for the coverage objective of 0.8415. The objective of signal-to-interference ratio (SIR) and the objective of cost obtained values of 0.9791 and 0.3333, respectively. Placing the RFID readers in a large facility while considering obstructions is a complicated problem. The GA and PSO algorithms still cannot achieve complete coverage, which is a limitation.

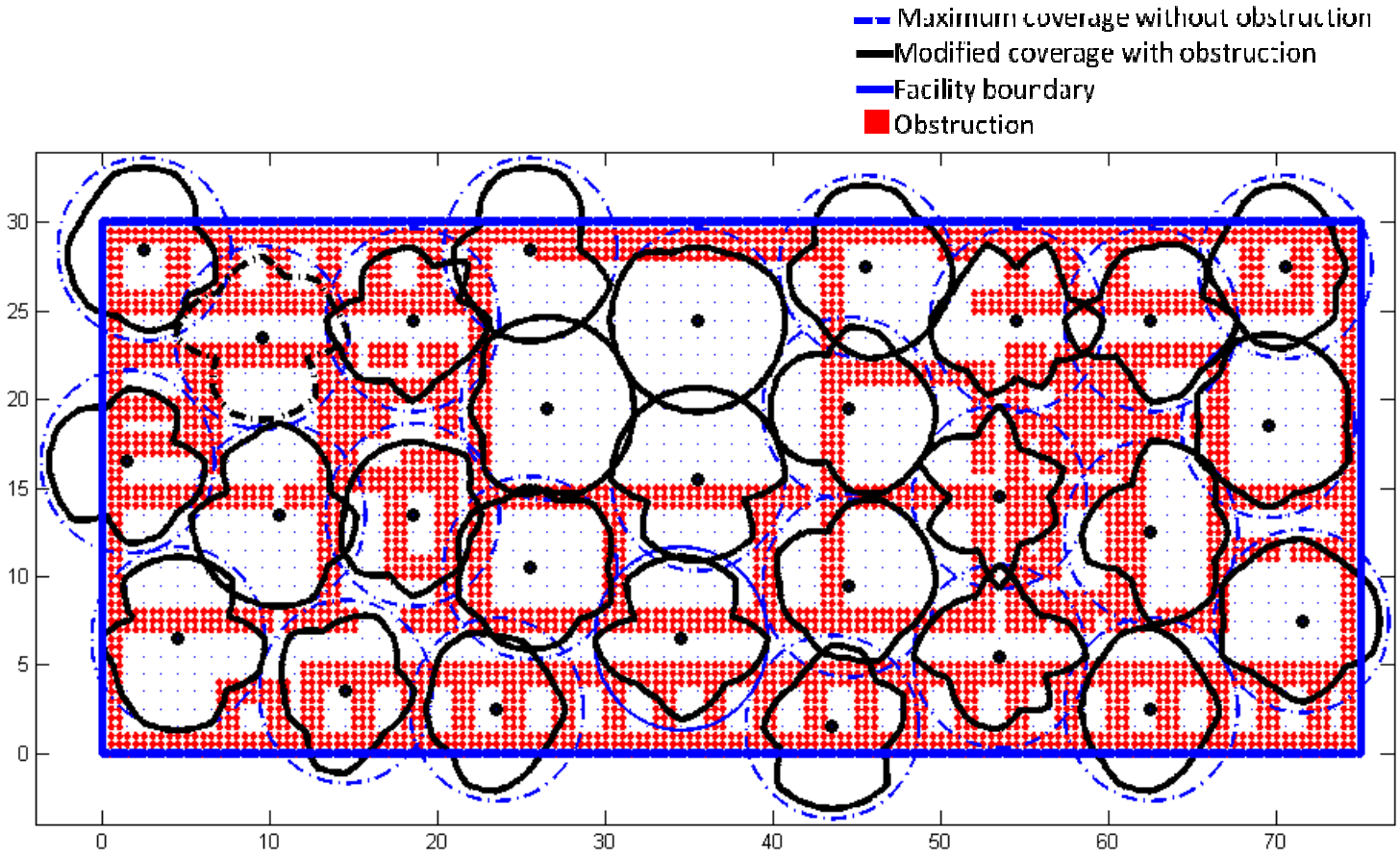

Figure 5.33 The placement of RFID readers in a large rectangular facility using the best configuration of RFID network design factors

5.4.4. Results with a Large Inverted-T Facility

The results of the multi-factor ANOVA for four RFID network design factors for a large inverted-T facility (i.e., Ji's facility) are shown in Table 5.14.

Table 5.14 Multi-factor ANOVA results for the large inverted-T facility

Source	*Sum of Squares*	*Df*	*Mean Square*	*F-Ratio*	*P-Value*
MAIN EFFECTS					
A: Grid size	0.00153454	1	0.00153454	5.37	**0.0270**
B: Power levels	0.00535096	1	0.00535096	18.73	**0.0001**
C: Model formulation	0.0010416	1	0.0010416	3.65	0.0652
D: Optimization algorithm	0.00976981	1	0.00976981	34.20	**0.0000**
INTERACTIONS					
AB	0.00233523	1	0.00233523	8.17	**0.0074**
AC	0.000458803	1	0.000458803	1.61	0.2142
AD	0.00003468	1	0.00003468	0.12	0.7298
BC	0.000253001	1	0.000253001	0.89	0.3537
BD	0.00111554	1	0.00111554	3.90	0.0568
CD	0.0000869408	1	0.0000869408	0.30	0.5850
ABC	0.000361901	1	0.000361901	1.27	0.2687
ABD	0.000196021	1	0.000196021	0.69	0.4136
ACD	0.000851767	1	0.000851767	2.98	0.0939
BCD	0.000268853	1	0.000268853	0.94	0.3393
ABCD	0.00167088	1	0.00167088	5.85	**0.0215**
RESIDUAL	0.00914195	32	0.000285686		
TOTAL (CORRECTED)	0.0344725	47			

Table 5.14 shows that the RFID network design factors *grid size*, *power levels*, and *optimization algorithm* have a statistically significant effect on the value of fitness. The RFID network design factor that does not have a statistically significant effect on the value of fitness is *model formulation*. However, *model formulation* has a statistically significant effect as part of four-factor interaction of grid size, power levels, model formulation, and optimization algorithm.

In the large inverted-T facility, the GA performed much better than the PSO algorithm and it found better values of fitness when the experiments were conducted using a grid size of one meter and a single power level, which can be observed on the Fisher's LSD interval plots depicted in Figure 5.34, Figure 5.35 and Figure 5.36, respectively.

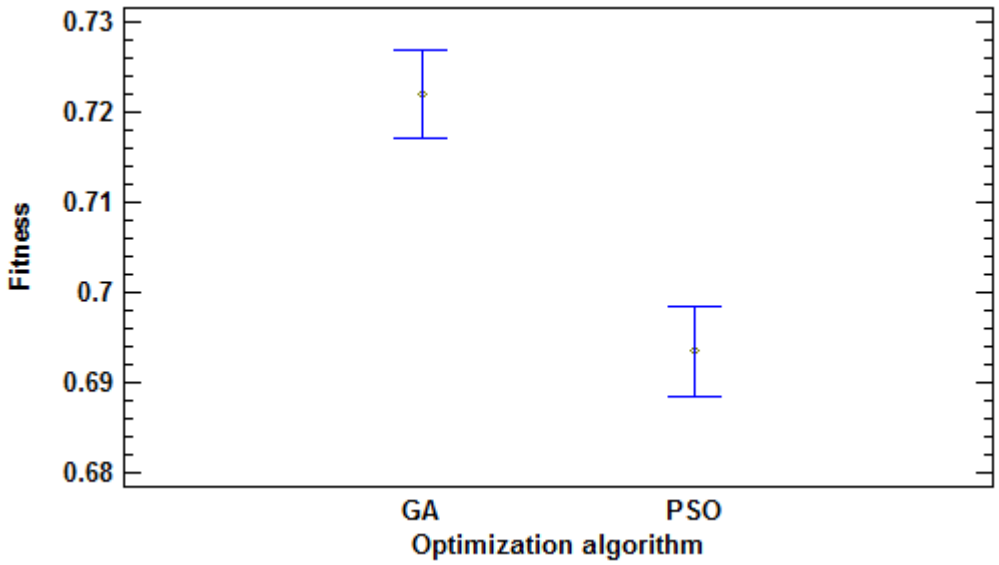

Figure 5.34 LSD interval plot of the RFID network design factor *optimization algorithm*

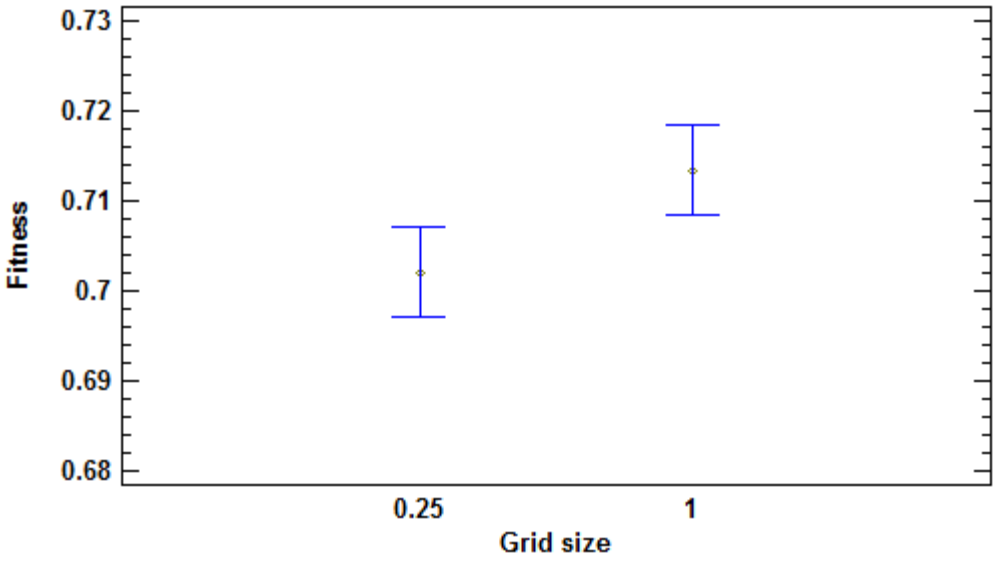

Figure 5.35 LSD interval plot of the RFID network design factor *grid size*

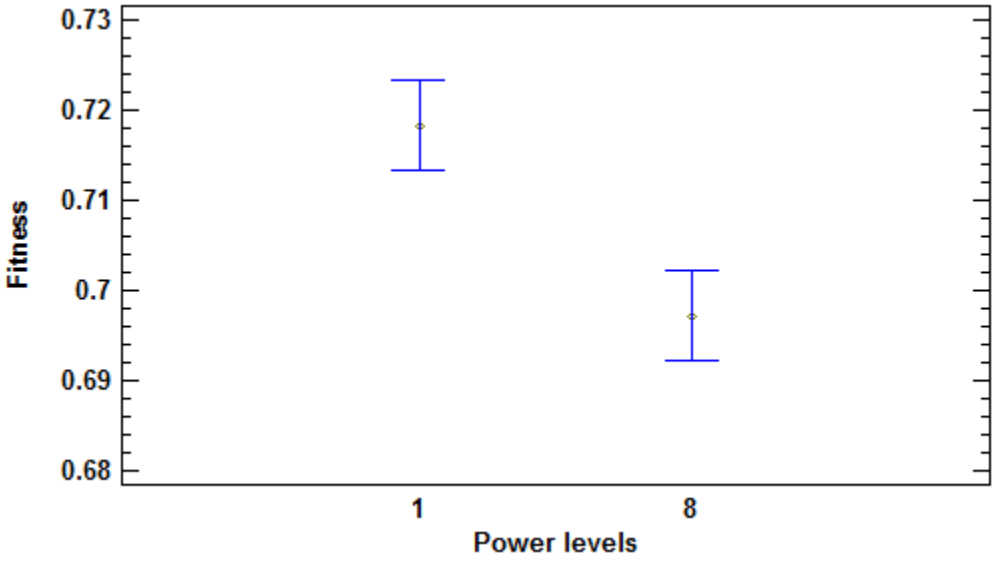

Figure 5.36 LSD interval plot of the RFID network design factor *power levels*

The configuration that resulted in the highest value of fitness for a large inverted-T facility included a grid size of one meter and a single power level using the GA algorithm and the CAC model formulation. This configuration is preferable because of its lower complexity.

The graphical results depicted in Figure 5.37 show the placement of RFID readers in a large inverted-T facility using the best configuration of RFID network design factors. The GA algorithm can find the best value of fitness of 0.7553. In this case, 2,029 out of 2,420 RFID tags were covered resulting in a value for the coverage objective of 0.8384. The objective of signal-to-interference ratio (SIR) and the objective of cost obtained values of 0.9549 and 0.3065, respectively. The size of the large inverted-T facility is much larger than that of the large rectangular facility; therefore, the problem is much more complex and the GA and PSO algorithms still cannot find a solution that ensures complete coverage.

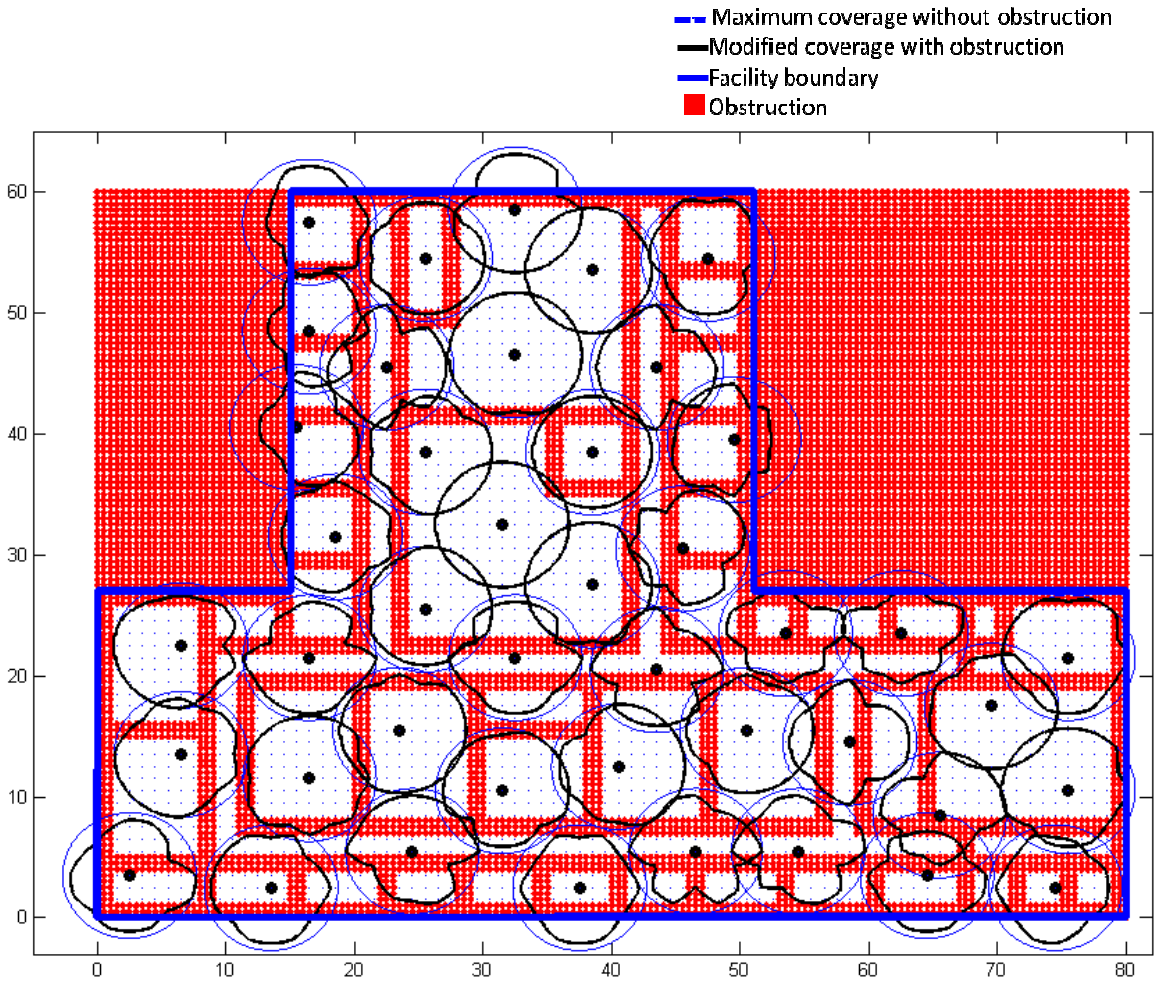

Figure 5.37 The placement of RFID readers in a large inverted-T facility using the best configuration of RFID network design factors

6. CONCLUSIONS AND OPPORTUNITIES FOR FUTURE WORK

A methodology to model and optimize the design of RFID networks for inventory management was developed in this research. The main objective of this methodology is to find the optimal *location* and *number* of RFID readers to ensure a desired level of coverage. Finding a solution that ensures the complete coverage of an entire facility (e.g., a warehouse) would allow an RFID network to support real-time inventory tracking and localization which can minimize shrinkage and prevent theft. The developed methodology is not limited to inventory management applications. For instance, it can also be applied in healthcare facilities where the quality of life of human beings is at stake. A good example of such an application is the RFID network deployed to support medical asset tracking reported by Oztekin et al. (2010).

Several contributions have been made by this research. To achieve the goal of the design of RFID networks for inventory management, the *circular antenna coverage* (CAC) and *elliptical antenna coverage* (EAC) model formulations were developed based on the type of antenna used by the RFID reader in the system. Most of the prior work in the literature proposes models to solve the RFID network problem (RNP) assuming that the antenna of the RFID readers produced a circular coverage; however, very few models have been proposed where an elliptical antenna coverage area is assumed. In this research, a dipole antenna having a circular antenna coverage was assumed in the CAC model formulation. However, RFID readers that use directional antennas with an elliptical antenna coverage area are more common in RFID networks. Therefore, the EAC model formulation was developed assuming the use of a patch antenna. It is expected that the development of the CAC and the EAC model formulations would results in a better understanding of the effect of both types of

antennas on the performance of an RFID network.

The consideration of the downlink communication and the uplink communication channels was also included in the CAC and EAC model formulations using the multipath propagation model and the radar cross section propagation model, respectively. The consideration of the uplink communication channel was found in only one previous work from the literature. The more realistic assumption of an elliptical antenna coverage as well as the use of two propagation models make the model formulations more practical and more accurate.

Finding solutions to the CAC and EAC model formulations is an NP-hard problem. Therefore, an automated tool was developed that implements two heuristic optimization algorithms based on *genetic algorithm* (GA) and *particle swarm optimization* (PSO) to find good solutions to the CAC and EAC model formulations within a reasonable computation time. In the process of finding the solutions, the attenuation due to the effect of obstructions (i.e., passive interference) was taken into account. The shape and size of the *maximum antenna coverage* without the effect of obstructions, i.e., perfect circular or ellipse, was changed to a *modified antenna coverage* after the effect of obstructions was assessed by using a *ray-tracing* approach. The consideration of obstructions made the GA and PSO algorithms more constrained to obtain better solutions. None of the prior research found in the literature considered the effect of obstructions in their RFID network design problem.

A full factorial experimental design was conducted to investigate the effect of the six RFID network design factors *facility shape, facility size, grid size, power levels, model formulation,* and *optimization algorithm* on the value of fitness (i.e., the response variable). The results of this experiment were analyzed using multi-factor ANOVA. Further experimentation was conducted to investigate the effect of the four RFID network design

factors *grid size, power levels, model formulation,* and *optimization algorithm* on the value of fitness with scenarios where it was assumed that the size and shape of the facility (as well as the locations of obstructions) were known. Understanding the effect of the six RFID network design factors in the first scenario would be beneficial when the designers would like to design an RFID network before a facility is built. If a facility is already available, the latter scenario could be applied to identify the effect of *grid size, power levels, model formulation,* and *optimization algorithm* on the value of fitness.

The rest of the chapter is organized as follows. Section 6.1 presents the conclusions reached in this study. Section 6.2 discusses the limitations of this research. Finally, section 6.3 presents the opportunities for future work.

6.1. Research Conclusions

The methodology developed to model and optimize the design of RFID networks for inventory management proved to work very well with small rectangular facilities and small inverted-T facilities, but there were some limitations when applying it to large facilities (see section 6.2).

The GA and PSO algorithms were able to find the optimal location and number of RFID readers required in the system that satisfied three objectives in the fitness function, i.e., maximize the RF coverage, minimize the level of interference and minimize the implementation cost. The performance of the GA and PSO algorithms was validated against the results reported by Chen et al. (2011). The validation results showed that the GA and PSO algorithm achieved much better coverage; 76 RFID tags were covered by the GA and 75 RFID tags were covered by the PSO algorithm. These results represent a 5.556% and a 4.167% performance improvement, respectively, compared to the 33 RFID tags covered by

Chen et al. (2011). Covering the entire indoor test facility was further investigated. The GA was able to cover all 99 RFID tags, but the PSO algorithm could only cover 97 RFID tags within 1,000 iterations.

In terms of the effectiveness and efficiency of GA and PSO algorithms, two scenarios in a small facility (10 meters by 10 meters) were tested with five runs each. The results obtained by GA and PSO algorithms were compared to the exact solution(s) obtained via exhaustive enumeration. In the first scenario, the CAC model formulation with three RFID readers and 50 random RFID tags was used. The results showed that the GA was 100% effective in achieving the exact solution, whereas the PSO algorithm obtained the exact solution four out of five runs for an effectiveness of 80%. The average computation time to obtain the exact solution (or near exact solution) over five runs compared to the computation time needed to obtain exact solution(s) via exhaustive enumeration was used to assess the efficiency of the GA and PSO algorithms. The efficiency of the GA and PSO algorithms were 98.95% and 88.34%. In the second scenario, the CAC model formulation with four RFID readers and RFID tags located at the center of grids was used. It was found that adding only one more RFID reader to the system made this problem much larger than that of the first scenario (i.e., the total solutions obtained via exhaustive enumeration increased from 161,700 to 3,921,225). The effectiveness of the GA and PSO algorithms decreased to 80% and 60% in the second scenario. However, their efficiencies improved significantly to 99.40% for the GA and 99.29% for the PSO algorithm.

The statistical analyses of the experimental data showed that the five RFID network design factors *facility shape, facility size, power levels, model formulation*, and *optimization algorithm* had a significant effect on the value of fitness. The RFID network design factors *grid size* was not statistically significant. The GA and PSO algorithms were able to obtain

better values of fitness for a facility with a rectangular shape (Tang's facility), a small size and a single power level of RFID readers. In terms of the model formulations, the CAC model formulation was able to achieve a better value of fitness than the EAC model formulation because of its lesser complexity.

In terms of the optimization algorithm, the GA resulted in better values of fitness than the PSO algorithm. This might be due to the fact that the problem in this research is a discrete problem. Rounding the updated value of position (x) in the PSO algorithm to the nearest integer was the approach used to make it a discrete PSO. A more sophisticated discrete PSO may be needed to obtain better (or comparable) results than those obtained with the GA.

It was also concluded that grid size had an interaction effect on the value of fitness, i.e., interaction of a facility size and a grid size. More specifically, the GA and PSO algorithms performed better with the smaller grid size when a small facility size was considered. When the large facility size was used, the grid size did not matter.

The configuration that resulted in the highest value of fitness involved a facility with a rectangular shape (Tang's facility), a small facility size, a small grid size (0.25 meter), a single power level of RFID readers, and using a CAC model formulation with the GA. This configuration resulted in the highest value of fitness of 0.8052, including the coverage objective of 0.8855, signal-to-interference ratio (SIR) objective of 0.9695, and the cost objective of 0.4.

For a specific facility shape and facility size, the best configurations for each layout and the resulting value of fitness are summarized in Table 6.1.

Table 6.1 The best configuration for a specific facility shape and facility size and its fitness

Best Configuration	Small Rectangular Facility	Small Inverted-T Facility	Large Rectangular Facility	Large Inverted-T Facility
Grid size	0.25	0.25	0.25 or **1**†	1
Power levels	1	1	1	1
Model formulation	CAC	**CAC**† or EAC	**CAC**† or EAC	**CAC**† or EAC
Optimization algorithm	GA or PSO	GA or PSO	GA	GA
Value of Fitness	0.8052	0.8003	0.7674	0.7553
Coverage	0.8855	1	0.8415	0.8384
SIR	0.9695	0.8766	0.9791	0.9549
Cost	0.4	0.125	0.3333	0.3065

† **Bold letters are preferable**

6.2. Research Limitations

The following are the main limitations of this research:

1. The GA and PSO algorithms can effectively search for the solution that guarantees the entire coverage of a small rectangular facility and a small inverted-T facility. However, the GA and PSO algorithms, especially the PSO, cannot work very well with the large facility size scenarios used in this research. Some parameters of the algorithms and the weights of each objective have to be investigated in more detail. Moreover, the termination criterion of algorithms when conducting the experiment was 1,000 iterations. It is anticipated that the solutions can be improved with a larger number of iterations.

2. The development the CAC and EAC model formulations to reflect a continuous problem such as the RFID network planning problem is complicated. This is the reason why no prior research was found where the mathematical model or model formulation for the RFID network design problem was formulated with a continuous placement location of RFID readers in the system. Therefore, the facilities used in this research were discretized into several small grids making them discrete problems. In general, the inertia-weighted PSO, used as a basis of the PSO algorithm developed in this research, was originally conceived for a continuous problem. Rounding the updated value of position (x) in the developed PSO algorithm to the nearest integer was the approach used to make it a discrete PSO. The method is simple and proved effective in dealing with small facility size problems. However, it did not work very well with large facility sizes. A more sophisticated discrete problem suggested in Rapaić et al., (2008) was applied. This algorithm used a hyperbolic tangent function to transform the continuous format of the velocity (v) parameter obtained from the original PSO to a discrete format referred to as the *saturated velocity*. The new parameter called *maximal displacement* was also introduced in the process of updating the position (x). However, this modified PSO algorithm did not find a better solution compared to that of the simple discrete PSO algorithm even with a small facility size. Some literature suggested the use of a binary discrete PSO algorithm. However, the particle representation has to be changed significantly and it is expected that the binary discrete PSO algorithm with the new particle representation will take much longer computation time because of the much longer particle length. Therefore, the binary discrete PSO will be suggested as one of opportunities for future work.

6.3. Opportunities for Future Work

Following are the research opportunities to be addressed to gain a better understanding and/or enhance the performance of the modeling and optimization of RFID networks for inventory management:

1. Develop a binary discrete PSO algorithm using a new format for the particle representation (i.e., a number of particles equal to the number of candidate grids) and set the candidate grids where the RFID reader is placed to "1" or set it to "0" otherwise. Then, perform a comparison of the results with those obtained with the developed PSO (and especially with those obtained when using a large facility size).
2. Conduct a new set of experiments with a larger number of iterations allowed, e.g., 10,000 iterations, before the algorithms are terminated. The objective of this strategy is to investigate whether or not the coverage objective improves.
3. Perform a detailed sensitivity analysis of the parameters in the GA. This includes the population size, the mutation rate, the parent selection, the crossover process, and the chromosome selection for the next generation.
4. Develop a graphical user interface (GUI), creating the executable file (.exe), and making the user manual for the source code in this research. It would be beneficial for the RFID network designer to use it in the design of the RFID network in the real facility. They can enter all necessary input parameters and the GUI will display the best configuration for a certain type of facility.
5. Investigate alternative representations for the elliptical antenna coverage (e.g., the placement location is at one of the focal points). This coverage pattern can represent the directional antenna having both the front lobe and back lobe.

BIBLIOGRAPHY

Adickes, M. D., Billo, R. E., Norman, B. A., Banerjee, S., Nnaji, B. O., & Rajgopal, J. A. (2002). Optimization of Indoor Wireless Communication Network Layouts. *IIE Transactions, 34*, 823-836.

Almanza-Ojeda, D. L., Hernandez-Gutierrez, A., & Ibarra-Manzano, M. A. (2006). Design and implementation of a vehicular access control using RFID. *IEEE Multiconference on Electronics and Photonics, 2006. MEP 2006*. 223-225.

Amazon.com Inc. (2012). Price of WLAN access point. Retrieved May 17, 2012, from http://www.amazon.com/s/ref=pd_lpo_k2_dp_sr_sq_top?ie=UTF8&keywords=price%20of%20wlan%20access%20point&index=blended&pf_rd_p=486539851&pf_rd_s=lpo-topstripe1&pf_rd_t=201&pf_rd_i=B00007KDVJ&pf_rd_m=ATVPDKIKX0DER&pf_rd_r=1S089D08Z4PSNFDEJADC.

Anderson, H. R., & McGeehan, J. P. (1994). Optimizing Microcell Base Station Locations using Simulated Annealing Techniques. *44th IEEE Vehicular Technology Conference*. 858-862.

Angeles, R. (2005). RFID Technologies: Supply-Chain Applications and Implementation Issues. *Information Systems Management, 22*, 51-65.

Anusha, S., & Iyer, S. (2005). RFIDcover - A Coverage Planning Tool for RFID Networks with Mobile Readers. *Master's Thesis, Indian Institute of Technology, Bombay*. Retrieved from http://citeseerx.ist.psu.edu/viewdoc/summary?doi=10.1.1.75.2537.

Balanis, C. A. (2005). *Antenna Theory: Analysis and Design, 3rd Edition* (3rd Ed.). Wiley-Interscience.

Bhattacharya, I., & Roy, U. K. (2010). Optimal Placement of Readers in an RFID Network Using Particle Swarm Optimization. *International Journal of Computer Networks & Communications (IJCNC), 2*(6), 225-234.

Bolic M., Simplot-Ry D.l, Stojmenovic I. (Editors), RFID Systems: Research Trends and Challenges, John Wiley and Sons, 2010.

Chande, A., Dhekane, S., Hemachandra, N., & Rangaraj, N. (2005). Perishable inventory management and dynamic pricing using RFID technology. *Sadhana, 30*(2-3), 445-462.

Chang, C.-H., & Lin, J.-L. (2007). A Systematic Layout Planning of Visualizing Devices on a Non-Rectangular Plane by Genetic Heuristics. *Proceedings of the 20th International Conference on Industrial, Engineering, and Other Applications of Applied Intelligent Systems*, IEA/AIE'07. 424–433. Berlin, Heidelberg: Springer-Verlag.

Chen, H., Zhu, Y., Hu, K., & Ku, T. (2011). RFID Network Planning using a Multi-Swarm Optimizer. *Journal of Network and Computer Applications*, *34*(3), 888-901.

Chen, Z. N., Qing, X., & Chung, H. L. (2009). A Universal UHF RFID Reader Antenna. *IEEE Transactions on Microwave Theory and Techniques, 57*(5), 1275-1282.

Circuit Design, Inc. (2009). Okumura - Hata Curve. Retrieved June 2, 2011, from http://www.cdt21.com/resources/siryo4_01.asp

Clerc, M., & Kennedy, J. 2002, "The particle swarm - explosion, stability, and convergence in a multi-dimensional complex space," IEEE Transactions on Evolutionary Computation, 6(1), 58-73.

Dobkin, D. M. (2004). *RF Engineering for Wireless Networks: Hardware, Antennas, and Propagation*. Newnes.

Dobkin, D. M. (2007). *The RF in RFID: Passive UHF RFID in Practice*. Newnes.

Eberhart, & Shi, Y. (2001). Particle Swarm Optimization: Developments, Applications andResources. *Proceedings of the IEEE 2001 Congress on Evolutionary Computation*. 81-86.

Efrat, A., Hoffmann, F., Knauer, C., Kriegel, K., Rote, G., & Wenk, C. (2004). Covering with Ellipse. *Algorithmica , 38*(1), 145-160.

Engels, D. W., & Sarma, S. E. (2002). The Reader Collision Problem. *2002 IEEE International Conference on Systems, Man and Cybernetics*.

EPCglobal. (2011). EPCglobal Class 1 Generation 2 UHF Air Interface Protocol Standard "Gen 2." Retrieved May 13, 2011, from http://www.gs1.org/gsmp/kc/epcglobal/uhfc1g2.

Ernst, & Young. (2003, May 13). Ernst & Young Study Estimates Retailers Lose $46 Billion Annually to Inventory Shrinkage; Employee Theft Is Biggest Problem. *Business Wire* .

Finkenzeller, D. K. (2003). *RFID Handbook: Fundamentals and Applications in Contactless Smart Cards and Identification.* 2nd Ed.. Wiley.

Giampaolo, E. D., Forni, F., & Marrocco, G. (2010). RFID-Network Planning by Particle Swarm Optimization. *2010 IEEE Proceedings of the Fourth European Conference on Antennas and Propagation (EuCAP)*. 1-5.

Goldberg, D. E., & Deb, K. (1991). A comparative analysis of selection schemes used in genetic algorithms. *Foundations of Genetic Algorithms*, *1*(90007), 69–93.

Greene, C. E. (2006, February 13). *Area of Operation for a Radio-Frequency Identification (RFID) Tag in the Far-Field.* PhD Thesis. University of Pittsburgh.

Guan, Q., Liu, Y., Yang, Y., & Yu, W. (2006). Genetic Approach for Network Planning in the RFID Systems. *Sixth International Conference on Intelligent Systems Design and Applications, 2006. ISDA '06*. 567-572.

Gupta, N., & Iyer, S. (2007). RFIDPlanner - A Coverage Planning Tool for RFID Networks. *Asian Intl Mobile Computing Conference (AMOC 2007)*. 1-8. Calcutta, India.

Han, J. K., Park, B. S., Choi, Y. S., & Park, H. K. (2001). Genetic Approach with a New Representation for Base StationPlacement in Mobile Communications. *54th IEEE Vehicular Technology Conference, VTC 2001 Fall.* 2703-2707.

Heppes, A., & Melissen, J. (1996). Covering a rectangle with equal circles. *Periodica Mathematica Hungarica, 34*, 65-81.

Holland, J. H. (1975). *Adaptation in Natural and Artificial Systems* University of Michigan Press.

Hougardy , S. (2011). On Packing Square into a Rectangle. *Computational Geometry, 44*(8), 456-463.

Huang, D. Y., & Boyle, K. (2008). *Antennas: From Theory to Practice.* 1st Ed.. Wiley.

Huang, H.-P., & Chang, Y.-T. (2011). Optimal Layout and Deployment for RFID Systems. *Advanced Engineering Informatics, 25*(1), 4-10.

Huang, H.-Z., Qu, J., & Zuo, M. J. (2009). Genetic Algorithm-based Optimal Apportionment of Reliability and Redundancy under Multiple Objectives. *IIE Transactions, 41*(4), 287-298.

Hughes, G., & Chraibi, M. (2011, January 1). Calculating Ellipse Overlap Areas. California Polytechnic State University, San Luis Obispo, CA. Retrieved from http://digitalcommons.calpoly.edu/stat_fac/17.

Imai, T. (2007). Ray-tracing Method for Estimating Radio Propagation Using Genetic. *NTT DoCoMo Technical Journal, 9*(3), 20–27.

Impinj, Inc. (2013). Impinj INDY® UHF RFID reader chips & Impinj MONZA® UHF RFID tag chips. Retrieved July 7, 2013, from http://www.impinj.com/RFID_Products/.

Ji, Z., Sarkar, T. K., & Li, B.H. (2002). Methods for optimizing the location of base stations for indoor wireless communications. *IEEE Transactions on Antennas and Propagation,* 10, 1481 – 1483.

Jones, P., Clarke-Hill, C., Comfort, D., Hillier, D., & Shears, P. (2005). Radio frequency identification and food retailing in the UK. *British Food Journal*, *107*(6), 356-360.

Jones, P., Clarke-Hill, C., Hillier, D., & Comfort, D. (2005). The Benefits, Challenges and Impacts of Radio Frequency Identification Technology (RFID) for Retailers in the UK. *Marketing Intelligence & Planning*, *23*(4), 395-402.

Kennedy, J., & Eberhart, R. (1995). Particle Swarm Optimization. *IEEE International Conference on Neural Networks,* 1942-1948.

Kern, C. (2004). Radio-frequency-identification for security and media circulation in libraries. *The Electronic Library*, *22*(4), 317-324.

Kim, D.-Y., Yoon, H.-G., Jang, B.-J., & Yook, J.-G. (2008). Interference Analysis of UHF RFID Systems. *Progress In Electromagnetics Research B*, *4*, 115-126.

Kim, D.-Y., Yoon, H.-G., Jang, B.-J., & Yook, J.-G. (2009). Effects of Reader-to-Reader Interference on the UHF RFID Interrogation Range. *IEEE Transactions on Industrial Electronics*, *56*(7), 2337-2346.

Knuth, D. E. (1998). *Art of Computer Programming, Volume 3: Sorting and Searching* (2nd Ed.). Addison-Wesley Professional.

Konak, A., Coit, D. W., & Smith, A. E. (2006). Multi-Objective Optimization using Genetic Algorithms: A Tutorial. *Reliability Engineering & System Safety*, *91*(9), 992-1007.

Marrocco, G., Giampaolo, E. D., & Aliberti, R. (2009). Estimation of UHF RFID Reading Regions in Real Environments. *IEEE Antennas and Propagation Magazine*, *51*(6), 44-57.

Michalewicz, Z. (1998). *Genetic Algorithms + Data Structures = Evolution Programs.* 3rd Ed.. Springer.

Montgomery, D. C. (2008). *Design and analysis of experiments*: 7th Ed., John Wiley & Sons Inc.

Nikitin, P. V., & Rao, K. V. . (2008). Antennas and Propagation in UHF RFID Systems. *2008 IEEE International Conference on RFID*. 277-288.

Orfanidis, S. J. (2010). Electromagnetic Waves and Antennas. *Chapter 15, p. 609*. Rutgers University, Piscataway, NJ. Retrieved from http://www.ece.rutgers.edu/~orfanidi/ewa/.

Oztekin, A., Mahdavi, F., Erande, K., Kong, Z. J., Swim, L. K., & Bukkapatnam, S. T. S. (2010). Criticality index analysis based optimal RFID reader placement models for asset tracking. *International Journal of Production Research*, *48*(9), 2679–2698.

Phongcharoenpanich, C. (2009). Investigation of Antennas for RFID Reader. *NTC International Conference 2009*.

Porter, J. D., Billo, R. E., & Mickle, M. H. (2006). Effect of Active Interference on the Performance of Radio Frequency Identification Systems. *International Journal of Radio Frequency Identification Technology and Applications*, *1(1)*, 4-23.

Prommak, C., Kabara, J., Tipper, D., & Charnsripinyo, C. (2002). Next Generation Wireless LAN System Design. *IEEE Proceedings of MILCOM 2002*. 473- 477.

Rapaić, M., Kanovic, Z., & Jelicic Z. (2008). Discrete particle swarm optimization algorithm for solving optimal sensor deployment problem. *Journal of Automatic Control, 18(1)*, 9-14.

Rappaport, T. S. (2002). *Wireless Communications: Principles and Practice*. 2nd Ed.. Prentice Hall.

Reza, A. W., & Geok, T. K. (2009). Investigation of Indoor Location Sensing via RFID Reader Network Utilizing Grid Covering Algorithm. *Wireless Personal Communications*, *49*(1), 67-80.

Rezende, M. C., Martin, I. M., Miacci, M. A. S., & Nohara, E. L. (2001). Radar cross section measurements (8-12 GHz) of flat plates painted with microwave absorbing materials. *IEEE Proceedings of Microwave and Optoelectronics Conference, 2001. 1*, 263–267.

RFID Journal LLC. (2012). How much do RFID readers cost today? Retrieved May 17, 2012, from http://www.rfidjournal.com/faq/20/86.

RNCOS Industry Research Solutions. (2012). *Global RFID Market Forecast to 2014*. Retrieved from http://www.rncos.com/Report/IM378.htm.

Sanghera, P. (2007). *RFID+: CompTIA RFID+ Study Guide and Practice Exam*. 1st Ed.. Syngress.

Sydänheimo, L., Ukkonen, L., & Kivikoski, M. (2006). Effects of Size and Shape of Metallic Objects on Performance of Passive Radio Frequency Identification. *The International Journal of Advanced Manufacturing Technology*, *30*, 897-905.

Talbi, L., & Delisle, G.-Y. (1999). Using directive antennas to reduce multipath fading in indoor PCN systems. *IEEE Antennas and Propagation Society International Symposium, 1999,* 4, 2448–2451.

Tang, K. S., Man, K. F., & Ko, K. T. (1997). Wireless LAN Design using Hierarchical Genetic Algorithm. *Proceedings of the Seventh International Conference on Genetic Algorithms*. 629–635.

Venkatesan, M., & Grauer, Z. (2004). Leveraging Radio Frequency Identification (RFID) Technology to Improve Laboratory Information Management. *American Laboratory*, *36*(18), 11-15.

Wikipedia. (2010, December 29). Radiation Pattern for an Omnidirectional Dipole Antenna. Retrieved May 19, 2011, from http://en.wikipedia.org/wiki/Talk:Radiation_pattern.

Wismans, W. M. G. (1999). Identification and registration of animals in the European Union. *Computers and Electronics in Agriculture*, *24*(1-2), 99-108.

APPENDICES

APPENDIX A

DETAILED DESCRIPTION OF SOME PARAMETERS IN THE NOTATION OF THE CIRCULAR ANTENNA COVERAGE MODEL FORMULATION

Initial number of RFID readers (*N*)

This is the number of RFID readers required to cover a rectangular facility. A circular shape for the radiation pattern for the RFID reader's antenna and a rectangular shape for the facility area are assumed in the CAC model formulation. The circle packing algorithm is used to obtain the initial number of RFID readers by using a square or a hexagon enclosed by a circle to cover the rectangular-shaped facility. As Figure 1 (square) and Figure 2 (hexagon) clearly show, eight (8) RFID readers are required as a starting point to cover the entire example rectangular facility.

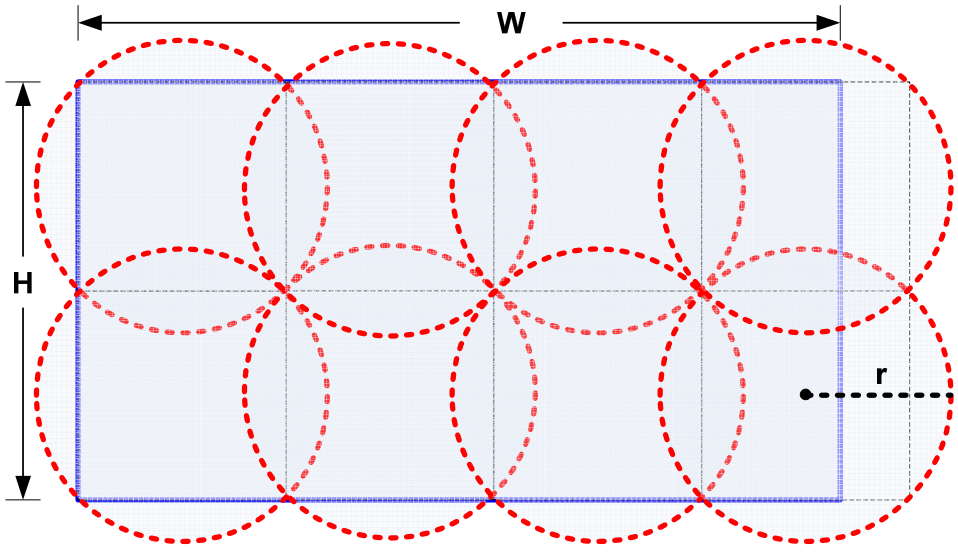

Figure 1 Example of applying the concept of circle packing by using a square enclosed by a circle to cover the rectangular-shaped facility

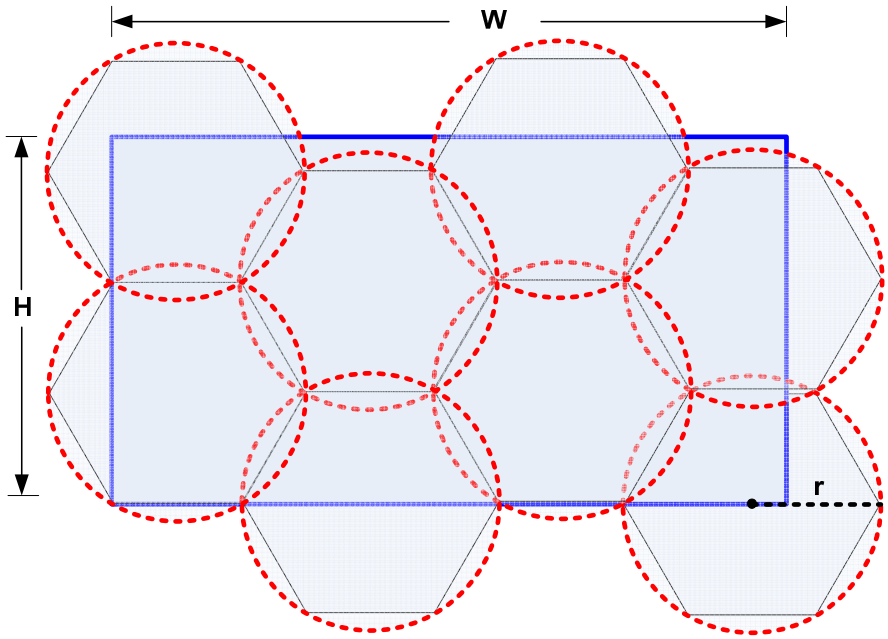

Figure 2 Example of applying the concept of circle packing by using a hexagon enclosed by a circle to cover the rectangular-shaped facility

The effectiveness of using a square or a hexagon enclosed by a circle to cover the rectangular-shaped facility very much depends on the shape and size of the facility. However, a square enclosed by a circle is used to cover the rectangular-shaped facility in this instance to make it easier for visualization.

APPENDIX B
ORDER OF EXPERIMENTS AND RESULTS FROM THE EXPERIMENTAL DESIGN

No	Facility Shape	Facility Size	Grid size	Power Levels	Model	Algorithm	Replication Number	Experiment Number	*Fitness*	*Coverage*	*SIR*	*Cost*	*Time*
	(Tang -, Ji +)	(Small -, Large +)	(0.25m -, 1m +)	(1 levels -, 8 levels +)	(CAC -, EAC+)	(GA -, PSO +)			*(Z)*	*(f_1)*	*(f_2)*	*(f_3)*	*(seconds)*
1	Tang	Small	0.25	1	CAC	GA	1	155	0.7981	0.8702	0.9801	0.4	344.63
							2	53	0.8023	0.8855	0.9551	0.4	337.26
							3	143	0.8038	0.8855	0.9626	0.4	339.29
2	Tang	Small	0.25	1	CAC	PSO	1	128	0.8009	0.8855	0.9482	0.4	211.35
							2	28	0.7995	0.8702	0.9870	0.4	220.73
							3	112	0.8052	0.8855	0.9695	0.4	219.27
3	Tang	Small	0.25	1	EAC	GA	1	119	0.7939	0.8855	0.9129	0.4	519.77
							2	148	0.7910	0.8702	0.9443	0.4	541.72
							3	68	0.7924	0.8702	0.9513	0.4	507.77
4	Tang	Small	0.25	1	EAC	PSO	1	102	0.7882	0.8702	0.9304	0.4	262.01
							2	172	0.7867	0.8473	0.9917	0.4	255.37
							3	80	0.7896	0.8626	0.9603	0.4	255.02
5	Tang	Small	0.25	8	CAC	GA	1	61	0.8052	0.8855	0.9695	0.4	336.11
							2	69	0.7995	0.8702	0.9870	0.4	347.14
							3	125	0.7981	0.8702	0.9801	0.4	329.50
6	Tang	Small	0.25	8	CAC	PSO	1	178	0.7981	0.8855	0.9343	0.4	225.69
							2	180	0.8052	0.8855	0.9695	0.4	221.11
							3	24	0.8023	0.8855	0.9551	0.4	234.18
7	Tang	Small	0.25	8	EAC	GA	1	152	0.7924	0.8702	0.9513	0.4	520.74
							2	4	0.7925	0.8702	0.9518	0.4	506.75
							3	162	0.7867	0.8702	0.9230	0.4	520.31
8	Tang	Small	0.25	8	EAC	PSO	1	132	0.7840	0.8473	0.9778	0.4	247.69
							2	149	0.7853	0.8626	0.9389	0.4	237.41
							3	103	0.7882	0.8473	0.9991	0.4	254.99
9	Tang	Small	1	1	CAC	GA	1	45	0.7910	0.8702	0.9443	0.4	354.04
							2	31	0.7953	0.8855	0.9199	0.4	352.85
							3	64	0.7952	0.8702	0.9652	0.4	347.45
10	Tang	Small	1	1	CAC	PSO	1	161	0.7953	0.8855	0.9199	0.4	198.95
							2	91	0.7953	0.8855	0.9199	0.4	188.09
							3	14	0.7952	0.8702	0.9652	0.4	197.50

APPENDIX B (Continued)
ORDER OF EXPERIMENTS AND RESULTS FROM THE EXPERIMENTAL DESIGN

No	Facility Shape	Facility Size	Grid size	Power Levels	Model	Algorithm	Replication Number	Experiment Number	*Fitness*	*Coverage*	*SIR*	*Cost*	*Time*
	(Tang -, Ji +)	(Small -, Large +)	(0.25m -, 1m +)	(1 levels -, 8 levels +)	(CAC -, EAC+)	(GA -, PSO +)			*(Z)*	*(f_1)*	*(f_2)*	*(f_3)*	*(seconds)*
11	Tang	Small	1	1	EAC	GA	1	49	0.7783	0.8473	0.9495	0.4	541.86
							2	73	0.7924	0.8702	0.9513	0.4	507.40
							3	154	0.7867	0.8702	0.9230	0.4	505.65
12	Tang	Small	1	1	EAC	PSO	1	130	0.7783	0.8473	0.9495	0.4	230.26
							2	34	0.7726	0.8626	0.8754	0.4	235.18
							3	82	0.7882	0.8702	0.9304	0.4	242.65
13	Tang	Small	1	8	CAC	GA	1	133	0.7953	0.8855	0.9199	0.4	351.03
							2	42	0.7896	0.8702	0.9374	0.4	363.99
							3	92	0.7655	0.8702	0.8168	0.4	341.60
14	Tang	Small	1	8	CAC	PSO	1	1	0.7783	0.8397	0.9724	0.4	176.88
							2	23	0.7953	0.8855	0.9199	0.4	187.98
							3	114	0.7952	0.8702	0.9652	0.4	184.46
15	Tang	Small	1	8	EAC	GA	1	74	0.7754	0.8397	0.9580	0.4	519.20
							2	104	0.7811	0.8702	0.8947	0.4	514.25
							3	158	0.7783	0.8626	0.9037	0.4	521.02
16	Tang	Small	1	8	EAC	PSO	1	40	0.7726	0.8626	0.8754	0.4	295.98
							2	16	0.7826	0.8702	0.9021	0.4	278.19
							3	98	0.7726	0.8626	0.8754	0.4	294.26
17	Tang	Large	0.25	1	CAC	GA	1	107	0.7547	0.8289	0.9297	0.3571	6,570.21
							2	57	0.7423	0.8275	0.9195	0.3095	7,174.80
							3	165	0.7139	0.8031	0.8746	0.2857	7,518.00
18	Tang	Large	0.25	1	CAC	PSO	1	137	0.7458	0.8101	0.9655	0.3333	3,614.08
							2	135	0.7560	0.8729	0.8756	0.2857	3,903.80
							3	38	0.7265	0.8268	0.9140	0.2381	4,091.20
19	Tang	Large	0.25	1	EAC	GA	1	79	0.7350	0.7751	0.9686	0.3810	9,749.80
							2	25	0.7462	0.8017	0.9689	0.3571	9,893.20
							3	118	0.7328	0.7940	0.9487	0.3333	10,848.8
20	Tang	Large	0.25	1	EAC	PSO	1	179	0.6887	0.7730	0.8387	0.2857	5,856.43
							2	124	0.6801	0.7542	0.8046	0.3333	5,963.71
							3	140	0.7257	0.8324	0.8456	0.2857	5,800.29

APPENDIX B (Continued)
ORDER OF EXPERIMENTS AND RESULTS FROM THE EXPERIMENTAL DESIGN

No	Facility Shape	Facility Size	Grid size	Power Levels	Model	Algorithm	Replication Number	Experiment Number	*Fitness*	*Coverage*	*SIR*	*Cost*	*Time*
	(Tang -, Ji +)	(Small -, Large +)	(0.25m -, 1m +)	(1 levels -, 8 levels +)	(CAC -, EAC+)	(GA -, PSO +)			*(Z)*	*(f_1)*	*(f_{21})*	*(f_3)*	*(seconds)*
21	Tang	Large	0.25	8	CAC	GA	1	122	0.7292	0.8380	0.9177	0.2143	7,820.20
							2	47	0.7138	0.8052	0.8678	0.2857	7,177.40
							3	182	0.7421	0.8156	0.9065	0.3571	6,506.60
22	Tang	Large	0.25	8	CAC	PSO	1	6	0.6995	0.7654	0.8681	0.3333	3,410.29
							2	115	0.6663	0.7437	0.8147	0.2857	3,626.86
							3	7	0.6597	0.7088	0.9340	0.2381	3,897.14
23	Tang	Large	0.25	8	EAC	GA	1	173	0.7475	0.8254	0.9041	0.3571	10,996.6
							2	90	0.7295	0.7912	0.9168	0.3571	10,683.8
							3	181	0.7423	0.8163	0.9530	0.3095	11,155.8
24	Tang	Large	0.25	8	EAC	PSO	1	99	0.6473	0.6865	0.8914	0.2857	5,982.14
							2	188	0.6598	0.6718	0.9026	0.3810	5,228.00
							3	156	0.6882	0.7353	0.9493	0.2857	5,966.60
25	Tang	Large	1	1	CAC	GA	1	19	0.7674	0.8415	0.9791	0.3333	6,888.40
							2	8	0.7136	0.8010	0.8080	0.3571	6,624.20
							3	171	0.7214	0.8094	0.8218	0.3571	6,673.80
26	Tang	Large	1	1	CAC	PSO	1	151	0.7214	0.7800	0.9098	0.3571	3,636.80
							2	21	0.7357	0.7975	0.9527	0.3333	3,669.80
							3	78	0.7136	0.7842	0.8820	0.3333	3,599.60
27	Tang	Large	1	1	EAC	GA	1	170	0.7209	0.7968	0.9046	0.3095	8,850.43
							2	48	0.7233	0.7619	0.9499	0.3810	7,640.57
							3	105	0.7547	0.8352	0.9346	0.3333	8,179.29
28	Tang	Large	1	1	EAC	PSO	1	144	0.6663	0.6969	0.9312	0.3095	5,435.57
							2	67	0.6987	0.7193	0.9547	0.3810	5,039.71
							3	138	0.7182	0.7807	0.9155	0.3333	5,546.29
29	Tang	Large	1	8	CAC	GA	1	75	0.7138	0.7709	0.9467	0.3095	6,919.00
							2	72	0.7233	0.7940	0.9726	0.2619	7,825.60
							3	174	0.7000	0.7849	0.9072	0.2381	8,158.20
30	Tang	Large	1	8	CAC	PSO	1	9	0.6987	0.7256	0.9597	0.3571	3,341.80
							2	108	0.6894	0.7367	0.9273	0.3095	3,556.40
							3	95	0.6977	0.7751	0.9012	0.2619	3,848.71

APPENDIX B (Continued)
ORDER OF EXPERIMENTS AND RESULTS FROM THE EXPERIMENTAL DESIGN

No	Facility Shape	Facility Size	Grid size	Power Levels	Model	Algorithm	Replication Number	Experiment Number	*Fitness*	*Coverage*	*SIR*	*Cost*	*Time*
	(Tang -, Ji +)	(Small -, Large +)	(0.25m -, 1m +)	(1 levels -, 8 levels +)	(CAC -, EAC+)	(GA -, PSO +)			*(Z)*	*(f_1)*	*(f_2)*	*(f_3)*	*(seconds)*
31	Tang	Large	1	8	EAC	GA	1	136	0.7209	0.7898	0.9256	0.3095	10,676.0
							2	33	0.7262	0.7751	0.9723	0.3333	10,386.2
							3	187	0.7041	0.7696	0.8547	0.3571	10,276.6
32	Tang	Large	1	8	EAC	PSO	1	186	0.6953	0.7318	0.9477	0.3333	5,612.30
							2	189	0.6658	0.7193	0.8855	0.2857	5,964.38
							3	51	0.6882	0.7535	0.8710	0.3095	5,637.80
33	Ji	Small	0.25	1	CAC	GA	1	46	0.7765	0.9830	0.8085	0.125	698.85
							2	2	0.8003	1.0000	0.8764	0.125	687.62
							3	101	0.7966	0.9532	0.8736	0.250	792.65
34	Ji	Small	0.25	1	CAC	PSO	1	192	0.7844	0.9744	0.8738	0.125	418.38
							2	120	0.7765	0.9744	0.8341	0.125	415.17
							3	87	0.7908	0.9957	0.8416	0.125	397.62
35	Ji	Small	0.25	1	EAC	GA	1	145	0.7919	0.9447	0.8753	0.250	1,133.73
							2	32	0.7797	0.9659	0.8755	0.125	1,015.63
							3	163	0.7839	0.9234	0.8994	0.250	1,057.74
36	Ji	Small	0.25	1	EAC	PSO	1	22	0.7781	0.9744	0.8421	0.125	529.75
							2	52	0.7931	0.9787	0.9045	0.125	568.53
							3	146	0.7681	0.8979	0.8967	0.250	628.96
37	Ji	Small	0.25	8	CAC	GA	1	5	0.7860	0.9830	0.8562	0.125	660.92
							2	116	0.7892	0.9787	0.8848	0.125	665.05
							3	131	0.7757	0.9702	0.8429	0.125	662.68
38	Ji	Small	0.25	8	CAC	PSO	1	157	0.7619	0.9915	0.8352	0.000	407.23
							2	121	0.7744	0.9021	0.9157	0.250	448.56
							3	159	0.7773	0.9744	0.8381	0.125	408.23
39	Ji	Small	0.25	8	EAC	GA	1	160	0.7812	0.9744	0.8579	0.125	1,019.08
							2	85	0.7728	0.9106	0.8823	0.250	1,122.61
							3	166	0.7820	0.9574	0.9129	0.125	888.19
40	Ji	Small	0.25	8	EAC	PSO	1	97	0.7836	0.9744	0.8697	0.125	571.80
							2	89	0.7829	0.9702	0.8786	0.125	576.26
							3	113	0.7852	0.9830	0.8521	0.125	528.51

APPENDIX B (Continued)
ORDER OF EXPERIMENTS AND RESULTS FROM THE EXPERIMENTAL DESIGN

No	Facility Shape	Facility Size	Grid size	Power Levels	Model	Algorithm	Replication Number	Experiment Number	*Fitness*	*Coverage*	*SIR*	*Cost*	*Time*
	(Tang -, Ji +)	(Small -, Large +)	(0.25m -, 1m +)	(1 levels -, 8 levels +)	(CAC -, EAC+)	(GA -, PSO +)			*(Z)*	*(f_1)*	*(f_2)*	*(f_3)*	*(seconds)*
41	Ji	Small	1	1	CAC	GA	1	81	0.7717	0.9659	0.8358	0.125	727.65
							2	30	0.7670	0.9574	0.8375	0.125	725.99
							3	117	0.7845	0.9830	0.8482	0.125	720.71
42	Ji	Small	1	1	CAC	PSO	1	10	0.7892	1.0000	0.8209	0.125	384.05
							2	177	0.7908	1.0000	0.8288	0.125	378.64
							3	184	0.7908	0.9830	0.8799	0.125	365.05
43	Ji	Small	1	1	EAC	GA	1	17	0.7837	0.9830	0.8442	0.125	1,026.36
							2	126	0.7828	0.9872	0.8275	0.125	909.63
							3	50	0.7797	0.9702	0.8627	0.125	1,018.19
44	Ji	Small	1	1	EAC	PSO	1	86	0.7694	0.9362	0.9134	0.125	505.01
							2	109	0.7694	0.9489	0.8751	0.125	510.23
							3	123	0.7694	0.9447	0.8877	0.125	510.63
45	Ji	Small	1	8	CAC	GA	1	18	0.7693	0.9574	0.8495	0.125	696.03
							2	167	0.7773	0.9702	0.8508	0.125	704.33
							3	3	0.7709	0.9489	0.8830	0.125	703.34
46	Ji	Small	1	8	CAC	PSO	1	70	0.7797	0.9787	0.8372	0.125	389.64
							2	54	0.7709	0.9489	0.8830	0.125	382.18
							3	66	0.7622	0.9659	0.7883	0.125	365.74
47	Ji	Small	1	8	EAC	GA	1	35	0.7813	0.9787	0.8451	0.125	931.50
							2	153	0.7813	0.9617	0.8962	0.125	985.69
							3	88	0.7804	0.9744	0.8539	0.125	1,039.07
48	Ji	Small	1	8	EAC	PSO	1	190	0.7820	0.9744	0.8618	0.125	543.65
							2	63	0.7733	0.9574	0.8693	0.125	511.33
							3	76	0.7749	0.9617	0.8644	0.125	514.17
49	Ji	Large	0.25	1	CAC	GA	1	147	0.7542	0.8169	0.9815	0.3387	20,424.6
							2	44	0.7340	0.8099	0.9015	0.3387	20,996.9
							3	176	0.7130	0.7851	0.8548	0.3548	19,315.3
50	Ji	Large	0.25	1	CAC	PSO	1	56	0.7357	0.8107	0.9398	0.3065	10,931.0
							2	11	0.7226	0.7814	0.9301	0.3387	10,477.5
							3	71	0.7074	0.7777	0.8974	0.3065	10,812.7

APPENDIX B (Continued)
ORDER OF EXPERIMENTS AND RESULTS FROM THE EXPERIMENTAL DESIGN

No	Facility Shape	Facility Size	Grid size	Power Levels	Model	Algorithm	Replication Number	Experiment Number	*Fitness*	*Coverage*	*SIR*	*Cost*	*Time*
	(Tang -, Ji +)	(Small -, Large +)	(0.25m -, 1m +)	(1 levels -, 8 levels +)	(CAC -, EAC+)	(GA -, PSO +)			*(Z)*	*(f_1)*	*(f_2)*	*(f_3)*	*(seconds)*
51	Ji	Large	0.25	1	EAC	GA	1	13	0.7319	0.8025	0.9779	0.2742	32,762.0
							2	134	0.7523	0.8318	0.9757	0.2903	31,872.0
							3	168	0.7062	0.7789	0.9039	0.2903	30,369.3
52	Ji	Large	0.25	1	EAC	PSO	1	12	0.6937	0.7293	0.9257	0.3548	14,150.7
							2	110	0.7063	0.7508	0.9242	0.3548	14,172.6
							3	60	0.6781	0.7074	0.9456	0.3226	15,404.2
53	Ji	Large	0.25	8	CAC	GA	1	62	0.7243	0.7669	0.9820	0.3387	19,271.8
							2	185	0.6966	0.7905	0.8373	0.2742	22,452.0
							3	96	0.7104	0.7926	0.9001	0.2742	23,242.8
54	Ji	Large	0.25	8	CAC	PSO	1	15	0.6773	0.7012	0.9602	0.3226	10,140.3
							2	127	0.6740	0.7322	0.8668	0.3065	10,605.2
							3	39	0.6685	0.7066	0.9001	0.3226	10,220.0
55	Ji	Large	0.25	8	EAC	GA	1	83	0.6966	0.7835	0.8423	0.2903	33,452.0
							2	36	0.6796	0.7657	0.7622	0.3387	29,528.0
							3	26	0.7073	0.7934	0.8821	0.2742	33,790.0
56	Ji	Large	0.25	8	EAC	PSO	1	191	0.6744	0.7161	0.8689	0.3548	14,312.6
							2	77	0.6475	0.6872	0.8533	0.3226	15,242.2
							3	55	0.6581	0.7058	0.8666	0.3065	15,525.6
57	Ji	Large	1	1	CAC	GA	1	20	0.7296	0.8256	0.8324	0.3387	19,234.2
							2	183	0.7168	0.8136	0.8044	0.3387	19,623.4
							3	129	0.7553	0.8384	0.9549	0.3065	21,161.4
58	Ji	Large	1	1	CAC	PSO	1	175	0.7072	0.7752	0.8556	0.3548	9,915.00
							2	111	0.6937	0.7781	0.7955	0.3387	10,067.2
							3	141	0.6784	0.7558	0.8181	0.3065	10,764.4
59	Ji	Large	1	1	EAC	GA	1	29	0.7081	0.7893	0.8501	0.3226	29,174.0
							2	43	0.7252	0.7884	0.9542	0.3065	30,720.0
							3	106	0.7063	0.8099	0.8114	0.2903	31,652.0
60	Ji	Large	1	1	EAC	PSO	1	142	0.7513	0.8099	0.9719	0.3548	14,297.8
							2	41	0.7074	0.7413	0.9743	0.3387	14,215.4
							3	100	0.7244	0.7744	0.9441	0.3548	14,607.1

APPENDIX B (Continued)
ORDER OF EXPERIMENTS AND RESULTS FROM THE EXPERIMENTAL DESIGN

61	Ji	Large	1	8	CAC	GA	1	150	0.7542	0.8388	0.9803	0.2742	22,570.0
							2	139	0.7222	0.7860	0.9628	0.2903	21,752.0
							3	164	0.7255	0.8041	0.9409	0.2742	23,358.5
62	Ji	Large	1	8	CAC	PSO	1	169	0.7051	0.7504	0.9195	0.3548	9,491.00
							2	65	0.6978	0.7256	0.9573	0.3548	9,485.86
							3	27	0.6937	0.7405	0.9083	0.3387	10,298.5
63	Ji	Large	1	8	EAC	GA	1	93	0.7521	0.8182	0.9834	0.3226	30,658.0
							2	58	0.7222	0.7860	0.9789	0.2742	33,956.0
							3	37	0.7042	0.7678	0.8951	0.3226	31,158.5
64	Ji	Large	1	8	EAC	PSO	1	59	0.7033	0.7393	0.9439	0.3548	14,104.2
							2	94	0.6789	0.7161	0.9075	0.3387	14,875.2
							3	84	0.6585	0.7045	0.8402	0.3387	15,028.0

APPENDIX C

CALCULATION OF RADIUS (*r*), SEMI-MAJOR AXIS (*a*) AND SEMI-MINOR AXIS (*b*)

The Calculation of the Radius (*r*) for the CAC Model Formulation

The radius of the coverage area of the RFID reader's antenna *(r)* is calculated by taking into account all important parameters of the RFID reader system compliant with the EPCglobal® standard mentioned in section 4.1. The multipath propagation model was used in the downlink communication. The radius of the coverage area of RFID reader's antenna (*r*) in the downlink communication can be computed as follows:

Given parameters:

Minimum tag power, $P_{r,tag} = -20\ dBm\ (10\mu W)$ (Impinj, Inc. , 2013)

Transmitted power, $P_t = 30\ dBm\ (1\,W)$

RFID reader's antenna gain, $G_{reader} = 0\,dB\ (1)$

Effective Isotropic Radiated Power, $EIRP = P_t G_{reader} = 1 \times 1 = 1\,W$

RFID tag's antenna gain, $G_{tag} = 2.15\,dB\ (1.64)$

Frequency, $f = 915MHz \rightarrow \lambda = \frac{300}{915} = 0.328m$

Path loss exponent, $n = 2.20$ (Rappaport, T. S., 2002)

Loss from multipath fading, $X = 4.75\ dB\ (3)$ (Rappaport, T. S., 2002)

As was shown in equation 3.5 and 3.6, the received signal power can be calculated as follows:

$$[P_{r,tag}]_{dBm} = [P_t]_{dBm} + [G_{reader}]_{dB} + [G_{tag}]_{dB} - L_P(d_0) - 10n \log\left(\frac{d}{d_0}\right) - X_{dB} \quad (1)$$

$$[P_{r,tag}]_{dBm} = [P_t]_{dBm} + [G_{reader}]_{dB} + [G_{tag}]_{dB} - 20\log\left(\frac{4\pi}{\lambda}\right) - 10n \log(d) - X_{dB} \quad (2)$$

Equation 2 can be rewritten in the format of a ratio as the follows:

$$P_{r,tag} = P_t \times G_{reader} \times G_{tag} \times \left(\frac{\lambda}{4\pi}\right)^2 \times \frac{1}{d^n} \times \frac{1}{10^{\frac{X}{10}}} \quad (3)$$

Rearranging some terms yields:

$$d = \left(\frac{P_t \times G_{reader} \times G_{tag}}{P_{r,tag} \times 10^{\frac{X}{10}}} \times \left(\frac{\lambda}{4\pi}\right)^2 \right)^{\frac{1}{n}} \quad (4)$$

Substituting in the known values gives:

$$d_{\max} = \left(\frac{1 \times 1.64}{10 \times 10^{-6} \times 10^{\frac{4.75}{10}}} \times \left(\frac{0.328}{4\pi}\right)^2 \right)^{\frac{1}{2.2}} \quad (5)$$

$$d_{\max} = 5.19\, meters$$

Therefore, the maximum distance at which the RFID tag can receive the minimum power of 10μW when optimally positioned given the aforementioned parameters is 5.19 meters.

The previous calculation is the calculation of *r* in the downlink communication that provides information on where the RFID tag could receive operational power from the RFID reader. There also needs to be a calculation of *r* in the uplink communication to determine if the backscattered signal from the RFID tag can be successfully read by the RFID reader.

The radar-cross section propagation model was used in the uplink communication. The radius of the coverage area of RFID reader's antenna (*r*) can be computed using equation 3.9b as follows:

$$P_{r,reader} = \frac{P_t \times G_{trasmitter} \times G_{receiver} \times \sigma \times \lambda^2}{(4\pi)^3} \times \frac{1}{r^{2n}} \times \frac{1}{10^{\frac{X}{10}}} \quad (6)$$

Rearranging some terms in equation 6 yields:

$$r = \left(\frac{P_t \times G_{trasmitter} \times G_{receiver} \times \sigma \times \lambda^2}{P_{r,reader} \times (4\pi)^3 \times 10^{\frac{X}{10}}} \right)^{\frac{1}{2n}} \quad (7)$$

Given parameters:

Transmitted power, $P_t = 30\ dBm\ (1\,W)$

Transmitter's antenna gain, $G_{trasmitter} = G_{reader} = 0\,dB$ (1)

Effective Isotropic Radiated Power, $EIRP = P_t G_{reader} = 1 \times 1 = 1\,W$

Receiver's antenna gain, $G_{receiver} = G_{reader} = 0\,dB$ (1)

RCS, $\sigma = \frac{4\pi \times (Area)^2}{\lambda^2} = \frac{4\pi \times (0.15 \times 0.15)^2}{0.328^2} = 0.06\ m^2$ (Rezende et al., 2001)

Frequency, $f = 915MHz \rightarrow \lambda = \frac{300}{915} = 0.328m$

Receiver's sensitivity, $P_{r,reader} = -95\ dBm\ (0.316\ nW)$ (Impinj, Inc. , 2013)

Path loss exponent, $n = 2.20$ (Rappaport, T. S., 2002)

Loss from multipath fading, $X = 4.75\ dB$ (3) (Rappaport, T. S., 2002)

Substituting in the known parameters into (7) gives:

$$r_{\max} = \left(\frac{1 \times 1 \times 1 \times 0.06 \times 0.328^2}{0.316 \times 10^{-9} \times (4\pi)^3 \times 10^{\frac{4.75}{10}}} \right)^{\frac{1}{2 \times 2.2}} \quad (8)$$

$$r_{\max} = 6.37\ meters$$

When the radii of the coverage of the RFID reader's antenna *(r)* in the downlink and the uplink communication channels are compared, it is found that the limitation is the downlink communication channel because the value of *r* is shorter than that of the uplink communication channel. In this case, the coverage area in the RFID system is limited by the RFID tag's sensitivity instead of the RFID reader's sensitivity. Therefore, the value of *r* is equal to 5.19 meters and this value is used for all experiments conducted with the CAC model formulation.

The Calculation of Semi-Major axis (*a*) and Semi-Minor Axis (*b*) for the EAC Model Formulation

The semi-major axis (*a)* can be calculated using equation 4.15. However, equation 4.15 has to be slightly modified (see equation 9) when considering the effect of the path loss exponent (*n*) and the loss from multipath fading (*X*) in the multipath propagation model. Once the value of *a* is obtained, the semi-minor axis (*b)* is calculated using equation (10).

$$2a = \left(\frac{P_t \times G_{reader} \times G_{tag} \times \chi}{P_{r,tag} \times 10^{\frac{X}{10}}} \times \left(\frac{\lambda}{4\pi} \right)^2 \right)^{\frac{1}{n}} \tag{9}$$

$$b = a \sqrt{\tan \frac{HPBW}{2} \frac{\sin \frac{HPBW}{2}}{\sqrt{2} - \cos \frac{HPBW}{2}}} \tag{10}$$

Most parameters used in the calculation of *r* in the downlink communication channel care also used in the calculation of *a* and *b* in the downlink communication channel for the EAC model formulation. However, two parameters, i.e., RFID reader's antenna gain (G_{reader}) and loss from multipath fading (X) are modified to reflect practical values to be used in the real RFID system. A directional patch antenna is used for the RFID reader in EAC model formulation. This type of antenna has more antenna gain than that of omnidirectional or dipole antenna used in CAC model formulation. This value is set to be maximum value allowed by FCC. FCC allows the maximum *EIRP* of 4 Watts; therefore, the RFID reader's antenna gain is set to be 6.02 dB or 4 in ratio, i.e., $EIRP = P_t \times G_{reader} = 1 \times 4 = 4\ W$. Talbi & Delisle (1999) suggested that the use of directional antennas can reduce multipath fading

in the indoor wireless environment. Therefore, the loss from multipath fading for the EAC model formulation should be less than that of CAC model formulation. This value is set to be 3 dB or 2 in ratio.

In addition, a new parameter, i.e., half power beam width of the RFID reader antenna (*HPBW*), is introduced for the calculation of *b* after *a* is obtained.

Given parameters:

RFID reader's antenna gain, $G_{reader} = 6.02\,dB$ (4)

Loss from multipath fading, $X = 3\ dB$ (2)

Half power beam width of the RFID reader antenna, $HPBW = 67^{\circ}$

Substituting all given parameters in equation 9 and 10 gives:

$$2a = \left(\frac{4 \times 1.64 \times 1}{10 \times 10^{-6} \times 10^{\frac{3}{10}}} \times \left(\frac{0.328}{4\pi} \right)^2 \right)^{\frac{1}{2.2}} \tag{11}$$

$$a_{\max} = 5.84\,meters$$

$$b = 5.84 \sqrt{\tan\frac{67^{\circ}}{2} \times \frac{\sin\frac{67^{\circ}}{2}}{\sqrt{2} - \cos\frac{67^{\circ}}{2}}} \tag{12}$$

$$b_{\max} = 4.63\,meters$$

A similar concept to that used in calculating the radius of the coverage area of the RFID reader's antenna *(r)* in the uplink communication channel for CAC model formulation

can be applied to find the semi-major axis (*a*) and semi-minor axis (*b*) for the EAC model formulation. In this case, it is found that $a_{\max}$ and $b_{\max}$ for the uplink communication channel are 6.55 meters and 5.20 meters, respectively. The limitation of signal communication between the RFID reader and the RFID tag is on the downlink communication channel; therefore, $a_{\max} = 5.84\,meters$ and $b_{\max} = 4.63\,meters$ are used for all experiments of EAC model formulation.